

Durham E-Theses

Magnetic Field Effect on Stability of Convection in Fluid and Porous Media

HARFASH, AKIL,JASSIM

How to cite:

HARFASH, AKIL,JASSIM (2014) *Magnetic Field Effect on Stability of Convection in Fluid and Porous Media*, Durham theses, Durham University. Available at Durham E-Theses Online:
<http://etheses.dur.ac.uk/3255/>

Use policy

The full-text may be used and/or reproduced, and given to third parties in any format or medium, without prior permission or charge, for personal research or study, educational, or not-for-profit purposes provided that:

- a full bibliographic reference is made to the original source
- a [link](#) is made to the metadata record in Durham E-Theses
- the full-text is not changed in any way

The full-text must not be sold in any format or medium without the formal permission of the copyright holders.

Please consult the [full Durham E-Theses policy](#) for further details.

Magnetic Field Effect on Stability of Convection in Fluid and Porous Media

Akil Jassim Harfash

A thesis presented for the degree of
Doctor of Philosophy



Numerical Analysis Group
Department of Mathematical Sciences
University of Durham
England

May 2014

Dedicated to

My family

Magnetic Field Effect on Stability of Convection in Fluid and Porous Media

Akil Jassim Harfash

Submitted for the degree of Doctor of Philosophy

January 2014

Abstract

We investigate the linear instability and nonlinear stability for some convection models, and present results and details of their computation in each case. The convection models we consider are: convection in a variable gravity field with magnetic field effect; magnetic effect on instability and nonlinear stability in a reacting fluid; magnetic effect on instability and nonlinear stability of double diffusive convection in a reacting fluid; Poiseuille flow in a porous medium with slip boundary conditions.

The structural stability for these convection models is studied. A priori bounds are derived. With the aid of these a priori bounds we are able to demonstrate continuous dependence of solutions on some coefficients. We further show that the solution depends continuously on a change in the coefficients.

Chebyshev collection, p order finite element, finite difference, high order finite difference methods are also developed for the evaluation of eigenvalues and eigenfunctions inherent in stability analysis in fluid and porous media, drawing on the experience of the implementation of the well established techniques in the previous work (cf. Drazin and Reid [46], Fox [53], Ng and Reid [132–134]) and Orszag [140]). These generate sparse matrices, where the standard homogeneous boundary conditions for both porous and fluid media problems are contained within the method.

When the difference between the linear (which predicts instability) and nonlinear (which predicts stability) thresholds is very large, the validity of the linear instability threshold to capture the onset of the instability is unclear. Thus, we develop a three dimensional simulation to test the validity of these thresholds. To achieve this we

transform the problem into a velocity-vorticity formulation and utilise second order finite difference schemes. We use both implicit and explicit schemes to enforce the free divergence equation.

Declaration

The work in this thesis is based on research carried out at the Numerical Analysis group, Department of Mathematical Sciences, England. No part of this thesis has been submitted elsewhere for any other degree or qualification and it is all my own work with the exception of Chapters 3 and 5, which contains work published in collaboration with Prof. B. Straughan, University of Durham, United Kingdom . The contents of Chapters 2 to 10 are published in [72]- [79] and [199].

Copyright © 2014 by Akil Jassim Harfash.

“The copyright of this thesis rests with the author. No quotations from it should be published without the author’s prior written consent and information derived from it should be acknowledged”.

Acknowledgements

I would like to thank my supervisor, Prof. Brian Straughan, for all the support he has given me over the past three years, and for helping to make my postgraduate studies both enjoyable and rewarding.

I would like to express my deepest gratitude to Dr James F. Blowey, for his effort, support and advice which played a key role to complete my thesis. I would like to thank Dr. Antony A. Hill for his comments that have led to improvements in my thesis. My thanks go to everyone in the Department of Mathematical Sciences, in particular the Numerical Analysis Group, for all their help and support. Thanks also to Imran M for preparing the LATEX template used for this thesis.

I am indebted to my father, my mother, my brothers, my sisters and the rest of my family for the huge support they have provided me during my studies. My sincere thanks are due to my wife, Huda for her help and support. I also address my thanks to my father and mother in law for their support and encouragement.

Finally, I would like to acknowledge the Iraqi ministry of higher education and scientific research for their financial support and otherwise.

Contents

Abstract	iii
Declaration	v
Acknowledgements	vi
1 Introduction	1
2 Convection in a variable gravity field with magnetic field effect	11
2.1 Introduction	11
2.2 Governing Equations	13
2.3 Linear instability	16
2.4 Nonlinear energy stability theory	18
2.5 Numerical methods	21
2.5.1 Chebyshev tau	21
2.5.2 Finite Difference Scheme	25
2.6 Results and conclusions	29
3 Magnetic effect on instability and nonlinear stability in a reacting fluid	41
3.1 Introduction	41
3.2 Basic Equations	42
3.3 Linear instability	45
3.4 Nonlinear stability	46
3.5 Numerical technique	49
3.6 Results and conclusions	52

4	Magnetic effect on instability and nonlinear stability of double diffusive convection in a reacting fluid	57
4.1	Introduction	57
4.2	Basic Equations	59
4.3	Linear instability	63
4.4	Nonlinear energy stability theory	66
4.5	Numerical method	68
4.6	Results and conclusions	73
5	Instability in Poiseuille flow in a porous medium with slip boundary conditions	85
5.1	Introduction	85
5.2	Basic equations	87
5.3	Numerical techniques	89
5.3.1	Chebyshev collocation method	89
5.3.2	Finite element method	91
5.4	Numerical results and conclusions	95
6	Numerical methods for solving some hydrodynamic stability problems	108
6.1	Introduction	108
6.2	The effect of boundary conditions on convective instability	108
6.3	Numerical methods for the eigenvalue system	113
6.3.1	Chebyshev tau	113
6.3.2	Finite difference scheme	116
6.3.3	Finite element method	119
6.3.4	Chebyshev collocation methods	124
6.3.5	Method 2.	127
6.4	Numerical results and conclusions	129
7	Structural stability for convection models in a reacting porous medium with magnetic field effect	141

7.1	Introduction	141
7.2	Continuous dependence for the first model	146
7.2.1	Continuous dependence on σ	147
7.2.2	Continuous dependence on K_1	148
7.3	Continuous dependence for the second model	149
7.3.1	Continuous dependence on σ	150
7.3.2	Continuous dependence on K_1	151
8	Structural stability for two convection models in a reacting fluid with magnetic field effect	153
8.1	Introduction	153
8.2	Continuous dependence for the first model	155
8.2.1	Continuous dependence on σ	160
8.2.2	Continuous dependence on K_1	162
8.3	Continuous dependence for the second model	163
8.3.1	Continuous dependence on σ	168
8.3.2	Continuous dependence on K_1	170
9	Continuous dependence on the coefficients for double diffusive con- vection in Darcy flow with Magnetic field effect	172
9.1	Introduction	172
9.2	A priori bounds	174
9.2.1	A bound for \mathbf{v}	175
9.2.2	A bound for T	175
9.2.3	A bound for C	177
9.2.4	Bounds for $\nabla T, \nabla C$	178
9.2.5	A bounds for ∇w	178
9.2.6	A bounds for $\nabla \mathbf{v}$	179
9.3	Continuous dependence on the coefficient σ	180
9.4	Continuous dependence on the coefficients g_i and h_i	186

10 Three dimensional simulation for the problem of a layer of non-Boussinesq fluid heated internally with prescribed heat flux on the lower boundary and constant temperature upper surface	188
10.1 Introduction	188
10.2 Governing equations	190
10.3 Linear and nonlinear energy stability theories	192
10.4 Velocity-vorticity formulation	193
10.5 Numerical schemes	194
10.6 Results and conclusions	196
11 Conclusions	209
Bibliography	214

List of Figures

2.1	Critical Rayleigh number Ra against M^2 with $\varepsilon = 0.9, 1.2, 1.5$ for two free surfaces. Linear instability and nonlinear stability curves as in in caption.	32
2.2	Critical Rayleigh number Ra against M^2 with $\varepsilon = 0.9, 1.2, 1.5$ for two fixed surfaces. Linear instability and nonlinear stability curves as in caption.	33
2.3	Comparison of the absolute error of critical Rayleigh numbers for FD and HFD methods with various values of h .	34
3.1	Critical Rayleigh number R_a against M^2 , with $\xi = 2$ for $\eta = 0, 2, 4$. Linear instability and nonlinear stability curves as in caption.	54
3.2	Critical Rayleigh number R_a against M^2 , with $\xi = 6$ for $\eta = 0, 2, 4$. Linear instability and nonlinear stability curves as in caption.	54
3.3	Critical Rayleigh number R_a against ξ , with $M^2 = 1$ for $\eta = 0, 2, 4$. Linear instability and nonlinear stability curves as in caption.	55
3.4	Critical Rayleigh number R_a against ξ , with $M^2 = 6$ for $\eta = 0$. Linear instability curve together with nonlinear stability one.	55
3.5	Critical Rayleigh number R_a against ξ , with $M^2 = 6$ for $\eta = 2$. Linear instability curve together with nonlinear stability one.	56
3.6	Critical Rayleigh number R_a against ξ , with $M^2 = 6$ for $\eta = 4$. Linear instability curve together with nonlinear stability one.	56
4.1	Critical Rayleigh number R_a against R with $M^2 = 0$, $\eta = 0$ and $H_1 = H_2 = +1$, for fixed-fixed boundary conditions. (a) $\xi = 10^{-10}$. (b) $\xi = 1$. (c) $\xi = 2$. (d) $\xi = 3$. Linear instability and nonlinear stability curves as in caption.	77

- 4.2 Critical Rayleigh number R_a against R with $M^2 = 0$, $\eta = 0$ and $H_1 = H_2 = +1$, for free-free boundary conditions. (a) $\xi = 10^{-10}$. (b) $\xi = 1$. (c) $\xi = 2$. (d) $\xi = 3$. Linear instability and nonlinear stability curves as in caption. 78
- 4.3 Critical Rayleigh number R_a against R with $\xi = 1$, $\eta = 1$ and $H_1 = H_2 = +1$. (a) $M^2 = 30$. (b) $M^2 = 60$. (c) $M^2 = 90$. (d) $M^2 = 30$. (e) $M^2 = 60$. (f) $M^2 = 90$. Linear instability and nonlinear stability curves as in caption. a, b, c represent the results of fixed-fixed boundary conditions and d, e, f for free-free boundary conditions 79
- 4.4 Critical Rayleigh number R_a against M^2 with $\xi = 1$, $\eta = 1$ and $H_1 = H_2 = +1$, for fixed-fixed boundary conditions. (a) $R_c = 30$. (b) $R_c = 35$. (c) $R_c = 40$. (d) $R_c = 45$. Linear instability and nonlinear stability curves as in caption. 80
- 4.5 Critical Rayleigh number R_a against M^2 with $\xi = 1$, $\eta = 1$ and $H_1 = H_2 = +1$, for free-free boundary conditions. (a) $R_c = 25$. (b) $R_c = 30$. (c) $R_c = 35$. (d) $R_c = 40$. Linear instability and nonlinear stability curves as in caption. 81
- 4.6 Critical Rayleigh number R_a for $\eta = 2, 4, 6$ for fixed-fixed boundary conditions. (a) R_a against M^2 with $\xi = 2, R_c = 15, H_1 = H_2 = +1$. (b) R_a against M^2 with $\xi = 2, R_c = 15, H_1 = +1, H_2 = -1$. (c) R_a against R with $\xi = 2, M^2 = 50, H_1 = H_2 = +1$. (d) R_a against R with $\xi = 2, M^2 = 50, H_1 = +1, H_2 = -1$. Linear instability curve together with nonlinear stability one. 82
- 4.7 Critical Rayleigh number R_a for $\eta = 2, 4, 6$ for free-free boundary conditions. (a) R_a against M^2 with $\xi = 2, R_c = 15, H_1 = H_2 = +1$. (b) R_a against M^2 with $\xi = 2, R_c = 15, H_1 = +1, H_2 = -1$. (c) R_a against R with $\xi = 2, M^2 = 50, H_1 = H_2 = +1$. (d) R_a against R with $\xi = 2, M^2 = 50, H_1 = +1, H_2 = -1$. Linear instability curve together with nonlinear stability one. 83

- 4.8 Critical Rayleigh number R_a against ξ for $M^2 = 50$, $R_c = 15$, $H_1 = H_2 = +1$ and $\eta = 2, 4, 6$ for fixed-fixed boundary conditions. Linear instability curve together with nonlinear stability one. 84
- 5.1 Critical Reynolds number Re_L against N_0 . The values of M are as indicated in the figures. 102
- 5.2 Critical wavenumber a_L against N_0 . The values of M are as indicated in the figures. 103
- 5.3 Critical value of c_r , namely c_L , against N_0 . The values of M are as indicated in the figures. 104
- 5.4 Spectral of growth rate $c = cr + ici$ at critical values with $M = 1$ (a) $N_0 = 0$, (b) $N_0 = 0.002$. (c) $N_0 = 0.01$. (d) $N_0 = 0.02$ 105
- 5.5 Spectral of growth rate $c = cr + ici$ at critical values with $M = 5$ (a) $N_0 = 0$. (b) $N_0 = 0.001$. (c) $N_0 = 0.002$. (d) $N_0 = 0.005$ 106
- 5.6 Spectral of growth rate $c = cr + ici$ at critical values with $M = 10$ (a) $N_0 = 0$. (b) $N_0 = 0.001$. (c) $N_0 = 0.002$. (d) $N_0 = 0.0025$ 107
- 10.1 The contours map at $z = 0.5$. $\tau = 4$, $\delta = -1$, $\hat{\gamma} = 0.3$, $R^2 = 155000$, $Lx = 1.4$, $Ly = 1.4$, $\Delta t = 5 \times 10^{-5}$, $\Delta x = \Delta y = \Delta z = 0.02$. (a) u , (b) v , (c) w , (d) θ 206
- 10.2 The contours map at $z = 0.5$, $\tau = 4$, $\delta = -1$, $\hat{\gamma} = 0.3$, $R^2 = 155000$, $Lx = 1.4$, $Ly = 1.4$, $\Delta t = 5 \times 10^{-5}$, $\Delta x = \Delta y = \Delta z = 0.02$. (a) ξ_1 , (b) ξ_2 , (c) ξ_3 207
- 10.3 The required time to arrive at steady state versus R at $\delta = -1$ a. $\hat{\gamma} = 0.28$, b. $\hat{\gamma} = 0.29$, c. $\hat{\gamma} = 0.3$, d. $\hat{\gamma} = 0.31$ e. $\hat{\gamma} = 0.32$, f. $\hat{\gamma} = 0.34$. 208

List of Tables

2.1	Comparison of the linear and nonlinear numerical values of critical Rayleigh for two free surfaces $\varepsilon = 0.3$	35
2.2	Comparison of the linear and nonlinear numerical values of critical Rayleigh for two fixed surfaces $\varepsilon = 0.3$	36
2.3	Comparison of the linear and nonlinear numerical values of critical Rayleigh for two free surfaces $\varepsilon = 0.6$	37
2.4	Comparison of the linear and nonlinear numerical values of critical Rayleigh for two fixed surfaces $\varepsilon = 0.6$	38
2.5	Comparison of the absolute error of critical Rayleigh numbers for FD, HFD and Che-tau methods with various values of h and number of polynomials.	39
5.1	Critical Rayleigh numbers with varying M , $N_0 = 0$. Che-C-1 denotes collocation method-1, Che-C-2 denotes collocation method-2, and FEM signifies finite element method. The notation no. polys. denotes number of Chebyshev polynomials used, N is the order of the polynomial in the finite element, and E signifies the number of finite elements employed. UN denotes the method is numerically unstable.	98

5.2	Critical Rayleigh numbers with varying M , $N_0 = 0.001$. Che-C-1 denotes collocation method-1, Che-C-2 denotes collocation method-2, and FEM signifies finite element method. The notation no. polys. denotes number of Chebyshev polynomials used, N is the order of the poly- nomial in the finite element, and E signifies the number of finite elements employed. UN denotes the method is numerically unstable.	99
5.3	Critical Rayleigh numbers with varying M , $N_0 = 0.002$. Che-C-1 denotes collocation method-1, Che-C-2 denotes collocation method-2, and FEM signifies finite element method. The notation no. polys. denotes number of Chebyshev polynomials used, N is the order of the poly- nomial in the finite element, and E signifies the number of finite elements employed. UN denotes the method is numerically unstable.	100
5.4	Critical Rayleigh numbers with varying M , $N_0 = 0.003$. Che-C-1 denotes collocation method-1, Che-C-2 denotes collocation method-2, and FEM signifies finite element method. The notation no. polys. denotes number of Chebyshev polynomials used, N is the order of the poly- nomial in the finite element, and E signifies the number of finite elements employed. UN denotes the method is numerically unstable.	101
6.1	Comparison of the absolute error of wavenumbers for finite elements method.	134
6.2	Comparison of the absolute error of critical Rayleigh num- bers for finite elements method.	135
6.3	Comparison of the absolute error of critical Rayleigh num- bers and wavenumbers for Chebyshev tau method.	136

6.4	Comparison of the absolute error of critical Rayleigh numbers and wavenumbers for Chebyshev collocation method-1.	137
6.5	Comparison of the absolute error of critical Rayleigh numbers and wavenumbers for Chebyshev collocation method-2.	138
6.6	Comparison of the absolute error of critical Rayleigh numbers and wavenumbers for finite differences (FD) and high order finite differences (HFD) methods.	139
6.7	The critical Rayleigh and wavenumbers for symmetric-slip case for a selection of λ values. These numbers are evaluated by using finite element, Chebyshev tau, Chebyshev collocation-1, Chebyshev collocation-2, finite difference and fourth order finite difference.	139
6.8	The critical Rayleigh and wavenumbers for fixed-slip case for a selection of λ_U values. These numbers are evaluated by using finite element, Chebyshev tau, Chebyshev collocation-2, finite difference and fourth order finite difference.	140
10.1	Critical Rayleigh and wavenumbers Ra_L , Ra_E , a_L^2 , a_E^2 at $\delta = -1$	198
10.2	Summary of numerical results for $\delta = -1$, $\hat{\gamma} = 0.28$, $Ra_L = 114766.015$, $Ra_E = 59632.1$, $Lx = 1.5$ and $Ly = 1.5$.	199
10.3	Summary of numerical results for $\delta = -1$, $\hat{\gamma} = 0.29$, $Ra_L = 133165.864$, $Ra_E = 64280.001$, $Lx = 1.5$ and $Ly = 1.4$	200
10.4	Summary of numerical results for $\delta = -1$, $\hat{\gamma} = 0.3$, $Ra_L = 154816.654$, $Ra_E = 68802.297$, $Lx = 1.4$ and $Ly = 1.4$. . .	201
10.5	Summary of numerical results for $\delta = -1$, $\hat{\gamma} = 0.31$, $Ra_L = 180365.749$, $Ra_E = 73174.607$, $Lx = 1.6$ and $Ly = 1.2$	202

10.6	Summary of numerical results for $\delta = -1$, $\hat{\gamma} = 0.32$, $Ra_L = 210613.017$, $Ra_E = 77376.734$, $Lx = 1.7$ and $Ly = 1.1$	203
10.7	Summary of numerical results for $\delta = -1$, $\hat{\gamma} = 0.34$, $Ra_L = 289395.588$, $Ra_E = 85204.774$, $Lx = 1.4$ and $Ly = 1.1$	204
10.8	Summary of numerical results for $\delta = -1$, $\hat{\gamma} = 0.36$, $Ra_L = 402309.378$, $Ra_E = 92178.900$, $Lx = 1.2$ and $Ly = 1.1$	205

Chapter 1

Introduction

The concept of stability in the mathematical study of a physical system has had a long and fruitful history. Real situations show that for the practical use of many technical systems stability properties can be a decisive criterion. Some examples where stability properties are important could be: engineering structures (bridges, plates, shells structures under pressure loading or unloading by flowing fluids), vehicles moving at high speed, truck-trailer combinations, railway trains, hydrodynamics problems.

Over the past decades, engineers have approached many of their stability problems using a linearised stability analysis. In addition, if a linear stability analysis does not seem to be sufficient, numerical simulations are employed. Such a numerical simulation allows one to check whether a linearised analysis provides practically useful results or not. However, contrary to the widespread belief that linearised stability analysis together with numerical simulation are a general method of treating stability problems, it has been proved that this is not the case. There exists a large number of problems where a linearised analysis does not give much information about the behaviour of the nonlinear system at all and, hence, a numerical simulation would be very costly without yielding much insight into the qualitative

To clarify the concept of stability in the context of a system of partial differential equations, we begin with a simple illustrative example. Suppose u is a solution of the nonlinear diffusion equation with a linear source term and subject to boundary

and initial conditions as follows, (cf. Straughan [196])

$$\begin{aligned}\frac{\partial u}{\partial t} + u \frac{\partial u}{\partial x} &= \frac{\partial^2 u}{\partial x^2} + au, & x \in (0, 1), & t > 0, \\ u(0, t) &= u(1, t) = 0, \\ u(x, 0) &= u_0(x).\end{aligned}\tag{1.0.1}$$

Here t and x are time and spatial point respectively, and a is some real, positive constant. Clearly $u = 0$, is a solution to equation (1.0.1), which is referred to as a stationary solution as none of the variables have time (t in the context of the example) dependence. It is the stability of this solution which we investigate by introducing a perturbation (i.e. disturbance) to it. If all the perturbations decay to zero as time progresses then the solution is said to be stable. Conversely if just a single disturbance grows in amplitude with time, then the solution is unstable. Let w be a perturbation to the solution $\bar{u} \equiv 0$, i.e. $u = \bar{u} + w$, such that

$$\frac{\partial w}{\partial t} + w \frac{\partial w}{\partial x} = \frac{\partial^2 w}{\partial x^2} + aw.\tag{1.0.2}$$

To discuss linearised instability we retain only the terms in (1.0.2) which are linear in w . As this is now a linear equation we may introduce exponential time dependence in w such that $w(x, t) = e^{\sigma t} z(x)$, for some, potentially complex, growth rate σ . This yields the equation

$$\sigma z = \frac{d^2 z}{dx^2} + az.\tag{1.0.3}$$

By imposing the boundary conditions, ($z = 0, x = 0, 1$), it is possible to find

$$z(x) = C \sin(kx), \quad \text{where} \quad k = n\pi, \quad n = \pm 1, \pm 2, \dots$$

for any constant C . Substituting this into (1.0.3) yields

$$\sigma = -k^2 + a, \quad \text{where} \quad k^2 = n^2 \pi^2, \quad n = \pm 1, \pm 2, \dots$$

The growth rate σ can now be used to assess whether the zero solution is unstable. Therefore, $\sigma \in \mathbb{R}$ and $\sigma < 0 \iff a < k^2 \iff a < k_{\min}^2 = \pi^2$. So for $a < \pi^2$ we say there is linear stability. On the other hand if $a > \pi^2$ then $\sigma > 0$ for $n = 1$ and there is linear instability. Hence $a = \pi^2$ is the linear instability-stability boundary.

In general the locus which separates instability and stability is known as the neutral stability curve. The neutral stability curve represents a marginal state between stability and instability. This marginal state exhibits one of two kinds of motion, stationary $\sigma \in \mathbb{R}$ or oscillatory $\sigma \in \mathbb{C}$. If the motion is stationary, perturbations grow (or are damped) aperiodically whereas if it is oscillatory they grow (or are damped) periodically. If instability sets in as stationary motion the principle of exchange of stabilities is said to hold. On the other hand if instability sets in as oscillatory motion then the system is said to be subject to overstability. One of the aims of this thesis is to generate neutral stability curves and investigate their state.

It is important to note, however, that this linear analysis approach assumes that the perturbation is small and so neglects terms of quadratic and higher order. Hence, if a system of partial differential equations contains nonlinear elements, these terms must be discarded to proceed. It has been proved that linear analysis often provides little information on the behaviour of the nonlinear system (see Straughan [196]), so in such cases only instability can be deduced from the linear thresholds, as any potential growth in the nonlinear terms is not considered.

To obtain sufficient conditions for stability with respect to arbitrary disturbances the full nonlinear equations must be considered. In order to establish the nonlinear stability of the steady solution, it is sufficient to show that all perturbations vanish rapidly as $t \rightarrow \infty$. For this is sufficient to prove that any relevant perturbation vanishes exponentially. One suitable way to demonstrate this is the energy method. A fuller account of the energy method and its applications on a various problems may be found in Straughan [196]. Nonlinear energy analysis, which is conducted throughout the thesis, is of particular importance as energy methods are creating much interest, see e.g. Kaiser and Mulone [93], Delgado et al. [41], and also because they delimit the parameter region of possible subcritical instability (the region between the linear instability and nonlinear stability thresholds).

Multiplying (1.0.1)₁ by u and integrating over $(0, 1)$ yields

$$\frac{1}{2} \int_0^1 \frac{\partial u^2}{\partial t} dx = \int_0^1 u \frac{\partial u^2}{\partial x^2} dx + a \int_0^1 u^2 dx.$$

It is possible to use the boundary conditions to derive that

$$\int_0^1 u \frac{\partial u^2}{\partial x^2} dx = [u \frac{\partial u}{\partial x}]_0^1 - \int_0^1 (\frac{\partial u}{\partial x})^2 dx = -\|u_x\|^2,$$

and

$$\int_0^1 u^2 \frac{\partial u}{\partial x} dx = \frac{1}{3}[u^3]_0^1 = 0,$$

where $u_x = du/dx$ and $\|\cdot\|$ denotes the norm on $L^2(0, 1)$ (where $L^2(0, 1)$ is the space of square integrable functions on $(0, 1)$), i.e.,

$$\|u\|^2 = \int_0^1 u^2 dx.$$

Defining an energy $E(t)$ by

$$E(t) = \frac{1}{2}\|u\|^2,$$

we have the inequality

$$\begin{aligned} \frac{dE}{dt} &= -\|u_x\|^2 + a\|u\|^2 = -a\|u_x\|^2 \left(\frac{1}{a} - \frac{\|u\|^2}{\|u_x\|^2} \right) \\ &\leq -a\|u_x\|^2 \left(\frac{1}{a} - \max_{\mathcal{H}} \frac{\|u\|^2}{\|u_x\|^2} \right), \end{aligned} \quad (1.0.4)$$

where \mathcal{H} is the space of admissible functions,

$$\mathcal{H} = \{u \in C^2(0, 1) \cap C([0, 1]) : u = 0, \quad x = 0, 1\},$$

and $C^m(0, 1)$ is the space of m continuously differentiable functions on $(0, 1)$, $0 \leq m \leq \infty$. Suppose now that R_E is defined by

$$\frac{1}{R_E} = \max_{\mathcal{H}} \frac{\|u\|^2}{\|u_x\|^2}$$

then (1.0.4) becomes

$$\frac{dE}{dt} \leq -a\|u_x\|^2 \left(\frac{1}{a} - \frac{1}{R_E} \right)$$

Using the Poincaré's inequality (i.e. $\|u_x\|^2 \geq \pi^2\|u\|^2$, see Appendix A.1 for further details), and assuming $c = 1/a - 1/R_E$ it can be deduced that

$$\frac{dE}{dt} \leq -ac\pi^2\|u\|^2 = -2ac\pi^2 E,$$

or, equivalently

$$\frac{d}{dt}(e^{2ac\pi^2 t} E) \leq 0,$$

which leads to

$$E(t) \leq e^{-2ac\pi^2 t} E(0).$$

Recall that $E(t) = \frac{1}{2}\|u\|^2$; therefore if $c > 0$

$$\|u\|^2 \leq e^{-2ac\pi^2 t} \|u_0\|^2 \longrightarrow 0 \text{ as } t \longrightarrow \infty,$$

Hence it has been shown that provided $a < R_E$, $\|u\| \longrightarrow 0$ at least exponentially as $t \longrightarrow \infty$, and so the zero solution to (1.0.1) is stable.

To find R_E let $I_1 = \|u\|^2$, $I_2 = \|u_x\|^2$ and recall that

$$\frac{1}{R_E} = \max_{\mathcal{H}} \frac{I_1}{I_2}$$

Suppose u is a maximising solution and consider solutions of the form $u + \epsilon\eta$ where ϵ is some constant and η is an arbitrary $C^2(0, 1)$ function such that $\eta(0) = \eta(1) = 0$. Clearly the maximum occurs at $\epsilon = 0$ so,

$$\left[\frac{d}{d\epsilon} \left(\frac{I_1}{I_2} \right) \right]_{\epsilon=0} = \left[\frac{1}{I_2} \frac{dI_1}{d\epsilon} - \frac{I_1}{I_2^2} \frac{dI_2}{d\epsilon} \right]_{\epsilon=0} = \delta I_1 \left[\frac{1}{I_2} \right]_{\epsilon=0} - \frac{\delta I_2}{R_E} \left[\frac{1}{I_2} \right]_{\epsilon=0} = 0,$$

where δ stands for the derivative with respect to ϵ evaluated at $\epsilon = 0$. Hence it can be deduced that

$$R_E \delta I_1 - \delta I_2 = 0. \tag{1.0.5}$$

where

$$\begin{aligned} \delta I_1 &= \left[\frac{d}{d\epsilon} \int_0^1 (u + \epsilon\eta)^2 dx \right]_{\epsilon=0} = 2 \int_0^1 u\eta dx, \\ \delta I_2 &= \left[\frac{d}{d\epsilon} \int_0^1 (u_x + \epsilon\eta_x)^2 dx \right]_{\epsilon=0} = 2 \int_0^1 u_x \eta_x dx, \end{aligned}$$

Therefore (1.5) yields

$$\int_0^1 (\eta R_E u - u_x \eta_x) dx = 0.$$

which can be integrated by parts to give

$$\int_0^1 \eta (R_E u + u_{xx}) dx = 0.$$

Apart from the continuity and boundary conditions it must satisfy, η is arbitrary hence it can be concluded that,

$$\frac{d^2 u}{dx^2} + R_E u = 0, \quad u(0) = u(1) = 0. \tag{1.0.6}$$

This is known as the Euler-Lagrange equation for the example at hand. It yields an eigenvalue problem for R_E .

The general solution of (1.0.6) is given by

$$u = A \sin(\sqrt{R_E} x) + B \cos(\sqrt{R_E} x),$$

where A, B are constants. The boundary condition $u(0) = 0$ implies that $B = 0$, hence

$$u = A \sin(\sqrt{R_E} x).$$

For a non arbitrary solution suppose $A \neq 0$, then $u(1) = 0$ implies that

$$\sqrt{R_E} = n\pi, \quad \text{where} \quad n = \pm 1, \pm 2, \dots$$

$$\text{i.e.} \quad R_E = \pi^2, 4\pi^2, 9\pi^2, \dots$$

Recall that stability requires $a < R_E$. The minimum value of R_E is π^2 so as expected, $a < \pi^2$, is the stability bound of the zero solution to (1.0.1).

In general it is found that the energy method yields some critical threshold below which everything is stable and a linear instability analysis some bounds above which everything is unstable. In the example above the energy method and normal mode analysis yield the same critical instability-stability boundary. This is due to the fact that the differential equation under consideration (1.0.1)₁ is linear. If nonlinearities are introduced then in general it is found that a nonlinear stability analysis will yield a different critical threshold to one obtained by a linear analysis. A linear analysis assumes that any perturbation is small and so neglects terms of quadratic order and higher, hence discrepancy between linear instability and nonlinear stability results can occur. One of the aims of this thesis, and energy theory in general, is to try and optimise the two thresholds to be as close together as possible and so reduce the possibility of subcritical instabilities which may occur below the linear instability bound and above the nonlinear stability threshold. Many techniques have been used to do this and the theory applied to a range of important physical problems. There are many references in the literature and significant advancement has been made in the last 50 years. For reference we mention some recent papers and the citations therein namely, Basurto and Lombardo [18] and Lombardo et al. [111, 112]. Many

more references and a thorough discussion of the energy method and its subtleties can be found in Straughan [196].

Conventionally, stability calculations involve determining eigenvalues and eigenfunctions, with few of the associated eigenvalue problems solvable analytically. Two powerful existing techniques for finding eigenvalues and eigenfunctions numerically are the compound matrix (cf. Drazin and Reid [46] and Ng and Reid [132–134]) and the Chebyshev tau method (cf. Fox [53] and Orszag [140]). These numerical methods are used in the linear and nonlinear analyses to yield generalised eigenvalue problems of the form,

$$Ax = \sigma Bx$$

where A and B are matrices and x is some vector, all of which depend upon the system under consideration. The compound matrix method, which belongs to the family of shooting techniques, performs competently for stiff differential equations, with the specific purpose of reducing rounding error, as explored in Greenberg and Marletta [68], Straughan and Walker [201], see also the references therein. The Chebyshev tau technique is a spectral method. This method calculates as many eigenvalues as required as opposed to just one at a time as is done in the compound matrix method. Straughan and Walker [201] applied these two techniques to linear and nonlinear stability problems for convection in porous media. Their paper provides an excellent summary of the two aforementioned methods. They compare the techniques and highlight the advantages and disadvantages of both when investigating stability problems.

These established methods, although useful, produce a variety of computational and storage problems, as highlighted in each instance of their utilisation in the thesis. The main difficulties with spectral methods are how to apply the boundary conditions which involve derivatives of order higher than one and significant rounding errors in the computational results. One of the techniques which was used to avoid these difficulties was to choose the spaces of test and trial functions such that these spaces satisfy the boundary conditions [64, 65]. One of the aims of Chapter 2 is to apply the Chebyshev tau method to solve the problem of convection in a variable gravity field with magnetic field effect with free-free and fixed-fixed boundary

conditions. We also consider the finite difference and the high order finite difference to solve our problem which are very flexible numerical methods. We believe that the comparison between these methods is very important where we discuss this in some detail.

In Chapter 3, we study the problem of convective movement of a reacting solute in a viscous incompressible fluid occupying a plane layer and subjected to a vertical magnetic field. The thresholds for linear instability are found and compared to those derived by a global nonlinear energy stability analysis. The finite difference method has been applied to get the numerical results of this problem. We show the effect of magnetic field and the chemical reaction on the critical Rayleigh number.

Double-diffusive convection takes place in a wide variety of technological application (e.g. solar ponds, crystallization and solidification processes, nuclear engineering) and in other scientific branches (e.g. geology, oceanography, astrophysics). One of the fundamental problems of double-diffusive convection is the stability of a statically stable horizontal fluid layer, stratified by two buoyancy components with different molecular diffusivities (e.g. heat and salt) which make opposite contributions to the overall vertical density distribution. In such systems, motion can arise even when the basic state density distribution is gravitationally stable.

In any realistic double-diffusive system the temperature or concentration gradient can cause considerable spatial variations of the physical properties of the fluid which, in turn, vary the gradient itself. In Chapter 4, we study the problem of double-diffusive convection in a reacting fluid and magnetic field effect based internal heat source. A linear instability analysis and nonlinear stability analysis are performed and using the finite element method of p order we get the corresponding numerical results. The numerical results are presented for fixed-fixed and free-free boundary conditions.

The classical hydrodynamic problem of stability of Poiseuille flow in a channel is a major one in fluid dynamics, see e.g. Joseph [92], Chapter 3, Straughan [195], Chapter 8. As these texts point out there are major problems in trying to develop a meaningful nonlinear energy stability theory for such flows since the nonlinear energy stability threshold is inevitably far away from the linear instability one. Additionally,

the eigenvalue problems associated with this class of flows are numerically very difficult, see e.g. Dongarra et al. [43]. The focus of attention in Chapter 5 is on the problem of Poiseuille flow in a channel which is filled with a porous medium saturated with a linear viscous fluid. In particular, we analyse the effect of slip boundary conditions on the onset of instability. Due to numerous applications in micro-electro-mechanical-systems (MEMS) and other microfluidic devices, we consider such a study to be essential. We accurately analyse when instability will commence and determine the critical Reynolds number as a function of the slip coefficient.

In Chapter 6, we apply the second order finite difference method, the high order finite difference scheme, p order finite element method, the Chebyshev collocation method-1 and method-2 and Chebyshev tau technique to solve the eigenvalue systems of standard thermal convection with free-free, slip-slip, and fixed-slip boundary conditions. Rayleigh [163] showed that, in the case of free-free boundary conditions, we may obtain an analytical result for Rayleigh number $Ra_{crit} = 27\pi^4/4$ (see also Chandrasekhar [32] and Drazin and Reid [46]), thus, we select free-free boundary conditions to check the accuracy of numerical methods. However, slip-slip, and fixed-slip boundary conditions have been selected to check the flexibility of the numerical methods in dealing with these boundary conditions.

Within the context of fluid flow in porous media, or simply within the theory of fluid flow, there has been substantial recent interest in deriving stability estimates where changes in coefficients are allowed, or even the model (the equations themselves) changes. This type of stability has earned the name structural stability, and is different from continuous dependence on the initial data. Structural stability is the focus of attention in, for example, Ames and Payne [1–4], Franchi and Straughan [54–57], Lin and Payne [106–110], Payne and Song [144–146], Payne and Straughan [149–151], Payne et al. [143], and also occupies attention in the books of Bellomo and Preziosi [19], Ames and Straughan [5] and Straughan [197]. Structural stability questions are fundamental in that one wishes to know whether a small change in a coefficient in an equation, or in the boundary data, or in the equations themselves, will induce a dramatic change in the solution. Thus structural stability constitutes a class of stability problems every bit as important as continuous

dependence on the initial data.

In Chapters 7, 8 and 9 we deal with obtaining stability estimates for solutions to some convection problems where changes in coefficients are allowed, or even the equations themselves change. Such stability estimates are fundamental to analysing whether a small change in a coefficient or other data leads to a drastic change in the solution. Chapters 7 and 8 continue the investigation of continuous dependence properties of models which were introduced in Chapters 3 and 4 when these models include porous media and fluid, respectively. For porous media case, we concentrate on a Brinkman model. For both models, we establish the continuous dependence on changes in the chemical reaction K_1 coefficient, and on changes in the coefficient of the magnetic term σ . Chapter 9 is devoted to studying the influence of the magnetic and the gravity vector coefficients on the double diffusive convective flow in a porous medium using the Darcy model.

The purpose of Chapter 10 is to study the effect of a heat source on the solution to the equations for an incompressible heat conducting viscous fluid. When the difference between the linear and nonlinear thresholds is very large, the comparison between these thresholds is very interesting and useful. Thus we repeat the stability analysis of Straughan [194] to select new situations which have very big subcritical region. Then, we develop a three dimensional simulation for the problem. To do this, firstly, we transform the problem to velocity- vorticity formulation, then we use second order finite difference schemes. We use implicit and explicit schemes to enforce the free divergence equation. The size of the box is evaluated according to the normal modes representation. Moreover, we adopt the periodic boundary conditions for velocity, temperature, and concentration in the x, y dimensions.

Chapter 11 contains some concluding remarks on the results and implications of the thesis, with suggestions on the development of future work.

Chapter 2

Convection in a variable gravity field with magnetic field effect

2.1 Introduction

In this chapter, we wish to analyse a model of convective instability created by a top heavy layer of fluid containing a solute or pollutant. Applications include environmental (atmospheric) physics where a polluted atmosphere at the Earth's surface is helped by convection overturning the air and mixing. Other applications concern studies involving a salt concentration in a fluid. The topic of pollution/contaminant spread in a shallow atmosphere, in a shallow layer of water, or in soils, is one of much current research interest with application to many environmental/geophysical concerns of modern life, cf. Franchi and Straughan [58] and the references therein.

The fundamental concept behind Magnetohydrodynamics (MHD) is that magnetic fields can induce currents in a moving conductive fluid, which in turn creates forces on the fluid and also changes the magnetic field itself. The set of equations which describe MHD are a combination of the Navier-Stokes equations of fluid dynamics and Maxwell's equations of electromagnetism. The MHD applies to many conductive fluid and plasma flows encountered in nature and in industrial applications ([179], [52] and the references therein). For instance, MHD equations would be relevant for the atmosphere of the sun, the influence of the solar wind on the Earth's atmosphere, nuclear fusion, and for the simulation of plasma thrusters for

active flow control in aerodynamics.

It is likely to be important to consider variable gravity effects in the large scale convection of atmospheres, see Pradhan and Samal [155]. The addition of viscosity will provide a more realistic situation. It could be argued that one should further include compressibility, but we prefer to treat at this stage the incompressible model as the results will certainly be more transparent; the mathematical complexities introduced by compressibility even with a constant gravity field are highly nontrivial, cf. Spiegel [191] and Padula [141]. However, it is necessary to include non-Boussinesq (penetrative) effects to describe a convective atmosphere (Veronis [220]).

The analogous problem which consider the effect of the magnetic field on the onset of thermal instability in fluids has received considerable attention, cf., Galdi and Straughan [61], Galdi [60], Sunil et al. [205], Sunil et al. [207], Sunil and Mahajan [209], Sunil et al. [208], Dragomirescu and Georgescu [44,62], Straughan [193], Zebib [229], Zakaria [228], Chertovskih et al. [34], Lee and Chun [104], Ghasemi et al. [63], Ashouri et al. [7], Varshney and Baig [219], Landeau and Aubert [99] and Umavathi and Malashetty [218].

Convictional hydrodynamic stability theory is mainly concerned with the determination of critical values of Rayleigh number, demarcating a region of stability from that of instability. To do this, we apply a quasi-static approximation as in Galdi and Straughan [61]. This still allows a full analysis of the effect of the magnetic field but avoids mathematical complication associated with the complete set of equations for magneto hydrodynamic, cf., Rionero [169], Galdi [60], Rionero and Mulone [177], Chandrasekhar [32], Roberts [179], Landau et al. [100]. Nevertheless, the model we develop is still highly nonlinear and very non-trivial.

Orszag in [140], introduced the earlier numerical study to the Orr-Sommerfeld problem. He solved this problem by using a direct (tau) spectral method. The other important papers was introduced by Dongarra et al. [43] and Straughan and Walker [201]. In [43] they analyze the Orr-Sommerfeld equation supplied with homogeneous boundary conditions which contain derivative up to the first order. S-

traughan and Walker in [201] solved other hydrodynamic stability problems using Chebyshev tau and compound matrix methods. Hill and Straughan in [86] apply high accuracy Legendre spectral element method for solving second order as well as higher order (especially fourth order) differential eigenvalue problems. Gheorghiu and Pop in [65], built up a Chebyshev tau method in order to solve a hydrodynamic stability problem connected with the Marangoni-Plateau-Gibbs convection. The eigenvalue problem was a non-standard one, i.e., two out of the four boundary conditions attached to the OrrSommerfeld equation contained derivatives of order two and three. In [64] Gheorghiu and Dragomirescu used Weighted residuals Galerkin method, Weighted residuals Petrov-Galerkin method and the Chebyshev collocation method to solve the linear hydrodynamic stability problem of a convective flow in varying gravity field.

In this Chapter, the problem of convection in a variable gravity field with magnetic field effect is studied by using methods of linear instability theory and nonlinear energy theory. Three numerical methods have been applied to get the numerical results of our problem, namely Chebyshev tau, finite difference FD and High order finite difference HFD. The plan of the chapter is as follows. In the next section we develop the basic equations. Then, both linear instability and unconditional nonlinear stability results are derived in Section 2.3 and 2.4, respectively. The numerical techniques are described with details in Section 2.5. In the final section, we present the numerical results which have been computed using the Chebyshev tau, finite differences and high order finite differences.

The results in this chapter are also presented in the manuscript Harfash [72].

2.2 Governing Equations

We suppose the fluid is contained in the plane layer $\{z \in (0, d)\} \times \mathbb{R}^2$, and is incompressible, although a Boussinesq approximation is employed in the buoyancy term in the momentum equation. The momentum equation for a fluid containing a solute and with an imposed magnetic field is then

$$\rho(v_{i,t} + v_j v_{i,j}) = -p_{,i} + \mu \Delta v_i - \rho \alpha_c k_i g(z)(c - c_\infty) + \mathbf{j} \times \mathbf{B}, \quad (2.2.1)$$

where ρ, \mathbf{v}, p, c are the constant density, velocity field, pressure, and concentration of solute. Additionally, α_c is the salt expansion coefficient, μ is the dynamic viscosity, $g(z) = 1 + \varepsilon h(z)$ is gravity field, c_∞ is a reference concentration, $\mathbf{k} = (0, 0, 1)$, \mathbf{j} is the current, and \mathbf{B} is the magnetic induction field. Throughout, we use standard indicial notation and the Einstein summation convention so that e.g. $v_{i,t} = \partial v_i / \partial t$, and $p_{,i} = \partial p / \partial x_i$, $v_j v_{i,j} \equiv (\mathbf{v} \cdot \nabla) \mathbf{v}$, and Δ is the Laplacian. The balance of mass equation is

$$v_{i,i} = 0. \quad (2.2.2)$$

The equation governing the evaluation of the solute concentration is, cf., Straughan [196], p.239,

$$c_t + v_i c_{,i} = \hat{D} \Delta c. \quad (2.2.3)$$

Here $c(\mathbf{x}, t)$ is the solute concentration, \hat{D} is the the solute diffusion coefficient. To make the convective overturning instability problem tractable we employ the quasi-static MHD approximation of Galdi and Straughan [61]. This assume that the electrical field \mathbf{E} is always derivable from a potential, i.e. $\mathbf{E}_i = -\phi_{,i}$. The magnetic and electrical fields, \mathbf{E}, \mathbf{H} , satisfy Maxwell's equations, cf. Roberts [179], Fabrizio and Morro [52], so that

$$\text{curl } \mathbf{H} = \mathbf{j}, \quad \text{curl } \mathbf{E} = -\frac{\partial \mathbf{B}}{\partial t}, \quad \text{div } \mathbf{B} = 0, \quad \text{div } \mathbf{j} = 0 \quad (2.2.4)$$

where \mathbf{j} is the current and $\mathbf{B} = \hat{\mu} \mathbf{H}$ is the magnetic induction. Then, from (2.2.4)₂ it follows that $\partial B_i / \partial t = 0$ and so B_i is a function of the spatial variable x_j only. Galdi and Straughan [61] take $\mathbf{B} = B_0 \mathbf{k}$ where $\mathbf{k} = (0, 0, 1)$, the convection layer being $\mathbb{R}^2 \times \{z \in (0, d)\}$. The current is given by $\mathbf{j} = \sigma(-\mathbf{E} + \mathbf{v} \times \mathbf{B})$, where σ is the electrical conductivity and \mathbf{v} is the fluid velocity, and then (2.2.4)₄ shows that

$$\sigma(-\Delta \phi + \mathbf{B} \cdot \nabla \times \mathbf{v} - \mathbf{v} \cdot \nabla \times \mathbf{B}) = 0. \quad (2.2.5)$$

It is now assumed that $w_3 = 0$, where \mathbf{w} is the vorticity, $\mathbf{w} = \text{curl } \mathbf{v}$. Then since $\mathbf{B} = B_0 \mathbf{k}$, we have $\mathbf{B} \cdot \nabla \times \mathbf{v} \equiv 0$. From equation (2.2.4)₁ and the expression for \mathbf{j} ,

$$\text{curl } \mathbf{B} = \frac{1}{\eta} (-\nabla \phi + \mathbf{v} \times \mathbf{B}), \quad (2.2.6)$$

where $\eta(= 1/\hat{\mu}\sigma)$ is the resistivity. We let $\eta \rightarrow \infty$ (which is equivalent to letting the magnetic Prandtl number $P_m = \nu/\eta \rightarrow 0$) and then from (2.2.6) we see that $\text{curl } \mathbf{B} = 0$. Therefore, the term $\mathbf{v} \cdot \nabla \times \mathbf{B} = 0$ in (2.2.5) and that equation reduces to $\Delta\phi = 0$. Since we suppose ϕ decays sufficiently rapidly at infinite we must have $\phi \equiv 0$ and then we arrive to $\mathbf{j} = \sigma(\mathbf{v} \times \mathbf{B})$ with $\mathbf{B} = B_0 \mathbf{k}$. Thus we have

$$\mathbf{j} \times \mathbf{B} = \sigma(\mathbf{v} \times B_0 \mathbf{k}) \times B_0 \mathbf{k}. \quad (2.2.7)$$

Now, substitute (2.2.7) in (2.2.1), thus, we find the equations for our model are

$$v_{i,t} + v_j v_{i,j} = -\frac{1}{\rho} p_{,i} + \nu \Delta v_i - \alpha_c g(z)(c - c_\infty)k_i + \frac{B_0^2 \sigma_1}{\rho} [(\mathbf{v} \times \mathbf{k}) \times \mathbf{k}]_i. \quad (2.2.8)$$

$$v_{i,i} = 0, \quad (2.2.9)$$

$$c_{,t} + v_i c_{,i} = \hat{D} \Delta c. \quad (2.2.10)$$

The model now consists of the six partial differential equations (2.2.8), (2.2.9) and (2.2.10) and the following boundary conditions are assumed to hold,

$$v_i = 0, \quad \text{at } z = 0, d; \quad c = c_U, \quad \text{at } z = d; \quad c = c_L, \quad \text{at } z = 0, \quad (2.2.11)$$

where c_U, c_L are constant with $c_U > c_L$. Let us now consider the basic steady state solution $(\bar{v}_i, \bar{p}, \bar{c})$ of the system, where, as there is no fluid flow, $\bar{v}_i \equiv 0$. Utilizing the boundary conditions and assuming that the basic steady state solutions are functions of z only

$$\bar{c} = \beta z + c_L, \quad (2.2.12)$$

where $\beta = (c_U - c_L)/d$. The steady pressure \bar{p} may then be found from (2.2.8) which reduces to

$$-\frac{1}{\rho} \bar{p}_{,i} - g(z) \alpha_c (\bar{c} - c_\infty) k_i = 0. \quad (2.2.13)$$

To study the stability of (2.2.8), (2.2.9) and (2.2.10) we introduce a perturbation (u_i, π, ϕ) to the steady state solution $(\bar{v}_i, \bar{p}, \bar{c})$, where

$$v_i = \bar{v}_i + u_i, \quad p = \bar{p} + \pi, \quad c = \bar{c} + \phi.$$

Using (2.2.12), (2.2.13) the perturbed system is

$$u_{i,t} + u_j u_{i,j} = -\frac{1}{\rho} \pi_{,i} + \nu \Delta u_i - g(z) \alpha_c \phi k_i + \frac{B_0^2 \sigma_1}{\rho} [(\mathbf{u} \times \mathbf{k}) \times \mathbf{k}]_i,$$

$$\phi_t + u_i \phi_{,i} = -\beta w + \hat{D} \Delta \phi,$$

where u_i is solenoidal, i.e. $u_{i,i} = 0$.

We now introduce non-dimensionalised variable with scaling of

$$\mathbf{x} = \mathbf{x}^* d, \quad t = t^* \frac{d^2}{\nu}, \quad \mathbf{u} = U \mathbf{u}^*, \quad \phi = T^\# \phi^*, \quad \pi = P \pi^*, \quad U = \frac{\nu}{d}, \quad P = \frac{\rho \nu^2}{d^2},$$

$$T^\# = U \sqrt{\frac{\nu \beta}{\hat{D} \alpha_c}}, \quad R = \sqrt{\frac{\alpha_c d^4 \beta}{\hat{D} \nu}}, \quad M = B_0 d \sqrt{\frac{\sigma_1}{\rho \nu}}, \quad Ps = \frac{\nu}{\hat{D}}.$$

Here Ps is the Prandtl number and R is the Rayleigh number. With this scaling the non-dimensional form of becomes (we are usually omit all stars even through the non-dimensionless form is understood)

$$u_{i,t} + u_j u_{i,j} = -\pi_{,i} + \Delta u_i - k_i R g(z) \phi + M^2 [(u \times k) \times k]_i,$$

$$u_{i,i} = 0, \tag{2.2.14}$$

$$Ps (\phi_t + u_i \phi_{,i}) = -R w + \Delta \phi.$$

The spatial domain is now $\{(x, y) \in \mathbb{R}^2\} \times \{z \in (0, 1)\}$. The perturbed boundary conditions are given by

$$u_i = 0, \quad \phi = 0, \quad \text{on } z = 0, 1, \tag{2.2.15}$$

and u_i, ϕ, π satisfy a plane tiling form in the (x, y) -plane, Chandrasekhar [32], Straughan [196].

2.3 Linear instability

Before discussing nonlinear energy stability of a solution to (2.2.14) we briefly digress into linearized instability theory. The governing equations are obtained from (2.2.14) by omitting the nonlinear terms. The resulting linearized equations possess solutions of the type

$$u_i(\mathbf{x}, t) = u_i(\mathbf{x}) e^{\sigma t}, \quad \phi(\mathbf{x}, t) = \phi(\mathbf{x}) e^{\sigma t}, \quad \pi(\mathbf{x}, t) = \pi(\mathbf{x}) e^{\sigma t},$$

where σ is the growth rate and a complex constant. So that $u_i(\mathbf{x}), \phi(\mathbf{x}), \pi(\mathbf{x})$ satisfy

$$-\pi_{,i} + \Delta u_i - k_i R g(z) \phi + M^2 [(u \times k) \times k]_i = \sigma u_i, \quad (2.3.16)$$

$$-Rw + \Delta \phi = \sigma P s \phi. \quad (2.3.17)$$

Taking the double *curl* of (2.3.16), using the third component, (and the fact that u is solenoidal) we have

$$\Delta^2 w - R g(z) \Delta^* \phi - M^2 D^2 w = \sigma \Delta w, \quad (2.3.18)$$

where $\Delta^* = \partial^2/\partial x^2 + \partial^2/\partial y^2$, $D = d/dz$. We now introduce normal modes of the form $w = W(z)f(x, y)$, and $\phi = \Phi(z)f(x, y)$ where $f(x, y)$ is a plan-form which tiles the plane (x, y) with

$$\Delta^* f = -a^2 f. \quad (2.3.19)$$

The plan-forms represent the horizontal shape of the convection cells formed at the onset of instability. These cells form a regular horizontal pattern tiling the (x, y) plane, where the wavenumber a (see [32]) is a measure of the width of the convection cell. Using (2.3.19), and applying the normal mode representations to (2.3.17) and (2.3.18) we find

$$(D^2 - a^2)^2 W + a^2 R g(z) \Phi - M^2 D^2 W = \sigma (D^2 - a^2) W, \quad (2.3.20)$$

$$(D^2 - a^2) \Phi - RW = \sigma P s \Phi, \quad (2.3.21)$$

where the boundary conditions become

$$\Phi = W = DW = 0, \quad z = 0, 1, \quad \text{for fixed boundaries,} \quad (2.3.22)$$

and

$$\Phi = W = D^2 W = 0, \quad z = 0, 1, \quad \text{for free boundaries.} \quad (2.3.23)$$

System (2.3.20)-(2.3.21) and (2.3.22) or (2.3.23) is solved using the Chebyshev tau, finite difference (FD) and high order finite difference (HFD) methods. Detailed numerical techniques and results are reported in sections 5 and 6, respectively. We have solved system (2.3.20)-(2.3.21) and (2.3.22) or (2.3.23) for eigenvalues σ_j by using the *QZ* algorithm from Matlab routines. Once the eigenvalues σ_j are found

we use the secant method to locate where σ_j^R , $\sigma_j = \sigma_j^R + \sigma_j^I$ being the real and imaginary parts of eigenvalue σ_j . The value of R which makes $\sigma_1^R = 0$, σ_1^R being the largest eigenvalue, is the critical value of R for a^2 fixed. We then use golden section search to minimize over a^2 and find the critical value of R^2 for linear instability.

2.4 Nonlinear energy stability theory

Linearized instability theory certainly shows where instability occurs. It does not, however, a priori yield any information on stability, nor does it necessarily predict the smallest instability threshold. To clarify this concept, we begin with a simple illustrative example. Consider the following systems

$$\begin{aligned}\dot{x} &= \alpha y - x^3, \\ \dot{y} &= -\alpha x - y^3,\end{aligned}\tag{2.4.24}$$

$$\begin{aligned}\dot{x} &= \alpha y + x^3, \\ \dot{y} &= -\alpha x + y^3.\end{aligned}\tag{2.4.25}$$

Note that, for both system, the linearization is simply a harmonic oscillator with eigenvalues $\pm i\alpha$. The exact solution of nonlinear system (2.4.24) may be found by separating variables:

$$x^2(t) + y^2(t) \leq \frac{x_0^2(t) + y_0^2(t)}{1 + 2t(x_0^2(t) + y_0^2)}.$$

Therefore, $x^2(t) + y^2(t) \rightarrow 0$ as $t \rightarrow \infty$ and thus we deduce that the solution is asymptotically stable. However, the solution of nonlinear system (2.4.25) lead to

$$x^2(t) + y^2(t) \geq \frac{x_0^2(t) + y_0^2(t)}{1 - 2t(x_0^2(t) + y_0^2)},$$

and thus system (2.4.25) is unstable as $t \rightarrow \infty$.

It is possible that nonlinear terms will make a system become unstable long before the threshold predicted by linear theory is reached. Such instabilities are called subcritical. If we have a threshold below which we know all nonlinear perturbations decay, in a precise mathematical way, then this will yield a nonlinear stability boundary. When this threshold is relatively close to the analogous threshold of

linear theory we may have some confidence that the linear results are actually predicting the physical picture correctly. Nonlinear energy stability theory is discussed in detail in the book by [196].

We now develop an unconditional (i.e. for all initial data) nonlinear energy stability theory for system (2.2.14). The numerical results for the nonlinear stability threshold turn out to be relatively close to those for the linear instability boundary, and hence they are practically useful. The numerical results are discussed in detail in section 6.

Let V be a period cell for a disturbance to (2.2.14), and let $\|\cdot\|$ and (\cdot, \cdot) be the norm and inner product on $L^2(V)$. We derive energy identities by multiplying (2.2.14)₁ by u_i and integrating over V , and (2.2.14)₂ by ϕ and integrating over V , to find

$$\frac{1}{2} \frac{d}{dt} \|\mathbf{u}\|^2 = -\|\nabla \mathbf{u}\|^2 - R(g\phi, w) - M^2[\|\mathbf{u}\|^2 - \|w\|^2], \quad (2.4.26)$$

$$\frac{Ps}{2} \frac{d}{dt} \|\phi\|^2 = -R(\phi, w) - \|\nabla \phi\|^2. \quad (2.4.27)$$

Letting λ be positive parameter to be selected at our discretion, we multiply (2.4.27). Adding this equation to (2.4.26) yields

$$\frac{d}{dt} \left(\frac{1}{2} \|\mathbf{u}\|^2 + \frac{\lambda Ps}{2} \|\phi\|^2 \right) = -R((g + \lambda)\phi, w) - \lambda \|\nabla \phi\|^2 - \|\nabla \mathbf{u}\|^2 - M^2(\|u\|^2 + \|v\|^2),$$

where \mathbf{u} is explicitly written as $\mathbf{u} = (u, v, w)$. Define

$$E(t) = \frac{1}{2} \|\mathbf{u}\|^2 + \frac{\lambda Ps}{2} \|\phi\|^2,$$

$$\mathcal{D} = \lambda \|\nabla \phi\|^2 + \|\nabla \mathbf{u}\|^2 + M^2(\|u\|^2 + \|v\|^2),$$

$$\mathcal{I} = -R((g + \lambda)\phi, w).$$

Adopting these definitions for (2.4.28) we find

$$\frac{dE}{dt} = \mathcal{I} - \mathcal{D}.$$

Thus we have

$$\frac{dE}{dt} \leq -\mathcal{D} \left(1 - \frac{1}{R_E} \right),$$

where $1/R_E = \max_{\mathcal{H}}(\mathcal{I}/\mathcal{D})$ and \mathcal{H} is the space of admissible functions, namely

$$\mathcal{H} = \{u_i, \phi \in C^2(0, 1) : \phi = w = Dw = 0, z = 0, 1\}.$$

For fixed surface and the same space for free surface with $D^2w = 0$ instead of $Dw = 0$. If $R_E > 1$, then with λ_1 being the constant in Poincaré's inequality for \mathbf{u} and ϕ we have $\mathcal{D} \geq cE$, where $c = \min\{2\lambda_1, 2\lambda_1 P s^{-1}\}$. Hence

$$\frac{dE}{dt} \leq -cE \left(\frac{R_E - 1}{R_E} \right).$$

Thus, letting $\gamma = c(R_E - 1)/R_E$ and integrating we have

$$E(t) \leq E(0)e^{\gamma t}.$$

If $R_E > 1$, then as $t \rightarrow \infty$, $E(t)$ tends to zero at least exponentially, so we have shown the decay of ϕ and \mathbf{u} . Now that the global stability has been established we must study the maximisation problem $1/R_E = \max_{\mathcal{H}}(\mathcal{I}/\mathcal{D})$ together with the condition $R_E > 1$. To solve the maximisation problem we study the Euler Lagrange equations. The Euler Lagrange equations are found from

$$R_E \delta \mathcal{I} - \delta \mathcal{D} = 0. \quad (2.4.28)$$

let χ and ψ be arbitrary, fixed $C^2(0, 1)$ functions which satisfy the boundary conditions. We now consider neighbouring function $u_i = u_i + \epsilon \eta(x_j)$ and $\phi = \phi + \epsilon \psi(x_j)$, Hence

$$\begin{aligned} \delta \mathcal{D} &= \frac{d}{d\epsilon} [\|\nabla \mathbf{u} + \epsilon \nabla \eta\|^2 + M^2 \|\mathbf{u} + \epsilon \eta\|^2 - M^2 \|w + \epsilon \eta_3\|^2 + \lambda \|\nabla \phi + \epsilon \nabla \psi\|^2]_{\epsilon=0} \\ &= \langle -2\Delta u_i + 2M^2 u_i - 2M^2 k_i w, \eta_i \rangle + \langle -2\lambda \Delta \phi, \psi \rangle, \end{aligned}$$

and

$$\begin{aligned} \delta \mathcal{I} &= \frac{d}{d\epsilon} [-R \langle (g + \lambda) \phi + \epsilon \psi, w + \epsilon \eta_3 \rangle]_{\epsilon=0} \\ &= \langle -(g + \lambda) R k_i \phi, \eta_i \rangle + \langle -(g + \lambda) R w, \psi \rangle. \end{aligned}$$

Thus, the Euler Lagrange equations which arise from the variational problem $1/R_E = \max_{\mathcal{H}}(\mathcal{I}/\mathcal{D})$ can be written as:

$$-(g + \lambda) R k_i \phi - 2M^2 u_i + 2\Delta u_i + 2k_i M^2 w = -\pi_{,i}, \quad (2.4.29)$$

$$-(g + \lambda)Rw + 2\lambda\Delta\phi = 0, \quad (2.4.30)$$

where π is a Lagrange multiplier. To remove the Lagrange multiplier we take the third component of the double *curl* of (2.4.29), and introducing the normal mode representation and notation as presented in section 3, thus system (2.4.29)-(2.4.30) then becomes

$$(D^2 - a^2)^2W - M^2D^2W = -(g + \lambda)\frac{a^2}{2}R\Phi, \quad (2.4.31)$$

$$(D^2 - a^2)\Phi = \frac{(g + \lambda)}{2\lambda}RW, \quad (2.4.32)$$

where the boundary conditions become

$$\Phi = W = DW = 0, \quad z = 0, 1, \quad \text{for fixed boundaries,} \quad (2.4.33)$$

and

$$\Phi = W = D^2W = 0, \quad z = 0, 1, \quad \text{for free boundaries.} \quad (2.4.34)$$

We can now determine the critical Rayleigh Ra_E for fixed a^2 and λ . Then, we employ golden section search to minimize in a^2 and then maximize in λ to determine Ra_E for nonlinear energy stability,

$$Ra_E = \max_{\lambda} \min_{a^2} R^2(a^2, \lambda). \quad (2.4.35)$$

where for all $R^2 < Ra_E$ we have stability.

2.5 Numerical methods

In this section we will discuss the numerical treatment which we used in this chapter to solve systems (2.3.20)-(2.3.21) and (2.4.31)-(2.4.32). The numerical results are presented for the gravity field $g(z) = 1 - \varepsilon z$, while the numerical routine is applicable to a wide variety of other fields. Three methods are used to solve these systems, thus we will introduce these methods as follows, respectively:

2.5.1 Chebyshev tau

For free surface, we introduce new function $A = (D^2 - a^2)W$. Therefore, the systems (2.3.20)-(2.3.21) and (2.4.31)-(2.4.32) become as follows

$$(D^2 - a^2)W = A, \quad (2.5.36)$$

$$(D^2 - a^2)A - M^2 a^2 W - M^2 A + a^2 R g \Phi = \sigma A, \quad (2.5.37)$$

$$(D^2 - a^2)\Phi - R w = \sigma P_s \Phi, \quad (2.5.38)$$

$$(D^2 - a^2)W = A, \quad (2.5.39)$$

$$(D^2 - a^2)A - M^2 a^2 W - M^2 A = -(g + \lambda) \frac{a^2}{2} R \Phi, \quad (2.5.40)$$

$$(D^2 - a^2)\Phi = \frac{(g + \lambda)}{2\lambda} R W, \quad (2.5.41)$$

and the boundary conditions will be

$$\Phi = W = A = 0, \quad \text{at } z = 0, 1. \quad (2.5.42)$$

To employ the Chebyshev tau technique, system (2.5.53)-(2.5.55) and (2.5.63)-(2.5.65) are converted to the Chebyshev domain $(-1, 1)$, and then W, A and Φ are written as a finite series of Chebyshev polynomials

$$W = \sum_{k=0}^{N+2} W_k T_k(z), \quad A = \sum_{k=0}^{N+2} A_k T_k(z), \quad \Phi = \sum_{k=0}^{N+2} \Phi_k T_k(z).$$

The weighted inner product of each equation is taken with some T_k and the orthogonality of the Chebyshev polynomial is utilised to form the generalised eigenvalue problem

$$\begin{pmatrix} 4D^2 - a^2 I & -I & O \\ -M^2 a^2 I & 4D^2 - (M^2 + a^2) I & a^2 R F1 \\ -R I & O & 4D^2 - a^2 I \end{pmatrix} \mathbf{Q} = \sigma \begin{pmatrix} O & O & O \\ O & I & O \\ O & O & P_s I \end{pmatrix} \mathbf{Q},$$

for linear problem and for nonlinear is

$$\begin{pmatrix} 4D^2 - a^2 I & -I & O \\ -M^2 a^2 I & 4D^2 - (M^2 + a^2) I & O \\ O & O & 4D^2 - a^2 I \end{pmatrix} \mathbf{Q} = \frac{R}{2} \begin{pmatrix} O & O & O \\ O & O & -a^2 F2 \\ \frac{1}{\lambda} F2 & O & O \end{pmatrix} \mathbf{Q},$$

where $\mathbf{Q} = (\hat{W}, \hat{A}, \hat{\Phi})^T$, $\hat{W} = (W_0, \dots, W_{N+2})^T$, $\hat{A} = (A_0, \dots, A_{N+2})^T$, $\hat{\Phi} = (\Phi_0, \dots, \Phi_{N+2})^T$, D^2 is the Chebyshev representation of d^2/dz^2 and $F1 = (1 - \varepsilon/2)I - (\varepsilon/2)Z$, $F2 = (1 + \lambda - \varepsilon/2)I - (\varepsilon/2)Z$, I is the identity matrix and Z is the matrix representation of z , for more details see [43]. Using the boundary conditions and the fact that $T_n(\pm 1) = (\pm 1)^n$ we remove the last two rows of each $(N+2) \times (N+2)$ block

and replace these rows by the discrete form of the boundary conditions (2.5.42). Also, we can adopt another technique to apply the boundary conditions where we can find the values of $W_{N+1}, W_{N+2}, A_{N+1}, A_{N+2}, \Phi_{N+1}$ and Φ_{N+2} from the boundary conditions then we substitute these values in the system and thus we remove the last two rows. The new system have the order $(N + 1) \times (N + 1)$ instead of $(N + 3) \times (N + 3)$ (see [43,201] for more clarification).

The conversion of the degree of the derivative from fourth to second, in order avoid the use of the fourth derivatives which will generate a D^4 matrix. In D^4 matrix, if we use a large number of Chebyshev functions, an instability in the calculation of the eigenvalues will be generated [43].

Firstly, let $C = (D - a)W$, $A = (D + a)C$, thus $A = (D^2 - a^2)w$. Hence, the systems (2.3.20)-(2.3.21) and (2.4.31)-(2.4.32) can be written respectively,

$$\begin{aligned} (D - a)W &= C, \\ (D + a)C &= A, \\ (D^2 - a^2)A - m^2 a^2 W - M^2 A + a^2 R\Phi &= \sigma(D^2 - a^2)W, \\ (D^2 - a^2)\Phi - R w &= \sigma P s \Phi, \end{aligned} \tag{2.5.43}$$

$$\begin{aligned} (D - a)W &= C, \\ (D + a)C &= A, \\ (D^2 - a^2)A - m^2 a^2 W - M^2 A &= -(1 + \lambda) \frac{a^2}{2} R\Phi, \\ (D^2 - a^2)\Phi &= \frac{(1 + \lambda)}{2\lambda} R W, \end{aligned} \tag{2.5.44}$$

with boundary conditions $C = W = \Phi = 0$ and $DC = A$ on $z = 0, 1$. The system (2.5.43) and (2.5.44) is transformed onto the Chebyshev domain $(-1, 1)$ and the solutions W, C, A and Φ are expanded as Chebyshev polynomials so that

$$W = \sum_{k=0}^{N+2} W_k T_k(z), \quad C = \sum_{k=0}^{N+2} C_k T_k(z), \quad A = \sum_{k=0}^{N+2} A_k T_k(z), \quad \Phi = \sum_{k=0}^{N+2} \Phi_k T_k(z).$$

Taking the weighted inner product with T_i , and defining D and D^2 to be the

Chebyshev representation of d/dz and d^2/dz^2 , the eigenvalue problem now becomes

$$\begin{aligned} & \begin{pmatrix} 2D - aI & -I & O & O \\ O & 2D + aI & -I & O \\ -M^2a^2 & O & 4D^2 - (M^2 + a^2)I & a^2RF1 \\ -RI & O & O & 4D^2 - a^2I \end{pmatrix} \mathbf{Q} \\ &= R \begin{pmatrix} O & O & O & O \\ O & O & O & O \\ 4D^2 - a^2I & O & O & O \\ O & O & O & P_s I \end{pmatrix} \mathbf{Q}, \end{aligned}$$

for linear problem and for nonlinear is

$$\begin{aligned} & \begin{pmatrix} 2D - aI & -I & O & O \\ O & 2D + aI & -I & O \\ -M^2a^2 & O & 4D^2 - (M^2 + a^2)I & O \\ O & O & O & 4D^2 - a^2I \end{pmatrix} \mathbf{Q} \\ &= \frac{R}{2} \begin{pmatrix} O & O & O & O \\ O & O & O & O \\ O & O & O & -a^2F2 \\ \frac{1}{\lambda}F2 & O & O & O \end{pmatrix} \mathbf{Q}, \end{aligned}$$

where $\mathbf{Q} = (\hat{W}, \hat{C}, \hat{A}, \hat{\Phi})^T$, $\hat{W} = (W_0, \dots, W_{N+2})^T$, $\hat{C} = (C_0, \dots, C_{N+2})^T$, $\hat{A} = (A_0, \dots, A_{N+2})^T$, $\hat{\Phi} = (\Phi_0, \dots, \Phi_{N+2})^T$, D^2 is the Chebyshev representation of d^2/dz^2 and $F1 = (1 - \varepsilon/2)I - (\varepsilon/2)Z$, $F2 = (1 + \lambda - \varepsilon/2)I - (\varepsilon/2)Z$, I is the identity matrix and Z is the matrix representation of z

Using the boundary conditions and the fact that $T_n(\pm 1) = (\pm 1)^n$ and $T'_n(\pm 1) = (\pm 1)^{n-1}n^2$ we can find $W_{N+1}, W_{N+2}, C_{N+1}, C_{N+2}, \Phi_{N+1}$ and Φ_{N+2} , then we can remove the $N + 1$ and $N + 2$ rows and columns. To find A_{N+1}, A_{N+2} we will use the condition $2dC/dz = A$. This condition allow to us to evaluate A_{N+1} and A_{N+2} because C_{N+1} and C_{N+2} known as functions of $\{C_i\}_{i=1}^N$, thus

$$A_{N+1} = - \sum_{\substack{i=0 \\ i \text{ even}}}^{N-1} A_i + \sum_{\substack{i=1 \\ i \text{ odd}}}^N (i^2 - (N+2)^2)C_i,$$

$$A_{N+2} = - \sum_{\substack{i=1 \\ i \text{ odd}}}^N A_i + \sum_{\substack{i=0 \\ i \text{ even}}}^{N-1} (i^2 - (N+1)^2)C_i.$$

Then we use QZ algorithm to solve these systems. Also, a golden section search method and secant method was employed to find the critical Rayleigh numbers.

2.5.2 Finite Difference Scheme

Standard Finite Difference

The standard second and fourth order central difference operators at grid point i can be written as:

$$\begin{aligned} \delta^2 u_i &= \frac{u_{i+1} - 2u_i + u_{i-1}}{h^2}, \\ \delta^4 u_i &= \frac{u_{i+2} - 4u_{i+1} + 6u_i - 4u_{i-1} + u_{i-2}}{h^4}. \end{aligned} \quad (2.5.45)$$

The second and the fourth order derivatives for the function u at grid point i can be approximated by a second order accuracy as

$$\begin{aligned} \left. \frac{d^2 u}{dz^2} \right|_i &= \delta^2 u_i - \frac{h^2}{12} \frac{d^4 u}{dz^4} + O(h^4), \\ \left. \frac{d^4 u}{dz^4} \right|_i &= \delta^4 u_i - \frac{h^2}{6} \frac{d^6 u}{dz^6} + O(h^4). \end{aligned} \quad (2.5.46)$$

By using these finite difference approximations, (2.3.22) and (2.4.31)-(2.4.32) can be discretized at a given grid point i respectively as,

$$\delta_z^4 W_i - (M^2 + 2a^2)\delta_z^2 W_i + a^4 W_i + a^2 R g_i \Phi_i = \sigma(\delta^2 - a^2)W_i, \quad (2.5.47)$$

$$\delta_z^2 \Phi_i - a^2 \Phi_i - R W_i = \sigma P s \Phi_i, \quad (2.5.48)$$

and

$$\delta_z^4 W_i - (M^2 + 2a^2)\delta_z^2 W_i + a^4 W_i = -\frac{a^2}{2}(g_i + \lambda)R\Phi_i, \quad (2.5.49)$$

$$\delta_z^2 \Phi_i - a^2 \Phi_i = \frac{(g_i + \lambda)}{2\lambda} R W_i. \quad (2.5.50)$$

The boundary conditions $D_z W = 0$ at $z = 0, 1$ are approximated using finite difference technique as $W_{-1} = W_1$ and $W_{N+1} = W_{N-1}$. In the same scheme the boundary condition $D_z^2 W = 0$ at $z = 0, 1$ has the approximation $W_{-1} = -W_1$

and $W_{N+1} = -W_{N-1}$. In this manner, equations (2.5.47), (2.5.48) and the fixed boundary conditions lead to the finite difference equations

$$\begin{aligned} \frac{W_{i+2}}{h^4} - \left(\frac{4}{h^4} + \frac{2a^2 + M^2}{h^2}\right)W_{i+1} + \left(\frac{6}{h^4} + \frac{2(2a^2 + M^2)}{h^2} + a^4\right)W_i - \left(\frac{4}{h^4} + \frac{2a^2 + M^2}{h^2}\right)W_{i-1} \\ + \frac{W_{i-2}}{h^4} + Ra^2 g_i \Phi_i = \sigma \left[\frac{W_{i+1}}{h^2} - \left(\frac{2}{h^2} + a^2\right)W_i + \frac{W_{i-1}}{h^2} \right], \end{aligned} \quad (2.5.51)$$

$$i = 2, \dots, N - 2,$$

$$\begin{aligned} \frac{\Phi_{i+1}}{h^2} - \left(\frac{2}{h^2} + a^2\right)\Phi_i + \frac{\Phi_{i-1}}{h^2} - R W_i = \sigma P s \Phi_i, \end{aligned} \quad (2.5.52)$$

$$i = 1, \dots, N - 1,$$

$$\begin{aligned} \frac{W_3}{h^4} - \left(\frac{4}{h^4} + \frac{2a^2 + M^2}{h^2}\right)W_2 + \left(\frac{7}{h^4} + \frac{2(2a^2 + M^2)}{h^2} + a^4\right)W_1 + Ra^2 g_1 \Phi_1 \\ = \sigma \left[\frac{W_2}{h^2} - \left(\frac{2}{h^2} + a^2\right)W_1 \right], \end{aligned} \quad (2.5.53)$$

which is the equation obtained from (2.5.47) with $i = 1$, and

$$\begin{aligned} \left(\frac{7}{h^4} + \frac{2(2a^2 + M^2)}{h^2} + a^4\right)W_{N-1} - \left(\frac{4}{h^4} + \frac{2a^2 + M^2}{h^2}\right)W_{N-2} + \frac{W_{N-3}}{h^4} + Ra^2 g_{N-1} \Phi_{N-1} \\ = \sigma \left[-\left(\frac{2}{h^2} + a^2\right)W_{N-1} + \frac{W_{N-2}}{h^2} \right], \end{aligned} \quad (2.5.54)$$

which arises from (2.5.47) with $i = N - 1$.

For free surface, the same equations still work and there two differences, where the third term in (2.5.53) and the first term in (2.5.54) are equal to $(5/h^4 + 2(2a^2 + M^2)/h^2 + a^4)W_1$. Similarly, equations (2.5.49), (2.5.50) and the fixed boundary conditions produce to the following finite difference equations

$$\begin{aligned} \frac{W_{i+2}}{h^4} - \left(\frac{4}{h^4} + \frac{2a^2 + M^2}{h^2}\right)W_{i+1} + \left(\frac{6}{h^4} + \frac{2(2a^2 + M^2)}{h^2} + a^4\right)W_i - \left(\frac{4}{h^4} + \frac{2a^2 + M^2}{h^2}\right)W_{i-1} \\ + \frac{W_{i-2}}{h^4} = -\frac{Ra^2}{2} (g_i + \lambda) \Phi_i, \end{aligned} \quad (2.5.55)$$

$$i = 2, \dots, N - 2,$$

$$\begin{aligned} \frac{\Phi_{i+1}}{h^2} - \left(\frac{2}{h^2} + a^2\right)\Phi_i + \frac{\Phi_{i-1}}{h^2} = \frac{R}{2\lambda} (g_i + \lambda) W_i, \end{aligned} \quad (2.5.56)$$

$$i = 1, \dots, N - 1,$$

$$\frac{W_3}{h^4} - \left(\frac{4}{h^4} + \frac{2a^2 + M^2}{h^2}\right)W_2 + \left(\frac{7}{h^4} + \frac{2(2a^2 + M^2)}{h^2} + a^4\right)W_1 = -\frac{Ra^2}{2} (g_1 + \lambda) \Phi_1, \quad (2.5.57)$$

which is the equation obtained from (2.5.49) with $i = 1$, and

$$\begin{aligned} & \left(\frac{7}{h^4} + \frac{2(2a^2 + M^2)}{h^2} + a^4\right)W_{N-1} - \left(\frac{4}{h^4} + \frac{2a^2 + M^2}{h^2}\right)W_{N-2} + \frac{W_{N-3}}{h^4} \\ & = -\frac{Ra^2}{2}(g_{N-1} + \lambda)\Phi_{N-1}, \end{aligned} \quad (2.5.58)$$

which arises from (2.5.49) with $i = N - 1$.

Equation (2.5.55)-(2.5.58) still the same with free surface with two differences in the terms, where the third term in (2.5.57) and and the first term in (2.5.58) are equal to $(5/h^4 + 2(2a^2 + M^2)/h^2 + a^4)W_1$.

High Order Finite Difference

The main idea of the high order finite difference scheme is to find the values of truncation errors from the original differential equation and substitute these values in the finite difference formula. In this scheme we can reduce the order of truncation errors. In our system we can easily find the value of D^6W and $D^4\Phi$ as follows

$$D^6W = (2a^2 - M^2 + \sigma)D^4W - (a^4 + \sigma a^2)D^2W - a^2R(gD^2\Phi + g'D\Phi + g''\Phi), \quad (2.5.59)$$

$$D^4\Phi = (a^2 + \sigma Ps)D^2\Phi + RD^2W, \quad (2.5.60)$$

where the first derivative $D\Phi$ can be approximate at grid point i as follows. Let

$$\delta u_i = \frac{u_{i+1} - u_{i-1}}{2h}. \quad (2.5.61)$$

Then the approximate value of the first derivative can written as

$$\left.\frac{du}{dz}\right|_i = \delta u_i - \frac{h^2}{6} \frac{d^3u}{dz^3} + O(h^4), \quad (2.5.62)$$

If we substitute the values of D^6W and $D^4\Phi$ in (2.5.46) for W and Φ , and then approximate D^2W , D^4W and $D^2\Phi$ by using standard second order finite difference we have the following fourth order finite difference formula

$$\left.\frac{d^2W}{dz^2}\right|_i = \delta^2 W_i - \frac{h^2}{12} \delta_z^4 (W_i + O(h^2)) + O(h^4), \quad (2.5.63)$$

$$\left.\frac{d^2\Phi}{dz^2}\right|_i = \delta^2 \Phi_i - \frac{h^2}{12} \{ (a^2 + \sigma Ps)(\delta^2 \Phi_i + O(h^2)) + R(\delta^2 W_i + O(h^2)) \} + O(h^4), \quad (2.5.64)$$

$$\begin{aligned} \left. \frac{d^4 W}{dz^4} \right|_i &= \delta^4 W_i - \frac{h^2}{6} \{ (2a^2 - M^2 + \sigma)(\delta^4 W_i + O(h^2)) - (a^4 + \sigma a^2)(\delta^2 W_i + O(h^2)) \\ &\quad - a^2 R(g_i(\delta^2 \Phi_i + O(h^2)) + g'_i(\delta \Phi_i + O(h^2)) + g''_i \Phi_i) \} + O(h^4). \end{aligned} \quad (2.5.65)$$

It is clear that the overall truncation error will be of $O(h^4)$. Using (2.5.63)-(2.5.65) finite difference approximations, (2.3.20)-(2.3.21) can be approximated at a grid point i respectively as,

$$\begin{aligned} r_2 \delta^4 W_i + r_1 \delta^2 W_i + a^4 W_i + a^2 R g_i \Phi_i + a^2 R \frac{h^2}{6} (g_i \delta^2 \Phi_i + 2g'_i \delta \Phi_i + g''_i \Phi_i) \\ = \sigma \left[\frac{h^2}{12} \delta^4 W_i + r_4 \delta^2 W_i - a^2 W_i \right], \end{aligned} \quad (2.5.66)$$

$$-R \left(1 + \frac{\Delta z^2}{12} \delta^2 \right) W_i + r_3 \delta_z^2 \Phi_i - a^2 \Phi_i = \sigma P_s \left(1 + \frac{\Delta z^2}{12} \delta^2 \right) \Phi_i, \quad (2.5.67)$$

where $r_1 = (h^2/6) a^4 - M^2 - 2a^2$, $r_2 = 1 - (h^2/12) (M^2 + 2a^2)$, $r_3 = 1 - (h^2/12) a^2$ and $r_4 = 1 - (h^2/6) a^2$. The boundary conditions under high order finite difference approximated still the same standard scheme for fixed and free surfaces. Thus, for fixed boundary condition, (2.5.66) and (2.5.67) produce the following high order finite difference equations

$$\begin{aligned} \frac{r_2}{h^4} W_{i+2} + \left(-\frac{4r_2}{h^4} + \frac{r_1}{h^2} \right) W_{i+1} + \left(\frac{6r_2}{h^4} - \frac{2r_1}{h^2} + a^4 \right) W_i + \left(-\frac{4r_2}{h^4} + \frac{r_1}{h^2} \right) W_{i-1} + \frac{r_2}{h^4} W_{i-2} \\ + R a^2 \left[\left(\frac{1}{6} - \frac{h}{6} g'_i \right) \Phi_{i-1} + \left(g_i + \frac{h^2}{6} g''_i - \frac{1}{3} \right) \Phi_i + \left(\frac{1}{6} + \frac{h}{6} g'_i \right) \Phi_{i+1} \right] \\ = \sigma \left[\frac{W_{i-2}}{12h^2} + \left(\frac{r_4}{h^2} - \frac{4}{12h^2} \right) W_{i-1} + \left(\frac{1}{2h^2} - \frac{2r_4}{h^2} - a^2 \right) W_i + \left(\frac{r_4}{h^2} - \frac{4}{12h^2} \right) W_{i+1} + \frac{W_{i+2}}{12h^2} \right], \end{aligned} \quad (2.5.68)$$

$$i = 2, \dots, N-2,$$

$$\begin{aligned} R \left[\frac{-1}{12} W_{i-1} - \frac{5}{6} W_i - \frac{1}{12} W_{i+1} \right] + r_3 \frac{\Phi_{i-1}}{h^2} - \left(\frac{2r_3}{h^2} + a^2 \right) \Phi_i + r_3 \frac{\Phi_{i+1}}{h^2} \\ = \sigma P_s \left[\frac{1}{12} \Phi_{i-1} + \frac{5}{6} \Phi_i + \frac{1}{12} \Phi_{i+1} \right], \end{aligned} \quad (2.5.69)$$

$$i = 1, \dots, N-1,$$

$$\begin{aligned} \frac{r_2}{h^4} W_3 + \left(-\frac{4r_2}{h^4} + \frac{r_1}{h^2} \right) W_2 + \left(\frac{7r_2}{h^4} - \frac{2r_1}{h^2} + a^4 \right) W_1 + R a^2 \left[\left(g_1 + \frac{h^2}{6} g''_1 - \frac{1}{3} \right) \Phi_1 + \left(\frac{1}{6} + \frac{h}{6} g'_1 \right) \Phi_2 \right] \\ = \sigma \left[\left(\frac{7}{12h^2} - \frac{2r_4}{h^2} - a^2 \right) W_1 + \left(\frac{r_4}{h^2} - \frac{4}{12h^2} \right) W_2 + \frac{W_3}{12h^2} \right], \end{aligned} \quad (2.5.70)$$

which is the equation obtained from (2.5.66) with $i = 1$, and

$$\left(\frac{7r_2}{h^4} - \frac{2r_1}{h^2} + a^4 \right) W_{N-1} + \left(-\frac{4r_2}{h^4} + \frac{r_1}{h^2} \right) W_{N-2} + \frac{r_2}{h^4} W_{N-3}$$

$$\begin{aligned}
& +Ra^2 \left[\left(\frac{1}{6} - \frac{h}{6} g'_{N-1} \right) \Phi_{N-2} + \left(g_{N-1} + \frac{h^2}{6} g''_{N-1} - \frac{1}{3} \right) \Phi_{N-1} \right] \\
= \sigma & \left[\frac{W_{N-3}}{12h^2} + \left(\frac{r_4}{h^2} - \frac{4}{12h^2} \right) W_{N-2} + \left(\frac{7}{12h^2} - \frac{2r_4}{h^2} - a^2 \right) W_{N-1} \right], \tag{2.5.71}
\end{aligned}$$

which arises from (2.5.66) with $i = N - 1$.

For free surface, (2.5.68) and (2.5.69) still the same, while (2.5.70) and (2.5.71) should be replaced by the following equations

$$\begin{aligned}
\frac{r_2}{h^4} W_3 + \left(-\frac{4r_2}{h^4} + \frac{r_1}{h^2} \right) W_2 + \left(\frac{5r_2}{h^4} - \frac{2r_1}{h^2} + a^4 \right) W_1 + Ra^2 \left[\left(g_1 + \frac{h^2}{6} g''_1 - \frac{1}{3} \right) \Phi_1 + \left(\frac{1}{6} + \frac{h}{6} g'_1 \right) \Phi_2 \right] \\
= \sigma \left[\left(\frac{5}{12h^2} - \frac{2r_4}{h^2} - a^2 \right) W_1 + \left(\frac{r_4}{h^2} - \frac{4}{12h^2} \right) W_2 + \frac{W_3}{12h^2} \right], \tag{2.5.72}
\end{aligned}$$

$$\begin{aligned}
& \left(\frac{5r_2}{h^4} - \frac{2r_1}{h^2} + a^4 \right) W_{N-1} + \left(-\frac{4r_2}{h^4} + \frac{r_1}{h^2} \right) W_{N-2} + \frac{r_2}{h^4} W_{N-3} \\
& + Ra^2 \left[\left(\frac{1}{6} - \frac{h}{6} g'_{N-1} \right) \Phi_{N-2} + \left(g_{N-1} + \frac{h^2}{6} g''_{N-1} - \frac{1}{3} \right) \Phi_{N-1} \right] \\
= \sigma & \left[\frac{W_{N-3}}{12h^2} + \left(\frac{r_4}{h^2} - \frac{4}{12h^2} \right) W_{N-2} + \left(\frac{5}{12h^2} - \frac{2r_4}{h^2} - a^2 \right) W_{N-1} \right]. \tag{2.5.73}
\end{aligned}$$

Generally, the finite difference and high order finite difference schemes produce a generalized matrix eigenvalue problem of form

$$A \mathbf{Q} = \sigma B \mathbf{Q}, \tag{2.5.74}$$

for the linear case and for the nonlinear case it takes the form

$$A \mathbf{Q} = R B \mathbf{Q}, \tag{2.5.75}$$

where \mathbf{Q} is the eigenfunction vector, the Matrices A and B have different values according to each case and R, σ represent the eigenvalues of our problem.

2.6 Results and conclusions

In this section we present the numerical results for the linear instability and the nonlinear energy theory. Figures [2.1, 2.2] and Tables [2.1, 2.2, 2.3, 2.4] give the critical Rayleigh number Ra against M^2 for different values of ε utilising the three numerical methods: FD, HFD and Chebyshev tau. For the FD and HFD techniques

convergence to 4 decimal places is achieved with $h = 0.005$ and $h = 0.01$, respectively. For the Chebyshev tau method, convergence to 8 decimal places is achieved with 20 Chebyshev polynomials. As the results are not distinguishable visually, Figures [2.1, 2.2] show the results from the Chebshev method only.

To investigate the possibility of a very widely varying gravity field (one which even changes sign) we choose ε to vary from 0 to 1.5 . Such fields are of interest in laboratory experiments in areas of crystal growth and other applications, although a plane layer would not be the geometry studied. Nevertheless, our results may help us to understand such situations.

Tables [2.1, 2.2, 2.3, 2.4] give the critical Rayleigh numbers for linear instability and nonlinear energy stability for $\varepsilon = 0, 0.3, 0.6$ and $0 \leq M^2 \leq 100$. In Figures [2.1, 2.2] we present the critical Rayleigh numbers for linear instability and nonlinear energy stability for $\varepsilon = 0.9, 1.2, 1.5$ and $0 \leq M^2 \leq 100$. When M^2 is small, it should be observed that the nonlinear Ra values are very close to the linear ones. Thus, the linear theory predicts the onset of convection accurately. However, the difference between the critical Rayleigh numbers for linear instability and nonlinear energy stability increases with increasing M^2 values, although, even for $M^2 = 100$, the two thresholds are comparable. Figures [2.1, 2.2] demonstrate that Ra increases with increasing M^2 which shows the stabilizing effect of the magnetic field. In addition, it should be observed that the effect of ε on the linear and nonlinear stability pictures has a similar behaviour to the effect of M^2 .

It is very important to make a comparison between the accuracy of the three numerical methods, with the crucial measurement here being the exact solution. As a tractable exact solution is not achievable for our problem we turn our attention to the solution of linear system for two free boundaries i.e. we will solve analytically system (2.3.20)-(2.3.21) with respect to the boundary conditions (2.3.23) with $\varepsilon = 0$ i.e. $g(z) = 1$. It is relatively straightforward to show that the solution which yields the smallest Rayleigh number has a z -dependence like $\sin \pi z$. Ra then satisfies

$$Ra = \frac{(\pi^2 + a^2)}{a^2} [(\pi^2 + a^2)^2 + \pi^2 M^2]. \quad (2.6.76)$$

The critical wavenumber is found by minimizing Ra in a^2 subject to

$$2a^6 + 3\pi^2 a^4 - (\pi^6 + \pi^4 M^2) = 0. \quad (2.6.77)$$

The critical value a_{crit}^2 can be evaluated by using the Newton-Raphson iteration method as follows:

$$a_{i+1}^2 = a_i^2 - \frac{(2a_i^6 + 3\pi^2 a_i^4 - (\pi^6 + \pi^4 M^2))}{(6a_i^4 + 6\pi^2 a_i^2)}. \quad (2.6.78)$$

Thus the critical Rayleigh number is found by utilising a_{crit}^2 from (2.6.78) in (2.6.76). Of course equations (2.6.78) and (2.6.76) provide semi exact results due to the use of the Newton-Raphson method to evaluate a_{crit}^2 , but these results have a very small error and they can give a very good comparison between our numerical results and the exact results. In the case of $g(z) = 1$, the system is symmetric and hence the critical Rayleigh number for linear theory is equal to the nonlinear one, thus, it is enough to solve the linear system to find the linear and nonlinear threshold. In Table 2.5, we report the absolute error of critical Rayleigh numbers for the FD, HFD and Chebyshev tau methods with various values of h and number of polynomials. It is very clear from Table 2.5 that the Chebyshev tau method has highly accuracy compared with the FD, HFD methods. Moreover, for FD and HFD methods, the absolute error increases with increasing the value of M , but for the Chebyshev tau method (when the number of polynomials is greater than or equal to 15) the absolute error does not increase. However, for Chebyshev tau with a high number of polynomials, the accuracy has an oscillated behaviour where the absolute error increases or decreases with an increasing the number of polynomials. This behaviour is very common when studying the hydrodynamic stability problems. As the number of polynomials increases, theoretically, the accuracy of the Chebyshev tau method should increase, however, as the number of polynomials increases, the computer calculations increase and thus the computer's error will be higher. Since hydrodynamic stability problems require the repeated solving of an eigenvalue system to locate the critical Rayleigh number, we expect the computer's error to make the absolute error higher than the theoretical one. This behaviour is very clear in Table 2.5, where the absolute error of FD and HFD methods is higher than the truncation error of these methods. The accuracy of the numerical methods increases with increasing

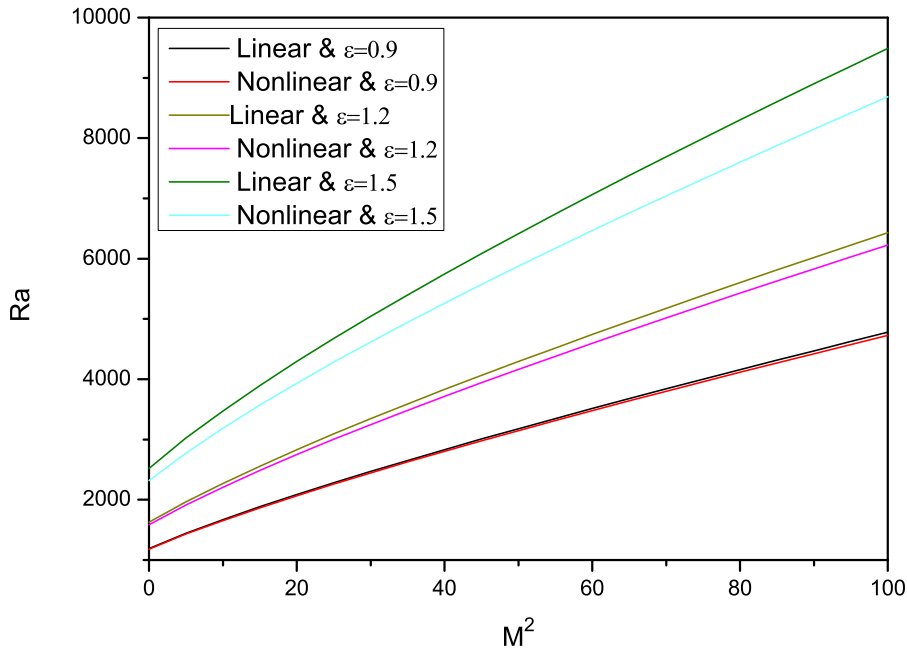


Figure 2.1: Critical Rayleigh number Ra against M^2 with $\varepsilon = 0.9, 1.2, 1.5$ for two free surfaces. Linear instability and nonlinear stability curves as in in caption.

the value of h and the number of polynomials until it arrive to the peak, then the behaviour of the accuracy become more oscillated due to the computer's error. In Figure 2.3, the absolute error of critical Rayleigh numbers are shown for FD and HFD methods with various values of h . Generally, the accuracy of the finite difference schemes corresponds with the value of h , where the accuracy increases with a decreasing value of h . However we can not take the value of h less than 0.005 for two reasons. Firstly, with $h = 0.005$ and after imposing the boundary conditions, the order of the eigenvalue matrices will be 399×399 , thus according to the computers' ability, this is an optimal choice. Secondly, we do not believe that small values h can give us more accurate results as the computations have to increase rapidly, and this is very important spatially when we solve nonlinear stability problems.

One of the key reasons to apply different numerical methods is to make a comparison between these methods and to conclude which is the best method in solving hydrodynamic stability problems. The advantage of Chebyshev tau method is that

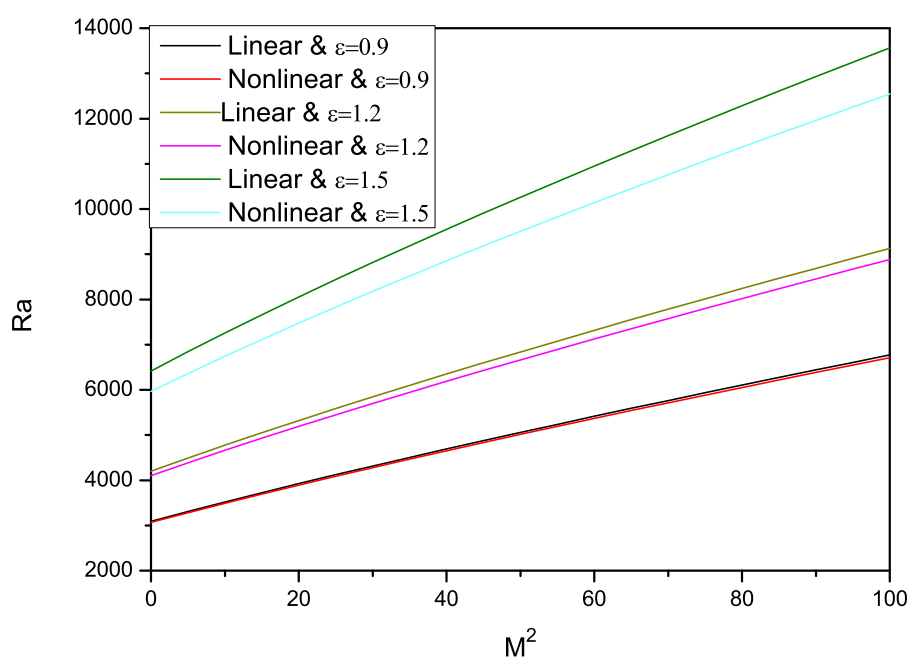


Figure 2.2: Critical Rayleigh number Ra against M^2 with $\epsilon = 0.9, 1.2, 1.5$ for two fixed surfaces. Linear instability and nonlinear stability curves as in caption.

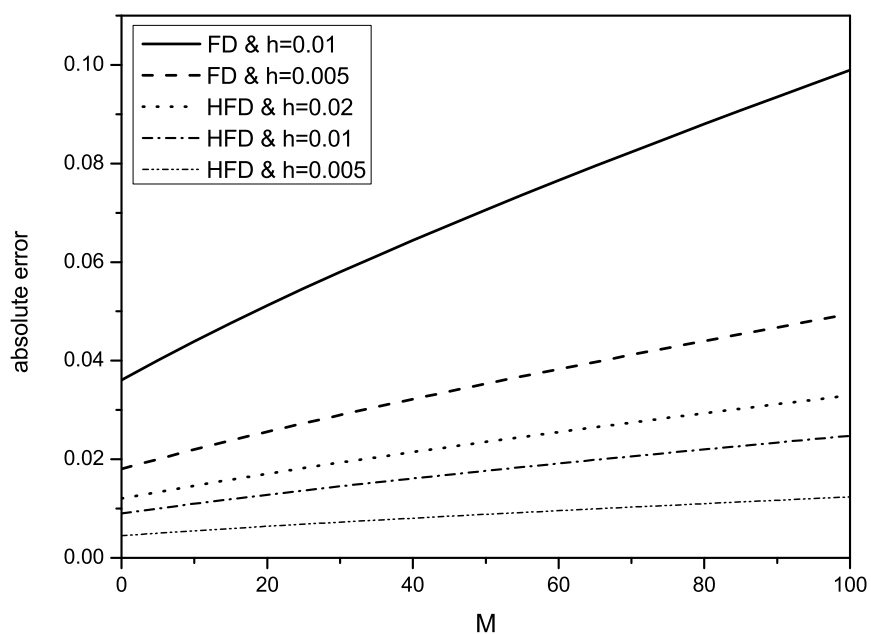


Figure 2.3: Comparison of the absolute error of critical Rayleigh numbers for FD and HFD methods with various values of h .

M^2	Che - tau		FD		HFD	
	Linear	Nonlinear	Linear	Nonlinear	Linear	Nonlinear
0	773.42255	773.12190	773.38012	773.02645	773.40841	773.09008
5	936.96280	936.57778	936.91563	936.46215	936.94708	936.53924
10	1085.71852	1085.25445	1085.66681	1085.12047	1085.70128	1085.20979
15	1224.98893	1224.44930	1224.93285	1224.29814	1224.97023	1224.39892
20	1357.49108	1356.87844	1357.43080	1356.71093	1357.47098	1356.82260
25	1484.84113	1484.15744	1484.77678	1483.97421	1484.81968	1484.09636
30	1608.09412	1607.34095	1608.02583	1607.14251	1608.07135	1607.27480
35	1727.98449	1727.16314	1727.91236	1726.94990	1727.96045	1727.09206
40	1845.04823	1844.15979	1844.97234	1843.93212	1845.02293	1844.08390
45	1959.69091	1958.73633	1959.61135	1958.49451	1959.66439	1958.65572
50	2072.22838	2071.20847	2072.14521	2070.95277	2072.20066	2071.12324
55	2182.91238	2181.82786	2182.82566	2181.55850	2182.88348	2181.73807
60	2291.94750	2290.79901	2291.85729	2290.51620	2291.91743	2290.70474
65	2399.50273	2398.29084	2399.40908	2397.99476	2399.47152	2398.19215
70	2505.71961	2504.44483	2505.62256	2504.13564	2505.68726	2504.34177
75	2610.71811	2609.38091	2610.61771	2609.05877	2610.68464	2609.27353
80	2714.60102	2713.20182	2714.49730	2712.86686	2714.56644	2713.09017
85	2817.45719	2815.99639	2817.35020	2815.64874	2817.42153	2815.88050
90	2919.36409	2917.84204	2919.25386	2917.48182	2919.32735	2917.72197
95	3020.38974	3018.80677	3020.27630	3018.43408	3020.35193	3018.68254
100	3120.59427	3118.95069	3120.47764	3118.56563	3120.55539	3118.82233

Table 2.1: Comparison of the linear and nonlinear numerical values of critical Rayleigh for two free surfaces $\varepsilon = 0.3$.

M^2	Che - tau		FD		HFD	
	Linear	Nonlinear	Linear	Nonlinear	Linear	Nonlinear
0	2008.65597	2007.94493	2008.26128	2007.69704	2008.52440	2007.86230
5	2150.61174	2149.83285	2150.18904	2149.56744	2150.47084	2149.74438
10	2288.50673	2287.66095	2288.05538	2287.37852	2288.35628	2287.56681
15	2422.92042	2422.00859	2422.43989	2421.70957	2422.76024	2421.90892
20	2554.30520	2553.32805	2553.79505	2553.01282	2554.13515	2553.22297
25	2683.02251	2681.98068	2682.48233	2681.64957	2682.84245	2681.87031
30	2809.36667	2808.26074	2808.80269	2807.91404	2809.17868	2808.14517
35	2933.58124	2932.41172	2932.98769	2932.04969	2933.38339	2932.29104
40	3055.87052	3054.63789	3055.24715	3054.26077	3055.66273	3054.51218
45	3176.40795	3175.11262	3175.75450	3174.72063	3176.19013	3174.98196
50	3295.34224	3293.98462	3294.65850	3293.57796	3295.11433	3293.84907
55	3412.80211	3411.38255	3412.08785	3410.96140	3412.56402	3411.24217
60	3528.89984	3527.41868	3528.15483	3526.98319	3528.65150	3527.27352
65	3643.73408	3642.19162	3642.95811	3641.74196	3643.47542	3642.04173
70	3757.39206	3755.78859	3756.58290	3755.32491	3757.12234	3755.63403
75	3869.95139	3868.28717	3869.11062	3867.80961	3869.67113	3868.12798
80	3981.48144	3979.75673	3980.60887	3979.26540	3981.19058	3979.59295
85	4092.04457	4090.25959	4091.13997	4089.75461	4091.74303	4090.09126
90	4201.69702	4199.85199	4200.76022	4199.33349	4201.38475	4199.67916
95	4310.48978	4308.58491	4309.52056	4308.05299	4310.16671	4308.40760
100	4418.46923	4416.50471	4417.46741	4415.95946	4418.13529	4416.32296

Table 2.2: Comparison of the linear and nonlinear numerical values of critical Rayleigh for two fixed surfaces $\varepsilon = 0.3$.

M^2	Che - tau		FD		HFD	
	Linear	Nonlinear	Linear	Nonlinear	Linear	Nonlinear
0	938.44198	936.30507	938.39033	936.18948	938.42477	936.26654
5	1136.65775	1133.92450	1136.60029	1133.78451	1136.63860	1133.87784
10	1316.91449	1313.62323	1316.85144	1313.46105	1316.89347	1313.56917
15	1485.64942	1481.82538	1485.58101	1481.64243	1485.62661	1481.76440
20	1646.16328	1641.82480	1646.08971	1641.62210	1646.13875	1641.75723
25	1800.41943	1795.58066	1800.34087	1795.35899	1800.39324	1795.50677
30	1949.69957	1944.37188	1949.61616	1944.13183	1949.67177	1944.29186
35	2094.89591	2089.08867	2094.80778	2088.83076	2094.86653	2089.00270
40	2236.65953	2230.38066	2236.56678	2230.10531	2236.62862	2230.28888
45	2375.48311	2368.73940	2375.38583	2368.44696	2375.45068	2368.64192
50	2511.75027	2504.54762	2511.64856	2504.23842	2511.71636	2504.44455
55	2645.76680	2638.11041	2645.66073	2637.78472	2645.73144	2638.00184
60	2777.78119	2769.67566	2777.67082	2769.33372	2777.74440	2769.56168
65	2907.99867	2899.44813	2907.88408	2899.09017	2907.96048	2899.32881
70	3036.59115	3027.59931	3036.47238	3027.22553	3036.55156	3027.47472
75	3163.70433	3154.27456	3163.58144	3153.88514	3163.66337	3154.14475
80	3289.46303	3279.59839	3289.33606	3279.19350	3289.42071	3279.46343
85	3413.97515	3403.67846	3413.84415	3403.25825	3413.93148	3403.53839
90	3537.33476	3526.60860	3537.19978	3526.17321	3537.28977	3526.46347
95	3659.62446	3648.47121	3659.48552	3648.02078	3659.57814	3648.32107
100	3780.91724	3769.33912	3780.77440	3768.87377	3780.86963	3769.18400

Table 2.3: Comparison of the linear and nonlinear numerical values of critical Rayleigh for two free surfaces $\varepsilon = 0.6$.

M^2	Che - tau		FD		HFD	
	Linear	Nonlinear	Linear	Nonlinear	Linear	Nonlinear
0	2436.26100	2431.21594	2435.78182	2430.91579	2436.10127	2431.11589
5	2608.25091	2602.72688	2607.73842	2602.40556	2608.08008	2602.61978
10	2775.30778	2769.31185	2774.76137	2768.96996	2775.12564	2769.19789
15	2938.13573	2931.67399	2937.55940	2931.31206	2937.94362	2931.55335
20	3097.28444	3090.36224	3096.67233	3089.98072	3097.08040	3090.23507
25	3253.19308	3245.81514	3252.54490	3245.41443	3252.97702	3245.68157
30	3406.21925	3398.38980	3405.53474	3397.97025	3405.99108	3398.24995
35	3556.65886	3548.38170	3555.93774	3547.94362	3556.41849	3548.23567
40	3704.76014	3696.03870	3704.00218	3695.58240	3704.50749	3695.88660
45	3850.73378	3841.57119	3849.93872	3841.09693	3850.46876	3841.41310
50	3994.76047	3985.15960	3993.92809	3984.66761	3994.48301	3984.99560
55	4136.99657	4126.96005	4136.12662	4126.45055	4136.70659	4126.79022
60	4277.57847	4267.10874	4276.67073	4266.58193	4277.27589	4266.93314
65	4416.62602	4405.72532	4415.68025	4405.18140	4416.31076	4405.54401
70	4554.24517	4542.91560	4553.26115	4542.35475	4553.91717	4542.72865
75	4690.53019	4678.77370	4689.50770	4678.19607	4690.18936	4678.58116
80	4825.56535	4813.38376	4824.50426	4812.78952	4825.21166	4813.18568
85	4959.42638	4946.82140	4958.32641	4946.21068	4959.05972	4946.61783
90	5092.18160	5079.15484	5091.04256	5078.52778	5091.80192	5078.94582
95	5223.89294	5210.44591	5222.71461	5209.80264	5223.50017	5210.23148
100	5354.61672	5340.75084	5353.39890	5340.09149	5354.21078	5340.53106

Table 2.4: Comparison of the linear and nonlinear numerical values of critical Rayleigh for two fixed surfaces $\varepsilon = 0.6$.

M^2	FD			HFD			Che-tau		
	h			No. of polynomials					
	0.02	0.01	0.005	0.02	0.01	0.005	10	15	20
0	0.432	0.036	0.018	0.012	0.009	0.005	3.6E-07	7.9E-10	5.8E-10
5	0.481	0.040	0.020	0.013	0.010	0.005	4.0E-07	7.9E-10	1.0E-09
10	0.527	0.044	0.022	0.015	0.011	0.005	4.4E-07	1.1E-10	4.6E-10
15	0.571	0.048	0.024	0.016	0.012	0.006	4.8E-07	1.6E-10	6.5E-10
20	0.614	0.051	0.026	0.017	0.013	0.006	5.2E-07	5.7E-09	3.0E-08
25	0.655	0.055	0.027	0.018	0.014	0.007	5.5E-07	4.4E-10	9.5E-09
30	0.696	0.058	0.029	0.019	0.014	0.007	5.8E-07	5.8E-10	1.8E-10
35	0.735	0.061	0.031	0.020	0.015	0.008	6.2E-07	2.4E-10	7.1E-10
40	0.773	0.064	0.032	0.021	0.016	0.008	6.5E-07	3.0E-10	2.2E-10
45	0.810	0.068	0.034	0.023	0.017	0.008	6.8E-07	8.7E-10	6.4E-10
50	0.847	0.071	0.035	0.024	0.018	0.009	7.1E-07	2.5E-09	2.6E-09
55	0.883	0.074	0.037	0.025	0.018	0.009	7.4E-07	2.0E-10	4.1E-10
60	0.919	0.077	0.038	0.026	0.019	0.010	7.7E-07	9.6E-10	9.5E-10
65	0.954	0.079	0.040	0.026	0.020	0.010	8.0E-07	9.0E-11	2.9E-10
70	0.988	0.082	0.041	0.027	0.021	0.010	8.1E-07	1.7E-08	9.7E-10
75	1.022	0.085	0.043	0.028	0.021	0.011	8.6E-07	2.0E-10	5.2E-10
80	1.056	0.088	0.044	0.029	0.022	0.011	8.9E-07	8.0E-11	2.0E-08
85	1.089	0.091	0.045	0.030	0.023	0.011	9.2E-07	9.5E-10	1.2E-09
90	1.122	0.094	0.047	0.031	0.023	0.012	9.4E-07	2.9E-10	3.2E-09
95	1.155	0.096	0.048	0.032	0.024	0.012	9.7E-07	1.1E-10	4.0E-09
100	1.187	0.099	0.049	0.033	0.025	0.012	1.0E-06	2.5E-10	5.0E-08

Table 2.5: Comparison of the absolute error of critical Rayleigh numbers for FD, HFD and Che-tau methods with various values of h and number of polynomials.

it can achieve the required accuracy using a small number of polynomials, and thus we can get very accurate results with very short run time. However, the FD method need a large number of divisions to reach the required accuracy, whilst the HFD method can reach to the desired accuracy by using less number of divisions. The FD method required $h = 0.005$ to achieve a good accuracy and convergence results, while we use $h = 0.01$ for the HFD method. For the Chebyshev tau method, 15 polynomials is enough to obtain a very good accuracy for two free boundaries, while, to arrive to the highest accuracy for two fixed boundaries, we use 20 polynomials. Generally, the run time of Chebyshev tau method is very short compare with FD and HFD.

On the other hand, the Chebyshev tau method is not easy to apply, where it requires a great effort to solve any system of equations. Concerning the problems of variable coefficients, the Chebyshev tau method is complicated to implement, as this method depends on writing all functions in the system of equations in the form of Chebyshev polynomials, which can present difficulties when using, for example, triangular and hyperbolic functions. In addition, the main disadvantages of this method is that it needs a new numerical treatment when we change the boundary conditions, where each type of boundary conditions requires different and special treatment. Also, Chebyshev tau method is unstable in equations which have high order derivative, where the values of a matrix increase significantly with increasing the order of derivatives.

In summary, although the Chebyshev tau method requires a great effort to set up the numerical scheme, it only requires a small number of polynomials to achieve an excellent level of accuracy and convergence. This point is very important as our numerical calculations required considerable calculation time (in some cases more than ten hours). Although the FD and HFD methods are very flexible methods, hydrodynamic stability problems need a method which can achieve an accurate solution within a short time period due to the requirement of repeated calculations. The FD and HFD lack this property and we see from the results that the FD method requires $h = 0.005$ to achieve a very good accuracy and convergence results, while we use $h = 0.01$ for HFD method.

Chapter 3

Magnetic effect on instability and nonlinear stability in a reacting fluid

3.1 Introduction

The convective instability created by a top heavy layer of fluid containing a solute is one with many applications in atmospheric physics, oceanography, and in pollution where the solute can cover a city and linger for long periods of time. A model for such behaviour was developed by Franchi and Straughan [58] and they completed a detailed instability analysis of their highly nonlinear model.

In a separate development Hayat and Nawaz [80] studied stagnation point flow in a rotating frame for a fluid containing a reacting solute with a superimposed magnetic field acting. Since convection in chemically reacting fluids has been a topic of much recent interest, cf., Malashetty and Biradar [120], Rahman and Al-Lawatia [157], and electro-magnetic field effects on such processes have likewise attracted much attention, cf., Eltayeb et al. [49, 50], Kaloni and Mahajan [94], Maehlmann and Papageorgiou [116], Nanjundappa et al. [130], Reddy et al. [164], Shivakumara et al. [187, 188], Sunil et al. [212], we deem it of great relevance to develop and analyse stability in detail for the solute instability problem of Franchi and Straughan [58],

but allowing for chemical reactions and an imposed magnetic field as in the work of Hayat and Nawaz [80]. We should point out that thermal convection interacting with other effects is a very hot current research topic, cf., Bera and Khalili [20], Bera et al. [21], Chen et al. [35], Yang et al. [226], Kumar et al. [97, 98], Papanicolaou et al. [142], Saravanan and Sivakumar [184], Saravanan and Brindha [183], Shivakumara et al. [185, 186].

To study the effect of a magnetic field we employ a quasi-static approximation as in Galdi and Straughan [61]. This still allows a full analysis of the effect of the magnetic field but avoids mathematical complications associated with the complete set of equations for magnetohydrodynamics, cf., Rionero [169], Galdi [60], Rionero and Mulone [177], Chandrasekhar [32], Roberts [179], Landau et al. [100]. Nevertheless, the model we develop is still highly nonlinear and very non-trivial.

The layout of this chapter is as follows. In the next section we present the basic model for convective motion in a fluid layer with a dissolved reacting fluid and a vertically imposed magnetic field. In Section 3.3 we analyse linear instability of the basic motion and Section 3.4 compliments this with a global nonlinear energy stability analysis. Since the stability analyses involve eigenvalue problems with non-constant coefficients these problems must be solved numerically and a suitable numerical method is described in the penultimate section. Finally, in section 6 we give detailed results and conclusions from our model.

The results in this chapter were published in the article Harfash and Straughan [73].

3.2 Basic Equations

We suppose the fluid is contained in the plane layer $\{z \in (0, d)\} \times \mathbb{R}^2$, and is incompressible, although a Boussinesq approximation is employed in the buoyancy term in the momentum equation. The momentum equation for a fluid containing a solute and with an imposed magnetic field is then

$$\rho(v_{i,t} + v_j v_{i,j}) = -p_{,i} + \mu \Delta v_i - \rho \alpha_c k_i g (c - c_\infty) + \mathbf{j} \times \mathbf{B}, \quad (3.2.1)$$

where ρ , \mathbf{v} , p , c are the constant density, velocity field, pressure, and concentration of solute. Additionally, α_c is the salt expansion coefficient, μ is the dynamic viscosity, g is gravity, c_∞ is a reference concentration, $\mathbf{k} = (0, 0, 1)$, \mathbf{j} is the current, and \mathbf{B} is the magnetic induction field. Throughout, we use standard indicial notation and the Einstein summation convention so that e.g. $v_{i,t} = \partial v_i / \partial t$, and $p_{,i} = \partial p / \partial x_i$, $v_j v_{i,j} \equiv (\mathbf{v} \cdot \nabla) \mathbf{v}$, and Δ is the Laplacian. The balance of mass equation is

$$v_{i,i} = 0 \quad (3.2.2)$$

The equation governing the evaluation of the solute concentration is, cf., Hayat and Nawaz [80],

$$c_{,t} + v_i c_{,i} = D \Delta c - K_1 (c - c_\infty). \quad (3.2.3)$$

Here $c(\mathbf{x}, t)$ is the solute concentration, D is the the solute diffusion coefficient, and K_1 is the chemical reaction rate, the chemical reaction being represented by the term $K_1(c - c_\infty)$.

To make the convective overturning instability problem tractable we employ the quasi-static MHD approximation of Galdi and Straughan [61] which has been explained in Chapter 2. According to this approximation we have

$$\mathbf{j} \times \mathbf{B} = \sigma_1 (\mathbf{v} \times \mathbf{B}_0) \times \mathbf{B}_0, \quad (3.2.4)$$

where σ_1 is the electrical conductivity and $\mathbf{B}_0 = (0, 0, B_0)$ is a magnetic field with only the vertical component. We now employ (3.2.4) in (3.2.1) and further replace $c - c_\infty$ by c , (we can always rescale equations (3.2.1) and (3.2.3) to achieve this). Thus, we find the equations for our model are

$$\begin{aligned} v_{i,t} + v_j v_{i,j} &= -\frac{1}{\rho} p_{,i} + \nu \Delta v_i - k_i g \alpha_c c + \frac{\sigma_1}{\rho} [(\mathbf{v} \times \mathbf{B}_0) \times \mathbf{B}_0]_i, \\ v_{i,i} &= 0, \\ c_{,t} + v_i c_{,i} &= D \Delta c - K_1 c. \end{aligned} \quad (3.2.5)$$

The boundary conditions to be satisfied are no-slip at the boundaries $z = 0$ and $z = d$ with the concentrations fixed there. Thus,

$$v_i = 0, \quad \text{at } z = 0, d; \quad c = c_U, \quad \text{at } z = d; \quad c = c_L, \quad \text{at } z = 0, \quad (3.2.6)$$

where c_U, c_L are constants with $c_U > c_L$.

We then find there is a steady solution $(\bar{v}_i, \bar{c}, \bar{p})$ whose stability we wish to examine, and this is

$$\begin{aligned} \bar{v}_i &\equiv 0, \\ \bar{c} &= \left[\frac{c_U - c_L \cosh(A_1 d)}{\sinh(A_1 d)} \right] \sinh(A_1 z) + c_L \cosh(A_1 z), \end{aligned} \quad (3.2.7)$$

where \bar{p} may then be found from (3.2.5), and where A_1 is given by

$$A_1^2 = \frac{K_1}{D}. \quad (3.2.8)$$

Next, we derive perturbation equations to this steady state. Hence, put $v_i = \bar{v}_i + u_i$, $c = \bar{c} + \phi$, $p = \bar{p} + \pi$, and employ the scales

$$\tau = \frac{d^2}{\nu}, \quad U = \frac{\nu}{d}, \quad P = \frac{\rho \nu U}{d}, \quad L = d,$$

where τ, U, L, P are time, velocity, length, and pressure scales. Define $\xi = A_1 d = (\sqrt{K_1/D})d$, and pick the concentration scale $C^\#$ as

$$C^\# = U \sqrt{\frac{\nu \Delta C}{D \alpha_c g d}}$$

where $\Delta C = c_U - c_L > 0$. Furthermore, define the salt Rayleigh number R^2 as

$$R^2 = \frac{\alpha_c g d^3 \Delta C}{D \nu}, \quad (3.2.9)$$

and the salt Prandtl number as $P_s = \nu/D$. We also need the non-dimensional numbers η and M where

$$\eta = \frac{c_L}{c_U - c_L} \quad \text{and} \quad M^2 = \frac{B_0^2 d^2 \sigma_1}{\rho \nu} \quad (3.2.10)$$

and further introduce the function $f(z; \xi, \eta)$ by

$$f(z; \xi, \eta) = \frac{\xi}{\sinh(\xi)} \{1 + \eta(1 - \cosh(\xi))\} \cosh(\xi z) + \xi \eta \sinh(\xi z). \quad (3.2.11)$$

Then, one may show the non-dimensional perturbation equations which arise from (3.2.5) are

$$\begin{aligned} u_{i,t} + u_j u_{i,j} &= -\pi_{,i} + \Delta u_i - R\phi k_i - M^2[(\mathbf{k} \times (\mathbf{u} \times \mathbf{k}))_i], \\ u_{i,i} &= 0, \\ P_s(\phi_{,t} + u_i \phi_{,i}) &= \Delta\phi - \xi^2\phi - Rf(z; \xi, \eta)w, \end{aligned} \tag{3.2.12}$$

where $w = u_3$, and now the spatial domain is $\mathbb{R}^2 \times \{z \in (0, 1)\}$.

The boundary conditions to be satisfied are

$$u_i = 0, \quad \phi = 0, \quad \text{on } z = 0, 1, \tag{3.2.13}$$

and u_i, ϕ, π satisfy a plane tiling form in the (x, y) -plane, cf., Chandrasekhar [32], Straughan [196].

Remark 3.2.1 *We observe that as $\xi \rightarrow 0$, $f \rightarrow 1$, the chemical reaction term disappears and we recover the concentration analogue of the thermal convection problem studied in Galdi and Straughan [61], pp. 216-217. However, the presence of the $f(z)$ term destroys the symmetry of the linear operator in (3.2.12) and considerably complicates the linear instability / nonlinear stability analysis.*

3.3 Linear instability

To obtain the threshold for linear instability where we know convection occurs we neglect the nonlinear terms $u_j u_{i,j}$ and $u_i \phi_{,i}$ in equations (3.2.12)₁ and (3.2.12)₃. Then, due to linearity we may seek solutions like $u_i(\mathbf{x}, t) = u_i(\mathbf{x})e^{\sigma t}$, $\phi(\mathbf{x}, t) = \phi(\mathbf{x})e^{\sigma t}$ and $\pi(\mathbf{x}, t) = \pi(\mathbf{x})e^{\sigma t}$, where σ is a complex constant. This leads to the system

$$\begin{aligned} \sigma u_i &= -\pi_{,i} + \Delta u_i - R\phi k_i + M^2[(\mathbf{u} \times \mathbf{k}) \times \mathbf{k}]_i, \\ u_{i,i} &= 0, \\ P_s \sigma \phi &= \Delta\phi - \xi^2\phi - Rfw. \end{aligned} \tag{3.3.14}$$

To proceed further we then take *curlcurl* of (3.3.14)₁, and retain the third component of the resulting equation, namely

$$\sigma \Delta w = \Delta^2 w - R \Delta^* \phi - M^2 D^2 w, \quad (3.3.15)$$

where $\Delta^* = \partial^2/\partial x^2 + \partial^2/\partial y^2$ and $D = \partial/\partial z$.

Next, due to the periodicity of the solution in the (x, y) variables we may write w and ϕ as

$$w = W(z)h(x, y) \quad \text{and} \quad \phi = \Phi(z)h(x, y),$$

where h is a plane-tiling planform so that

$$\Delta^* h = -a^2 h, \quad (3.3.16)$$

where a is the wavenumber. Such planforms are discussed in detail in Chandrasekhar [32], p.43-52 and Straughan [196], p.51. With D now denoting $D = d/dz$ equations (3.3.15) and (3.3.14)₃ reduce to

$$\begin{aligned} (D^2 - a^2)^2 W + R a^2 \Phi - M^2 D^2 W &= \sigma (D^2 - a^2) W, \\ (D^2 - a^2) \Phi - \xi^2 \Phi - R f(z; \xi, \eta) W &= \sigma P_s \Phi. \end{aligned} \quad (3.3.17)$$

The boundary conditions we employ herein are those appropriate to two fixed surfaces and so

$$W = DW = 0 \quad \text{and} \quad \Phi = 0, \quad \text{on} \quad z = 0, 1. \quad (3.3.18)$$

System (3.3.17) and (3.3.18) represents an eigenvalue problem for the eigenvalues σ with parameters a, M, ξ, η, P_s and R . Numerical results are presented in section 6 and the numerical method employed is described in section 3.5.

3.4 Nonlinear stability

The linear instability boundary yields a Rayleigh number threshold such that once $R_a = R^2$ exceeds this threshold convective instability certainly occurs. However, in general, linear theory yields no information on whether a solution with a Rayleigh number below this is definitely stable, cf., Straughan [196]. In fact, it is possible for a solution to become unstable with a Rayleigh number well below the linear instability threshold. Such instabilities are sub-critical instabilities and we here wish to employ

a nonlinear energy stability technique to yield a threshold for global nonlinear stability. Fortunately, the nonlinear threshold determined herein is relatively close to the linear instability one and this is important since it demonstrates that the linear instability analysis is correctly capturing the physics of the onset of convection. The energy method for nonlinear stability is attracting a lot of attention, cf., Capone et al. [24–27], Hill and Carr [83], Saravanan and Brindha [183], Sunil et al. [209,214].

To develop a nonlinear energy stability analysis, let V be a period cell for the disturbance solution in equations (3.2.12). Let $\|\cdot\|$ and (\cdot, \cdot) be the norm and inner product on the Hilbert space $L^2(V)$. We multiply equation (3.2.12)₁ by u_i and integrate over V . After some integrations by parts, use of the boundary conditions (3.2.13), and employing equation (3.2.12)₂ we derive the identity

$$\frac{1}{2} \frac{d}{dt} \|\mathbf{u}\|^2 = -\|\nabla \mathbf{u}\|^2 - R(w, \phi) - M^2(\|\mathbf{u}\|^2 - \|w\|^2). \quad (3.4.19)$$

Next, multiply equation (3.2.12)₃ by ϕ and integrate over V , to see that after further integrations by parts and use of (3.2.13) and (3.2.12)₂, we obtain

$$\frac{P_s}{2} \frac{d}{dt} \|\phi\|^2 = -R(fw, \phi) - \xi^2 \|\phi\|^2 - \|\nabla \phi\|^2. \quad (3.4.20)$$

The idea is to now add (3.4.19) + λ (3.4.20) for a positive parameter λ which we later select optimally. This leads to the energy equation

$$\frac{dE}{dt} = \mathcal{I} - \mathcal{D}, \quad (3.4.21)$$

where E, \mathcal{I} and \mathcal{D} are defined by

$$\begin{aligned} E(t) &= \frac{1}{2} \|\mathbf{u}\|^2 + \frac{\lambda P_s}{2} \|\phi\|^2, \\ \mathcal{I} &= -R(w, \phi[1 + \lambda f]), \\ \mathcal{D} &= \|\nabla \mathbf{u}\|^2 + \lambda \|\nabla \phi\|^2 + \lambda \xi^2 \|\phi\|^2 + M^2(\|u\|^2 + \|v\|^2), \end{aligned} \quad (3.4.22)$$

where \mathbf{u} is explicitly written as $\mathbf{u} = (u, v, w)$. Define now

$$\frac{1}{R_E} = \max_{\mathcal{H}} \frac{\mathcal{I}}{\mathcal{D}}, \quad (3.4.23)$$

where \mathcal{H} is the set of admissible functions defining \mathcal{I} and \mathcal{D} . This set is restricted to divergence free functions due to equation (3.2.12)₂. To impose this restriction we use a Lagrange multiplier and add the term $-\int_{\Omega} \zeta u_{i,i}$ to \mathcal{I} so that now

$$\mathcal{I} = -R(w, \phi[1 + \lambda f]) - (\zeta, u_{i,i}).$$

where ζ is a lagrange multiplier. Then from (3.4.21) we find

$$\frac{dE}{dt} \leq \mathcal{D}\left(\frac{1}{R_E} - 1\right) \quad (3.4.24)$$

If $R_E > 1$, then with λ_1 being the constant in Poincare's inequality for \mathbf{u} and ϕ , we have

$$\mathcal{D} \geq c E,$$

where $c = \min\{2\lambda_1, 2(\lambda_1 + \xi^2)P_s^{-1}\}$, and from (3.4.24) we may show

$$\frac{dE}{dt} \leq -c \frac{(R_E - 1)}{R_E} E. \quad (3.4.25)$$

Exponential decay of $E(t)$ follows from (3.4.25) and then R_E defined by (3.4.23) represents a global (for all initial data) nonlinear stability threshold.

The equations which satisfy the condition (3.4.23) are the Euler-Lagrange equations and in order to find these we must first derive $\delta\mathcal{I}$ and $\delta\mathcal{D}$. To do this we vary the perturbation variables \mathbf{u} and ϕ , by arbitrary functions χ and ψ , respectively. This method is described in detail in Chapter 1. The Euler-Lagrange equations which arise from (3.4.23) are:

$$\begin{aligned} 2\Delta u_i - R_E k_i (1 + \lambda f)\phi - 2M^2(u_i - k_i w) &= \zeta_i, \\ u_{i,i} &= 0, \\ 2\lambda\Delta\phi - 2\lambda\xi^2\phi - R_E(1 + \lambda f)w &= 0, \end{aligned} \quad (3.4.26)$$

This system is solved subject to boundary conditions (3.2.13) by numerical means and we determine

$$\max_{\lambda} R_E,$$

as our global nonlinear stability bound. Brief details are provided in section 3.5 and detailed numerical output is contained in section 3.6.

3.5 Numerical technique

To solve system (3.3.17) and (3.3.18) we expand the operator in (3.3.17)₁, and solve the system as

$$\begin{aligned} D^4W - (2a^2 + M^2)D^2W + a^4W + R a^2\Phi &= \sigma(D^2 - a^2)W, \\ (D^2 - a^2)\Phi - \xi^2\Phi - R f(z; \xi, \eta)W &= \sigma P_s \Phi. \end{aligned} \quad (3.5.27)$$

The above system is discretized using finite differences. To do this note that the spatial domain is $z \in (0, 1)$ and divide $(0, 1)$ into N equal subintervals of length $h = 1/N$. Let W_i denote the value of W at $z = ih$ and then we recall the standard second and fourth order differentiation operators are

$$\begin{aligned} \delta^2W_i &= \frac{W_{i+1} - 2W_i + W_{i-1}}{h^2}, \\ \delta^4W_i &= \frac{W_{i+2} - 4W_{i+1} + 6W_i - 4W_{i-1} + W_{i-2}}{h^4}. \end{aligned} \quad (3.5.28)$$

By expanding $W(ih \pm h)$ and $W(ih \pm 2h)$ in Taylor series we obtain approximations to the second and fourth order derivatives as

$$\begin{aligned} D^2W(ih) &= \delta^2W_i - \frac{h^2}{12}D^4W_i + O(h^4), \\ D^4W(ih) &= \delta^4W_i - \frac{h^2}{6}D^6W_i + O(h^4). \end{aligned} \quad (3.5.29)$$

The second and fourth order derivatives in (3.5.27) are replaced by (3.5.28) and (3.5.29) to $O(h^2)$ accuracy, i.e. we solve

$$\begin{aligned} \delta^4W_i - (M^2 + 2a^2)\delta^2W_i + a^4W_i + a^2R\Phi_i &= \sigma(\delta^2W_i - a^2W_i), \\ \delta^2\Phi_i - (a^2 + \xi^2)\Phi_i - R f(ih; \xi, \eta)W_i &= \sigma P_s \Phi_i. \end{aligned} \quad (3.5.30)$$

The boundary conditions for (3.5.30) are

$$W = 0, \quad DW = 0, \quad \Phi = 0, \quad z = 0, 1. \quad (3.5.31)$$

Hence, we are here concentrating on the realistic case of two fixed surfaces. Conditions (3.5.31) are equivalent to

$$W_0 = W_N = 0, \quad \Phi_0 = \Phi_N = 0, \quad (3.5.32)$$

and for DW we use a central difference and the fictitious points $z = -ih, z = 1 + ih$, to employ W_{-1} and W_{N+1} to see that $W_{-1} = W_1$ and $W_{N+1} = W_{N-1}$ to order

$O(h^2)$ accuracy. The latter representations are employed in (3.5.29) with $i = 1$ and $i = N - 1$ to remove W_{-1} and W_{N+1} when utilizing (3.5.28). In this manner, equations (3.5.29) and the boundary conditions lead to the finite difference equations

$$\begin{aligned} \frac{W_{i+2}}{h^4} - \left(\frac{4}{h^4} + \frac{2a^2 + M^2}{h^2}\right)W_{i+1} + \left(\frac{6}{h^4} + \frac{2(2a^2 + M^2)}{h^2} + a^4\right)W_i - \left(\frac{4}{h^4} + \frac{2a^2 + M^2}{h^2}\right)W_{i-1}, \\ + \frac{W_{i-2}}{h^4} + Ra^2\Phi_i = \sigma \left[\frac{W_{i+1}}{h^2} - \left(\frac{2}{h^2} + a^2\right)W_i + \frac{W_{i-1}}{h^2} \right], \end{aligned} \quad (3.5.33)$$

$$i = 2, \dots, N - 2,$$

$$\begin{aligned} \frac{\Phi_{i+1}}{h^2} - \left(\frac{2}{h^2} + a^2 + \xi^2\right)\Phi_i + \frac{\Phi_{i-1}}{h^2} - Rf(ih; \xi, \eta)W_i = \sigma P_s \Phi_i, \end{aligned} \quad (3.5.34)$$

$$i = 1, \dots, N - 1,$$

$$\begin{aligned} \frac{W_3}{h^4} - \left(\frac{4}{h^4} + \frac{2a^2 + M^2}{h^2}\right)W_2 + \left(\frac{7}{h^4} + \frac{2(2a^2 + M^2)}{h^2} + a^4\right)W_1 + Ra^2\Phi_1, \\ = \sigma \left[\frac{W_2}{h^2} - \left(\frac{2}{h^2} + a^2\right)W_1 \right], \end{aligned} \quad (3.5.35)$$

which is the equation obtained from (3.5.29)₁ with $i = 1$, and

$$\begin{aligned} \left(\frac{7}{h^4} + \frac{2(2a^2 + M^2)}{h^2} + a^4\right)W_{N-1} - \left(\frac{4}{h^4} + \frac{2a^2 + M^2}{h^2}\right)W_{N-2} + \frac{W_{N-3}}{h^4} + Ra^2\Phi_{N-1}, \\ = \sigma \left[-\left(\frac{2}{h^2} + a^2\right)W_{N-1} + \frac{W_{N-2}}{h^2} \right], \end{aligned} \quad (3.5.36)$$

which arises from (3.5.29)₁ with $i = N - 1$.

Equations (3.5.33)-(3.5.36) yield a generalized matrix eigenvalue problem of form

$$A \mathbf{x} = \sigma B \mathbf{x}, \quad (3.5.37)$$

where $\mathbf{x} = (W_1, \dots, W_{N-1}, \Phi_1, \dots, \Phi_{N-1})^T$ and A and B are $(2N - 2) \times (2N - 2)$ block structured matrices of form

$$A = \begin{pmatrix} A_1 & A_2 \\ A_3 & A_4 \end{pmatrix}, \quad B = \begin{pmatrix} B_1 & O \\ O & B_2 \end{pmatrix},$$

where A_1 is a pentadiagonal matrix, A_4 is tridiagonal, A_2 and A_3 are diagonal matrices with entries a^2R and $-Rf(ih)$, respectively. The matrices in B are such that B_1 is tridiagonal while B_2 is diagonal.

We have solved system (3.5.37) for eigenvalues σ_j by using LU decomposition using our own code and by the QZ algorithm from Matlab routines. Excellent agreement was found with both methods. Once the eigenvalues σ_j are found we use the secant method to locate where σ_j^R , $\sigma_j = \sigma_j^R + \sigma_j^I$ being the real and imaginary parts of eigenvalue σ_j . The value of R which makes $\sigma_1^R = 0$, σ_1^R being the largest eigenvalue, is the critical value of R for a^2 fixed. We then use golden section search to minimize over a^2 and find the critical value of R^2 for linear instability. Numerical results are reported in section 3.6. We have checked convergence and found that convergence to 10 decimal places is achieved with $h = 0.01$. In all of our calculations we found that $\sigma_1^I = 0$ at criticality and so the onset of instability is by stationary convection.

Remark 3.5.1 *We have chosen to employ a finite difference method to solve (3.3.17) and (3.3.18) rather than Chebyshev tau or compound matrices, such as in Dongarra et al. [43], Straughan and Walker [201–203]. This is largely due to the ease in implementation with the function $f(z)$. Also, the finite difference method leads to B non-singular in (3.5.37) and so we may employ LU decomposition, unlike the D^2 and D methods of Dongarra et al. [43] which necessarily have B singular and so necessitate use of the QZ algorithm. The banded nature of A and B would also lead naturally to solution by an Arnoldi technique. In addition, we found no occurrence of spurious eigenvalues as frequently arises with the Chebyshev tau method, cf., Dongarra et al. [43].*

To solve the energy eigenvalue problem (3.4.26) we remove the ζ term by taking *curlcurl* of (3.4.26)₁ to arrive at the system

$$\begin{aligned} 2\Delta^2 w - 2M^2 w_{,zz} - R_E(1 + \lambda f)\Delta^* \phi &= 0, \\ 2\lambda\Delta\phi - 2\lambda\xi^2\phi - R_E(1 + \lambda f)w &= 0. \end{aligned} \tag{3.5.38}$$

Again, the representations $w = W(z)h(x, y)$ and $\phi = \Phi(z)h(x, y)$ are introduced and we solve (3.5.38) as

$$\begin{aligned} 2(D^2 - a^2)^2 W - 2M^2 D^2 W &= -a^2 R_E(1 + \lambda f)\Phi, \\ 2\lambda(D^2 - a^2)\Phi - 2\lambda\xi^2\Phi &= R_E(1 + \lambda f)W, \end{aligned} \tag{3.5.39}$$

together with boundary conditions (3.3.18). Now, however, the eigenvalue is R_E .

We again use finite differences to solve for the smallest eigenvalue R_E for fixed a^2 and λ . Then, we employ golden section search to minimize in a^2 and then maximize in λ to determine the critical Rayleigh number for nonlinear energy stability,

$$R_{a_E}^{crit} = \max_{\lambda > 0} \min_{a^2} R_E^2(a^2; \lambda).$$

Numerical results are reported in section 3.6 and compared to those of linear instability theory.

3.6 Results and conclusions

In this section we report on numerical solution of the linear instability system (3.3.17), (3.3.18), and on the nonlinear energy stability system (3.4.26), (3.3.18).

Figures [3.1, 3.2] show the effect of increasing magnetic field M^2 on the critical Rayleigh number for various values of ξ and η . It is very noteworthy that the nonlinear stability curves are close to those of linear theory. This shows that possible sub-critical instabilities may only arise in a very small range of Rayleigh numbers, and it also demonstrates that linear instability theory is correctly capturing the physics of the onset of convection. Figures [3.1, 3.2] demonstrate that Ra increases with increasing M^2 which shows the stabilizing effect of the magnetic field.

Figure 3.3 shows how increasing ξ corresponds, in general, to greater stabilization. Figures 3.4, 3.5 show the same effect but for larger magnetic field strength. All these Figures demonstrate quantitatively the stabilizing effect of the chemical reaction. Again, it is very noticeable that the nonlinear energy stability curves are close to those of linear instability. This is reinforcing the fact that the linear curves are a true representation that the physics of the onset of convection is being correctly reflected. The gap between the curves represents the small band where sub-critical bifurcation may possibly occur.

Figure 3.6 again shows the stabilizing effect of increasing ξ , at least for $\xi \geq 3$. The decrease in Ra in Figure 3.3 when $\eta = 4$ and in Figure 3.6 (where again $\eta = 4$), is to be expected due to the definition of η in (3.2.10). For example, $\eta = 4$ corresponds to $c_U = 5c_L/4$. If we take $\eta = 6$ this corresponds to $c_U = 7c_L/6$. The coefficient of c_L decreases as η increases and this means that the destabilizing effect due to heavier fluid above is lessening.

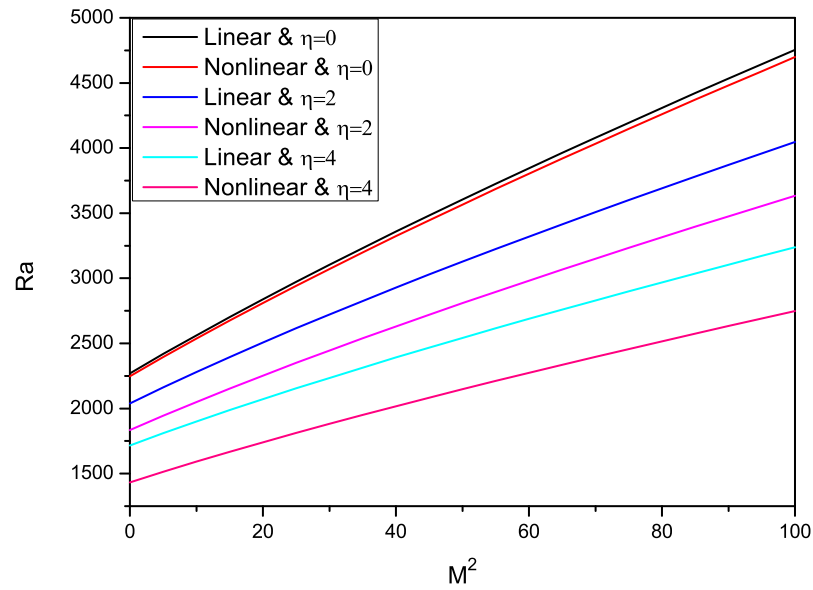


Figure 3.1: Critical Rayleigh number R_a against M^2 , with $\xi = 2$ for $\eta = 0, 2, 4$. Linear instability and nonlinear stability curves as in caption.

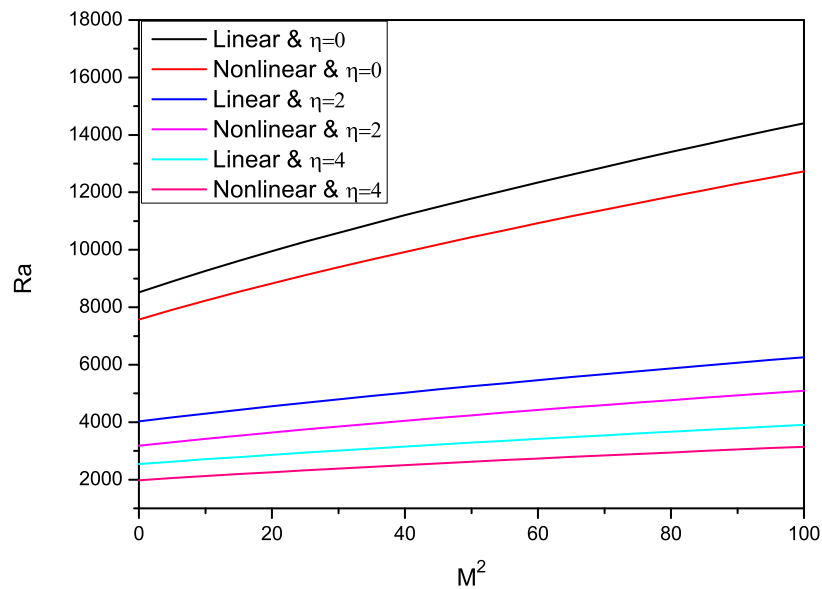


Figure 3.2: Critical Rayleigh number R_a against M^2 , with $\xi = 6$ for $\eta = 0, 2, 4$. Linear instability and nonlinear stability curves as in caption.

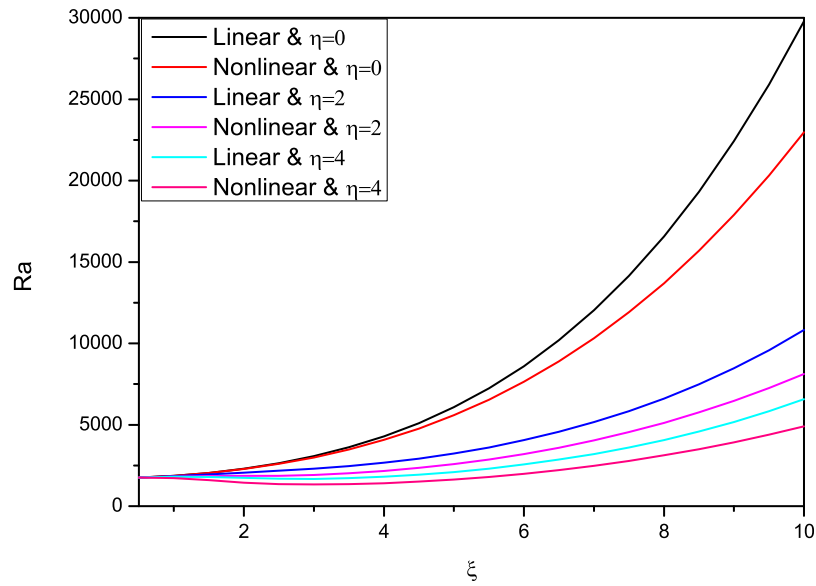


Figure 3.3: Critical Rayleigh number R_a against ξ , with $M^2 = 1$ for $\eta = 0, 2, 4$. Linear instability and nonlinear stability curves as in caption.

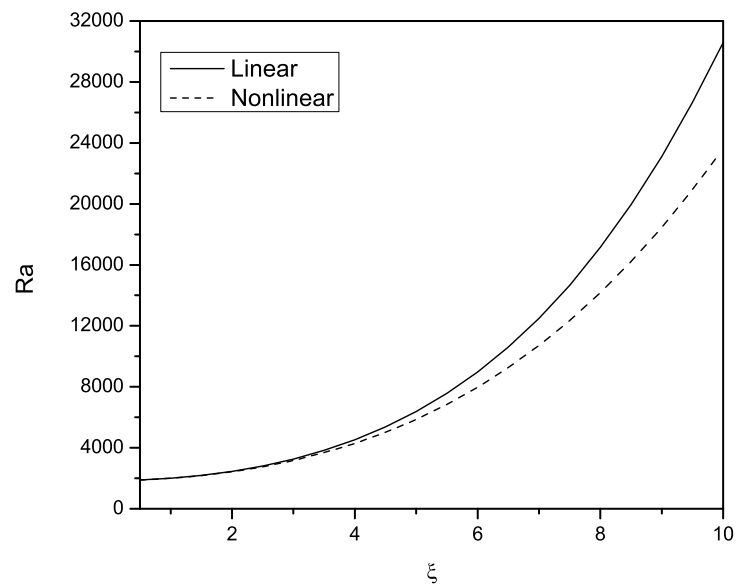


Figure 3.4: Critical Rayleigh number R_a against ξ , with $M^2 = 6$ for $\eta = 0$. Linear instability curve together with nonlinear stability one.

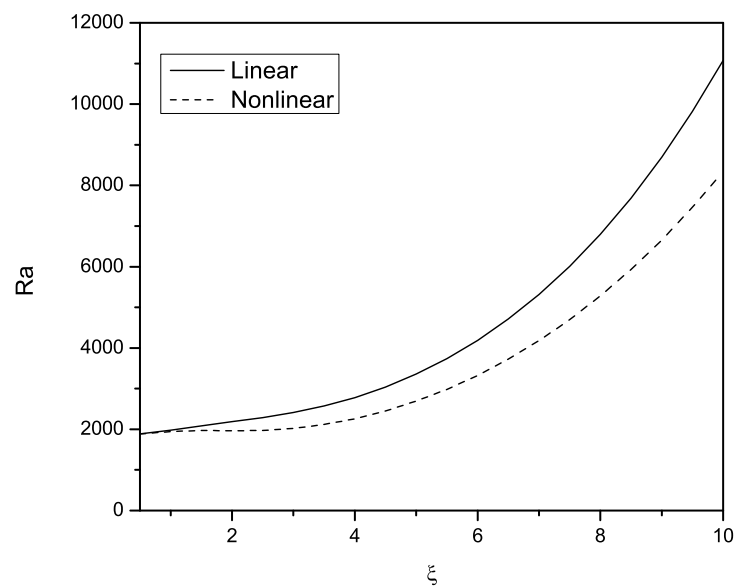


Figure 3.5: Critical Rayleigh number R_a against ξ , with $M^2 = 6$ for $\eta = 2$. Linear instability curve together with nonlinear stability one.

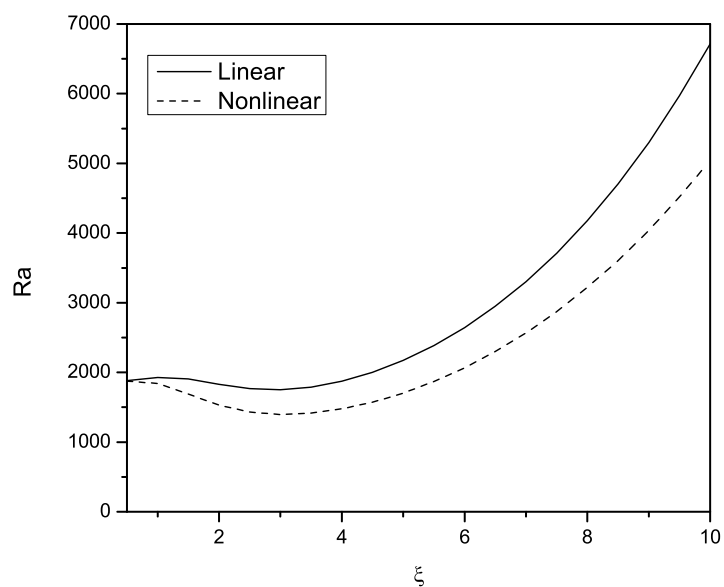


Figure 3.6: Critical Rayleigh number R_a against ξ , with $M^2 = 6$ for $\eta = 4$. Linear instability curve together with nonlinear stability one.

Chapter 4

Magnetic effect on instability and nonlinear stability of double diffusive convection in a reacting fluid

4.1 Introduction

The problem of double diffusive convection in fluid and porous media has attracted considerable interest during the last 50 years. This is because of its wide range of applications, for instance modeling geothermal reservoirs [36, 70, 180]. Bioremediation, where micro-organisms are introduced to change the chemical composition of contaminants is a very topical area, cf. Celia et al. [30], Chen et al. [33], Suchomel et al. [204]. Contaminant movement or pollution transport is a further area of multi-component, flow in porous media which is of much interest in environmental engineering, cf. Curran and Allen [40], Ewing and Weekes [51], Franchi and Straughan [58]. Other very important and topical areas of double diffusive occur in oil reservoir simulation, e.g. Ludvigsen et al. [114], and salinization in desert-like areas, Gilman and Bear [67]. Solar ponds are a particularly promising means of harnessing energy from the Sun by preventing convective overturning in thermohaline system by salting from below, cf., Leblanca et al. [103] and Nie et al. [135].

Recently, double diffusive convection in a viscous flow has been extensively investigated, both theoretically and experimentally [59, 115, 117, 159, 206, 211, 215, 216]. Moreover, convection in chemically reacting fluids has been a topic of much recent interest, cf., Malashetty and Biradar [120], Rahman and Al-Lawatia [157]. Also, Magnetoconvection (convection in the presence of a magnetic field) on such processes has been intensively studied by many authors, cf., Eltayeb et al. [49, 50], Kaloni and Mahajan [94], Maehlmann and Papageorgiou [116], Nanjundappa et al. [130], Reddy et al. [164], Shivakumara et al. [187, 188], Sunil et al. [212]. Thus, we deem it of great relevance to develop and analyse stability in detail for the double diffusive convection problem of Joseph [91], but allowing for chemical reactions and an imposed magnetic field.

The two important articles on the nonlinear energy stability of double diffusive convection problem was presented by Joseph [91] and Mulone [129]. A detailed review of problems related to this problem can be found in the book by Straughan [196]. A comprehensive review of the literature concerning double diffusive natural convection in a fluid-saturated porous medium may be found in the book by Nield and Bejan [138]. Useful review articles on double diffusive convection in porous media include those by Mojtabi and Charrier-Mojtabi [127] and Mamou [124].

Baines and Gill [11] introduced a detailed linear stability theory for problem of convection with temperature and salt fields in a fluid and the similar situation in porous medium was studied by Nield [136]. Rudraiah et al. [182] have used nonlinear perturbation theory to study the onset of double diffusive convection in a horizontal porous layer. The linear stability analysis of the thermosolutal convection is carried out by Poulikakos [154] using the Darcy-Brinkman model. The double diffusive convection in porous media in the presence of cross-diffusion effects is analyzed by Rudraiah and Malashetty [181]. Malashetty et al. [121] have studied the double diffusive convection in a fluid-saturated rotating porous layer when the fluid and solid phases are not in local thermal equilibrium, using both linear and nonlinear stability

analyses. Sunil and Mahajan [210] have derived a rigorous nonlinear stability result by introducing a suitable generalized energy functional for a magnetized ferrofluid layer heated and saluted from below with magnetic field-dependent (MFD) viscosity, for stress-free boundaries. Sunil et al. [213] have derived a nonlinear stability result for a double-diffusive magnetized ferrofluid layer rotating about a vertical axis for stress-free boundaries via generalized energy method.

The outline of this chapter is as follows. We begin by formulating a governing model for double diffusive convection with a dissolved reacting fluid and a vertically imposed magnetic field. We then find an instability bound for the linearized system and a global stability bound for the nonlinear system. Finally we introduce the numerical method used to solve our system, then we present and discuss the numerical results.

The results in this chapter have been published in the article Harfash [74].

4.2 Basic Equations

We suppose the fluid is contained in the plane layer $\{z \in (0, d)\} \times \mathbb{R}^2$, and is incompressible, although a Boussinesq approximation is employed in the buoyancy term in the momentum equation. The z direction is denoted by the vector k with i, j, k being the standard Cartesian basis. Gravity acts in the negative z direction and we assume that the density ρ is constant, everywhere except the body force. Then, the Navier-Stokes equation for the fluid motion are

$$\rho(v_{i,t} + v_j v_{i,j}) = -p_{,i} + \mu \Delta v_i + \rho k_i g(\alpha T - \alpha_c c) + \mathbf{j} \times \mathbf{B}, \quad (4.2.1)$$

where ρ, \mathbf{v}, p, c are the constant density, velocity field, pressure, and concentration of solute. Additionally, α and α_c are the thermal and salt expansion coefficients respectively, μ is the dynamic viscosity, g is gravity, $\mathbf{k} = (0, 0, 1)$, \mathbf{j} is the current, and \mathbf{B} is the magnetic induction field. Throughout, we use standard indicial notation and the Einstein summation convention so that e.g. $v_{i,t} = \partial v_i / \partial t$, and $p_{,i} = \partial p / \partial x_i$, $v_j v_{i,j} \equiv (\mathbf{v} \cdot \nabla) \mathbf{v}$, and Δ is the Laplacian. The balance of mass equation is

$$v_{i,i} = 0. \quad (4.2.2)$$

The heat equation governing the temperature field is defined as

$$T_{,t} + v_i T_{,i} = K\Delta T, \quad (4.2.3)$$

where T is the temperature field and K is the thermal diffusivity.

The equation governing the evaluation of the solute concentration is, cf., Hayat and Nawaz [80],

$$c_{,t} + v_i c_{,i} = D\Delta c - K_1 c. \quad (4.2.4)$$

Here $c(\mathbf{x}, t)$ is the solute concentration, D is the the solute diffusion coefficient, and K_1 is the chemical reaction rate.

Now, according to the quasi-static MHD approximation of Galdi and Straughan [61], we have

$$\mathbf{j} \times \mathbf{B} = \sigma_1(\mathbf{v} \times \mathbf{B}_0) \times \mathbf{B}_0, \quad (4.2.5)$$

where σ_1 is the electrical conductivity and $\mathbf{B}_0 = (0, 0, B_0)$ is a magnetic field with only the vertical component. We now employ (4.2.5) in (4.2.1). Thus, we find the equations for our model are

$$v_{i,t} + v_j v_{i,j} = -\frac{1}{\rho} p_{,i} + \nu \Delta v_i + g k_i (\alpha T - \alpha_c c) + \frac{B_0^2 \sigma_1}{\rho} [(\mathbf{v} \times \mathbf{k}) \times \mathbf{k}]_i, \quad (4.2.6)$$

$$v_{i,i} = 0, \quad (4.2.7)$$

$$T_{,t} + v_i T_{,i} = K\Delta T, \quad (4.2.8)$$

$$c_{,t} + v_i c_{,i} = D\Delta c - K_1 c, \quad (4.2.9)$$

where $\nu = \mu/\rho$. The model now consists of the six partial differential equations (4.2.6)-(4.2.9), on the boundaries $z = 0, d$ and the following boundary conditions are assumed to hold,

$$v_i = 0, \quad \text{at } z = 0, d; \quad c = c_U, T = T_U, \quad \text{at } z = d; \quad c = c_L, T = T_L, \quad \text{at } z = 0, \quad (4.2.10)$$

where c_U, c_L, T_U, T_L are constant.

Under these boundary conditions, our system admits the stationary solution whose stability we investigate, namely,

$$\begin{aligned}\bar{v}_i &\equiv 0, \\ \frac{d\bar{c}}{dz} &= -\frac{\Delta C}{d} f\left(\frac{z}{d}; \xi, \eta\right), \\ \bar{T} &= -H_1 \beta z + T_L, \\ \frac{d\bar{p}}{dz} &= -\rho g \alpha_c \bar{c} - \rho g \alpha \bar{T},\end{aligned}\tag{4.2.11}$$

where

$$\begin{aligned}f\left(\frac{z}{d}; \xi, \eta\right) &= \frac{\xi}{\sinh(\xi)} \{H_2 - \eta(1 - \cosh(\xi))\} \cosh\left(\xi \frac{z}{d}\right) - \xi \eta \sinh\left(\xi \frac{z}{d}\right), \\ \xi &= A_1 d, \quad A_1^2 = \frac{K_1}{D}, \quad \Delta C = |c_L - c_U|, \quad \Delta T = |T_L - T_U|, \quad \eta = \frac{c_L}{\Delta C}, \quad \beta = \frac{\Delta T}{d}, \\ H_1 &= \text{sign}(T_L - T_U), \quad H_2 = \text{sign}(c_L - c_U).\end{aligned}$$

To study the stability of (4.2.5)-(4.2.9), we introduce a perturbation (u_i, π, ϕ, θ) to the steady state solution $(\bar{v}_i, \bar{p}, \bar{c}, \bar{T})$, by

$$v_i = \bar{v}_i + u_i, \quad p = \bar{p} + \pi, \quad c = \bar{c} + \phi, \quad T = \bar{T} + \theta.$$

Using (4.2.11), the nonlinear perturbation equations have the form

$$\begin{aligned}u_{i,t} + u_j u_{i,j} &= -\frac{1}{\rho} \pi_{,i} + \nu \Delta u_i + g k_i (\alpha \theta - \alpha_c \phi) + \frac{B_0^2 \sigma_1}{\rho} [(\mathbf{u} \times \mathbf{k}) \times \mathbf{k}]_i, \\ \theta_t + u_i \theta_{,i} &= H_1 \beta w + K \Delta \theta, \\ \phi_t + u_i \phi_{,i} &= \frac{\Delta C}{d} f\left(\frac{z}{d}; \xi, \eta\right) w + D \Delta \phi - K_1 \phi,\end{aligned}\tag{4.2.12}$$

where u_i is solenoidal, i.e. $u_{i,i} = 0$.

These equations are conveniently non-dimensionalised with the variables

$$\begin{aligned}\mathbf{x} &= \mathbf{x}^* d, \quad t = t^* \frac{d^2}{\nu}, \quad \mathbf{u} = U \mathbf{u}^*, \quad \theta = T_\theta^\# \theta^*, \quad \phi = T_\phi^\# \phi^*, \quad \pi = P \pi^*, \\ U &= \frac{\nu}{d}, \quad P = \frac{\rho \nu^2}{d^2}, \quad T_\phi^\# = U \sqrt{\frac{\nu \Delta C}{D \alpha_c g d}}, \quad R_c = \sqrt{\frac{\alpha_c g d^3 \Delta C}{D \nu}}, \quad T_\theta^\# = U \sqrt{\frac{\nu \beta}{K \alpha g}}, \\ R_t &= \sqrt{\frac{\beta \alpha g d^4}{K \nu}}, \quad M = B_0 d \sqrt{\frac{\sigma}{\rho \nu}}, \quad P_s = \frac{\nu}{D}, \quad P_r = \frac{\nu}{K}.\end{aligned}$$

Here P_s and P_r is the Prandtl numbers and R_c and R_t is the Rayleigh numbers. Equations (4.2.12) in non-dimensional form (dropping stars) become,

$$\begin{aligned} u_{i,t} + u_j u_{i,j} &= -\pi_{,i} + \Delta u_i + k_i(R_t \theta - R_c \phi) + M^2[(\mathbf{u} \times \mathbf{k}) \times \mathbf{k}]_i, \\ P_r(\theta_t + u_i \theta_{,i}) &= H_1 R_t w + \Delta \theta, \\ P_s(\phi_t + u_i \phi_{,i}) &= R_c f(z; \xi, \eta) w + \Delta \phi - \xi^2 \phi. \end{aligned} \quad (4.2.13)$$

The spatial domain is now $\{(x, y) \in \mathbb{R}^2\} \times \{z \in (0, 1)\}$. These equations are to be solved together with the boundary conditions

$$\phi = \theta = u_i = 0, \quad \text{on } z = 0, 1, \quad (4.2.14)$$

together with the fact that the (x, y) behaviour of u_i, θ, ϕ, π satisfies a plane tiling periodic pattern, Chandrasekhar [32], Straughan [196]. In this study, we will discuss three cases:

1. $T_L > T_U, c_L > c_U$, i.e. heating below and salting below, $H_1 = +1$ and $H_2 = +1$.
2. $T_L < T_U, c_L > c_U$, i.e. heating above and salting below, $H_1 = -1$ and $H_2 = +1$.
3. $T_L > T_U, c_L < c_U$, i.e. heating below and salting above, $H_1 = +1$ and $H_2 = -1$.

It should be point out that when $\xi \rightarrow 0$ and thus $f(z) \rightarrow H_2$ and if the layer is salty above and heated below, then both are destabilizing, and the linearized system is symmetric, therefore, the linear and the nonlinear boundaries coincide and no sub-critical instabilities can occur. However, if the layer is salted below, which is a stabilizing effect, while the layer is heated from below, which is a destabilizing effect, thus, there are two physical effects are competing against each other. Due to this competition, it means that the linear theory of instability does not always capture the physics of instability completely and sub-critical instabilities may arise before the linear threshold is reached. Due to the possibility of sub-critical instabilities occurring, it is very important to obtain nonlinear stability thresholds which

guarantee bounds below which convective overturning will not occur.

4.3 Linear instability

Linear instability results for stationary convection are obtained via the application of standard procedures to the linearized version of (4.2.13). To find the critical Rayleigh number of linear theory, we neglect the nonlinear terms in (4.2.13) and assume a temporal growth rate like $e^{\sigma t}$, thus we obtain the linearised system

$$\begin{aligned} -\pi_{,i} + \Delta u_i + k_i(R_t\theta - R_c\phi) + M^2[(\mathbf{u} \times \mathbf{k}) \times \mathbf{k}]_i &= \sigma u_i, \\ H_1 R_t w + \Delta\theta &= \sigma P_r \theta, \\ R_c f(z; \xi, \eta)w + \Delta\phi - \xi^2\phi &= \sigma P_s \phi. \end{aligned} \quad (4.3.15)$$

To eliminate the pressure in (4.3.15)₁, we take the *curlcurl* of both sides. Then, setting $i = 3$ we obtain

$$\Delta^2 w + (R_t \Delta^* \theta - R_c \Delta^* \phi) - M^2 D^2 w = \sigma \Delta w, \quad (4.3.16)$$

where Δ^* is the horizontal Laplacian $\Delta^* = \partial^2/\partial x^2 + \partial^2/\partial y^2$, $D = d/dz$.

Assuming a normal mode representation for w, θ and ϕ of the form $w = W(z)h(x, y)$, $\theta = \Theta(z)h(x, y)$ and $\phi = \Phi(z)h(x, y)$ where $h(x, y)$ is some horizontal plan form satisfying

$$\Delta^* h = -a^2 h. \quad (4.3.17)$$

The plan-forms represent the horizontal shape of the convection cells formed at the onset of instability. These cells form a regular horizontal pattern tiling the (x, y) plane, where the wavenumber a (see [32]) is a measure of the width of the convection cell. Using (4.3.17), and applying the normal mode representations to (4.3.15)₂, (4.3.15)₃ and (4.3.16) we find

$$\begin{aligned} (D^2 - a^2)^2 W - a^2(R_t \Theta - R_c \Phi) - M^2 D^2 W &= \sigma(D^2 - a^2)W, \\ (D^2 - a^2)\Theta + H_1 R_t W &= \sigma P_r \Theta, \\ (D^2 - a^2)\Phi - \xi^2 \Phi + R_c f(z; \xi, \eta)W &= \sigma P_s \Phi, \end{aligned} \quad (4.3.18)$$

where the boundary conditions become

$$\Theta = \Phi = W = DW = 0, \quad z = 0, 1, \quad (4.3.19)$$

for fixed surface and

$$\Theta = \Phi = W = D^2W = 0, \quad z = 0, 1, \quad (4.3.20)$$

for free surface. System (4.3.18) and (4.3.19) or (4.3.20) is solved using the finite difference (FD) method. Detailed numerical results are reported in section 6. We can now determine the critical Rayleigh number given $Ra_L = \min_{a^2} R_t^2(a^2)$, such that $\sigma(R_t) = 0$ where for all $R^2 > Ra_L$ we have instability. In section 6 we will introduce specific details about the algorithm which we use in evaluation the Rayleigh numbers.

Although the linear analysis has been completed numerically, it is possible to use analytic methods to provide a general idea about the stationary and oscillatory neutral lines. In the linear instability analysis, the values of Prandtl numbers play a crucial role in determine where the linear curve is an oscillatory curve or stationary curve. Thus, it is useful to obtain an analytic solution for the problem. Before we start with analytic analysis we suppose that $M^2 = 0, \eta = 0$ and $\xi \rightarrow 0$, thus $f(z) \rightarrow 1$. Now, we can discuss the analytic analysis because the function $f(z)$ are removed. Note that without this assumptions it is impossible to establish the analytic solution, and we can get this solution just for two free boundaries i.e. we will solve analytically system (4.3.18) with respect to the boundary conditions (4.3.20). Moreover, according to our numerical results, we note that case 2 is always stable and in case 3, we found that $\sigma \in \mathbb{R}$. Thus, we discuss just case 1, i.e. $H_1 = +1$ and $H_2 = +1$. Now, according to the above assumptions, our system can be simplified to the following form

$$\begin{aligned} \sigma(D^2 - a^2)W &= (D^2 - a^2)^2W - a^2(R_t\Theta - R_c\Phi), \\ \sigma P_r\Theta &= (D^2 - a^2)\Theta + R_tW, \\ \sigma P_s\Phi &= (D^2 - a^2)\Phi + R_cW. \end{aligned} \quad (4.3.21)$$

Hence, letting $\mathfrak{L}_1 = (D^2 - a^2) - \sigma P_r$ and $\mathfrak{L}_2 = (D^2 - a^2) - \sigma P_s$, Thus, from (4.3.18)₂ and (4.3.18)₃ we have

$$\mathfrak{L}_1 \Theta = (D^2 - a^2)\Theta - \sigma P_r \Theta = -R_t W, \quad (4.3.22)$$

and

$$\mathfrak{L}_2 \Phi = (D^2 - a^2)\Phi - \sigma P_r \Phi = -R_c W. \quad (4.3.23)$$

Now, re-applying \mathfrak{L}_1 and \mathfrak{L}_2 to (4.3.18)₁ to get

$$\sigma \mathfrak{L}_1 \mathfrak{L}_2 (D^2 - a^2)W = \mathfrak{L}_1 \mathfrak{L}_2 (D^2 - a^2)^2 W + a^2 R_t^2 \mathfrak{L}_2(W) - a^2 R_c^2 \mathfrak{L}_1(W). \quad (4.3.24)$$

After make simple calculation we have

$$\begin{aligned} & \sigma (D^2 - a^2 - \sigma P_s)(D^2 - a^2 - \sigma P_r)(D^2 - a^2)W \\ &= (D^2 - a^2 - \sigma P_s)(D^2 - a^2 - \sigma P_r)(D^2 - a^2)^2 W \\ &+ a^2 R_t^2 (D^2 - a^2 - \sigma P_s)W - a^2 R_c^2 (D^2 - a^2 - \sigma P_r)W. \end{aligned} \quad (4.3.25)$$

Because of the boundary conditions $W = 0$, $D^2 W = 0$ on $z = 0, 1$ (non-dimensional boundaries), then W can be expanded as a *sine* series of terms like $\sin(n\pi z)$. In fact, we can show $n = 1$ yields the lowest instability boundary. Then, with $\Lambda = \pi^2 + a^2$, a being a wavenumber, from system (4.3.25) we derive

$$\begin{aligned} & -\sigma \Lambda^3 - \sigma^2 (P_r + P_s) \Lambda^2 - \sigma^3 \Lambda P_r P_s \\ &= \Lambda^4 + \sigma (P_r + P_s) \Lambda^3 + \sigma^2 \Lambda^2 P_r P_s + a^2 (R_c^2 - R_t^2) \Lambda + a^2 (P_r R_c^2 - P_s R_t^2) \sigma. \end{aligned} \quad (4.3.26)$$

The stationary convection curve ($\sigma = 0$) is then given by

$$R_t^2 = \frac{\Lambda^3}{a^2} + R_c^2. \quad (4.3.27)$$

Then we minimize (4.3.27) with respect to a^2 thus we have $a_c^2 = \pi^2/2$. Substituting this a^2 value into (4.3.27) we can evaluate

$$Ra_L = \frac{27}{4} \pi^4 + R_c^2. \quad (4.3.28)$$

For the general case (4.3.26) we put ($\sigma = \sigma_r + i\sigma_i$) and the instability boundary is found when $\sigma_r = 0$. Thus, we follow the method of Chandrasekhar [32], P.114, and

put $\sigma = i\sigma_i$ in (4.3.26). Taking real and imaginary parts of the resulting equation and then eliminating σ_i^2 we derive the equation for overstability,

$$R_t^2 = \frac{\Lambda^3 (1 - P_s P_2)}{a^2 (1 - P_s P_1)} + R_c^2 \frac{(1 - P_r P_1)}{(1 - P_s P_1)}, \quad (4.3.29)$$

where $P_1 = ((P_r + P_s)/P_r P_s) + 1$ and $P_2 = P_r + P_s + 1$. Now we minimize (4.3.29) with respect to a^2 we find that $a_c^2 = \pi^2/2$ and

$$Ra_L = \frac{27\pi^4 (1 - P_s P_2)}{4 (1 - P_s P_1)} + R_c^2 \frac{(1 - P_r P_1)}{(1 - P_s P_1)}. \quad (4.3.30)$$

4.4 Nonlinear energy stability theory

Linear instability analysis provides a boundary for which all R^2 greater than the critical Rayleigh number in instability, where no assumptions can be made about stability when R^2 is below this boundary, as the solution may become unstable before the threshold predicted by the linear theory is reached. A nonlinear energy analysis produces stability boundaries with our aim being to show that these thresholds are close enough to those of linear theory, so that we can conclude that linear instability theory effectively captures the physics of the onset of convection.

Let V be a period cell for a disturbance to (4.2.13), and let $\|\cdot\|$ and (\cdot, \cdot) be the norm and inner product on $L^2(V)$. We derive energy identities by multiplying (4.2.13)₁ by u_i and integrating over V , and (4.2.13)₂ by ϕ and integrating over V , to find

$$\frac{1}{2} \frac{d}{dt} \|\mathbf{u}\|^2 = -\|\nabla \mathbf{u}\|^2 + R_t(w, \theta) - R_c(w, \phi) - M^2[\|\mathbf{u}\|^2 - \|w\|^2], \quad (4.4.31)$$

$$\frac{P_r}{2} \frac{d}{dt} \|\theta\|^2 = H_1 R_t(w, \theta) - \|\nabla \theta\|^2, \quad (4.4.32)$$

$$\frac{P_s}{2} \frac{d}{dt} \|\phi\|^2 = R_c(f(z)w, \phi) - \xi^2 \|\phi\|^2 - \|\nabla \phi\|^2. \quad (4.4.33)$$

We introduce positive parameters λ_1 and λ_2 , and define

$$\begin{aligned} E(t) &= \frac{1}{2} \|\mathbf{u}\|^2 + \frac{\lambda_1 P_r}{2} \|\theta\|^2 + \frac{\lambda_2 P_s}{2} \|\phi\|^2, \\ \mathcal{D} &= \lambda_2 \xi^2 \|\phi\|^2 + \lambda_1 \|\nabla \theta\|^2 + \lambda_2 \|\nabla \phi\|^2 + \|\nabla \mathbf{u}\|^2 + M^2[\|u\|^2 + \|v\|^2], \\ \mathcal{I} &= R_t(w, \theta) - R_c(w, \phi) + H_1 \lambda_1 R_t(w, \theta) + \lambda_2 R_c(f(z)w, \phi), \end{aligned} \quad (4.4.34)$$

where \mathbf{u} is explicitly written as $\mathbf{u} = (u, v, w)$. From (4.4.31), (4.4.32) and (4.4.34) we derive

$$\begin{aligned}\frac{dE}{dt} &= \mathcal{I} - \mathcal{D}, \\ \frac{dE}{dt} &\leq -\mathcal{D}\left(1 - \frac{1}{R_E}\right),\end{aligned}$$

where $1/R_E = \max_{\mathcal{H}}(\mathcal{I}/\mathcal{D})$ and H is the space of admissible functions, namely

$$\mathcal{H} = \{u_i, \theta, \phi \in C^2(0, 1) : \theta = \phi = w = Dw = 0, \quad z = 0, 1.\}$$

For fixed surface and the same space for free surface with $D^2w = 0$ instead of $Dw = 0$. If $R_E > 1$ then with χ_1 being the constant in Poincaré's inequality, it follows that $\mathcal{D} > cE$ where $c = \min\{2\chi_1, 2(\chi_1 + \xi^2)P_s^{-1}, 2\chi_1P_r^{-1}\}$. Hence it follows that

$$\frac{dE}{dt} \leq -cE\left(\frac{R_E - 1}{R_E}\right).$$

Thus, letting $\epsilon = c(R_E - 1)/R_E$ we have $E(t) \leq E(0)e^{-\epsilon t}$ which tends to 0 as $t \rightarrow \infty$, so we have shown the decay of ϕ, θ and \mathbf{u} . We now turn our attention to the maximisation problem $1/R_E = \max_{\mathcal{H}}(\mathcal{I}/\mathcal{D})$ with $R_E > 1$. We do this for the threshold case $R_E = 1$ which yields the sharpest stability boundary. To solve the maximisation problem we study the Euler Lagrange equations. The Euler Lagrange equations are found from

$$R_E \delta \mathcal{I} - \delta \mathcal{D} = 0. \quad (4.4.35)$$

let χ, ϑ and ψ be arbitrary, fixed $C^2(0, 1)$ functions which satisfy the boundary conditions. We now consider neighbouring function $u_i = u_i + \epsilon \eta(x_j)$, $\theta = \theta + \epsilon \vartheta(x_j)$ and $\phi = \phi + \epsilon \psi(x_j)$, Hence

$$\begin{aligned}\delta \mathcal{D} &= \frac{d}{d\epsilon} [\|\nabla \mathbf{u} + \epsilon \nabla \eta\|^2 + M^2 \|\mathbf{u} + \epsilon \eta\|^2 - M^2 \|w + \epsilon \eta_3\|^2 + \lambda_1 \|\nabla \theta + \epsilon \nabla \vartheta\|^2 \\ &\quad + \lambda_2 \|\nabla \phi + \epsilon \nabla \psi\|^2 + \lambda_2 \xi^2 \|\phi + \epsilon \psi\|^2]_{\epsilon=0}\end{aligned}$$

$$= \langle -2\Delta u_i + 2M^2 u_i - 2k_i M^2 w, \eta_i \rangle + \langle -2\lambda_1 \Delta \theta, \vartheta \rangle + \langle 2\lambda \xi^2 \phi - 2\lambda_2 \Delta \phi, \psi \rangle,$$

and

$$\begin{aligned}
\delta\mathcal{I} &= \frac{d}{d\varepsilon} [R_t \langle w + \varepsilon\eta_3, \theta + \varepsilon\vartheta \rangle + H_1 \lambda_1 R_t \langle w + \varepsilon\eta_3, \theta + \varepsilon\vartheta \rangle \\
&\quad - R_c \langle w + \varepsilon\eta_3, \phi + \varepsilon\psi \rangle + \lambda_2 R_c \langle f(z)(w + \varepsilon\eta_3), \phi + \varepsilon\psi \rangle]_{\varepsilon=0} \\
&= \langle -R_c k_i \phi + \lambda_2 R_c k_i f(z)\phi + R_t k_i \theta + H_1 \lambda_1 R_t k_i \theta, \eta_i \rangle \\
&\quad + \langle R_t w + H_1 \lambda_1 R_t w, \vartheta \rangle + \langle -R_c w + \lambda_2 R_c f(z)w, \psi \rangle.
\end{aligned}$$

Thus, the Euler lagrange equations which arise from the variational problem $1/R_E = \max_{\mathcal{H}}(\mathcal{I}/\mathcal{D})$ can write as:

$$\begin{aligned}
&- R_t k_i \theta - H_1 \lambda_1 R_t k_i \theta + R_c k_i \phi - \lambda_2 R_c k_i f(z)\phi - 2\Delta u_i + 2M^2 u_i - 2k_i M^2 w = -\pi_{,i}, \\
&R_t w + H_1 \lambda_1 R_t w + 2\lambda_1 \Delta \theta = 0, \\
&- R_c w + \lambda_2 R_c f(z)w - 2\lambda_2 \xi^2 \phi + 2\lambda_2 \Delta \phi = 0,
\end{aligned} \tag{4.4.36}$$

where π is a lagrange multiplier. To remove the lagrange multiplier we Take the third component of the double *curl* of (4.4.36)₁, and introducing the normal mode representation and notation as presented in section 3, thus (4.4.36) then becomes

$$\begin{aligned}
(D^2 - a^2)^2 W - M^2 D^2 W + (1 - \lambda_2 f(z)) \frac{a^2}{2} R_c \Phi &= \frac{a^2 R_t}{2} (1 + H_1 \lambda_1) \Theta, \\
(D^2 - a^2) \Theta &= -\frac{R_t}{2} \left(\frac{1}{\lambda_1} + H_1 \right) W, \\
(D^2 - a^2) \Phi - \xi^2 \Phi - \frac{R_c}{2\lambda_2} (1 - \lambda_2 f(z)) W &= 0.
\end{aligned} \tag{4.4.37}$$

We can now determine the critical Rayleigh number given by

$$Ra_E = \max_{\lambda_1 \lambda_2} \min_{a^2} R_t^2(a^2, \lambda),$$

where for all $R_t^2 < Ra_E$ we have stability.

4.5 Numerical method

In this section we will discuss the finite element method which is used to solve systems (4.3.18) and (4.4.37). We shall explain how the linear system have been solved and then the solution of the nonlinear system follows directly using the same argument. Firstly, we introduce a new variable $A = D^2 W$, Therefore, system (4.3.18)

become as follows

$$\begin{aligned}
D^2W &= A, \\
D^2A - (2a^2 + M^2)A + a^4W - a^2(R_t\Theta - R_c\Phi) &= \sigma(A - a^2W), \\
(D^2 - a^2)\Theta + H_1R_tW &= \sigma P_r\Theta, \\
(D^2 - a^2)\Phi - \xi^2\Phi + R_c fW &= \sigma P_s\Phi.
\end{aligned} \tag{4.5.38}$$

For free surface the boundary conditions will be $W = A = \Theta = \Phi = 0$, while for fixed surface the situation require careful treatment and we shall deal with this treatment after introducing the finite element approximation.

Firstly, we divided the period $0 \leq x \leq 1$ into n elements, each element e having $p+1$ nodes n_1, n_2, \dots, n_{p+1} . In term of its $p+1$ nodal values, the variables W, A, Θ, Φ may be uniquely interpolated as a polynomial of $p+1$ order, the interpolation being given by

$$W^e = N^e \delta_W^e, \quad A^e = N^e \delta_A^e, \quad \Theta^e = N^e \delta_\Theta^e, \quad \Phi^e = N^e \delta_\Phi^e, \tag{4.5.39}$$

where $\delta_W^e = \{W_{n_1}, W_{n_2}, \dots, W_{n_{p+1}}\}$, $\delta_A^e = \{A_{n_1}, A_{n_2}, \dots, A_{n_{p+1}}\}$, $\delta_\Theta^e = \{\Theta_{n_1}, \Theta_{n_2}, \dots, \Theta_{n_{p+1}}\}$ and $\delta_\Phi^e = \{\Phi_{n_1}, \Phi_{n_2}, \dots, \Phi_{n_{p+1}}\}$, and the shape function matrix is

$$N^e = [N_{n_1}^p, N_{n_2}^p, \dots, N_{n_{p+1}}^p].$$

Therefore the over-all finite element approximation is given by

$$W = \sum_{e=1}^n W^e, \quad A = \sum_{e=1}^n A^e, \quad \Theta = \sum_{e=1}^n \Theta^e, \quad \Phi = \sum_{e=1}^n \Phi^e. \tag{4.5.40}$$

The variational formulations of (4.5.38) is

$$\text{Minimize } I_W[W] = \int_0^1 (-(DW)^2 - 2AW) dx, \tag{4.5.41}$$

$$\begin{aligned}
\text{Minimize } I_A[A] &= \int_0^1 (-(DA)^2 - (2a^2 + M^2)A^2 + 2a^4WA - 2a^2(R_t\Theta A - R_c\Phi A) \\
&\quad - \sigma(A^2 - 2a^2WA)) dx,
\end{aligned} \tag{4.5.42}$$

$$\text{Minimize } I_\Theta[\Theta] = \int_0^1 (-(D\Theta)^2 - a^2\Theta^2 + 2H_1R_tW\Theta - \sigma P_r\Theta^2) dx, \tag{4.5.43}$$

$$\text{Minimize } I_\Phi[\Phi] = \int_0^1 (-(D\phi)^2 - (a^2 + \xi^2)\Phi^2 + 2R_c fW\Phi - \sigma P_s\Phi^2) dx. \tag{4.5.44}$$

Substitution of (4.5.40) into variational formulations (4.5.41)-(4.5.44) gives

$$I_W[W] = \sum_{e=1}^n \int_e (-(DW^e)^2 - 2A^e W^e) dx = \sum_{e=1}^n I_W^e, \quad (4.5.45)$$

$$I_A[A] = \sum_{e=1}^n \int_e (-(DA^e)^2 - (2a^2 + M^2)(A^e)^2 + 2a^4 W^e A^e - 2a^2 (R_t \Theta^e A - R_c \Phi^e A) - \sigma((A^e)^2 - 2a^2 W^e A^e)) dx = \sum_{e=1}^n I_A^e, \quad (4.5.46)$$

$$I_\Theta[\Theta] = \sum_{e=1}^n \int_e (-(D\Theta^e)^2 - a^2(\Theta^e)^2 + 2H_1 R_t W^e \Theta^e - \sigma P_r(\Theta^e)^2) dx = \sum_{e=1}^n I_\Theta^e, \quad (4.5.47)$$

$$I_\Phi[\Phi] = \sum_{e=1}^n \int_e (-(D\phi^e)^2 - (a^2 + \xi^2)(\Phi^e)^2 + 2R_c f W^e \Phi^e - \sigma P_s(\Phi^e)^2) dx = \sum_{e=1}^n I_\Phi^e, \quad (4.5.48)$$

here, we use the fact that the functions $W^e, A^e, \theta^e, \phi^e$ are equivalent to zero outside the element e . Using (4.5.45), (4.5.46), (4.5.47) and (4.5.48) we obtain

$$I_W[W] = I_W(W_1, W_2, \dots, W_m),$$

$$I_A[A] = I_A(A_1, A_2, \dots, A_m),$$

$$I_\Theta[\Theta] = I_\Theta(\Theta_1, \Theta_2, \dots, \Theta_m),$$

$$I_\Phi[\Phi] = I_\Phi(\Phi_1, \Phi_2, \dots, \Phi_m),$$

where m is the number of all nodes in all elements. Then using the Rayleigh-Ritz procedure to minimize $I_W[W], I_A[A], I_\Theta[\Theta], I_\Phi[\Phi]$, with respect to the variational parameters $W_i, A_i, \Theta_i, \Phi_i$ respectively, gives

$$\frac{\partial I_W}{\partial W_i} = \sum_{e=1}^n \frac{\partial I_W^e}{\partial W_i} = 0, \quad i = 1, \dots, m, \quad (4.5.49)$$

$$\frac{\partial I_A}{\partial A_i} = \sum_{e=1}^n \frac{\partial I_A^e}{\partial A_i} = 0, \quad i = 1, \dots, m, \quad (4.5.50)$$

$$\frac{\partial I_\Theta}{\partial \Theta_i} = \sum_{e=1}^n \frac{\partial I_\Theta^e}{\partial \Theta_i} = 0, \quad i = 1, \dots, m, \quad (4.5.51)$$

$$\frac{\partial I_\Phi}{\partial \Phi_i} = \sum_{e=1}^n \frac{\partial I_\Phi^e}{\partial \Phi_i} = 0, \quad i = 1, \dots, m. \quad (4.5.52)$$

Using (4.5.39), (4.5.49), (4.5.50), (4.5.51) and (4.5.52), we have

$$\frac{\partial I_W^e}{\partial W_{n_i}} = -2 \int_e \frac{dN_{n_i}^p}{dz} \frac{dN^e}{dz} \delta_W^e dx - 2 \int_e N_{n_i}^p N^e \delta_A^e dx = 0, \quad (4.5.53)$$

$$\begin{aligned} \frac{\partial I_A^e}{\partial A_{n_i}} &= 2a^4 \int_e N_{n_i}^p N^e \delta_W^e dx - 2 \int_e \left(\frac{dN_{n_i}^p}{dz} \frac{dN^e}{dz} + (2a^2 + M^2) N_{n_i}^p N^e \right) \delta_A^e dx \\ -2a^2 R_t \int_e N_{n_i}^p N^e \delta_\Theta^e dx &+ 2a^2 R_c \int_e N_{n_i}^p N^e \delta_\Phi^e dx - 2\sigma \int_e [N_{n_i}^p N^e \delta_A^e - 2a^2 N_{n_i}^p N^e \delta_W^e] dx = 0, \end{aligned} \quad (4.5.54)$$

$$\begin{aligned} \frac{\partial I_\Theta^e}{\partial \Theta_{n_i}} &= -2 \int_e \left(\frac{dN_{n_i}^p}{dz} \frac{dN^e}{dz} + a^2 N_{n_i}^p N^e \right) \delta_\Theta^e dx \\ + 2H_1 R_t \int_e N_{n_i}^p N^e \delta_W^e dx &- 2P_r \sigma \int_e N_{n_i}^p N^e \delta_\Theta^e dx = 0, \end{aligned} \quad (4.5.55)$$

$$\begin{aligned} \frac{\partial I_\Phi^e}{\partial \Phi_{n_i}} &= -2 \int_e \left[\frac{dN_{n_i}^p}{dz} \frac{dN^e}{dz} + (a^2 + \xi^2) N_{n_i}^p N^e \right] \delta_\Phi^e dx \\ + 2R_c \int_e f N_{n_i}^p N^e \delta_W^e dx &- 2P_s \sigma \int_e N_{n_i}^p N^e \delta_\Phi^e dx = 0. \end{aligned} \quad (4.5.56)$$

Then, the matrix representation for the system of equation of element e take the form

$$\begin{aligned} &\begin{pmatrix} -D_2^e & -F_1^e & O & O \\ a^4 F_1^e & -D_2^e - (2a^2 + M^2) F_1^e & -a^2 R_t F_1^e & a^2 R_c F_1^e \\ H_1 R_t F_1^e & O & -D_2^e - a^2 F_1^e & O \\ R_c F_2^e & O & O & -D_2^e - (a^2 + \xi^2) F_1^e \end{pmatrix} \begin{pmatrix} \delta_W^e \\ \delta_A^e \\ \delta_\Theta^e \\ \delta_\Phi^e \end{pmatrix} \\ &= \sigma \begin{pmatrix} O & O & O & O \\ -a^2 F_1^e & F_1^e & O & O \\ O & O & P_r F_1^e & O \\ O & O & O & P_s F_1^e \end{pmatrix} \begin{pmatrix} \delta_W^e \\ \delta_A^e \\ \delta_\Theta^e \\ \delta_\Phi^e \end{pmatrix}, \end{aligned} \quad (4.5.57)$$

where

$$\begin{aligned} O_{ij} &= 0, \quad D_{2ij}^e = \int_{-1}^1 \frac{dN_{n_i}^p}{dz} \frac{dN_{n_j}^p}{dz} dz, \quad F_{1ij}^e = \int_{-1}^1 N_{n_i}^p N_{n_j}^p dz, \\ F_{2ij}^e &= \int_{-1}^1 f(z) N_{n_i}^p N_{n_j}^p dz, \quad i = 1, \dots, p+1, \quad j = 1, \dots, p+1. \end{aligned}$$

The above integral can be evaluated by applying the classical finite element nodal

basis functions in one dimension on the standard element $\Omega_{st} = (-1, 1)$. The standard shape functions are defined by the set of Lagrange polynomials

$$N_{n_i}^p(\zeta) = \prod_{j=n_1, j \neq i}^{n_{p+1}} \frac{\zeta - \zeta_j}{\zeta_i - \zeta_j}, \quad (4.5.58)$$

where $\zeta = 2/h(z - z_m)$, h is the length of element and z_m is the mid-point. Thus these integrations take the form:

$$D_{2ij}^e = \frac{2}{h} \int_{-1}^1 \frac{dN_{n_i}^p}{d\zeta} \frac{dN_{n_j}^p}{d\zeta} d\zeta,$$

$$F_{1ij}^e = \frac{h}{2} \int_{-1}^1 N_{n_i}^p N_{n_j}^p d\zeta,$$

$$F_{2ij}^e = \frac{h}{2} \int_{-1}^1 f\left(\frac{h}{2}\zeta + z_m\right) N_{n_i}^p N_{n_j}^p d\zeta,$$

$$i = 1, \dots, p+1, \quad j = 1, \dots, p+1.$$

All these integrals were calculated analytically using Matlab routines. Finally, we assemble the systems of all elements $e = 1, \dots, n$ to get the main system which have the form

$$A\mathbf{x} = \sigma B\mathbf{x}, \quad (4.5.59)$$

where $\mathbf{x} = (W_1, \dots, W_m, A_1, \dots, A_m, \Theta_1, \dots, \Theta_2, \Phi_1, \dots, \Phi_m)^T$.

For free surface boundary conditions, we imposing the boundary conditions easily by removing $W_1, W_m, A_1, A_m, \Theta_1, \Theta_2, \Phi_1, \Phi_m$ from the system and thus we remove the rows and columns of order $1, m, m+1, 2m, 2m+1, 3m, 3m+1$ and $4m$. However, for fixed boundary conditions, we change the conditions $DW = 0$ at $z = 0, 1$, to another conditions related with new function A . To do this, let the first element is $[0, a]$ and the last element is $[b, 1]$. Firstly, we integrate (4.5.38)₁ for first and the last elements and use the boundary conditions, to arrive to the following conditions

$$DW^1(a) = \int_0^a A^1 dx, \quad (4.5.60)$$

$$-DW^n(b) = \int_b^1 A^n dx, \quad (4.5.61)$$

where 1, n refer to the first and the last element. Next, we transform equations (4.5.60) and (4.5.61) to the local coordinate ζ and use (4.5.39) to obtain

$$\frac{2}{h} \frac{dN(1)}{d\zeta} \delta_W^1 = \frac{h}{2} \int_{-1}^1 N(\zeta) \delta_A^1 d\zeta, \quad (4.5.62)$$

$$-\frac{2}{h} \frac{dN(-1)}{d\zeta} \delta_W^n = \frac{h}{2} \int_{-1}^1 N(\zeta) \delta_A^n d\zeta. \quad (4.5.63)$$

Now, let $d_i = dN_i(1)/d\zeta$, $e_i = \int_{-1}^1 N_i(\zeta) d\zeta$, and $f_i = dN_i(-1)/d\zeta$. In addition, suppose that the nodes for the first element and for the last element have the order 1, 2, ..., $p+1$ and $m-p, m-p+1, \dots, m$, respectively. Then, (4.5.62) and (4.5.64) lead to the following computational conditions

$$A_1 = \frac{4}{h^2 e_1} [d_2 W_2 + \dots + d_{p+1} W_{p+1}] - \frac{1}{e_1} [e_2 A_2 + \dots + e_{p+1} A_{p+1}], \quad (4.5.64)$$

$$A_m = -\frac{4}{h^2 e_{p+1}} [f_1 W_{m-p} + f_2 W_{m-p+1} + \dots + f_p W_{m-1}] - \frac{1}{e_{p+1}} [e_1 A_{m-p} + \dots + e_p A_{m-1}]. \quad (4.5.65)$$

Now, we substitute the values of A_1 and A_m in (4.5.59) thus the columns of order $m+1$ and $2m$ will be zeros. Now, we can remove the rows and columns of order 1, $m, m+1, 2m, 2m+1, 3m, 3m+1$ and $4m$.

4.6 Results and conclusions

In this section we report our numerical solution of the linear instability and the nonlinear energy theory. Firstly, we have checked convergence and found that convergence to 8 decimal places is achieved with 2 elements and each element have 10 nodes for two free-free boundary conditions, while for fixed-fixed boundary conditions the convergence to 8 decimal places can be achieved using 3 elements and each element have 11 nodes. It should be point out that we use the finite element method to solve our problem because it is very flexible especially for problems which have variable coefficients and give very accurate result. Moreover, the finite element has a fast convergence to the required results.

We found that when the layer is heated above and salty below system (4.2.13) is always stable. For the case of the layer is salty above and heated below i.e. $H_1 = +1$

and $H_2 = -1$, the spectrum σ is found numerically to be always real. In the case of the layer is salty below and heated below i.e. $H_1 = +1$ and $H_2 = +1$, the linear analysis stability is more difficult because it include an oscillatory convection. We found that the values of wave numbers for oscillatory convection are very close to the values of wave numbers for stationary convection, thus the computations of the critical Rayleigh numbers will be difficult especially in the period around the intersection points.

For the case of the layer is salty below and heated below, we present in Figures 4.1 and 4.2 the critical Rayleigh number R_a against R_c^2 for fixed-fixed and free-free boundary conditions, respectively, for $M^2 = 0$ and $\eta = 0$ $\xi = 10^{-10}, 1, 2, 3$. The picture of nonlinear energy bound with the linear curves in these figures is a classical picture for double diffusive convection. These Figures show the effect of increasing ξ on oscillatory and steady convection, where as ξ increase, the switching of convection from steady to oscillatory will be late. Figure 4.3 present the critical Rayleigh number R_a against R_c but with different values ξ, η, M^2 , where the new values are $\xi = 1, \eta = 1$ and $M^2 = 30, 60, 90$. Figure 4.3 demonstrates that Ra increases with increasing M^2 which shows the stabilizing effect of the magnetic field. In addition, figures 4.1, 4.2 and 4.3 show that the subcritical instability regions become bigger with increasing R_c , and this is to be expected for classical double diffusive convection. Also, figures 4.1, 4.2 and 4.3 show that the switching of convection from steady to oscillatory for free-free boundary conditions occurs before the switching for fixed-fixed boundary conditions. Thus the switching do not occurs in the same point, and this is very important because many researchers make an analytic test to their system with free-free boundary conditions to see where the switching occurs.

Again, for the case of the layer is salty below and heated below, figures 4.4 and 4.5 present the critical Rayleigh number R_a against M^2 with $\xi = \eta = 1$, for fixed-fixed and free-free boundary conditions. As we mention above, the switching of convection occurs for the free-free boundary conditions before the fixed-fixed boundary conditions according to the R_c values, thus, for fixed-fixed boundary conditions we select $R_c = 30, 35, 40, 45$, while for free-free boundary conditions we select

$R_c = 25, 30, 35, 40$. It is very clear the stabilizing effect of the magnetic field where the values of Ra increases with increasing M^2 . The distance between the energy and linear bound increases with increasing R_c , thus with large values of R_c we have wide subcritical regions. Note that as R_c increases the nonlinearity of the linear curves decreases. The very important point in these figures is that the oscillatory convection appears before the stationary convection. This happen because we have two competitive effects, the magnetic field effect M^2 which have stabilizing effect and R_c effect which have destabilizing effect. Thus, when the the values of M^2 are small such that the destabilizing effect of R_c is stronger than the stabilizing effect of M^2 , we expected that the convection will be oscillatory and as M^2 increase the convection will be very close to the stationary. For example, in figure 4.4 when $R_c = 30$ the switching of convection from oscillatory to stationary occurs in the period $M^2 \in (20, 25)$, while with $R_c = 45$ the switching appear in the period $M^2 \in (225, 230)$.

In figure 4.6 and 4.7 we plot the critical Rayleigh number R_a against M^2 and R for $\eta = 2, 4, 6$ and fixed-fixed and free-free boundary conditions. We select the values of parameters such that oscillatory convection do not occurs for the case $H_1 = H_2 = +1$. This is because we wish to make a comparison between the two cases $H_1 = H_2 = +1$ and $H_1 = +1, H_2 = -1$. Figures 4.6 and 4.7 *a, b* present R_a against M^2 with $\xi = 2$ and $R_c = 15$, while Figures 4.6 and 4.7 *c, d* present R_a against R_c with $\xi = 2$ and $M^2 = 50$. Again, for both cases it is clear the stabilizing effect of M^2 and destabilizing effect of η and R_c . Also, we note that the system for the case of the layer is salty above and heated below is more stable than the case of the layer is salty below and heated below.

Finally, figure 4.8 present critical Rayleigh number R_a against ξ for $M^2 = 50$, $R_c = 15$, $H_1 = H_2 = +1$ and $\eta = 2, 4, 6$ for fixed-fixed boundary conditions. Again, We select $P_r = P_s = 1$, such that oscillatory convection do not occurs. We note that how increasing ξ corresponds, in general, to destabilizing. The linear critical Rayleigh numbers always decrease with increasing ξ . The nonlinear critical Rayleigh number start with $R_a = 2801.657676$ for all η , then in the period $0 < \xi < 4$, the

value of R_a decrease with decreasing ξ . Next, for $\xi > 4$, the value of R_a increase with increasing ξ until they arrive to the starting value $R_a = 2801.657676$ for large value of ξ . It is very clear that this decreasing and increasing has a different values according to the values of η .

Finally, we should mention that in this study the stability analyses on this problem have yield regions of potential subcritical instabilities where the linear instability and nonlinear stability thresholds do not coincide. However, recently, an operative technique have been applied to yield a sharp conditional nonlinear stability in subcritical instabilities regions, for more details see [82, 84].

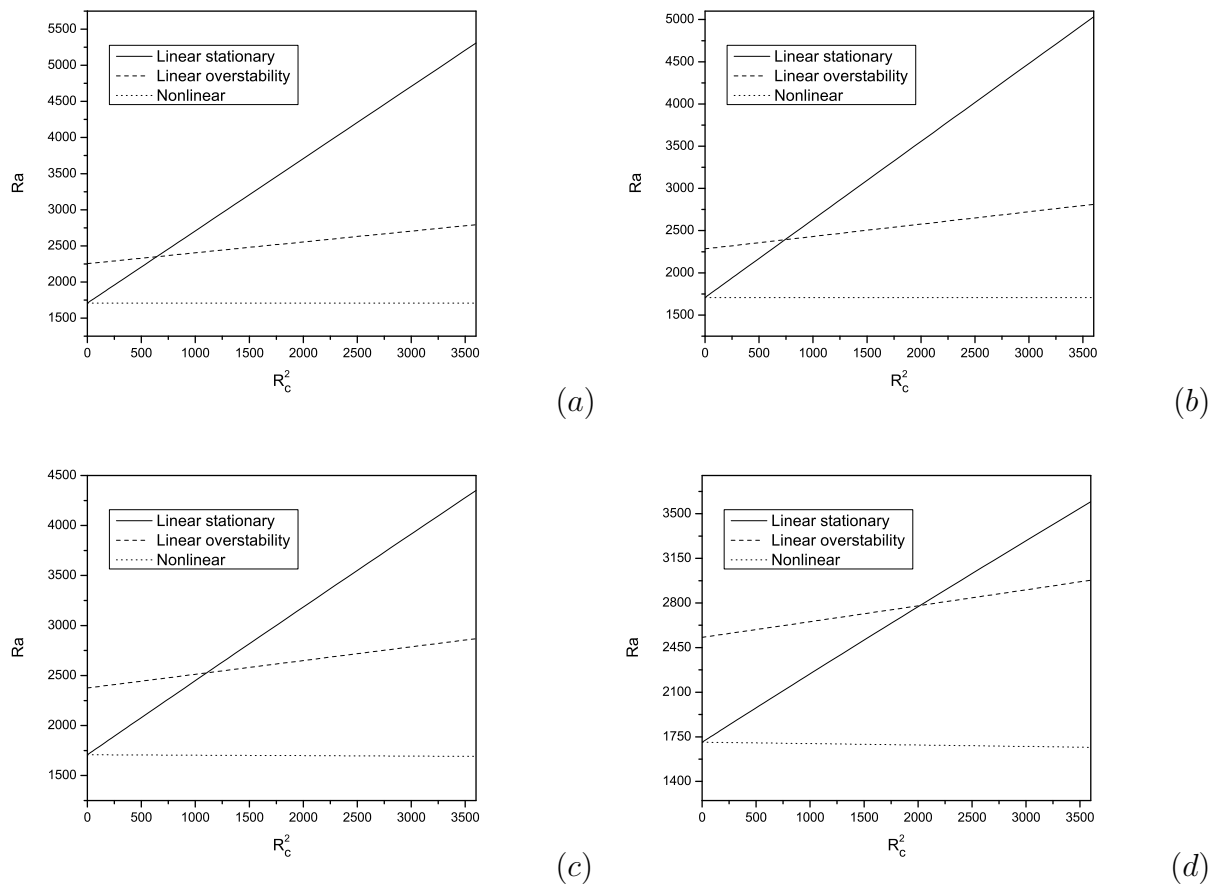
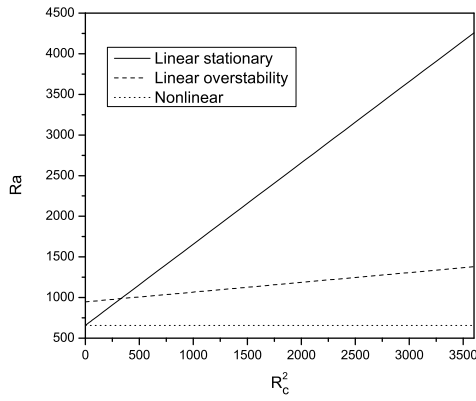
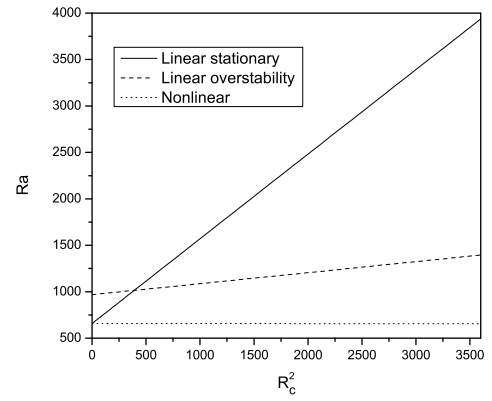


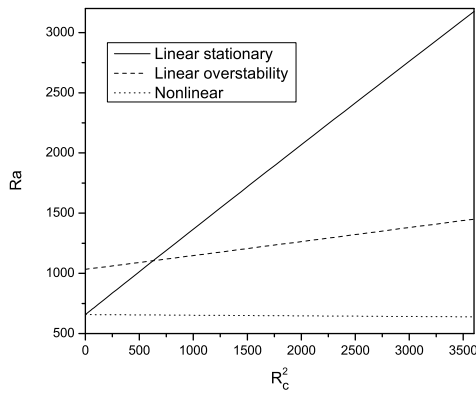
Figure 4.1: Critical Rayleigh number R_a against R with $M^2 = 0$, $\eta = 0$ and $H_1 = H_2 = +1$, for fixed-fixed boundary conditions. (a) $\xi = 10^{-10}$. (b) $\xi = 1$. (c) $\xi = 2$. (d) $\xi = 3$. Linear instability and nonlinear stability curves as in caption.



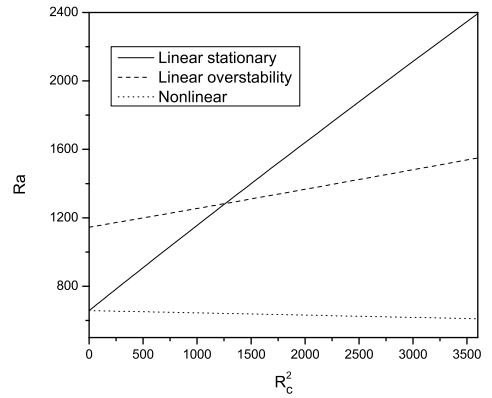
(a)



(b)

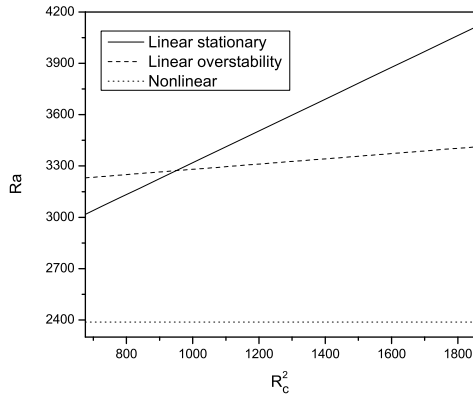


(c)

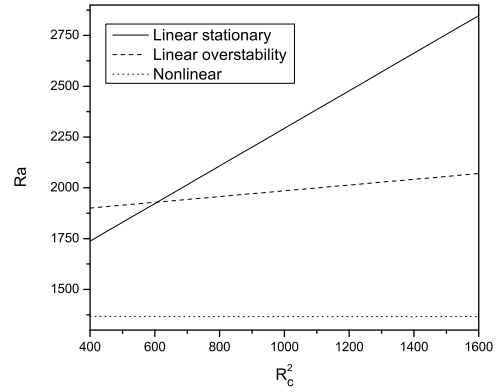


(d)

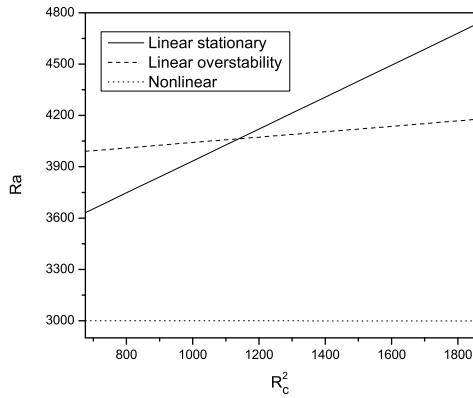
Figure 4.2: Critical Rayleigh number R_a against R with $M^2 = 0$, $\eta = 0$ and $H_1 = H_2 = +1$, for free-free boundary conditions. (a) $\xi = 10^{-10}$. (b) $\xi = 1$. (c) $\xi = 2$. (d) $\xi = 3$. Linear instability and nonlinear stability curves as in caption.



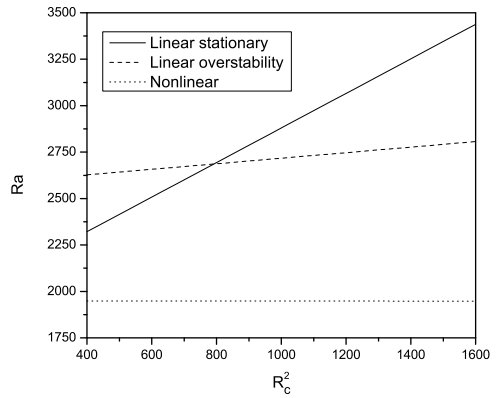
(a)



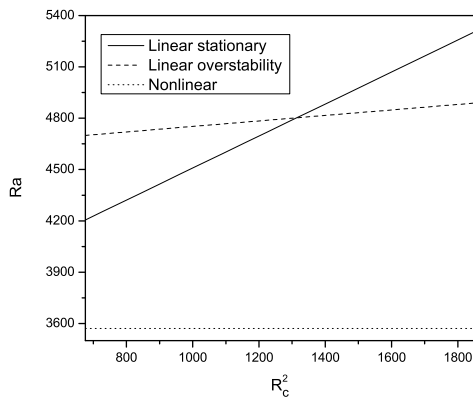
(d)



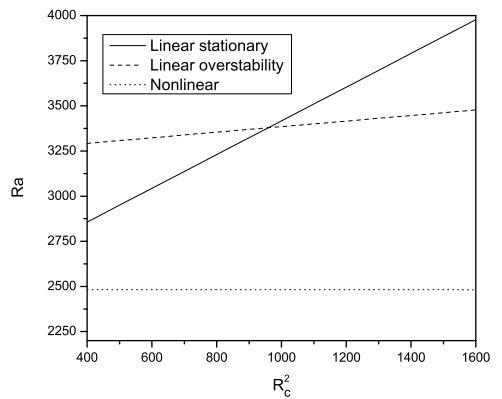
(b)



(e)



(c)



(f)

Figure 4.3: Critical Rayleigh number R_a against R with $\xi = 1$, $\eta = 1$ and $H_1 = H_2 = +1$. (a) $M^2 = 30$. (b) $M^2 = 60$. (c) $M^2 = 90$. (d) $M^2 = 30$. (e) $M^2 = 60$. (f) $M^2 = 90$. Linear instability and nonlinear stability curves as in caption. a, b, c represent the results of fixed-fixed boundary conditions and d, e, f for free-free boundary conditions

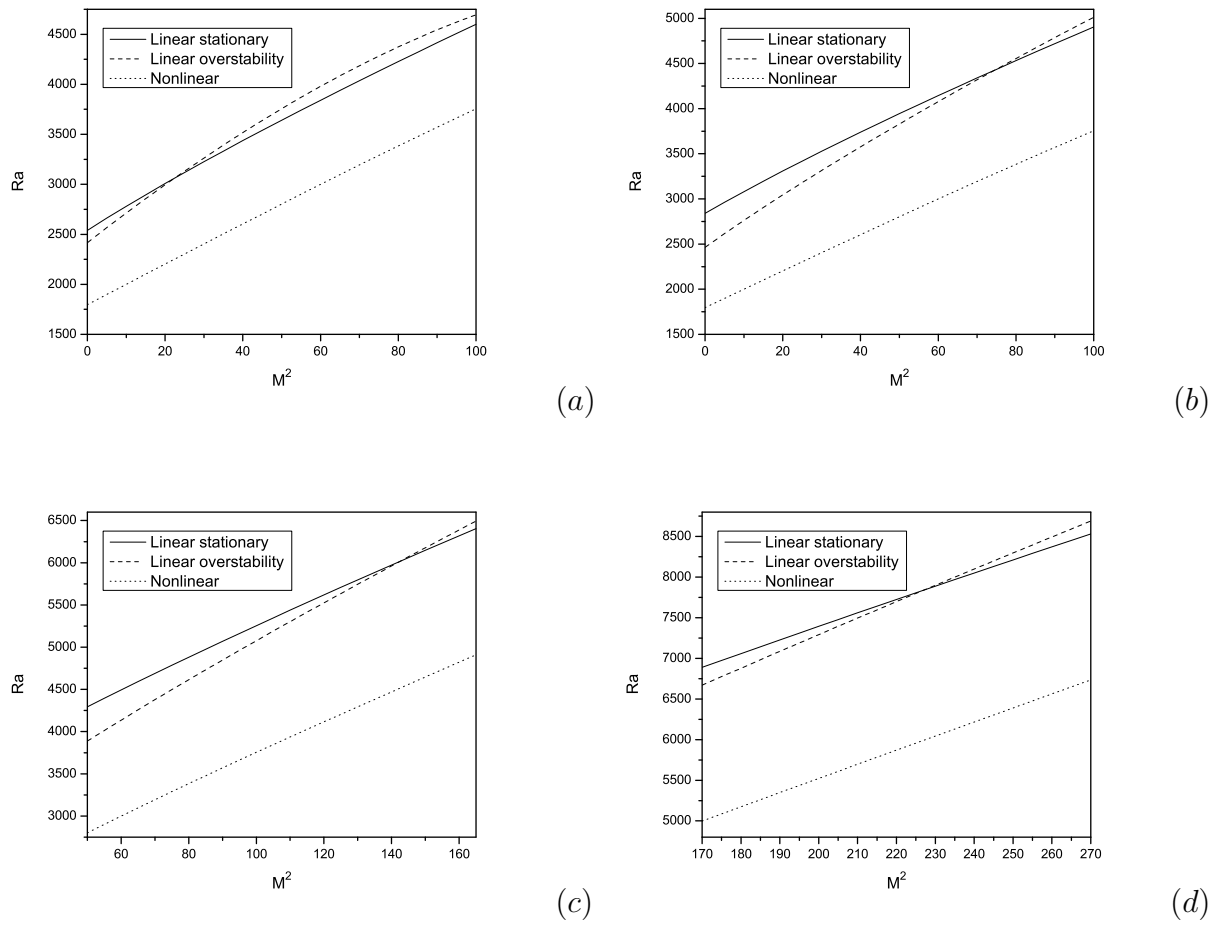


Figure 4.4: Critical Rayleigh number R_a against M^2 with $\xi = 1$, $\eta = 1$ and $H_1 = H_2 = +1$, for fixed-fixed boundary conditions. (a) $R_c = 30$. (b) $R_c = 35$. (c) $R_c = 40$. (d) $R_c = 45$. Linear instability and nonlinear stability curves as in caption.

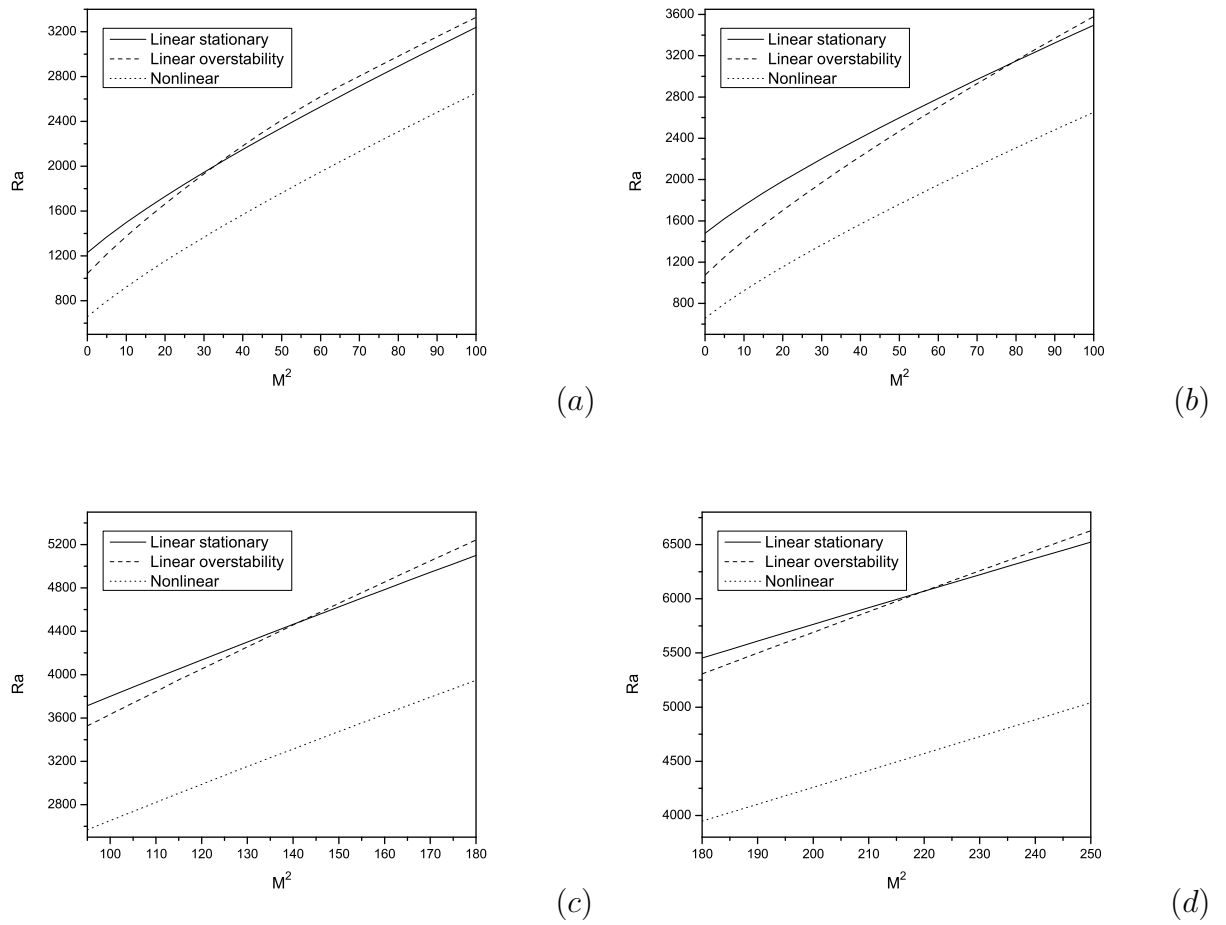


Figure 4.5: Critical Rayleigh number R_a against M^2 with $\xi = 1$, $\eta = 1$ and $H_1 = H_2 = +1$, for free-free boundary conditions. (a) $R_c = 25$. (b) $R_c = 30$. (c) $R_c = 35$. (d) $R_c = 40$.

Linear instability and nonlinear stability curves as in caption.

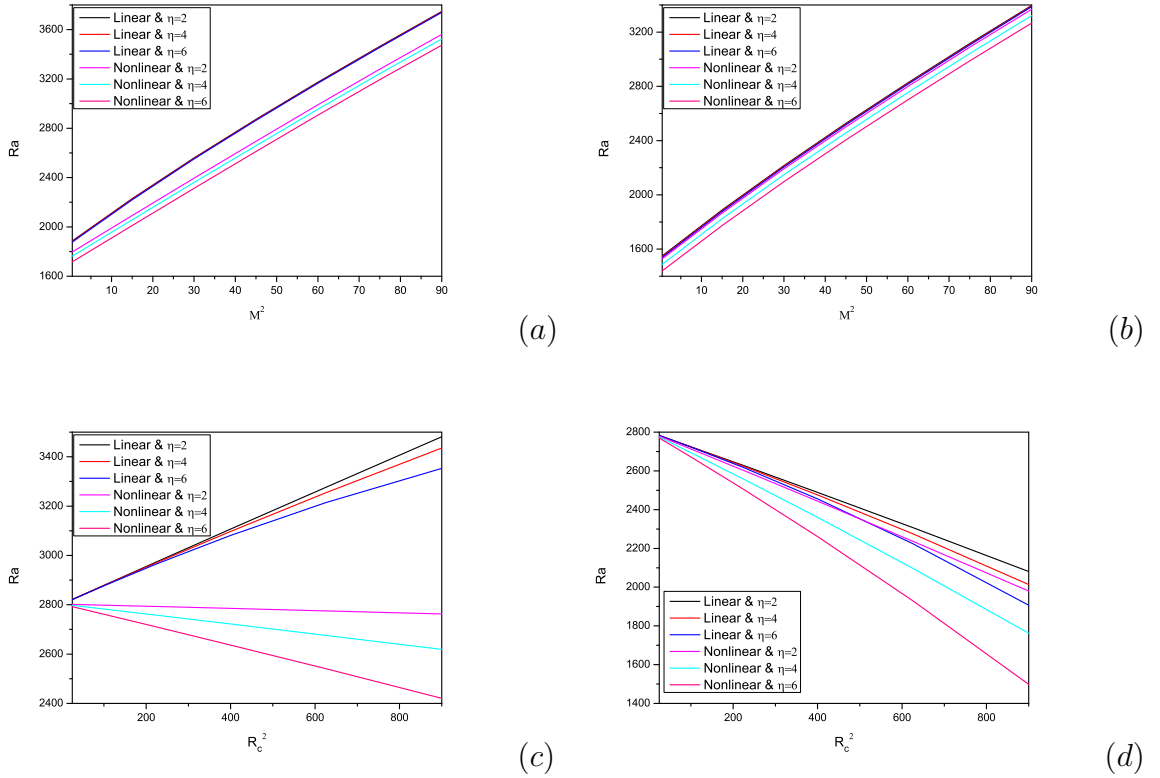


Figure 4.6: Critical Rayleigh number R_a for $\eta = 2, 4, 6$ for fixed-fixed boundary conditions. (a) R_a against M^2 with $\xi = 2, R_c = 15, H_1 = H_2 = +1$. (b) R_a against M^2 with $\xi = 2, R_c = 15, H_1 = +1, H_2 = -1$. (c) R_a against R with $\xi = 2, M^2 = 50, H_1 = H_2 = +1$. (d) R_a against R with $\xi = 2, M^2 = 50, H_1 = +1, H_2 = -1$. Linear instability curve together with nonlinear stability one.

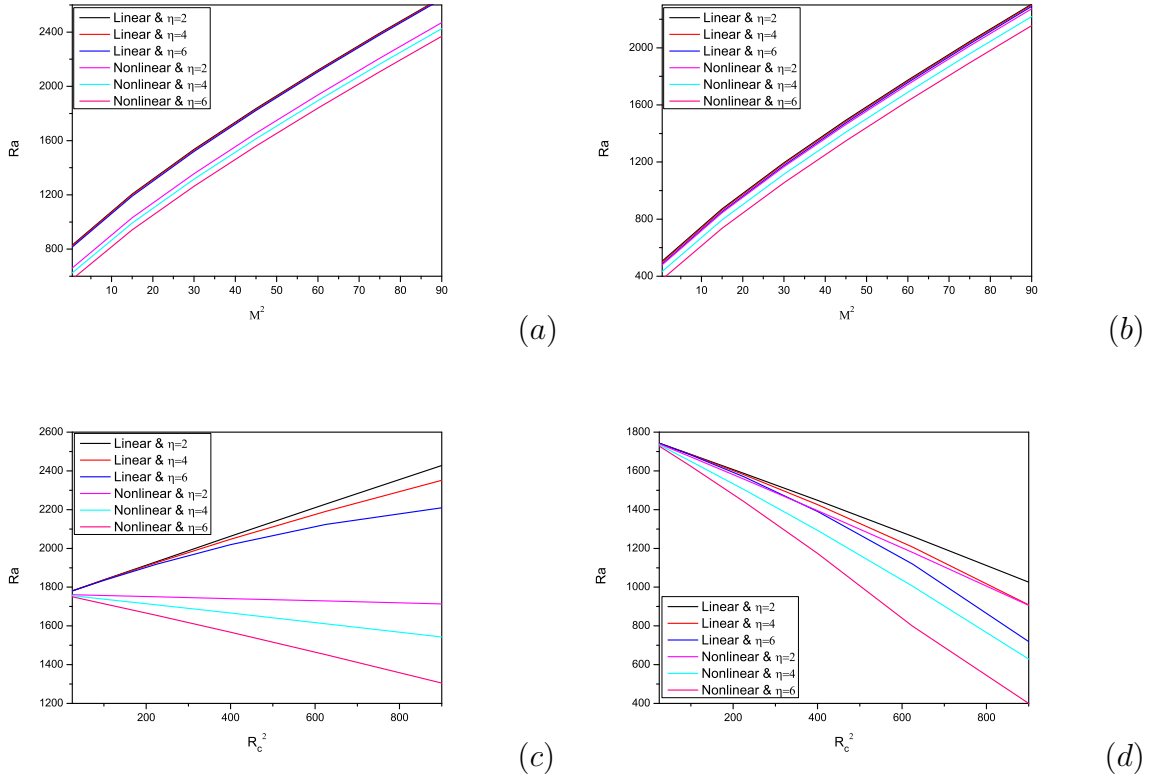


Figure 4.7: Critical Rayleigh number R_a for $\eta = 2, 4, 6$ for free-free boundary conditions. (a) R_a against M^2 with $\xi = 2, R_c = 15, H_1 = H_2 = +1$. (b) R_a against M^2 with $\xi = 2, R_c = 15, H_1 = +1, H_2 = -1$. (c) R_a against R with $\xi = 2, M^2 = 50, H_1 = H_2 = +1$. (d) R_a against R with $\xi = 2, M^2 = 50, H_1 = +1, H_2 = -1$. Linear instability curve together with nonlinear stability one.

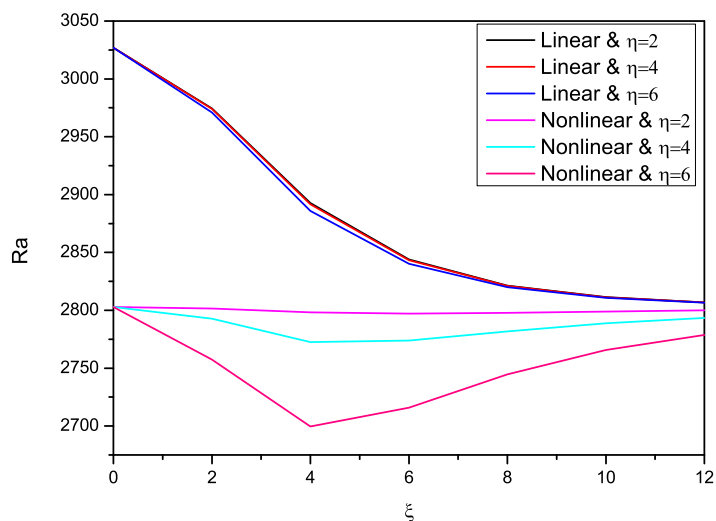


Figure 4.8: Critical Rayleigh number R_a against ξ for $M^2 = 50$, $R_c = 15$, $H_1 = H_2 = +1$ and $\eta = 2, 4, 6$ for fixed-fixed boundary conditions. Linear instability curve together with nonlinear stability one.

Chapter 5

Instability in Poiseuille flow in a porous medium with slip boundary conditions

5.1 Introduction

There is increasing interest in micro-electro-mechanical-systems (MEMS), and flow in microfluidic channels due to their applications in the electronics and related industries. In particular, at nanoscales there is increasing evidence that boundary conditions of slip type are needed rather than those of no-slip, cf. Badur *et al.* [10], Cercignani [31], Duan [48], Duan & Muzychka [47], Lauga *et al.* [101], Morini *et al.* [128], Priezjev [156], Rahman *et al.* [158], Shojaeian & Shojaeian [189], Stebel [192], Yong & Zhang [227], Zhang *et al.* [230], Zhang *et al.* [231]. An especially important application of microscale flow involving slip boundary conditions is to flow in porous metallic foams. Lefebvre *et al.* [105] give many industrial examples of this and provide a thorough review of the state of the art. The goal of this article is to provide a critical analysis of instability of flow in a channel occupied by a sparse porous medium when the boundary conditions are those of slip type.

The instability problem of flow in a channel occupied by a linearly viscous fluid, and subject to slip boundary conditions, has an interesting history. Chu [38] and Chu [37] report that increasing slip length in the slip boundary condition has the ef-

fect of decreasing the critical Reynolds number for the commencement of instability. However, Lauga & Cossu [102] and Spille *et al.* [190] report precisely the opposite. Namely, increasing the slip length has a stabilizing effect, thereby increasing the critical Reynolds number at which instability begins, according to linear theory. Webber [223] used a highly accurate Chebyshev tau method to analyse this instability problem and his results are in agreement with those of Lauga & Cossu [102] and Spille *et al.* [190].

The topic of instability of parallel shear flows in a channel and the associated numerical methods to accurately determine the instability thresholds is one of immense interest in the applied mathematics and engineering literature, cf. Avila *et al.* [8], Bandyopadhyay *et al.* [12], Bassom *et al.* [17], Dongarra *et al.* [43], Dragomirescu & Gheorghiu [45], Gheorghiu & Dragomirescu [64], Gheorghiu & Rommes [66], Hibino *et al.* [81], Khoshnood & Jalali [95], Malik & Hooper [122], Massa & Jha [125]. The difficulty with this class of problem is that the mathematical operators which arise in the instability analysis are non-symmetric and the resulting eigenfunctions are close to being linearly dependent. This makes finding an accurate numerical solution a challenging problem. This difficulty persists in the problem tackled here and we address the issue carefully.

The problem of instability of channel flow in a porous medium of Brinkman type with no-slip boundary conditions is itself of recent origin. Nield [137] initiated this study and this work is described in Straughan [197], pp. 234–236, where the correct equations are derived. Hill & Straughan [87] perform an accurate analysis of instability of flow in a fluid saturated channel of porous medium. Their results largely confirm the findings of Nield [137]. It should be stressed that these papers consider only no-slip boundary conditions. The conditions of slip at the boundary, which are believed to be highly relevant in microfluidic situations, are (we believe) analysed for the first time in this article.

The results in this chapter were published in the article Straughan and Harfash [199].

5.2 Basic equations

The equations for Poiseuille flow in a Brinkman porous material are derived in Nield [137] and in Straughan [197], p. 234. With v_i being the velocity field, p the pressure, R being the Reynolds number, and M^2 a non-dimensional Darcy (friction) coefficient the governing equations are

$$\begin{aligned} R \left(\frac{\partial v_i}{\partial t} + v_j \frac{\partial v_i}{\partial x_j} \right) &= - \frac{\partial p}{\partial x_i} + \Delta v_i - M^2 v_i, \\ \frac{\partial v_i}{\partial x_i} &= 0, \end{aligned} \tag{5.2.1}$$

where standard indicial notation is employed, a free index taking values 1,2 or 3, and a repeated index summing from 1 to 3, Δ is the Laplacian, and equations (5.2.1) hold in the domain $\{(x, y) \in \mathbb{R}^2\} \times \{z \in (-1, 1)\} \times \{t > 0\}$.

Slip boundary conditions have been suggested for a long time starting with the early work of Navier [131] and Maxwell [126]. They are the subject of intense recent work, especially in microfluidic and nanofluidic situations, as witnessed by Badur *et al.* [10], Duan [48], Duan & Muzychka [47], Lauga & Cossu [102], Morini *et al.* [128], Priezjev [156], Yong & Zhang [227], Zhang *et al.* [230], Zhang *et al.* [231], and many references including historical ones are given in these articles. A lucid historical account of the origin of slip boundary conditions is also given in chapter 1 of Webber [223]. The specific boundary conditions which solutions to equations (5.2.1) satisfy are, cf. Webber [223], chapter 3,

$$\begin{aligned} N_0 \frac{\partial v_1}{\partial z} &= v_1, \quad N_0 \frac{\partial v_2}{\partial z} = v_2, \quad v_3 = 0, \quad \text{on } z = -1, \\ N_0 \frac{\partial v_1}{\partial z} &= -v_1, \quad N_0 \frac{\partial v_2}{\partial z} = -v_2, \quad v_3 = 0, \quad \text{on } z = +1, \end{aligned} \tag{5.2.2}$$

where N_0 is a dimensionless parameter which measures the slip length. We assume that in equations (5.2.2) the slip on the lower boundary is the same as that on the upper boundary, for mathematical simplicity, since we are interested in the effect of the terms N_0 and M on the critical instability value of the Reynolds number R . One could easily generalize this work to allow for different slip coefficients on the upper and lower boundaries.

The basic solution whose stability we are interested in is one where the fluid is

driven along the channel in the x -direction by a constant pressure gradient of form

$$-\frac{\partial \bar{p}}{\partial x} = K^2 > 0,$$

where an overbar denotes the basic state. The basic velocity field corresponding to this pressure gradient has form $\bar{\mathbf{v}} = (U(z), 0, 0)$. Then one finds U must satisfy the boundary value problem

$$-K^2 = U'' - M^2 U, \quad -1 < z < 1, \quad (5.2.3)$$

subject to boundary conditions

$$\begin{aligned} N_0 U' + U &= 0, & z &= 1, \\ N_0 U' - U &= 0, & z &= -1. \end{aligned} \quad (5.2.4)$$

If in our non-dimensionalization we pick K^2 so that $K^2 = M^2 \cosh M / (\cosh M - 1)$ then U is found to be

$$U(z) = \frac{\cosh M}{\cosh M - 1} \left(1 - \frac{\cosh Mz}{N_0 M \sinh M + \cosh M} \right). \quad (5.2.5)$$

Note that when $N_0 = 0$, U reduces to

$$U = \frac{\cosh M - \cosh Mz}{\cosh M - 1},$$

in agreement with the basic solution employed by Nield [137] and by Hill & Straughan [87].

We now wish to investigate the stability of solution (5.2.5) and so let $\mathbf{u} = (u, v, w)$ be a perturbation to $\bar{\mathbf{v}}$ with corresponding pressure perturbation π . The perturbation equations are derived in detail in Straughan [197], p. 235, and he shows that after linearization and assuming spatial and time dependence like $\exp(i\alpha x + i\beta y - ict)$ then one may show that $w(z)$ satisfies the equation

$$(D^2 - a^2)^2 w - M^2(D^2 - a^2)w = iaR(U - c)(D^2 - a^2)w - iaRU''w, \quad (5.2.6)$$

where $D = d/dz$, $a^2 = \alpha^2 + \beta^2$, and $z \in (-1, 1)$. The boundary conditions which w must satisfy are derived from the conditions $N_0 u_{,z} = \pm u$, $z = \mp 1$, $N_0 v_{,z} = \pm v$, $z = \mp 1$, and the incompressibility condition $u_{,x} + v_{,y} + w_{,z} = 0$, are

$$w = 0; \quad N_0 w_{,zz} = \pm w_{,z}; \quad \text{on } z = \mp 1. \quad (5.2.7)$$

In terms of the D notation these boundary conditions are

$$\begin{aligned} N_0 D^2 w &= Dw, \quad \text{on } z = -1; & N_0 D^2 w &= -Dw, \quad \text{on } z = 1; \\ w &= 0 \quad \text{on } z = \pm 1. \end{aligned} \tag{5.2.8}$$

In the next section we briefly describe the numerical methods employed to solve equation (5.2.6) together with (5.2.8).

5.3 Numerical techniques

5.3.1 Chebyshev collocation method

Since solving (5.2.6) and (5.2.8) is a difficult numerical problem, we adopt the Chebyshev collocation method to solve the eigenvalue systems. We apply two variations of the Chebyshev collocation method in order to incorporate the boundary conditions, and also two methods provide an independent check. Firstly we introduce the function $B = Dw$, and then equation (5.2.6) may be written as the system

$$\begin{aligned} Dw - B &= 0, \\ D^3 B - (2a^2 + M^2)DB + (a^4 + a^2 M^2)w + iaRU''w & \\ &= iaR(U - c)(DB - a^2 w). \end{aligned} \tag{5.3.9}$$

The boundary conditions (5.2.8) now become

$$\begin{aligned} w &= 0, \quad z = \pm 1, \\ N_0 DB + B &= 0, \quad z = 1, \\ N_0 DB - B &= 0, \quad z = -1. \end{aligned} \tag{5.3.10}$$

Method 1.

Here we expand w and B as (truncated) series in trial functions θ_n, ϕ_n , so that

$$w = \sum_{n=1}^N w_n \theta_n(z), \quad B = \sum_{n=1}^N B_n \phi_n(z), \tag{5.3.11}$$

where θ_n, ϕ_n are defined by

$$\begin{aligned} \theta_n(z) &= (1 - z^2)T_{2n-2}(z), \\ \phi_n(z) &= \left[1 - z^2 + \frac{2N_0}{1 + N_0(2n-1)^2} \right] T_{2n-1}(z), \end{aligned} \tag{5.3.12}$$

and $T_n(z)$ are the Chebyshev polynomials of the first kind, cf. Dongarra *et al.* [43], which is defined by:

$$\begin{aligned} T_0(z) &= 1, & T_1(z) &= z \\ T_{n+1}(z) - 2zT_n(z) + T_{n-1}(z) &= 0, & -1 \leq z \leq 1 \end{aligned}$$

or

$$T_n(z) = \cos(n \arccos(z)), \quad -1 \leq z \leq 1$$

The reason for the choice of the basis functions θ_n and ϕ_n is that in this way the functions w and B satisfy the boundary conditions (5.3.10). The next step is to substitute expressions (5.3.11) into equations (5.3.9) and (5.3.10), and then require that equations (5.3.9) and (5.3.10) be satisfied at N collocation points z_1, \dots, z_N , where z_i are defined by $z_i = \cos([i - 1]/[2N - 1]\pi)$, $i = 1, \dots, N$. This results in a $2N \times 2N$ system of algebraic equations in the coefficients $w_1, \dots, w_N, B_1, \dots, B_N$:

$$\begin{pmatrix} D\theta & -I\phi \\ A\theta & A\phi \end{pmatrix} X = c \begin{pmatrix} O & O \\ ia^3RI\theta & -iaRD\phi \end{pmatrix} X,$$

where $X = (w_1, \dots, w_N, B_1, \dots, B_N)$, O is the zeros matrix, $A\theta(n_1, n_2) = (a^4 + a^2M^2 + iaRU''(z_{n_1}) + ia^3RU(z_{n_1}))I\theta(n_1, n_2)$, $A\phi(n_1, n_2) = D\phi^3(n_1, n_2) - (2a^2 + M^2 + iaRU(z_{n_1}))D\phi(n_1, n_2)$, $I\theta(n_1, n_2) = \theta_{n_2}(z_{n_1})$, $I\phi(n_1, n_2) = \phi_{n_2}(z_{n_1})$, $D\theta(n_1, n_2) = \theta'_{n_2}(z_{n_1})$, $D\phi(n_1, n_2) = \phi'_{n_2}(z_{n_1})$, $D\phi^3(n_1, n_2) = \phi'''_{n_2}(z_{n_1})$, $n_1, n_2 = 1, \dots, N$.

This matrix eigenvalue system is solved by using the QZ algorithm, cf. Dongarra *et al.* [43].

Method 2.

In order to implement the second technique we approximate the solutions to equations (5.3.9) and (5.3.10) as truncated series of Chebyshev polynomials as follows,

$$w = \sum_{n=0}^N w_n T_n(z), \quad B = \sum_{n=0}^N B_n T_n(z). \quad (5.3.13)$$

These expressions are employed in equations (5.3.9) and (5.3.10) and then the resulting equations are evaluated at Gauss-Lobatto points y_i defined by $y_i = \cos(\pi i/[N -$

3]), $i = 0, \dots, N-2$. This leads to $2N-2$ algebraic equations for $2N+2$ unknowns $w_0, \dots, w_N, B_0, \dots, B_N$. The remaining 4 equations are furnished by the boundary conditions (5.3.10) which become

$$\begin{aligned} \sum_{n=0}^N w_n = 0, \quad \sum_{n=0}^N (-1)^n w_n = 0, \\ \sum_{n=0}^N (N_0 n^2 + 1) B_n = 0, \quad \sum_{n=0}^N [(-1)^{n+1} N_0 n^2 - 1] B_n = 0, \end{aligned} \quad (5.3.14)$$

and these equations are added as rows to the matrices generated above to yield a $(2N+2) \times (2N+2)$ matrix eigenvalue equation. Then, we obtain the generalised eigenvalue problem:

$$\begin{pmatrix} D & -I \\ BC_1 & 0 \dots 0 \\ BC_2 & 0 \dots 0 \\ A_1 & A_2 \\ 0 \dots 0 & BC_3 \\ 0 \dots 0 & BC_4 \end{pmatrix} X = c \begin{pmatrix} O & O \\ 0 \dots 0 & 0 \dots 0 \\ 0 \dots 0 & 0 \dots 0 \\ ia^3 RI & -iaRD \\ 0 \dots 0 & 0 \dots 0 \\ 0 \dots 0 & 0 \dots 0 \end{pmatrix} X,$$

where $X = (w_0, \dots, w_N, B_0, \dots, B_N)$, O is the zeros matrix, $A_1(n_1, n_2) = (a^4 + a^2 M^2 + iaRU''(y_{n_1}) + ia^3 RU(y_{n_1}))I(n_1, n_2)$, $A_2(n_1, n_2) = D^3(n_1, n_2) - (2a^2 + M^2 + iaRU(y_{n_1}))D(n_1, n_2)$, $I(n_1, n_2) = T_{n_2}(y_{n_1})$, $D(n_1, n_2) = T'_{n_2}(y_{n_1})$, $D^3(n_1, n_2) = T'''_{n_2}(y_{n_1})$, $n_1 = 0, \dots, N-2$, $n_2 = 0, \dots, N$.

This is solved by the QZ algorithm.

5.3.2 Finite element method

As an additional check we have also employed a finite element method to solve equations (5.2.6) and (5.2.8). This consists of introducing another variable $A = D^2 w$ and writing equation (5.2.6) as a system of two equations involving $A = D^2 w$ and (5.2.6) written in terms of A and w as follows

$$D^2 w = A, \quad (5.3.15)$$

$$D^2 A - (2a^2 + M^2)A + (a^4 + a^2 M^2)w + iaRU''w - iaRU(A - a^2 w) = -iaRc(A - a^2 w), \quad (5.3.16)$$

$$\begin{aligned}
w &= 0, & \text{at } z &= \mp 1, \\
N_0 A - Dw &= 0, & \text{at } z &= -1, \\
N_0 A + Dw &= 0, & \text{at } z &= 1.
\end{aligned} \tag{5.3.17}$$

Firstly, we divided the period $-1 \leq x \leq 1$ into n elements, each element e having $p+1$ nodes n_1, n_2, \dots, n_{p+1} . In term of its $p+1$ nodal values, the variables w, A may be uniquely interpolated as a polynomial of $p+1$ order, the interpolation being given by

$$w^e = N^e \delta_w^e, \quad A^e = N^e \delta_A^e, \tag{5.3.18}$$

where $\delta_w^e = \{w_{n_1}, w_{n_2}, \dots, w_{n_{p+1}}\}$, $\delta_A^e = \{A_{n_1}, A_{n_2}, \dots, A_{n_{p+1}}\}$, and the shape function matrix is

$$N^e = [N_{n_1}^p, N_{n_2}^p, \dots, N_{n_{p+1}}^p].$$

Therefore the over-all finite element approximation is given by

$$w = \sum_{e=1}^n w^e, \quad A = \sum_{e=1}^n A^e, \tag{5.3.19}$$

The variational formulations of (5.3.15) and (5.3.16) are

$$\text{Minimize } I_w[w] = \int_0^1 (-(Dw)^2 - 2Aw) dx, \tag{5.3.20}$$

$$\begin{aligned}
\text{Minimize } I_A[A] &= \int_0^1 (-(DA)^2 - (2a^2 + M^2)A^2 + 2(a^4 + a^2 M^2)wA \\
&+ 2iaRU''wA - iaRU A^2 + 2iRU a^3 wA + iaRcA^2 - 2iRca^3 wA) dx,
\end{aligned} \tag{5.3.21}$$

Substitution of (5.3.19) into variational formulations (5.3.20) and (5.3.21) gives

$$I_w[w] = \sum_{e=1}^n \int_e (-(Dw^e)^2 - 2A^e w^e) dx = \sum_{e=1}^n I_w^e, \tag{5.3.22}$$

$$\begin{aligned}
I_A[A] &= \sum_{e=1}^n \int_e (-(DA^e)^2 - (2a^2 + M^2)(A^e)^2 + 2(a^4 + a^2 M^2)w^e A^e \\
&+ 2iaRU''w^e A^e - iaRU(A^e)^2 + 2iRU a^3 w^e A^e + iaRc(A^e)^2 - 2iRca^3 w^e A^e) dx = \sum_{e=1}^n I_A^e,
\end{aligned} \tag{5.3.23}$$

here, we use the fact that the functions w^e, A^e are equivalent to zero outside the element e . Using (5.3.22) and (5.3.23) we obtain

$$I_w[w] = I_w(w_1, w_2, \dots, w_m),$$

$$I_A[A] = I_A(A_1, A_2, \dots, A_m),$$

where m is the number of all nodes in all elements. Then using the Rayleigh-Ritz procedure to minimize $I_w[w], I_A[A]$, with respect to the variational parameters w_i, A_i respectively, gives

$$\frac{\partial I_w}{\partial w_i} = \sum_{e=1}^n \frac{\partial I_w^e}{\partial w_i} = 0, \quad i = 1, \dots, m, \quad (5.3.24)$$

$$\frac{\partial I_A}{\partial A_i} = \sum_{e=1}^n \frac{\partial I_A^e}{\partial A_i} = 0, \quad i = 1, \dots, m, \quad (5.3.25)$$

Then matrix representation for the system of equations at the element e take the form

$$\begin{aligned} & \begin{pmatrix} & -D_2^e & & -F_1^e \\ (a^4 + a^2 M^2)F_1^e + iaRF_3^e + ia^3RF_2^e & & -D_2^e - (2a^2 + M^2)F_1^e - iaRF_2^e & \end{pmatrix} \begin{pmatrix} \delta_w^e \\ \delta_A^e \end{pmatrix} \\ & = c \begin{pmatrix} O & O \\ iRa^3F_1^e & -iaRF_1^e \end{pmatrix} \begin{pmatrix} \delta_w^e \\ \delta_A^e \end{pmatrix}, \end{aligned} \quad (5.3.26)$$

where $O_{ij} = 0$, $D_{2ij}^e = \int_{-1}^1 \frac{dN_{n_i}^p}{dz} \frac{dN_{n_j}^p}{dz} dz$, $F_{1ij}^e = \int_{-1}^1 N_{n_i}^p N_{n_j}^p dz$,
 $F_{2ij}^e = \int_{-1}^1 U(z) N_{n_i}^p N_{n_j}^p dz$, $F_{3ij}^e = \int_{-1}^1 U''(z) N_{n_i}^p N_{n_j}^p dz$, $i, j = 1, \dots, p+1$.

The above integrals can be evaluated by applying the classical finite element nodal basis functions in one dimension on the standard element $\Omega_{st} = (-1, 1)$. The standard shape functions are defined by the set of Lagrange polynomials

$$N_{n_i}^p(\zeta) = \prod_{j=n_1, j \neq i}^{n_{p+1}} \frac{\zeta - \zeta_j}{\zeta_i - \zeta_j}, \quad (5.3.27)$$

where $\zeta = 2/h(z - z_m)$, h is the length of element and z_m is the mid-point. Thus these integrations take the form:

$$D_{2ij}^e = \frac{2}{h} \int_{-1}^1 \frac{dN_{n_i}^p}{d\zeta} \frac{dN_{n_j}^p}{d\zeta} d\zeta,$$

$$\begin{aligned}
F_{1ij}^e &= \frac{h}{2} \int_{-1}^1 N_{n_i}^p N_{n_j}^p d\zeta \\
F_{2ij}^e &= \frac{h}{2} \int_{-1}^1 U\left(\frac{h}{2}\zeta + z_m\right) N_{n_i}^p N_{n_j}^p d\zeta, \\
F_{3ij}^e &= \frac{h}{2} \int_{-1}^1 U''\left(\frac{h}{2}\zeta + z_m\right) N_{n_i}^p N_{n_j}^p d\zeta, \\
i &= 1, \dots, p+1, \quad j = 1, \dots, p+1.
\end{aligned}$$

All these integrals were calculated analytically using Matlab routines. Finally, we assemble the systems of all elements $e = 1, \dots, n$ to get the main system which have the form

$$B_1 \mathbf{x} = \sigma B_2 \mathbf{x}, \quad (5.3.28)$$

where $\mathbf{x} = (w_1, \dots, w_m, A_1, \dots, A_m)^T$.

For slip-slip boundary conditions, firstly, we transform these condition to the local coordinate ζ . Thus these boundary condition take the form

$$\begin{aligned}
w &= 0, & \text{at } \zeta &= -1, 1, \\
N_0 A - \frac{2}{h} D w &= 0, & \text{at } \zeta &= -1, \\
N_0 A + \frac{2}{h} D w &= 0, & \text{at } \zeta &= 1.
\end{aligned} \quad (5.3.29)$$

Now we can impose the boundary conditions (5.3.29)₁ by removing the rows and columns of order 1 and m , while we can apply the boundary conditions (5.3.29)_{2,3} by substituting $\zeta = -1$ in (5.3.29)₂ and $\zeta = 1$ in (5.3.29)₃ and then use (5.3.19) to arrive to the following final equations

$$A_1 = \frac{2}{N_0 h e_1} [d_2 w_2 + \dots + d_{p+1} w_{p+1}] - \frac{1}{e_1} [e_2 A_2 + \dots + e_{p+1} A_{p+1}], \quad (5.3.30)$$

$$A_m = -\frac{2}{N_0 h g_{p+1}} [f_1 w_{m-p} + f_2 w_{m-p+1} + \dots + f_p w_{m-1}] - \frac{1}{g_{p+1}} [g_1 A_{m-p} + \dots + g_p A_{m-1}]. \quad (5.3.31)$$

where $d_i = dN_i(-1)/d\zeta$, $e_i = N_i(-1)$, $g_i = N_i(1)$ and $f_i = dN_i(1)/d\zeta$.

Now, we substitute the values of A_1 and A_m in (5.3.28) thus the columns of order $m+1$ and $2m$ will be zeros and thus we can remove the $m+1$ and $2m$ rows and

columns.

We have found the finite element method to be more unstable numerically than either of the two collocation methods reported above. However, we include in table 5.1 numerical results to compare the performance of the collocation and finite element methods. We report this for $N_0 = 0, 0.001, 0.002, 0.003$; however, we have computed for several other N_0 values and the trend is always the same. All methods require more care as M increases and also as N_0 increases, both of which correspond to increasing critical Rayleigh number. The values reported in table 5.1 give the number of polynomials and elements required to achieve the same level of accuracy for all three methods. From tables 5.1, 5.2, 5.3, 5.4 we see that as M increases the number of Chebyshev polynomials increases for both collocation methods 1 and 2. For the finite element method both the polynomial order of the element and the number of elements must strongly increase as M increases and, indeed, for M greater than 5 we found it impossible to obtain satisfactory results, whereas the collocation methods still worked.

5.4 Numerical results and conclusions

The numerical results reported are based on the leading eigenvalue of the system (5.3.9) and (5.3.10). By this we mean that when one employs the time representation in w and B of form e^{-ict} with $c = c_r + ic_i$ then this results in w and B having terms of form $\exp(-ic_r t) \cdot \exp(c_i t)$. The eigenvalues are found such that the largest value of c_i is $c_i = 0$ and then the result is minimized over the wavenumber a . The resulting R value is then the critical Reynolds number with corresponding wavenumber. The value $c_i = 0$ is chosen because this is the threshold at which the solution becomes unstable according to linearized theory. For, if $c_i > 0$ then w and B grow rapidly like $\exp(c_i t)$ and the solution is unstable.

In figures 5.1 we display the critical Reynolds numbers at which instability begins as a function of the slip coefficient, N_0 . These graphs are given for values of M ranging from 0 to 10. The graphs are interpreted as follows. For example, when

$M = 0$ consider the lowest curve in figure 5.1₁. For values of R_E and N_0 lying below this curve the solution is linearly stable, i.e. all eigenvalues in this range are such that $c_i < 0$. If R_E and N_0 correspond to a value which is above the $M = 0$ curve then at least one eigenvalue has $c_i > 0$ and the solution is growing exponentially and is unstable. A similar interpretation holds for the other curves when $M = 0.5, 1, 2$, etc. We observe that as M increases for a fixed N_0 the critical Reynolds number increases substantially, in agreement with the results of Hill & Straughan [87]. In addition, for fixed M we witness that increasing N_0 leads to a strong stabilizing effect. This effect is particularly pronounced as M also increases. Thus, the increasing slip length and increasing Darcy term both combine to strongly increase the threshold at which instability commences. Thus, for a microfluidic channel filled with a porous metallic foam, we may expect a much greater instability threshold than in a clean channel. Figures 5.1 quantify this effect so once sufficiently accurate values of N_0 and M are known for a particular material, we may accurately determine when instability will commence (according to linearized instability theory).

Figures 5.2 display the corresponding critical wavenumber curves against N_0 for fixed M , M varying over the range $M = 0$ to $M = 10$. Again the curves are interpreted as those for R_E , i.e. above a curve we have instability, below linear stability. Increasing N_0 leads to decreasing critical a and this means the periodic cells of the w solution become larger in the x and y directions. The critical a values as a function of M , for fixed N_0 decrease as M increases from 0, but then this effect reverses in the range $M = 2$ to 3, and with M greater than this a_{crit} increases leading to smaller periodic cells in the x, y directions.

Finally we include in figures 5.3, critical values of c_r as a function of N_0 for various M . This indicates how oscillatory the solution is in time at the start of instability, as N_0 and M vary.

The spectrum which is plotted in Figures 5.4, 5.5 and 5.6, is similar to that found in Poiseuille flow in a porous medium with no-slip boundary conditions by Hill and Straughan [87], the eigenvalues displaying a Y shape in the (c_r, c_i) diagram. As M increase, the eigenvalues at the intersection of the three lines in the Y become more numerically unstable, and as M increases this effect is very pronounced.

The spectrum of (5.3.9) and (5.3.10) behaves very like that of the Orr-Sommerfeld problem for classical Poiseuille flow. For example, for higher Reynolds numbers we witnessed mode crossing of eigenvalues. For example, for $M = 0, 0.5, 1.0$, the first and second eigenvalues interchange places for R between 80822 and 80828, 86852 and 86854, and 106618 and 106620, respectively, with the previous first eigenvalue moving down the list as R increases. This behaviour is very similar to that observed by Dongarra et al. [43]. Moreover, the spectrum is very sensitive and care must be taken with the number of polynomials used in the numerical approximation, and in the arithmetical precision used in the calculation (those presented here are all in 64 bit arithmetic). For different values of N_0 , the spectrum for $M = 1, 5$ and 10 at the critical values are shown in Figures 5.4, 5.5 and 5.6, respectively. Since U is an even function of z , the proper solution of eigenvalue system (5.3.9) and (5.3.10) falls into two non-combining groups of even and odd solutions. However, Chebyshev collection method 1 produce the approximate eigenvalues with even modes for plane Poiseuille flow, while the Chebyshev collection method 2 give the approximate eigenvalues with even and odd modes.

The values presented here will be useful for any experiment or any device in which pressure gradient driven flow in a micro-channel is needed, especially when that channel is filled with a porous material for which a Brinkman system is suitable. Such a porous material is we believe, one of porous metallic foam type.

M	Che-C-1		Che-C-2		FEM		
	n. of pol.	Ra	n. of pol.	Ra	n. of N.	n. of E.	Ra
0	30	5772.22	50	5772.22	14	20	5771.92
0.5	30	6710.37	60	6710.36	16	25	6710.01
1	35	10033.15	60	10033.15	18	30	10032.63
2	40	28663.46	70	28663.48	24	35	28661.98
3	45	65266.01	90	65265.98	30	40	65262.56
4	55	112555.67	110	112555.47	36	45	112549.58
5	60	164298.23	120	164298.36	42	50	164289.76
6.03	65	219727.26	130	219726.34			UN
7.64	75	308610.10	150	308610.86			UN
10	85	440224.15	170	440220.18			UN

Table 5.1: Critical Rayleigh numbers with varying M , $N_0 = 0$. Che-C-1 denotes collocation method-1, Che-C-2 denotes collocation method-2, and FEM signifies finite element method. The notation no. polys. denotes number of Chebyshev polynomials used, N is the order of the polynomial in the finite element, and E signifies the number of finite elements employed. UN denotes the method is numerically unstable.

M	Che-C-1		Che-C-2		FEM		
	n. of pol.	Ra	n. of pol.	Ra	n. of N.	n. of E.	Ra
0	30	5769.99	50	5769.99	14	20	5769.68
0.5	30	6713.21	60	6713.19	16	25	6712.84
1	35	10059.17	60	10059.17	18	30	10058.65
2	40	28933.72	70	28933.74	24	35	28932.24
3	45	66530.99	90	66530.96	30	40	66527.54
4	55	116278.33	110	116278.13	36	45	116272.24
5	60	172615.47	120	172615.60	42	50	172607.00
6.03	65	235714.86	130	235713.93			UN
7.64	75	344379.92	150	344380.68			UN
10	85	528034.63	170	528030.66			UN

Table 5.2: Critical Rayleigh numbers with varying M , $N_0 = 0.001$. Che-C-1 denotes collocation method-1, Che-C-2 denotes collocation method-2, and FEM signifies finite element method. The notation no. polys. denotes number of Chebyshev polynomials used, N is the order of the polynomial in the finite element, and E signifies the number of finite elements employed. UN denotes the method is numerically unstable.

M	Che-C-1		Che-C-2		FEM		
	n. of pol.	Ra	n. of pol.	Ra	n. of N.	n. of E.	Ra
0	30	5795.26	50	5795.26	14	20	5794.96
0.5	30	6751.96	60	6751.95	16	25	6751.60
1	35	10158.12	60	10158.12	18	30	10157.60
2	40	29668.13	70	29668.15	24	35	29666.65
3	45	69913.72	90	69913.69	30	40	69910.27
4	55	126294.04	110	126293.84	36	45	126287.95
5	60	195251.94	120	195252.07	42	50	195243.47
6.03	65	280053.24	130	280052.32			UN
7.64	75	448165.57	150	448166.33			UN
10	85	810199.46	170	810195.48			UN

Table 5.3: Critical Rayleigh numbers with varying M , $N_0 = 0.002$. Che-C-1 denotes collocation method-1, Che-C-2 denotes collocation method-2, and FEM signifies finite element method. The notation no. polys. denotes number of Chebyshev polynomials used, N is the order of the polynomial in the finite element, and E signifies the number of finite elements employed. UN denotes the method is numerically unstable.

M	Che-C-1		Che-C-2		FEM		
	n. of pol.	Ra	n. of pol.	Ra	n. of N.	n. of E.	Ra
0	30	5845.03	50	5845.03	14	20	5844.73
0.5	30	6822.69	60	6822.68	16	25	6822.33
1	35	10321.94	60	10321.94	18	30	10321.42
2	40	30817.51	70	30817.53	24	35	30816.03
3	45	75255.54	90	75255.51	30	40	75252.09
4	55	142553.57	110	142553.37	36	45	142547.48
5	60	233567.17	120	233567.30	42	50	233558.70
6.03	65	359501.74	130	359500.81			UN
7.64	75	657199.37	150	657200.13			UN
10	85	1530026.58	170	1530022.61			UN

Table 5.4: Critical Rayleigh numbers with varying M , $N_0 = 0.003$. Che-C-1 denotes collocation method-1, Che-C-2 denotes collocation method-2, and FEM signifies finite element method. The notation no. polys. denotes number of Chebyshev polynomials used, N is the order of the polynomial in the finite element, and E signifies the number of finite elements employed. UN denotes the method is numerically unstable.

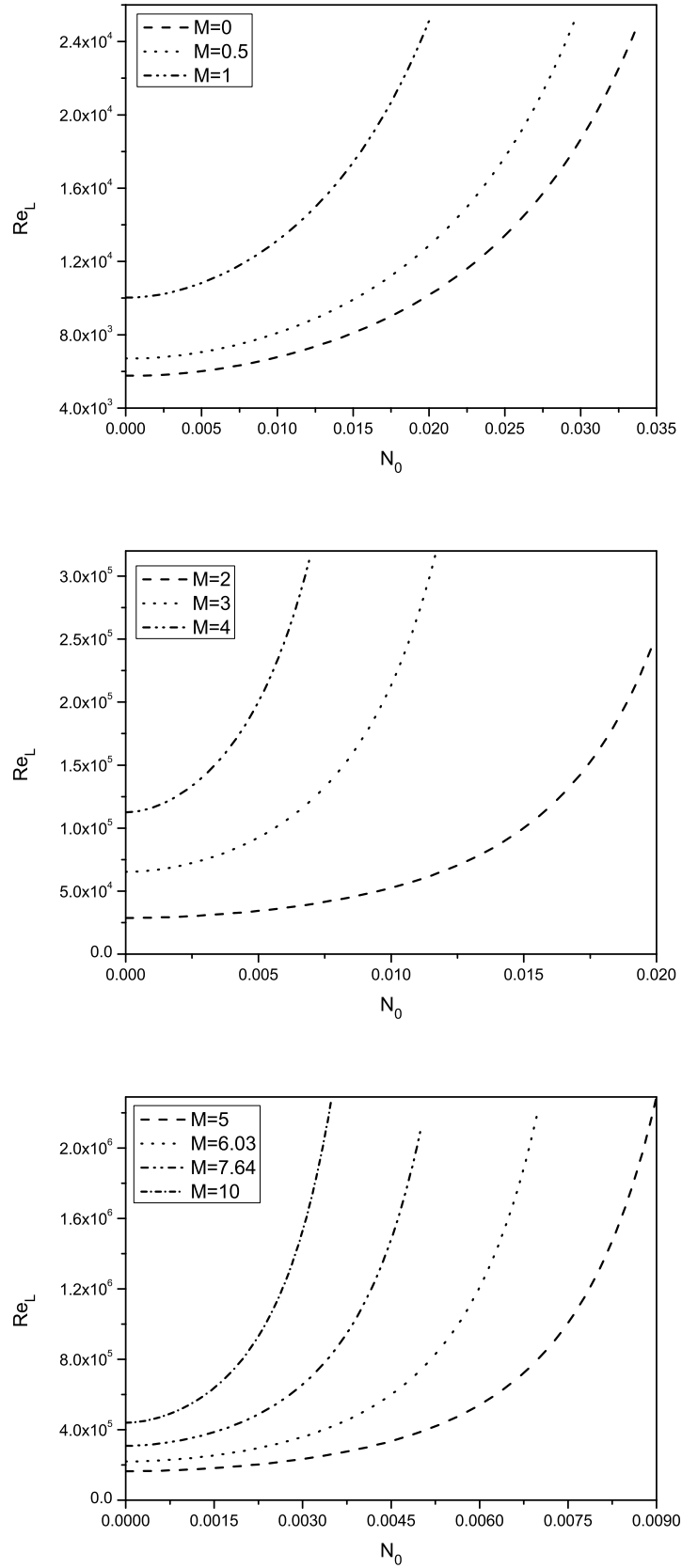


Figure 5.1: Critical Reynolds number Re_L against N_0 . The values of M are as indicated in the figures.

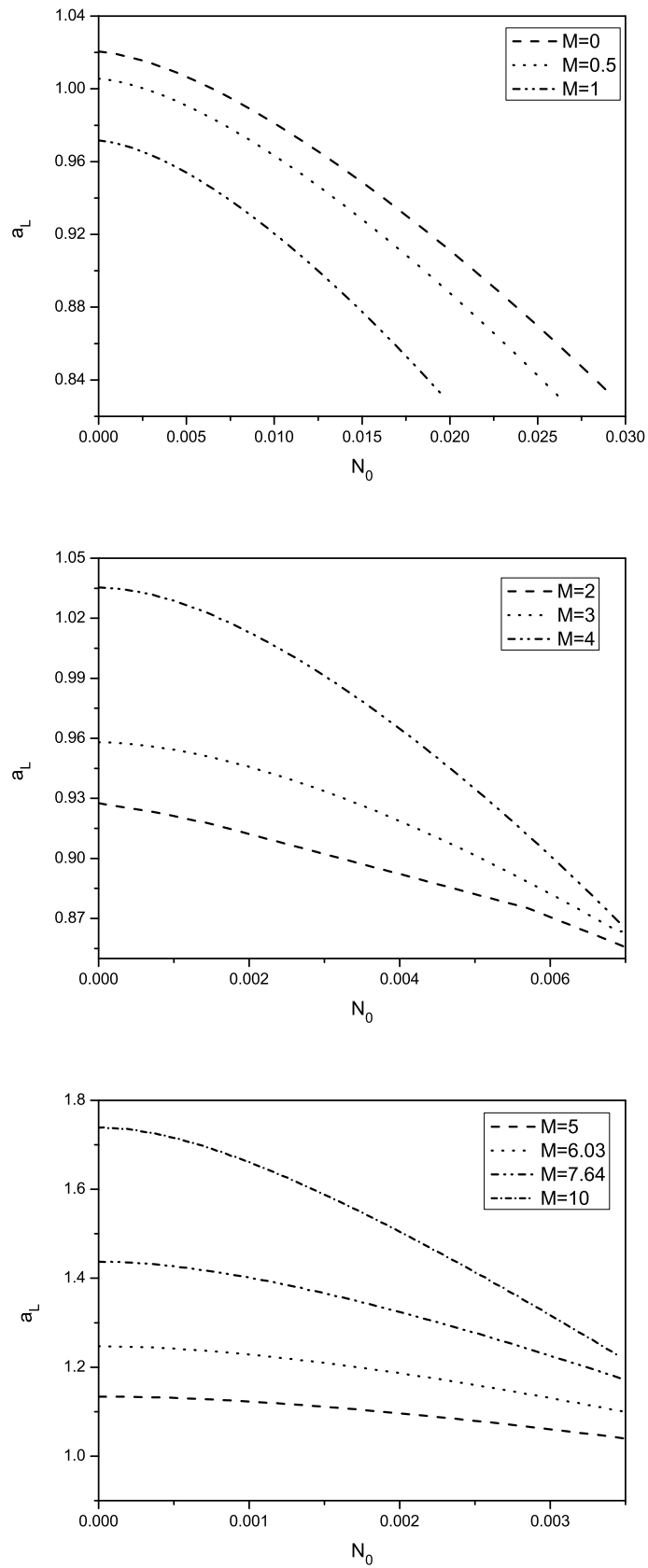


Figure 5.2: Critical wavenumber a_L against N_0 . The values of M are as indicated in the figures.

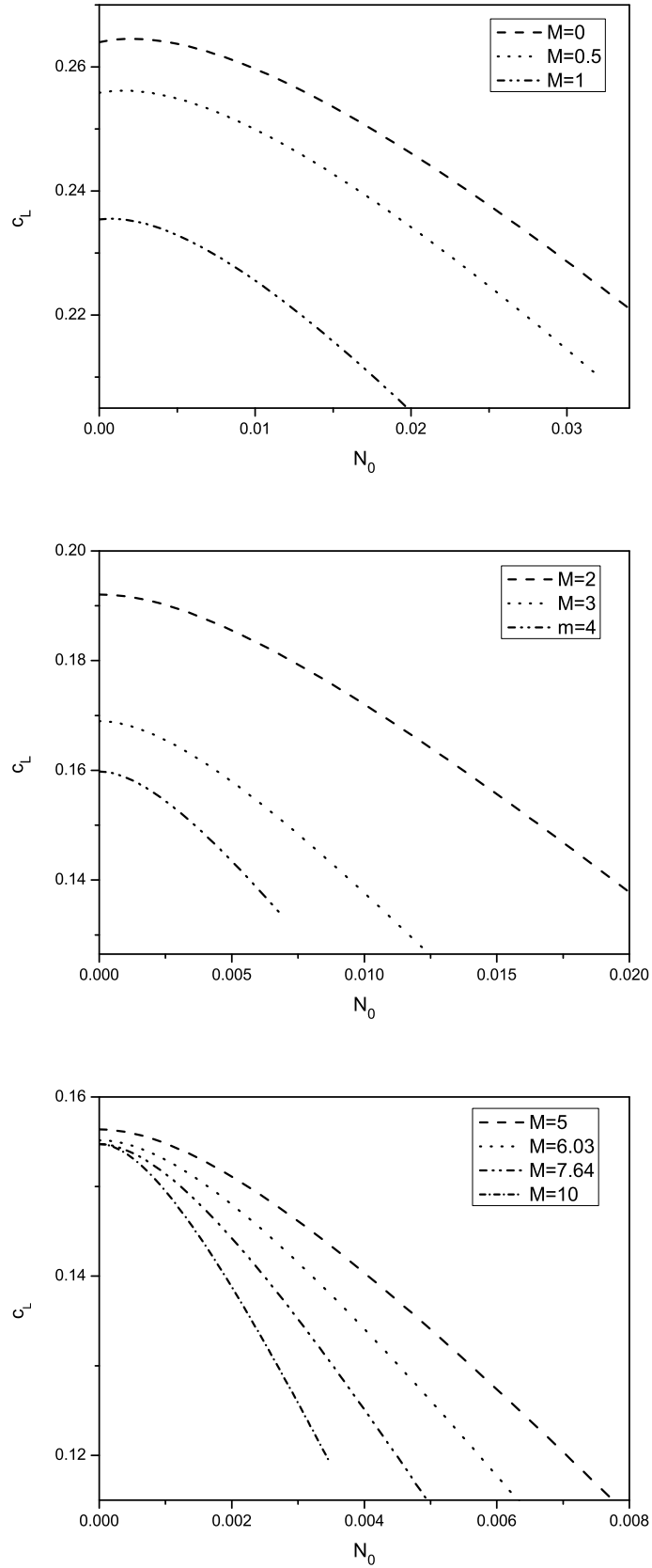


Figure 5.3: Critical value of c_r , namely c_L , against N_0 . The values of M are as indicated in the figures.

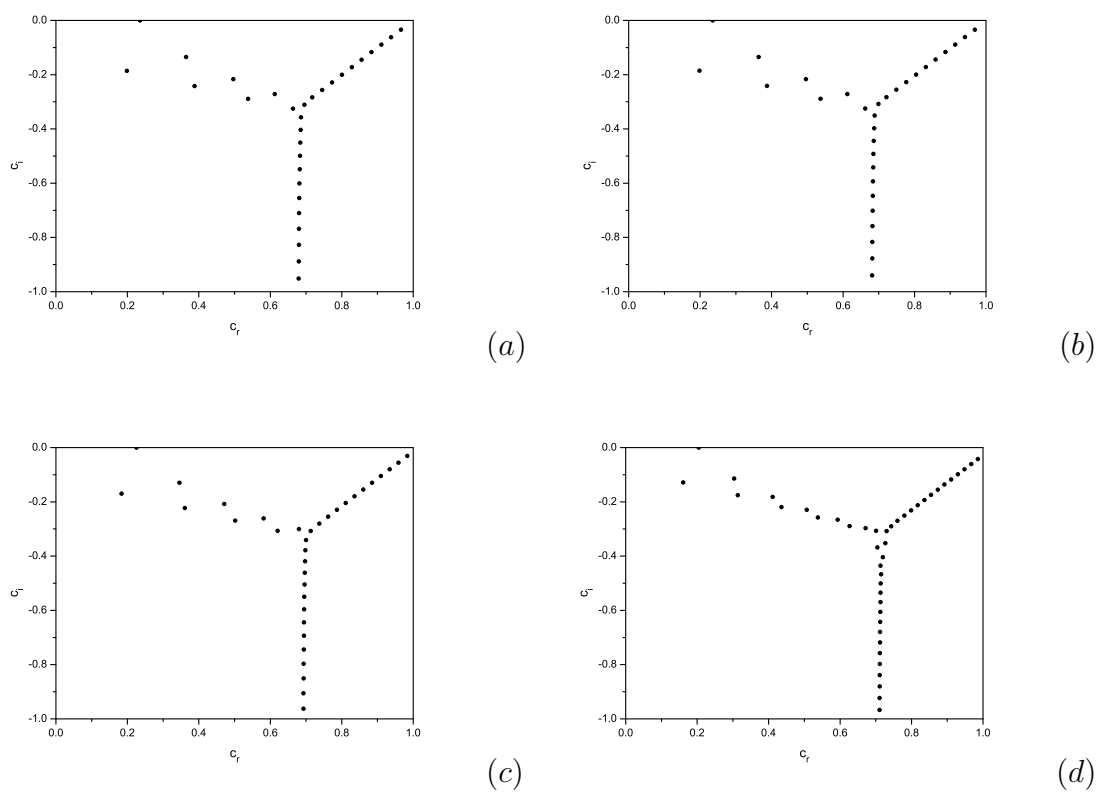


Figure 5.4: Spectral of growth rate $c = cr + ici$ at critical values with $M = 1$ (a) $N_0 = 0$, (b) $N_0 = 0.002$. (c) $N_0 = 0.01$. (d) $N_0 = 0.02$.

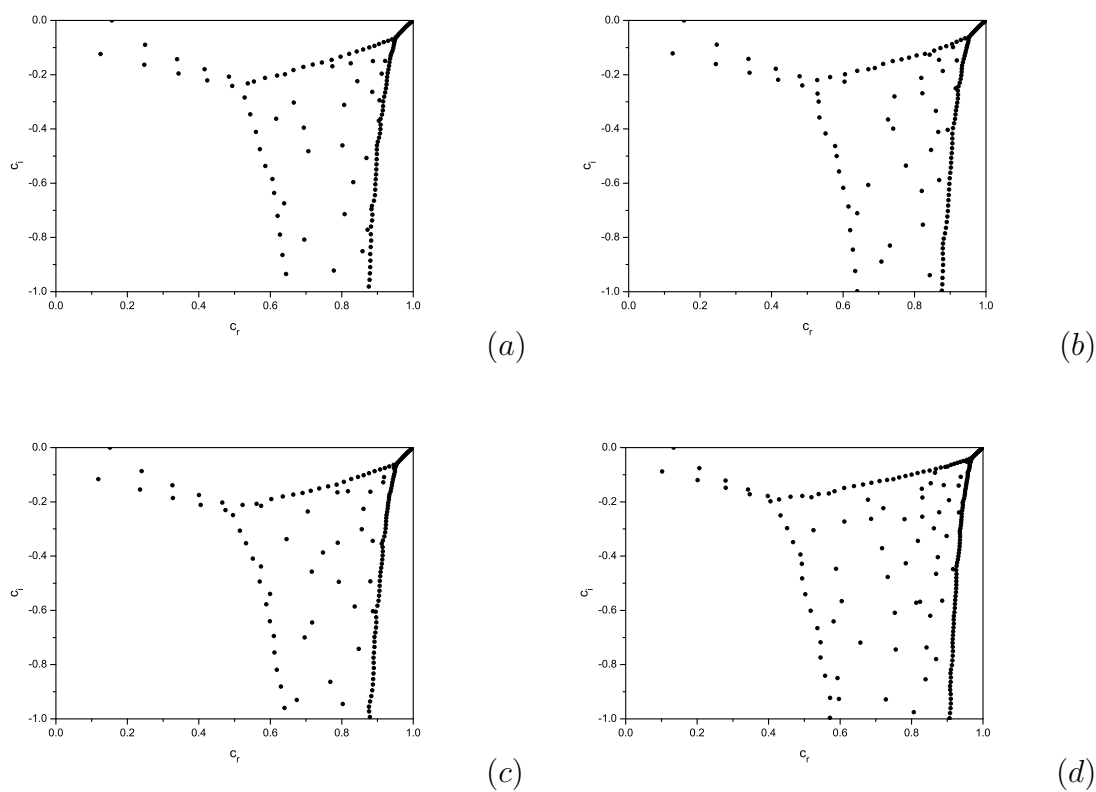


Figure 5.5: Spectral of growth rate $c = cr + ici$ at critical values with $M = 5$ (a) $N_0 = 0$. (b) $N_0 = 0.001$. (c) $N_0 = 0.002$. (d) $N_0 = 0.005$.

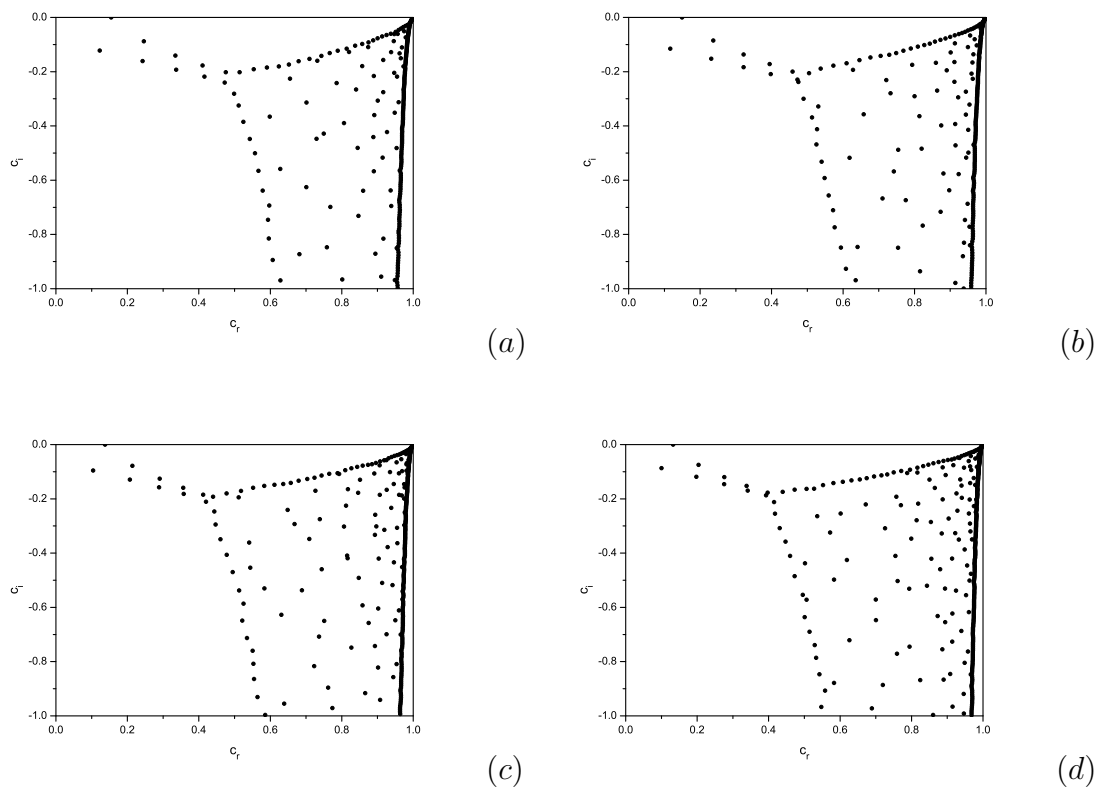


Figure 5.6: Spectral of growth rate $c = cr + ici$ at critical values with $M = 10$ (a) $N_0 = 0$. (b) $N_0 = 0.001$. (c) $N_0 = 0.002$. (d) $N_0 = 0.0025$.

Chapter 6

Numerical methods for solving some hydrodynamic stability problems

6.1 Introduction

The purpose of this chapter is to describe six very efficient numerical methods for solving a representative example of the stability problem of standard thermal convection in a thin fluid layer. The techniques referred to are the second order finite difference method, the high order finite difference scheme, p order finite element method, the Chebyshev collocation method-1 and method-2 and Chebyshev tau technique. Free-free, slip-slip, and fixed-slip boundary conditions are included.

The results in this chapter are also presented in the manuscript Harfash [75].

6.2 The effect of boundary conditions on convective instability

Let $x = (x, y, z)$ denote Cartesian coordinates in \mathbb{R}^3 . We consider a fluid contained in the region $\Omega \subset \mathbb{R}^3$, which is the infinite layer defined by $\Omega = (-\infty, \infty) \times (-\infty, \infty) \times [0, d]$. The behaviour of this fluid is described by the Boussinesq equations (6.2.1)-

(6.2.3), which comprise the Navier-Stokes equations and an energy balance equation:

$$\rho(v_{i,t} + v_j v_{i,j}) = -p_{,i} + \mu \Delta v_i - \rho k_i g [1 - \alpha(T - T_m)], \quad (6.2.1)$$

$$v_{i,i} = 0, \quad (6.2.2)$$

$$T_t + v_i T_{,i} = \kappa \Delta T, \quad (6.2.3)$$

where $\mathbf{v} = (u, v, w)$, p and T are velocity field, pressure, and temperature, respectively. Additionally, α is the thermal expansion coefficient, μ is the dynamic viscosity, g is the acceleration due to gravity, ρ is the density at the reference temperature T_m , κ is the thermometric conductivity and $\mathbf{k} = (0, 0, 1)$. Throughout, we use standard indicial notation and the Einstein summation convention so that e.g. $v_{i,t} = \partial v_i / \partial t$, $p_{,i} = \partial p / \partial x_i$, $v_j v_{i,j} \equiv (\mathbf{v} \cdot \nabla) \mathbf{v}$, and Δ is the Laplacian.

Ω is bounded above by the plane $z = d$ and below by the plane $z = 0$. The temperature at the upper and lower surfaces is kept constant

$$T|_{z=0} = T_L, \quad T|_{z=d} = T_U, \quad (6.2.4)$$

for constants $T_L > T_U$, and thus the layer is heated from below.

Navier [131] proposed a linear boundary condition relating \mathbf{v} to the shear rate, which has become standard in the study of boundary slip problems. Letting the surface $\partial\Omega$ have unit normal $n(x)$ directed out of the fluid, and $t(x)$ be any of the vectors tangent to $\partial\Omega$ at $x \in \partial\Omega$, this boundary condition can be expressed as

$$v_i n_i |_{\partial\Omega} = V_i n_i |_{\partial\Omega} \quad (6.2.5)$$

$$v_i t_i |_{\partial\Omega} = (V_i - \lambda \epsilon_{ij} n_j) t_i |_{\partial\Omega} \quad (6.2.6)$$

where $\epsilon = \epsilon(\mathbf{v})$ is the shear strain tensor, and $V_i = V_i(\partial\Omega)$ is the i th component of the local surface velocity. The model is essentially to set the component of \mathbf{v} normal to $\partial\Omega$ to be zero, thus imposing a condition of zero flux across the surface, while setting the two tangential components of \mathbf{v} proportional to the corresponding components of shear stress. We denote the constant of proportionality $\lambda \geq 0$, which has the dimension of length, and it can be seen that $\lambda = 0$ in (6.2.5) and (6.2.6) recovers the no-slip boundary condition.

We now apply the boundary conditions (6.2.5)-(6.2.6) to the Boussinesq model. Since the fluid is confined to Ω , from (6.2.5) we impose,

$$w = 0, \quad \text{at} \quad z = 0, d, \quad (6.2.7)$$

and we note that since there is no variation of w in the surfaces $\partial\Omega_L$ and $\partial\Omega_U$, we must have

$$w_{,x} = w_{,y} = 0, \quad \text{at} \quad z = 0, d. \quad (6.2.8)$$

Let λ_L be the slip length associated with the fluid-solid interface at $\partial\Omega_L$, and define λ_U similarly. Then, from (6.2.6) we have

$$u - \lambda_L u_{,z} = 0, \quad v - \lambda_L v_{,z} = 0, \quad \text{at} \quad z = 0, \quad (6.2.9)$$

$$u - \lambda_U u_{,z} = 0, \quad v - \lambda_U v_{,z} = 0, \quad \text{at} \quad z = d. \quad (6.2.10)$$

We note that these boundary conditions allow the zero solution $\mathbf{v} = 0$, which represents a fluid at rest. Let us now consider the basic steady state solution $(\bar{\mathbf{v}}, \bar{p}, \bar{T})$ of the system, where, as there is no fluid flow, $\bar{\mathbf{v}} \equiv 0$. Utilizing the boundary conditions and assuming that the basic steady state solutions are functions of z only

$$\bar{T} = -\beta z + T_L, \quad (6.2.11)$$

where $\beta = (T_L - T_U)/d$. The steady pressure \bar{p} may then be found from (6.2.1) which reduces to

$$-\frac{1}{\rho} \bar{p}_{,i} - k_i g [1 - \alpha(T - T_m)] = 0. \quad (6.2.12)$$

To study the stability of (6.2.1)-(6.2.3), we introduce a perturbation $(\mathbf{u}, \pi, \theta)$ to the steady state solution $(\bar{\mathbf{v}}, \bar{p}, \bar{T})$, where

$$v_i = \bar{v}_i + u_i, \quad p = \bar{p} + \pi, \quad T = \bar{T} + \theta.$$

Using (6.2.11), (6.2.12) the perturbed system is

$$u_{i,t} + u_j u_{i,j} = -\frac{1}{\rho} \pi_{,i} + \nu \Delta u_i + g \alpha k_i \theta, \quad (6.2.13)$$

$$\theta_t + u_i \theta_{,i} = \beta w + \kappa \Delta \theta, \quad (6.2.14)$$

where u_i is solenoidal, i.e. $u_{i,i} = 0$ and $\nu = \mu/\rho$.

We now introduce non-dimensionalised variable with scaling of

$$\mathbf{x} = \mathbf{x}^*d, \quad t = t^*\frac{d^2}{\nu}, \quad \mathbf{u} = U\mathbf{u}^*, \quad \theta = T^\sharp\theta^*, \quad \pi = P\pi^*, \quad U = \frac{\nu}{d}, \quad P = \frac{\rho\nu^2}{d^2},$$

$$T^\sharp = U\sqrt{\frac{\nu\beta}{\kappa\alpha g}}, \quad R = \sqrt{\frac{\alpha g d^4 \beta}{\kappa\nu}}, \quad Pr = \frac{\nu}{\kappa}.$$

Here Pr is the Prandtl number and $Ra = R^2$ is the Rayleigh number. With this scaling the non-dimensional form of (6.2.13)-(6.2.14) becomes (omitting the stars for ease of notation)

$$u_{i,t} + u_j u_{i,j} = -\pi_{,i} + \Delta u_i + k_i R\theta, \quad (6.2.15)$$

$$u_{i,i} = 0, \quad (6.2.16)$$

$$Pr(\theta_t + u_i \theta_{,i}) = R\omega + \Delta\theta. \quad (6.2.17)$$

The spatial domain is now $\{(x, y) \in \mathbb{R}^2\} \times \{z \in (0, 1)\}$. The perturbed boundary conditions are given by

$$u - \lambda_L u_{,z} = 0, \quad v - \lambda_L v_{,z} = 0, \quad \text{at } z = 0, \quad (6.2.18)$$

$$u - \lambda_U u_{,z} = 0, \quad v - \lambda_U v_{,z} = 0, \quad \text{at } z = 1, \quad (6.2.19)$$

$$\theta = 0, \quad \text{on } z = 0, 1. \quad (6.2.20)$$

We have reduced the problem of finding conditions for the onset of convection in our fluid layer to that of investigating the stability of the basic steady state solutions with respect to perturbations \mathbf{u}, π, θ as defined above. In this way we aim to find, for fixed λ_L and λ_U , the critical Rayleigh number $R_{crit}^2(\lambda_L, \lambda_U)$ such that solutions to (2.20)-(2.22) decay over time for $R < R_{crit}$ and grow for $R > R_{crit}$, regardless of the initial data .

We do this by showing that there exists R_L such that thermal instability will occur for $R > R_L$, and R_E such that $R < R_E$ guarantees stability of the the basic steady state solutions. It has been shown that $R_E = R_L = R_{crit}$ for system (6.2.15)-(6.2.17) for no-slip boundary conditions (see Joseph [89, 90]) and for slip boundary conditions (see Webber [222]), thus, it is enough to solve the linear system to find

the linear and nonlinear threshold and hence we can solve the system with solutions of the form of single Fourier modes.

The linearised equations are obtained from (6.2.15)-(6.2.17) by omitting a non-linear terms. The resulting linearized equations possess solutions of type

$$u_i(\mathbf{x}, t) = u_i(\mathbf{x})e^{\sigma t}, \theta(\mathbf{x}, t) = \theta(\mathbf{x})e^{\sigma t}, \pi(\mathbf{x}, t) = \pi(\mathbf{x})e^{\sigma t},$$

where σ is the growth rate and a complex constant. $u_i(\mathbf{x}), \phi(\mathbf{x}), \pi(\mathbf{x})$ then satisfy

$$-\pi_{,i} + \Delta u_i + k_i R \theta = \sigma u_i, \quad (6.2.21)$$

$$Rw + \Delta \theta = \sigma P_r \theta. \quad (6.2.22)$$

Taking the double *curl* of (6.2.21), using the third component, (and the fact that u is solenoidal) we have

$$\Delta^2 w + R \Delta^* \theta = \sigma \Delta w, \quad (6.2.23)$$

where $\Delta^* = \partial^2/\partial x^2 + \partial^2/\partial y^2$, $D = d/dz$. We now introduce normal modes of the form $w = W(z)f(x, y)$, and $\theta = \Theta(z)f(x, y)$ where $f(x, y)$ is a plan-form which tiles the plane (x, y) with

$$\Delta^* f = -a^2 f. \quad (6.2.24)$$

The plan-forms represent the horizontal shape of the convection cells formed at the onset of instability. These cells form a regular horizontal pattern tiling the (x, y) plane, where the wavenumber a (see [32] and [196]) is a measure of the width of the convection cell. Using (6.2.24), and applying the normal mode representations to (6.2.22) and (6.2.23) we find

$$(D^2 - a^2)^2 W - a^2 R \Theta = \sigma (D^2 - a^2) W, \quad (6.2.25)$$

$$(D^2 - a^2) \Theta + RW = \sigma P_r \Theta, \quad (6.2.26)$$

where $D = d/dz$, and $z \in (0, 1)$. It is easy to show that $\sigma \in \mathbb{R}$, and therefore the principle of "exchange of stabilities" applies to the linearized system, and thus it is enough to solve system (6.2.25)-(6.2.26) with $\sigma = 0$ i.e we shall solve the following system

$$(D^2 - a^2)^2 W = a^2 R \Theta, \quad (6.2.27)$$

$$(D^2 - a^2)\Theta = -RW. \quad (6.2.28)$$

The boundary conditions which w must satisfy are derived from the conditions (6.2.18) and (6.2.19) and the incompressibility condition $u_{,x} + v_{,y} + w_{,z} = 0$, are

$$w(0) = w(1) = 0, \quad \lambda_L w''(0) - w'(0) = 0, \quad \lambda_U w''(1) + w'(1) = 0, \quad (6.2.29)$$

and the boundary conditions for Θ are

$$\Theta(0) = \Theta(1) = 0. \quad (6.2.30)$$

Equations (6.2.27) and (6.2.28) are the classic stability equations for the Bénard problem. We note that in the limit $\lambda_U \rightarrow 0$ we obtain from (6.2.29) the no-slip boundary condition at $z = 1$, while for $\lambda_U \rightarrow \infty$ we recover the free boundary condition (and similarly for λ_L at $z = 0$). In the next section, six numerical methods are used to solve this system (6.2.27) and (6.2.28).

6.3 Numerical methods for the eigenvalue system

6.3.1 Chebyshev tau

Equation (6.2.27) has a fourth order derivative. Dongarra et al. [43] show that high order differentiation matrices, for instance in this case the D^4 matrix, can introduce significant round off errors. Therefore we use what is described in the literature as a D^2 method, and make the substitution. Letting λ_U and $\lambda_L \rightarrow \infty$, then we obtain from (6.2.29) the free boundary condition at $z = 0$ and $z = 1$. We introduce new function $A = (D^2 - a^2)W$. Rewriting equations (6.2.27) and (6.2.28) in terms of the new variable A , we require to solve

$$(D^2 - a^2)W = A, \quad (6.3.31)$$

$$(D^2 - a^2)A = a^2 R \Theta, \quad (6.3.32)$$

$$(D^2 - a^2)\Theta = -RW, \quad (6.3.33)$$

with boundary conditions

$$\Theta = W = A = 0, \quad \text{at } z = 0, 1. \quad (6.3.34)$$

To employ the Chebyshev tau technique, system (6.3.31)-(6.3.34) is converted to the Chebyshev domain $(-1, 1)$, and then W, A and Φ are written as a finite series of Chebyshev polynomials

$$W = \sum_{k=0}^{N+2} W_k T_k(z), \quad A = \sum_{k=0}^{N+2} A_k T_k(z), \quad \Theta = \sum_{k=0}^{N+2} \Theta_k T_k(z).$$

The weighted inner product of each equation is taken with some T_k and the orthogonality of the Chebyshev polynomial is utilised to form the generalised eigenvalue problem

$$\begin{pmatrix} 4D_2 - a^2 I & -I & O \\ O & 4D_2 - a^2 I & O \\ O & O & 4D_2 - a^2 I \end{pmatrix} \mathbf{Q} = R \begin{pmatrix} O & O & O \\ O & O & a^2 I \\ -I & O & O \end{pmatrix} \mathbf{Q},$$

where $\mathbf{Q} = \left(\hat{W}, \hat{A}, \hat{\Phi} \right)^T$, $\hat{W} = (W_0, \dots, W_{N+2})^T$, $\hat{A} = (A_0, \dots, A_{N+2})^T$, $\hat{\Phi} = (\Theta_0, \dots, \Theta_{N+2})^T$, D_2 is the Chebyshev representation of D^2 , and I is the identity matrix. Using the boundary conditions and the fact that $T_n(\pm 1) = (\pm 1)^n$ we remove the last two rows of each $(N+2) \times (N+2)$ block and replace these rows by the discrete form of the boundary conditions (6.3.34) which have the form

$$BC_1 : \sum_{n=0}^N W_n = 0, \quad (6.3.35)$$

$$BC_2 : \sum_{n=0}^N (-1)^n W_n = 0, \quad (6.3.36)$$

$$BC_3 : \sum_{n=0}^N A_n = 0, \quad (6.3.37)$$

$$BC_4 : \sum_{n=0}^N (-1)^n A_n = 0, \quad (6.3.38)$$

$$BC_5 : \sum_{n=0}^N \phi_n = 0, \quad (6.3.39)$$

$$BC_6 : \sum_{n=0}^N (-1)^n \phi_n = 0. \quad (6.3.40)$$

Then, the final eigenvalue system has the following form

$$\begin{pmatrix} 4D^2 - a^2I & -I & O \\ BC_1 & 0\dots 0 & 0\dots 0 \\ BC_2 & 0\dots 0 & 0\dots 0 \\ O & 4D^2 - a^2I & O \\ 0\dots 0 & BC_3 & 0\dots 0 \\ 0\dots 0 & BC_4 & 0\dots 0 \\ O & O & 4D^2 - a^2I \\ 0\dots 0 & 0\dots 0 & BC_5 \\ 0\dots 0 & 0\dots 0 & BC_6 \end{pmatrix} \mathbf{Q} = R \begin{pmatrix} O & O & O \\ 0\dots 0 & 0\dots 0 & 0\dots 0 \\ 0\dots 0 & 0\dots 0 & 0\dots 0 \\ O & O & a^2I \\ 0\dots 0 & 0\dots 0 & 0\dots 0 \\ 0\dots 0 & 0\dots 0 & 0\dots 0 \\ -I & O & O \\ 0\dots 0 & 0\dots 0 & 0\dots 0 \\ 0\dots 0 & 0\dots 0 & 0\dots 0 \end{pmatrix} \mathbf{Q}. \quad (6.3.41)$$

We solve this eigenvalue system by passing the above matrices to the Matlab's QZ subroutine. For an initial value of the wave number a , we obtain a spectrum of eigenvalues then we select the smallest eigenvalue R_m such that the fluid is stable for all $R < R_m$. We then repeat for other values of a , so that we may build the neutral curve of $Ra = R_m^2$ against a , along which the fluid is neutrally stable. By iterating over a we are thus able to obtain the critical Rayleigh number Ra_{crit} as the minimum value on this curve, which occurs at wavenumber a_{crit} .

Also, we can adopt another technique to apply the boundary conditions where we can find the values of W_{N+1} , W_{N+2} , A_{N+1} , A_{N+2} , Φ_{N+1} and Φ_{N+2} from the boundary conditions then we substitute these values in the system and thus we remove the last two rows. The new system have the order $(N+1) \times (N+1)$ instead of $(N+3) \times (N+3)$.

However, if λ_U and λ_L are fixed finite numbers, and thus our boundary conditions are slip-slip. The solution of (6.3.31)-(6.3.33) with slip-slip boundary conditions produces the same eigenvalue system to (6.3.41). The boundary conditions $BC1, BC2, BC5, BC6$ still the same as in (6.3.41), while the changes will be in the $BC3, BC4$ which have the following new forms:

$$BC_3 : \sum_{n=0}^N 2N_0 A_n + \sum_{n=0}^N n^2 W_n = 0, \quad (6.3.42)$$

$$BC_4: \sum_{n=0}^N 2N_0(-1)^n A_n + \sum_{n=0}^N (-1)^{n+1} n^2 W_n = 0, \quad (6.3.43)$$

Finally, letting $\lambda_U \rightarrow 0$ and λ_L a fixed finite numbers, i.e. we have fixed-slip boundary conditions. We introduce new function $\Psi = DW$, then system (6.2.27) and (6.2.28) can written in the following form:

$$DW - \Psi = 0, \quad (6.3.44)$$

$$D^3\Psi - 2a^2 DA + a^4 W - a^2 R\Theta = 0, \quad (6.3.45)$$

$$(D^2 - a^2)\Phi + RW = 0, \quad (6.3.46)$$

hence, the boundary conditions have the form

$$W = \phi = 0, \quad z = 0, 1, \quad (6.3.47)$$

$$N_0 D\Psi + \Psi = 0, \quad z = 1, \quad (6.3.48)$$

$$\Psi = 0, \quad z = 0, \quad (6.3.49)$$

then, we can apply the same procedure which are used for free-free and slip-slip boundary conditions to produce the eigenvalue system.

6.3.2 Finite difference scheme

Standard finite difference

The standard second and fourth order central difference operators at grid point i can be written as:

$$\begin{aligned} \delta^2 u_i &= \frac{u_{i+1} - 2u_i + u_{i-1}}{h^2}, \\ \delta^4 u_i &= \frac{u_{i+2} - 4u_{i+1} + 6u_i - 4u_{i-1} + u_{i-2}}{h^4}. \end{aligned} \quad (6.3.50)$$

The second and the fourth order derivatives for the function u at grid point i can be approximated by a second order accuracy as

$$\begin{aligned} \left. \frac{d^2 u}{dz^2} \right|_i &= \delta^2 u_i - \frac{h^2}{12} \frac{d^4 u}{dz^4} + O(h^4), \\ \left. \frac{d^4 u}{dz^4} \right|_i &= \delta^4 u_i - \frac{h^2}{6} \frac{d^6 u}{dz^6} + O(h^4). \end{aligned} \quad (6.3.51)$$

By using these finite difference approximations, (6.2.27) and (6.2.28) can be discretized at a given grid point i respectively as,

$$\delta_z^4 W_i - 2a^2 \delta_z^2 W_i + a^4 W_i - a^2 R \Theta_i = 0, \quad (6.3.52)$$

$$\delta_z^2 \Theta_i - a^2 \Theta_i + R W_i = 0, \quad (6.3.53)$$

The boundary conditions $D_z^2 W = 0$ at $z = 0, 1$ are approximated using finite difference technique as $W_{-1} = -W_1$ and $W_{N+1} = -W_{N-1}$. In this manner, equations (6.3.52) and (6.3.53) and the fixed boundary conditions lead to the finite difference equations

$$\begin{aligned} \frac{W_{i+2}}{h^4} - \left(\frac{4}{h^4} + \frac{2a^2}{h^2}\right)W_{i+1} + \left(\frac{6}{h^4} + \frac{4a^2}{h^2} + a^4\right)W_i - \left(\frac{4}{h^4} + \frac{2a^2}{h^2}\right)W_{i-1} \\ + \frac{W_{i-2}}{h^4} - Ra^2 \Theta_i = 0, \end{aligned} \quad (6.3.54)$$

$$i = 2, \dots, N - 2,$$

$$\frac{\Theta_{i+1}}{h^2} - \left(\frac{2}{h^2} + a^2\right)\Theta_i + \frac{\Theta_{i-1}}{h^2} + R W_i = 0, \quad (6.3.55)$$

$$i = 1, \dots, N - 1,$$

$$\frac{W_3}{h^4} - \left(\frac{4}{h^4} + \frac{2a^2}{h^2}\right)W_2 + \left(\frac{5}{h^4} + \frac{4a^2}{h^2} + a^4\right)W_1 + Ra^2 \Phi_1 = 0, \quad (6.3.56)$$

which is the equation obtained from (6.3.52) with $i = 1$, and

$$\left(\frac{5}{h^4} + \frac{4a^2}{h^2} + a^4\right)W_{N-1} - \left(\frac{4}{h^4} + \frac{2a^2}{h^2}\right)W_{N-2} + \frac{W_{N-3}}{h^4} + Ra^2 \Phi_{N-1} = 0, \quad (6.3.57)$$

which arises from (6.3.52) with $i = N - 1$.

For slip-slip boundary conditions, we adapt equations (6.3.56) and (6.3.57). At $i = 1$, we substitute $W_0 = 0$ and $W_{-1} = -(N0/h^2 - 1/2h)/(N0/h^2 + 1/2h)W_1$ in (6.3.54) to get the equivalent equation to (6.3.56). At $i = N$, we substitute $W_N = 0$ $W_{N+1} = -(N0/h^2 - 1/2h)/(N0/h^2 + 1/2h)W_{N-1}$ in (6.3.54) to get the equivalent equation to (6.3.57). For fixed-slip boundary conditions, At $i = N$, we substitute $W_N = 0$ $W_{N+1} = W_{N-1}$ in (6.3.54) to get the equivalent equation to (6.3.57). At $i = 1$ the equation still the same with slip-slip boundary conditions.

High order finite difference

The main idea of the high order finite difference scheme is to find the values of truncation errors from the original differential equation and substitute these values in the finite difference formula. In this scheme we can reduce the order of truncation errors. In our system we can easily find the value of D^6W and $D^4\Theta$ as follows

$$D^6W = (2a^2 - M^2)D^4W - a^4D^2W + a^2RD^2\Theta, \quad (6.3.58)$$

$$D^4\Theta = a^2D^2\Phi - RD^2W, \quad (6.3.59)$$

Substituting the values of D^6W and $D^4\Theta$ in (6.3.51), and then approximate D^2W , D^4W and $D^2\Theta$ by using standard second order finite difference we have the following fourth order finite difference formula

$$\left. \frac{d^2W}{dz^2} \right|_i = \delta^2W_i - \frac{h^2}{12}\delta_z^4(W_i + O(h^2)) + O(h^4), \quad (6.3.60)$$

$$\left. \frac{d^2\Theta}{dz^2} \right|_i = \delta^2\Theta_i - \frac{h^2}{12}\{a^2(\delta^2\Phi_i + O(h^2)) - R(\delta^2W_i + O(h^2))\} + O(h^4), \quad (6.3.61)$$

$$\left. \frac{d^4W}{dz^4} \right|_i = \delta^4W_i - \frac{h^2}{6}\{2a^2(\delta^4W_i + O(h^2)) - a^4(\delta^2W_i + O(h^2)) + a^2R(\delta^2\Theta_i + O(h^2))\} + O(h^4). \quad (6.3.62)$$

It is clear that the overall truncation error will be of $O(h^4)$. Using (6.3.60)-(6.3.62) finite difference approximations, (6.2.27) and (6.2.28) can be approximated at a grid point i respectively as,

$$r_2\delta^4W_i + r_1\delta^2W_i + a^4W_i - a^2R(1 + \frac{h^2}{6}\delta^2)\Theta_i = 0, \quad (6.3.63)$$

$$R(1 + \frac{\Delta z^2}{12}\delta^2)W_i + r_3\delta_z^2\Theta_i - a^2\Phi_i = 0, \quad (6.3.64)$$

where $r_1 = (h^2/6)a^4 - 2a^2$, $r_2 = 1 - (h^2/6)a^2$, $r_3 = 1 - (h^2/12)a^2$ and $r_4 = 1 - (h^2/6)a^2$. Thus, for free-free boundary conditions, (6.3.63) and (6.3.64) produce the following high order finite difference equations

$$\begin{aligned} \frac{r_2}{h^4}W_{i+2} + (-\frac{4r_2}{h^4} + \frac{r_1}{h^2})W_{i+1} + (\frac{6r_2}{h^4} - \frac{2r_1}{h^2} + a^4)W_i + (-\frac{4r_2}{h^4} + \frac{r_1}{h^2})W_{i-1} + \frac{r_2}{h^4}W_{i-2} \\ - Ra^2[\frac{1}{6}\Theta_{i-1} + \frac{2}{3}\Theta_i + \frac{1}{6}\Theta_{i+1}] = 0, \end{aligned} \quad (6.3.65)$$

$$i = 2, \dots, N - 2,$$

$$-R \left[\frac{-1}{12} W_{i-1} - \frac{5}{6} W_i - \frac{1}{12} W_{i+1} \right] + r_3 \frac{\Theta_{i-1}}{h^2} - \left(\frac{2r_3}{h^2} + a^2 \right) \Theta_i + r_3 \frac{\Theta_{i+1}}{h^2} = 0, \quad (6.3.66)$$

$$i = 1, \dots, N - 1,$$

$$\frac{r_2}{h^4} W_3 + \left(-\frac{4r_2}{h^4} + \frac{r_1}{h^2} \right) W_2 + \left(\frac{5r_2}{h^4} - \frac{2r_1}{h^2} + a^4 \right) W_1 - Ra^2 \left[\frac{2}{3} \Theta_1 + \frac{1}{6} \Theta_2 \right] = 0, \quad (6.3.67)$$

which is the equation obtained from (6.3.63) with $i = 1$, and

$$\left(\frac{5r_2}{h^4} - \frac{2r_1}{h^2} + a^4 \right) W_{N-1} + \left(-\frac{4r_2}{h^4} + \frac{r_1}{h^2} \right) W_{N-2} + \frac{r_2}{h^4} W_{N-3} - Ra^2 \left[\frac{1}{6} \Theta_{N-2} + \frac{2}{3} \Theta_{N-1} \right] = 0, \quad (6.3.68)$$

which arises from (6.3.63) with $i = N - 1$.

For slip-slip boundary conditions, we change the equations (6.3.67) and (6.3.68) by new equations. At $i = 1$, we substitute $W_0 = 0$ and $W_{-1} = -(N0/h^2 - 1/2h)/(N0/h^2 + 1/2h)W_1$ in (6.3.65) to get the equivalent equation to (6.3.67). At $i = N$, we substitute $W_N = 0$ $W_{N+1} = -(N0/h^2 - 1/2h)/(N0/h^2 + 1/2h)W_{N-1}$ in (6.3.65) to get the equivalent equation to (6.3.68). For fixed-slip boundary conditions, At $i = N$, we substitute $W_N = 0$ $W_{N+1} = W_{N-1}$ in (6.3.65) to get the equivalent equation to (6.3.68). At $i = 1$, the equation is still the same with slip-slip boundary conditions.

Generally, the finite difference and high order finite difference schemes produce a generalized matrix eigenvalue problem of form

$$\Lambda \Sigma = R \Xi \Sigma, \quad (6.3.69)$$

where Σ is the eigenfunction vector, the Matrices Λ and Ξ have different values according to each case and R represent the eigenvalues of our problem.

6.3.3 Finite element method

In this section we will discuss the finite element method which is used to solve systems (6.2.27) and (6.2.28). Firstly, we introduce a new variable $\Upsilon = D^2W$, Therefore, system (6.2.27) and (6.2.28) become as follows

$$D^2W = \Upsilon,$$

$$D^2\Upsilon - 2a^2\Upsilon + a^4W - a^2R\Theta = 0, (D^2 - a^2)\Theta + RW = 0, \quad (6.3.70)$$

with free-free boundary conditions

$$W = \Upsilon = \Theta = 0, \quad \text{at } z = 0, 1, \quad (6.3.71)$$

or with slip-slip boundary conditions

$$\begin{aligned} W = \Theta = 0, & \quad \text{at } z = 0, 1, \\ \lambda_L\Upsilon - DW = 0, & \quad \text{at } z = 0, \\ \lambda_U\Upsilon + DW = 0, & \quad \text{at } z = 1, \end{aligned} \quad (6.3.72)$$

or with fixed-slip boundary conditions

$$\begin{aligned} W = \Theta = 0, & \quad \text{at } z = 0, 1, \\ DW = 0, & \quad \text{at } z = 0, \\ \lambda_U\Upsilon + DW = 0, & \quad \text{at } z = 1, \end{aligned} \quad (6.3.73)$$

Firstly, we divided the period $0 \leq x \leq 1$ into n elements, each element e having $p + 1$ nodes n_1, n_2, \dots, n_{p+1} . In term of its $p + 1$ nodal values, the variables W, Υ, Θ may be uniquely interpolated as a polynomial of $p + 1$ order, the interpolation being given by

$$W^e = N^e \delta_W^e, \quad \Upsilon^e = N^e \delta_\Upsilon^e, \quad \Theta^e = N^e \delta_\Theta^e, \quad (6.3.74)$$

where $\delta_W^e = \{W_{n_1}, \dots, W_{n_{p+1}}\}$, $\delta_\Upsilon^e = \{\Upsilon_{n_1}, \dots, \Upsilon_{n_{p+1}}\}$ and $\delta_\Theta^e = \{\Theta_{n_1}, \dots, \Theta_{n_{p+1}}\}$, and the shape function matrix is

$$N^e = [N_{n_1}^p, \dots, N_{n_{p+1}}^p].$$

Therefore the over-all finite element approximation is given by

$$W = \sum_{e=1}^n W^e, \quad \Upsilon = \sum_{e=1}^n \Upsilon^e, \quad \Theta = \sum_{e=1}^n \Theta^e, \quad (6.3.75)$$

The variational formulations of (6.3.70) is

$$\text{Minimize } I_W[W] = \int_0^1 (-(DW)^2 - 2\Upsilon W) dx, \quad (6.3.76)$$

$$\text{Minimize } I_\Upsilon[\Upsilon] = \int_0^1 (-(D\Upsilon)^2 - 2a^2\Upsilon^2 + 2a^4W\Upsilon - 2a^2R\Theta\Upsilon) dx, \quad (6.3.77)$$

$$\text{Minimize } I_{\Theta}[\Theta] = \int_0^1 (-(D\Theta)^2 - a^2\Phi^2 + 2RW\Theta)dx. \quad (6.3.78)$$

Substitution of (6.3.75) into variational formulations (6.3.76)-(6.3.78) gives

$$I_W[W] = \sum_{e=1}^n \int_e (-(DW^e)^2 - 2\Upsilon^e W^e)dx = \sum_{e=1}^n I_W^e, \quad (6.3.79)$$

$$I_{\Upsilon}[\Upsilon] = \sum_{e=1}^n \int_e (-(D\Upsilon^e)^2 - 2a^2(\Upsilon^e)^2 + 2a^4 W^e \Upsilon^e - 2a^2 R\Theta^e \Upsilon)dx = \sum_{e=1}^n I_{\Upsilon}^e, \quad (6.3.80)$$

$$I_{\Theta}[\Theta] = \sum_{e=1}^n \int_e (-(D\Theta^e)^2 - a^2(\Theta^e)^2 + 2RfW^e \Theta^e)dx = \sum_{e=1}^n I_{\Theta}^e, \quad (6.3.81)$$

here, we use the fact that the functions $W^e, \Upsilon^e, \Theta^e$ are equivalent to zero outside the element e . Using (6.3.79)- (6.3.81), we obtain

$$I_W[W] = I_W(W_1, \dots, W_m),$$

$$I_{\Upsilon}[\Upsilon] = I_{\Upsilon}(\Upsilon_1, \dots, \Upsilon_m),$$

$$I_{\Theta}[\Theta] = I_{\Theta}(\Theta_1, \dots, \Theta_m),$$

where m is the number of all nodes in all elements. Then using the Rayleigh-Ritz procedure to minimize $I_W[W], I_{\Upsilon}[\Upsilon], I_{\Theta}[\Theta]$, with respect to the variational parameters $W_i, \Upsilon_i, \Theta_i$ respectively, gives

$$\frac{\partial I_W}{\partial W_i} = \sum_{e=1}^n \frac{\partial I_W^e}{\partial W_i} = 0, \quad i = 1, \dots, m, \quad (6.3.82)$$

$$\frac{\partial I_{\Upsilon}}{\partial \Upsilon_i} = \sum_{e=1}^n \frac{\partial I_{\Upsilon}^e}{\partial \Upsilon_i} = 0, \quad i = 1, \dots, m, \quad (6.3.83)$$

$$\frac{\partial I_{\Theta}}{\partial \Theta_i} = \sum_{e=1}^n \frac{\partial I_{\Theta}^e}{\partial \Theta_i} = 0, \quad i = 1, \dots, m. \quad (6.3.84)$$

Hence, we arrive to following formula

$$\frac{\partial I_W^e}{\partial W_{n_i}} = -2 \int_e \frac{dN_{n_i}^p}{dz} \frac{dN^e}{dz} \delta_W^e dx - 2 \int_e N_{n_i}^p N^e \delta_{\Upsilon}^e dx = 0, \quad (6.3.85)$$

$$\frac{\partial I_{\Upsilon}^e}{\partial \Upsilon_{n_i}} = 2a^4 \int_e N_{n_i}^p N^e \delta_W^e dx - 2 \int_e \left(\frac{dN_{n_i}^p}{dz} \frac{dN^e}{dz} + 2a^2 N_{n_i}^p N^e \right) \delta_{\Upsilon}^e dx$$

$$-2a^2R \int_e N_{n_i}^p N^e \delta_\Theta^e dx = 0, \quad (6.3.86)$$

$$\frac{\partial I_\Theta^e}{\partial \Theta_{n_i}} = -2 \int_e \left[\frac{dN_{n_i}^p}{dz} \frac{dN^e}{dz} + a^2 N_{n_i}^p N^e \right] \delta_\Theta^e dx + 2R \int_e N_{n_i}^p N^e \delta_W^e dx = 0. \quad (6.3.87)$$

Then, the matrix representation for the system of equation of element e take the form

$$\begin{aligned} & \begin{pmatrix} -D_2^e & -F_1^e & O \\ a^4 F_1^e & -D_2^e - 2a^2 F_1^e & O \\ O & O & -D_2^e - a^2 F_1^e \end{pmatrix} \begin{pmatrix} \delta_W^e \\ \delta_\Upsilon^e \\ \delta_\Theta^e \end{pmatrix} \\ &= R \begin{pmatrix} O & O & O \\ O & O & a^2 F_1^e \\ -F_1^e & O & O \end{pmatrix} \begin{pmatrix} \delta_W^e \\ \delta_\Upsilon^e \\ \delta_\Theta^e \end{pmatrix}, \end{aligned} \quad (6.3.88)$$

where

$$O_{ij} = 0, \quad D_{2ij}^e = \int_{-1}^1 \frac{dN_{n_i}^p}{dz} \frac{dN_{n_j}^p}{dz} dz, \quad F_{1ij}^e = \int_{-1}^1 N_{n_i}^p N_{n_j}^p dz, \quad i = 1, \dots, p+1, \quad j = 1, \dots, p+1.$$

The above integral can be evaluated by applying the classical finite element nodal basis functions in one dimension on the standard element $\Omega_{st} = (-1, 1)$. The standard shape functions are defined by the set of Lagrange polynomials

$$N_{n_i}^p(\zeta) = \prod_{j=n_1, j \neq i}^{n_{p+1}} \frac{\zeta - \zeta_j}{\zeta_i - \zeta_j}, \quad (6.3.89)$$

where $\zeta = 2/h(z - z_m)$, h is the length of element and z_m is the mid-point. Thus these integrations take the form:

$$D_{2ij}^e = \frac{2}{h} \int_{-1}^1 \frac{dN_{n_i}^p}{d\zeta} \frac{dN_{n_j}^p}{d\zeta} d\zeta,$$

$$F_{1ij}^e = \frac{h}{2} \int_{-1}^1 N_{n_i}^p N_{n_j}^p d\zeta$$

$$i = 1, \dots, p+1, \quad j = 1, \dots, p+1.$$

The integral were calculated analytically using Matlab routines. Finally, we assemble the systems of all elements $e = 1, \dots, n$ to get the main system which has the form

$$\Lambda \Sigma = R \Xi \Sigma, \quad (6.3.90)$$

where $\Sigma = (W_1, \dots, W_m, \Upsilon_1, \dots, \Upsilon_m, \Theta_1, \dots, \Theta_m)^T$.

For free surface boundary conditions, we can impose the boundary conditions easily by removing $W_1, W_m, \Upsilon_1, \Upsilon_m, \Theta_1, \Theta_m$ from the system and thus we remove the rows and columns of order $1, m, m + 1, 2m, 2m + 1$ and $3m$.

For slip-slip boundary conditions, firstly, we transform these condition to the local coordinate ζ and thus these boundary condition take the form

$$\begin{aligned} W = \Theta = 0, & \quad \text{at } \zeta = -1, 1, \\ \lambda_L \Upsilon - \frac{2}{h} DW = 0, & \quad \text{at } \zeta = -1, \\ \lambda_U \Upsilon + \frac{2}{h} DW = 0, & \quad \text{at } \zeta = 1. \end{aligned} \quad (6.3.91)$$

Now we can impose the boundary conditions (6.3.91)₁ by removing the rows and columns of order $1, m, 3m + 1$ and $3m$, while we can apply the boundary conditions (6.3.91)_{2,3} by substituting $\zeta = -1$ in (6.3.91)₂ and $\zeta = 1$ in (6.3.91)₃ and then use (6.3.70) to arrive to the following final equations

$$\Upsilon_1 = \frac{2}{\lambda_L h e_1} [d_2 W_2 + \dots + d_{p+1} W_{p+1}] - \frac{1}{e_1} [e_2 \Upsilon_2 + \dots + e_{p+1} \Upsilon_{p+1}], \quad (6.3.92)$$

$$\Upsilon_m = -\frac{2}{\lambda_U h g_{p+1}} [f_1 W_{m-p} + f_2 W_{m-p+1} + \dots + f_p W_{m-1}] - \frac{1}{g_{p+1}} [g_1 \Upsilon_{m-p} + \dots + g_p \Upsilon_{m-1}], \quad (6.3.93)$$

where $d_i = dN_i(-1)/d\zeta$, $e_i = N_i(-1)$, $g_i = N_i(1)$ and $f_i = dN_i(1)/d\zeta$.

Now, we substitute the values of A_1 and A_m in (6.3.90) thus the columns of order $m + 1$ and $2m$ will be zeros and thus we can remove the $m + 1$ and $2m$ rows and columns.

However, for fixed-slip boundary conditions, we change the conditions $DW = 0$ at $z = 0$, to another conditions related with function Υ . To do this, let the first element is $[0, a]$, then, we integrate (6.3.70)₁ for first element and use the boundary

condition $W = 0$ at $z = 0$, to arrive to the following conditions

$$DW^1(a) = \int_0^a \Upsilon^1 dx, \quad (6.3.94)$$

where 1 refer to the first element. Next, to make (6.3.94) are useful in our computational, we transform this condition to the local coordinate ζ and use (6.3.74) to obtain

$$\frac{2}{h} \frac{dN(1)}{d\zeta} \delta_W^1 = \frac{h}{2} \int_{-1}^1 N(\zeta) \delta_A^1 d\zeta. \quad (6.3.95)$$

Now, let $\tau_i = dN_i(1)/d\zeta$ and $\xi_i = \int_{-1}^1 N_i(\zeta) d\zeta$. In addition, suppose that the nodes for the first element and for the last element have the order $1, 2, \dots, p+1$ and $m-p, m-p+1, \dots, m$, respectively. Then, (6.3.95) leads to the following computational conditions

$$\Upsilon_1 = \frac{4}{h^2 \xi_1} [\tau_2 W_2 + \dots + \tau_{p+1} W_{p+1}] - \frac{1}{\xi_1} [\xi_2 \Upsilon_2 + \dots + \xi_{p+1} \Upsilon_{p+1}]. \quad (6.3.96)$$

Now, we substitute the value of Υ_1 from (6.3.96) and the value of Υ_m from (6.3.93) in (6.3.90) thus the columns of order $m+1$ and $2m$ will be zeros. Now, we can remove the rows and columns of order $1, m, m+1, 2m, 2m+1$ and $3m$.

6.3.4 Chebyshev collocation methods

In this section, we use the Chebyshev collocation method to solve the eigenvalue system (6.2.27) and (6.2.28). We apply two techniques of Chebyshev collocation method to impose the boundary conditions.

Method 1.

For free-free boundary conditions, we use the same transformation which have been used in the finite element method, to arrive

$$\begin{aligned} D^2 W &= \Phi, \\ D^2 \Phi - 2a^2 \Phi + a^4 W - a^2 R \Theta &= 0, \\ (D^2 - a^2) \Theta + RW &= 0, \end{aligned} \quad (6.3.97)$$

with the same boundary conditions (6.3.71). In the first technique, we choose the trial functions such that these functions satisfy the boundary conditions as follows:

$$W = \sum_{n=1}^N W_n \theta_n(z), \quad (6.3.98)$$

$$\Phi = \sum_{n=1}^N \Phi_n \theta_n(z), \quad (6.3.99)$$

$$\Theta = \sum_{n=1}^N \Theta_n \theta_n(z), \quad (6.3.100)$$

where

$$\theta_n(z) = (1 - z^2)T_{2n-2}(z). \quad (6.3.101)$$

Here $T_n(z)$ is the n th-degree of Chebyshev polynomial of the first kind, which is defined by

$$T_0(z) = 1, \quad T_1(z) = z,$$

$$T_{n+1}(z) - 2zT_n(z) + T_{n-1}(z) = 0, \quad -1 \leq z \leq 1,$$

or

$$T_n(z) = \cos(n \arccos(z)), \quad -1 \leq z \leq 1,$$

It is clear that w, Φ and Θ satisfies the boundary conditions (6.3.71). Now, Substituting (6.3.98)-(6.3.100) into (6.3.97), and requiring that (6.3.97) be satisfied at N collocation points z_1, \dots, z_N , where

$$z_i = \cos\left(\frac{i-1}{2N-1}\pi\right), \quad i = 1, \dots, N, \quad (6.3.102)$$

we obtain $2N$ algebraic equations for $2N$ unknowns $w_1, \dots, w_N, A_1, \dots, A_N, \phi_1, \dots, \phi_N$:

$$\begin{pmatrix} 4D^2 & -I & O \\ a^4I & 4D^2 - 2a^2I & O \\ O & O & 4D^2 - a^2I \end{pmatrix} X = R \begin{pmatrix} O & O & O \\ O & O & a^2RI \\ -RI & O & O \end{pmatrix} X,$$

where $X = (w_1, \dots, w_N, \Phi_1, \dots, \Phi_N, \Theta_1, \dots, \Theta_N)$, O is the zeros matrix, $I(n_1, n_2) = \theta_{n_2}(z_{n_1})$, $D^2(n_1, n_2) = \theta''_{n_2}(z_{n_1})$, $n_1 = 1, \dots, N$, $n_2 = 1, \dots, N$.

Now, to deal with the solution of (6.2.27) and (6.2.28) with slip-slip boundary conditions and $\lambda_L = \lambda_U = \lambda$. Firstly, we introduce a new function $\vartheta = Dw$, then our system can be written in the following form:

$$Dw - \vartheta = 0, \quad (6.3.103)$$

$$D^3\vartheta - 2a^2D\vartheta + a^4W - a^2R\Theta = 0, \quad (6.3.104)$$

$$(D^2 - a^2)\Theta + RW = 0, \quad (6.3.105)$$

Then, according to this transform, the boundary conditions have the form

$$W = \Theta = 0, \quad \text{at } z = 0, 1, \quad (6.3.106)$$

$$\lambda D\vartheta + \vartheta = 0, \quad z = 1, \quad (6.3.107)$$

$$\lambda D\vartheta - \vartheta = 0, \quad z = 0. \quad (6.3.108)$$

We choose the trial functions such that these functions satisfy the boundary conditions as follows:

$$W = \sum_{n=1}^N W_n \theta_n(z), \quad (6.3.109)$$

$$\vartheta = \sum_{n=1}^N \vartheta_n \psi_n(z), \quad (6.3.110)$$

where

$$\theta_n(z) = (1 - z^2)T_{2n-2}(z), \quad (6.3.111)$$

$$\psi_n(z) = \left(1 - z^2 + \frac{2\lambda}{1 + \lambda(2n-1)^2}\right)T_{2n-1}(z). \quad (6.3.112)$$

It is clear that W and ϑ satisfy the boundary conditions (6.3.106)-(6.3.108). Now we can apply the same procedure which are used for free-free boundary conditions. For fixed-slip boundary conditions, we are unable to solve the problem because it is not easy to suggest a function which satisfies two different boundary conditions. However, if $\lambda_L \neq \lambda_U$, it is not easy to find a trial function such that these functions satisfy the boundary conditions.

6.3.5 Method 2.

For free-free boundary conditions we adopt the modified system (6.3.97). We expand the solutions of the governing stability equations (6.3.97) as truncated series of Chebyshev polynomials

$$W = \sum_{n=0}^N w_n T_n(z), \quad \Phi = \sum_{n=0}^N \Phi_n T_n(z), \quad \Theta = \sum_{n=0}^N \Theta_n T_n(z), \quad (6.3.113)$$

then, we insert (6.3.113) into the equations (6.3.97), and then substitute the Gauss-Labatto points which are defined by

$$y_i = \cos\left(\frac{\pi i}{N-3}\right), \quad i = 0, \dots, N-2. \quad (6.3.114)$$

Thus, we obtain $3N - 3$ algebraic equations for $3N + 3$ unknowns $W_0, \dots, W_N, \Phi_0, \dots, \Phi_N, \Theta_0, \dots, \Theta_N$. Now, we can add six rows using the boundary conditions (6.3.71) as follows

$$BC_1: \quad \sum_{n=0}^N W_n = 0, \quad (6.3.115)$$

$$BC_2: \quad \sum_{n=0}^N (-1)^n W_n = 0, \quad (6.3.116)$$

$$BC_3: \quad \sum_{n=0}^N \Phi_n = 0, \quad (6.3.117)$$

$$BC_4: \quad \sum_{n=0}^N (-1)^n \Phi_n = 0, \quad (6.3.118)$$

$$BC_5: \quad \sum_{n=0}^N \Theta_n = 0, \quad (6.3.119)$$

$$BC_6: \quad \sum_{n=0}^N (-1)^n \Theta_n = 0. \quad (6.3.120)$$

Then, we obtain the generalised eigenvalue problem

$$\begin{pmatrix} 4D^2 & -I & O \\ BC_1 & 0\dots 0 & 0\dots 0 \\ BC_2 & 0\dots 0 & 0\dots 0 \\ a^4I & 4D^2 - 2a^2I & O \\ 0\dots 0 & BC_3 & 0\dots 0 \\ 0\dots 0 & BC_4 & 0\dots 0 \\ O & O & 4D^2 - a^2I \\ 0\dots 0 & 0\dots 0 & BC_5 \\ 0\dots 0 & 0\dots 0 & BC_6 \end{pmatrix} X = R \begin{pmatrix} O & O & O \\ 0\dots 0 & 0\dots 0 & 0\dots 0 \\ 0\dots 0 & 0\dots 0 & 0\dots 0 \\ O & O & a^2RI \\ 0\dots 0 & 0\dots 0 & 0\dots 0 \\ 0\dots 0 & 0\dots 0 & 0\dots 0 \\ -RI & O & O \\ 0\dots 0 & 0\dots 0 & 0\dots 0 \\ 0\dots 0 & 0\dots 0 & 0\dots 0 \end{pmatrix} X,$$

where $X = (W_0, \dots, W_N, \Phi_0, \dots, \Phi_N, \Theta_0, \dots, \Theta_N)$, O is the zeros matrix, $I(n_1, n_2) = T_{n_2}(z_{n_1})$, $D^2(n_1, n_2) = T_{n_2}''(z_{n_1})$, $n_1 = 0, \dots, N - 2$, $n_2 = 0, \dots, N$.

However, for numerical solutions of (6.2.27) and (6.2.28) with slip-slip boundary conditions, we adopt system (6.3.103)-(6.3.105) with boundary conditions (6.3.106)-(6.3.108) but with general values of λ_U, λ_L i.e. $\lambda_U \neq \lambda_L$. Then, we apply the same procedure which are used for free-free boundary conditions to arrive to the following eigenvalue problem system

$$\begin{pmatrix} 2D & -I & O \\ BC_1 & 0\dots 0 & 0\dots 0 \\ BC_2 & 0\dots 0 & 0\dots 0 \\ a^4I & 8D^3 - 4a^2D & O \\ 0\dots 0 & BC_3 & 0\dots 0 \\ 0\dots 0 & BC_4 & 0\dots 0 \\ O & O & 4D^2 - a^2I \\ 0\dots 0 & 0\dots 0 & BC_5 \\ 0\dots 0 & 0\dots 0 & BC_6 \end{pmatrix} X = R \begin{pmatrix} O & O & O \\ 0\dots 0 & 0\dots 0 & 0\dots 0 \\ 0\dots 0 & 0\dots 0 & 0\dots 0 \\ O & O & a^2RI \\ 0\dots 0 & 0\dots 0 & 0\dots 0 \\ 0\dots 0 & 0\dots 0 & 0\dots 0 \\ -RI & O & O \\ 0\dots 0 & 0\dots 0 & 0\dots 0 \\ 0\dots 0 & 0\dots 0 & 0\dots 0 \end{pmatrix} X,$$

where $X = (W_0, \dots, W_N, \vartheta_0, \dots, \vartheta_N, \Theta_0, \dots, \Theta_N)$, O is the zeros matrix, $I(n_1, n_2) = T_{n_2}(z_{n_1})$, $D(n_1, n_2) = T_{n_2}(z_{n_1})$, $D^3(n_1, n_2) = T_{n_2}'''(z_{n_1})$, $n_1 = 0, \dots, N - 2$, $n_2 = 0, \dots, N$. The boundary conditions $BC1, BC2, BC5, BC6$ have the same form of

the free-free boundary conditions, while $BC3$ and $BC4$ have different form which is related with slip boundary conditions and these written in the following form:

$$BC_3 : \sum_{n=0}^N (2\lambda_U n^2 + 1) \vartheta_n = 0, \quad (6.3.121)$$

$$BC_4 : \sum_{n=0}^N (2(-1)^{n+1} \lambda_L n^2 - 1) \vartheta_n = 0. \quad (6.3.122)$$

For fixed-slip boundary conditions, the system have the same form of slip-slip with $\lambda_L = 0$. This show the flexibility of this method, and thus, we believe that this method is more flexible than the other numerical methods. Moreover, this method is very accurate and not need to difficult numerical treatments.

6.4 Numerical results and conclusions

In this section we report our numerical results of (6.2.27) and (6.2.28) with free-free, slip-slip and fixed-slip boundary conditions. It is very important to make a comparison between the accuracy of the methods with the crucial measurement being the exact solution. As we mention in the introduction, Rayleigh [163] showed that, in the case of free-free boundary conditions, we may obtain the analytical result of the Rayleigh number $Ra_{crit} = 27\pi^4/4$ and $a_{crit}^2 = \pi^2/2$. Thus, we compute the absolute error of the critical Rayleigh and the wavenumbers from the relation:

$$e_a = |a_{exact} - a_{numer}|, \quad e_R = |R_{exact} - R_{numer}|$$

where e_a , e_R , a_{exact} , a_{numer} , R_{exact} and R_{numer} are the absolute error of wavenumber, the absolute error of critical Rayleigh number, the exact value of wavenumber, the numerical value of wavenumber, the exact value of the critical Rayleigh number and the numerical value of the critical Rayleigh number, respectively. We report the absolute error of the critical Rayleigh and the wavenumbers for the numerical methods with free-free boundary conditions in Tables 6.1-6.6.

In Table 6.1, the absolute errors of the wavenumber which are produce from the finite element method are introduced. The table demonstrates that the absolute error of the wavenumbers does not change when increasing the number of nodes

and number elements, where, in general, the values of absolute error 9.15×10^{-6} or very close to this value can be seen. When the number of elements are 2, 3, 4 and the number of nodes is 4, the accuracy is less than normal i.e. the accuracy is less than 9.15×10^{-6} which is very much to be expected as the approximation in these situations is of a low order. However, with a high number of elements and nodes, the accuracy values oscillate where the absolute error is less or greater than the normal value. Furthermore, this behaviour is to be expected in studying hydrodynamic stability problems. As the number of nodes and element increase, theoretically, the accuracy of the finite element method should increase. However, as the number of nodes and elements increase, the computer calculations increase and thus computer error will be greater. Since hydrodynamic stability problems require solving the eigenvalue system many times in order to achieve the critical Rayleigh number which corresponds to the critical wavenumber, computer error is expected to make the absolute error greater than the theoretical one. This behaviour is very clear in Table 6.6, where the absolute error is higher than the truncation error of FD and HFD methods. For both the absolute error of the critical Rayleigh and wave numbers, the accuracy increases with a higher number of nodes and elements until it reaches a peak, at which point the behaviour of the accuracy oscillates.

Similar behaviour of the absolute error of the wavenumber can be found in the Chebyshev tau, Chebyshev collection 1 and 2 schemes (see Tables 6.3, 6.4 and 6.5). However, the accuracy of the wave number for standard and high order finite difference methods is less than in the Chebyshev methods and finite element methods. Generally, the accuracy of the finite difference schemes corresponds with the value of h , where accuracy increases as the value of h decreases. However, the value of h cannot be taken as less than 0.01 for two reasons. First, with $h = 0.01$ and after imposing the boundary conditions, the order of the eigenvalue matrices will be 199×199 , and thus, according to the computers ability, this is an optimal choice. Secondly, it is difficult to believe that low h values can provide more accurate results as the computations have to increase rapidly, which is very important spatially when the nonlinear stability problems are solved.

Table 6.2 presents the absolute errors of the Rayleigh number generated from

the finite element method. Unlike the behaviour of the wavenumber, whereby the required accuracy with a low number of elements and nodes can be achieved, the accuracy of the Rayleigh numbers require a greater number of elements and nodes. Additionally, the absolute errors of the Rayleigh number are less than the absolute errors of the wavenumber. Similar to the wave numbers accuracy, the accuracy of the Rayleigh number increases with an increased number of nodes and elements up to the normal absolute error which is 2×10^{-10} . At this point the accuracy behaviour oscillates more. Table 6.2 shows that the required accuracy can be achieved with 2 elements and 8 nodes and this choice is the best according to the computer run time. In other words, using this choice the best accuracy with the smallest eigenvalue matrices can be achieved. This means that the order of eigenvalue matrices will be 30×30 . Now, from the results of the other numerical methods in Tables 6.3, 6.4 and 6.5, it can be seen the following observations

- The Chebyshev tau method can achieve the required accuracy using at least 11 Chebyshev polynomials, thus the order of eigenvalue matrices will be 26×26 after adding the two rows of boundary conditions.
- The Chebyshev collection method 1 can achieve the required accuracy using 6 Chebyshev polynomials. Thus the order of the eigenvalue matrices will be 16×16 after adding the two rows of boundary conditions. Here we should mention that the Chebyshev collection method 1 achieves the required accuracy with a smaller number of Chebyshev polynomials because it uses only the even polynomials - i.e. this method uses the polynomials T_0, T_2, \dots . So when the required accuracy with 6 Chebyshev polynomials is reached, this signifies that it uses the polynomials of order 0, 2, 4, 6, 8, 10. This is a very significant advantage of this method, achieving a high level of accuracy with low numbers of polynomials.
- The Chebyshev collection method 2 can achieve the required accuracy using 10 Chebyshev polynomials. Thus the order of eigenvalue matrices will be 24×24 after adding the two rows of boundary conditions.

Here, it is very important to mention that these numerical methods reach a

high level of accuracy with these numbers of polynomials, nodes and elements for free-free boundary conditions. However, there is a need to increase these numbers when dealing with other kinds of boundary conditions. Accordingly, the results of numerical methods are reported in Tables 6.7 and 6.8 for slip-slip and fixed-slip boundary conditions with selected numbers of polynomials, nodes and elements and h . The convergence has been checked and with the result that 8 decimal places for slip-slip and fixed-slip boundary conditions is achieved using 20, 10 and 20 Chebyshev polynomials for Chebyshev tau, Chebyshev collection method 1 and Chebyshev collection method 2, respectively, while for the finite element method the convergence to 8 decimal places required at least 3 elements and 10 nodes. Additionally, the required convergence was satisfied with $h = 0.001$, $h = 0.01$ for FD and HFD, respectively. Therefore, the numerical results in Tables 6.7 and 6.8 are reported according to these choices.

One of the important reasons for applying different numerical methods for solving the system (6.2.27) and (6.2.28) is to make a comparison between these methods so that a conclusion can be reached regarding which of these methods is the best in solving hydrodynamic stability problems. The advantage in using the Chebyshev Tau method is that it can achieve the required accuracy using a small number of polynomials, allowing the achievement of highly accurate results with a short run time. On the other hand, the Chebyshev tau method is not easy to apply, as a considerable effort to solve any system of equations is required. With regard to problems of variable coefficients, the Chebyshev tau method presents complications in finding the solution because this method depends on the writing of all functions in the system of the equation in the form of Chebyshev polynomial series, which proves difficult when functions such as triangular and hyperbolic functions are present.

The FD method need a large number of divisions to reach the required accuracy, while the HFD method can reach to the desired accuracy by using less number of divisions. We see from the results that the FD method require $h = 0.001$ to achieve a very good accuracy and convergence results, while we use $h = 0.01$ for HFD method. However, the FD and HFD methods leads to non-singular matrices in the eigenvalue systems and so we may employ LU decomposition, unlike the other nu-

merical methods which necessarily have singular matrices in the eigenvalue systems and so necessitate use of the QZ algorithm. The banded nature of matrices in the eigenvalue systems would also lead naturally to solution by an Arnoldi technique. In addition, we found no occurrence of spurious eigenvalues as frequently arise with the Chebyshev methods, cf., Dongarra et al. [43].

We believe that the finite element method is one of the best choices in solving the hydrodynamic stability problems as it is a flexible method and it can give very accurate results. However, the disadvantage of this method is that the required run time is longer than the Chebyshev numerical methods. Thus, using this method for linear theory problem is recommended. Moreover, it could be a suitable choice for nonlinear problems but with no more than two maximised parameters. The Chebyshev collection method 1 is an inflexible method where if the boundary conditions are not symmetric it becomes impossible to find trial functions satisfying the boundary conditions. However, this method has the highest accuracy between the numerical methods and requires a smaller number of polynomials to achieve excellent accuracy and convergence. This point is of great value because our numerical calculations require great computational time, with a run time in some cases of more than ten hours.

Finally, the Chebyshev collection method 2 is the most flexible method among the other numerical methods and can achieve high accuracy using a reasonable number of Chebyshev polynomials. Usually, we used this method in my work because of the highly accurate results within a short time. The author strongly recommends this method for use in solving hydrodynamic stability problems.

No. elements	No. of nodes						
	4	5	6	7	8	9	10
2	6.8E-04	9.2E-06	9.2E-06	9.2E-06	9.2E-06	9.2E-06	9.2E-06
3	6.7E-05	9.2E-06	9.2E-06	9.2E-06	9.2E-06	9.2E-06	7.0E-06
4	1.9E-05	9.2E-06	9.2E-06	9.2E-06	9.2E-06	9.2E-06	9.2E-06
5	9.2E-06	9.2E-06	9.2E-06	9.2E-06	9.2E-06	9.2E-06	9.2E-06
6	9.2E-06	9.2E-06	9.2E-06	9.2E-06	9.2E-06	7.0E-06	9.2E-06
7	9.2E-06	9.2E-06	9.2E-06	9.2E-06	9.2E-06	7.0E-06	9.2E-06
8	9.2E-06	9.2E-06	9.2E-06	9.2E-06	9.2E-06	9.2E-06	7.0E-06
9	9.2E-06	9.2E-06	9.2E-06	9.2E-06	9.2E-06	7.9E-06	8.3E-06
10	9.2E-06	9.2E-06	9.2E-06	9.2E-06	7.0E-06	7.3E-06	2.7E-05
11	9.2E-06	9.2E-06	9.2E-06	4.6E-06	7.0E-06	9.2E-06	1.4E-05
12	9.2E-06	9.2E-06	9.2E-06	9.2E-06	9.2E-06	8.9E-07	7.7E-05
13	9.2E-06	9.2E-06	9.2E-06	9.2E-06	9.2E-06	9.2E-06	2.0E-05
14	9.2E-06	9.2E-06	9.2E-06	9.2E-06	6.8E-06	1.6E-05	6.1E-05
15	9.2E-06	9.2E-06	9.2E-06	9.2E-06	9.2E-06	3.5E-05	9.2E-06
16	9.2E-06	9.2E-06	9.2E-06	9.2E-06	1.1E-05	3.3E-05	6.1E-06
17	9.2E-06	8.1E-07	9.2E-06	9.2E-06	4.0E-06	3.5E-05	3.2E-06
18	9.2E-06	9.2E-06	9.2E-06	9.2E-06	9.2E-06	3.0E-06	2.9E-05
19	9.2E-06	9.2E-06	9.2E-06	9.2E-06	2.8E-05	6.6E-06	6.2E-06
20	9.2E-06	8.1E-07	8.1E-07	7.0E-06	1.5E-05	4.6E-05	7.5E-05

Table 6.1: Comparison of the absolute error of wavenumbers for finite elements method.

No. elements	No. of nodes						
	4	5	6	7	8	9	10
2	1.8E-01	1.8E-03	1.1E-05	5.0E-08	8.5E-10	5.2E-10	8.2E-10
3	1.7E-02	7.3E-05	2.0E-07	1.1E-09	6.7E-10	2.3E-10	4.9E-08
4	3.0E-03	7.4E-06	1.2E-08	7.4E-10	9.5E-10	5.1E-10	9.9E-08
5	7.9E-04	1.2E-06	1.9E-09	6.7E-10	4.0E-10	1.5E-09	1.2E-07
6	2.7E-04	2.9E-07	8.9E-10	3.1E-10	3.0E-08	5.1E-08	1.2E-07
7	1.1E-04	8.6E-08	4.4E-10	2.8E-10	3.5E-08	5.3E-08	1.3E-07
8	4.8E-05	3.0E-08	7.6E-10	9.5E-10	4.0E-08	6.0E-08	1.1E-07
9	2.4E-05	1.2E-08	6.7E-10	4.4E-10	4.0E-08	5.3E-08	1.1E-07
10	1.2E-05	5.6E-09	7.8E-10	7.4E-10	4.6E-08	5.8E-08	9.2E-08
11	7.1E-06	2.7E-09	1.4E-09	3.2E-10	4.8E-08	6.6E-08	9.4E-08
12	4.2E-06	1.3E-09	6.7E-10	6.1E-08	5.0E-08	7.4E-08	6.0E-08
13	2.6E-06	7.6E-10	5.7E-10	6.0E-08	5.0E-08	8.2E-08	1.0E-07
14	1.7E-06	8.4E-10	5.4E-10	6.0E-08	5.5E-08	8.2E-08	7.6E-08
15	1.1E-06	8.6E-10	4.8E-10	6.1E-08	5.0E-08	6.1E-08	1.1E-07
16	7.5E-07	5.2E-10	5.1E-08	5.7E-08	5.1E-08	6.1E-08	1.1E-07
17	5.2E-07	3.3E-10	5.0E-08	6.0E-08	6.9E-08	5.5E-08	8.0E-08
18	3.7E-07	2.3E-10	5.3E-08	5.8E-08	5.0E-08	9.3E-08	1.3E-07
19	2.7E-07	5.6E-10	5.2E-08	5.6E-08	5.2E-08	5.3E-08	8.7E-08
20	2.0E-07	2.0E-10	5.2E-08	5.8E-08	5.7E-08	8.0E-08	1.8E-07

Table 6.2: Comparison of the absolute error of critical Rayleigh numbers for finite elements method.

No. of pol.	Ra	a_c^2	No. of pol.	Ra	a_c^2
4	9.67E-01	3.63E-03	27	5.08E-10	3.16E-06
5	3.06E-03	6.97E-06	28	1.12E-09	8.11E-07
6	1.10E-02	6.97E-06	29	1.13E-09	1.31E-05
7	2.14E-05	9.15E-06	30	1.31E-09	9.15E-06
8	7.69E-05	9.15E-06	31	4.91E-09	2.53E-05
9	5.89E-08	9.15E-06	32	1.66E-08	4.25E-05
10	3.63E-07	9.15E-06	33	7.98E-11	9.15E-06
11	8.51E-10	9.15E-06	34	2.49E-07	9.15E-06
12	1.86E-09	9.15E-06	35	4.30E-11	1.30E-05
13	8.50E-10	9.15E-06	36	8.36E-08	2.53E-05
14	7.62E-10	9.15E-06	37	7.58E-09	3.52E-05
15	2.72E-11	8.11E-07	38	5.63E-09	2.55E-05
16	6.03E-10	9.15E-06	39	1.85E-09	1.62E-05
17	5.68E-11	9.15E-06	40	4.05E-10	3.00E-06
18	6.80E-10	9.15E-06	41	7.75E-09	9.15E-06
19	2.29E-11	3.00E-06	42	2.69E-09	1.31E-05
20	7.69E-10	9.15E-06	43	1.21E-08	3.87E-07
21	1.09E-09	9.15E-06	44	3.04E-09	9.88E-06
22	7.22E-10	9.15E-06	45	5.46E-09	2.19E-05
23	7.55E-08	9.15E-06	46	4.44E-09	2.93E-05
24	3.61E-10	9.15E-06	47	3.77E-11	1.94E-05
25	2.98E-10	8.11E-07	48	1.34E-06	3.16E-06
26	6.42E-10	9.15E-06	49	6.41E-09	9.15E-06

Table 6.3: Comparison of the absolute error of critical Rayleigh numbers and wavenumbers for Chebyshev tau method.

No. of pol.	Ra	a_c^2	No. of pol.	Ra	a_c^2
4	1.34E-05	9.15E-06	27	7.47E-10	9.15E-06
5	9.05E-08	9.15E-06	28	7.53E-10	9.15E-06
6	6.07E-10	9.15E-06	29	7.54E-10	9.15E-06
7	7.55E-10	9.15E-06	30	7.54E-10	9.15E-06
8	7.47E-10	9.15E-06	31	7.55E-10	9.15E-06
9	7.52E-10	9.15E-06	32	7.43E-10	9.15E-06
10	7.50E-10	9.15E-06	33	7.44E-10	9.15E-06
11	7.47E-10	9.15E-06	34	7.41E-10	9.15E-06
12	7.51E-10	9.15E-06	35	7.52E-10	9.15E-06
13	7.49E-10	9.15E-06	36	7.48E-10	9.15E-06
14	7.45E-10	9.15E-06	37	7.51E-10	9.15E-06
15	7.48E-10	9.15E-06	38	7.39E-10	9.15E-06
16	7.49E-10	9.15E-06	39	7.44E-10	9.15E-06
17	7.54E-10	9.15E-06	40	7.46E-10	9.15E-06
18	7.48E-10	9.15E-06	41	7.54E-10	9.15E-06
19	7.50E-10	9.15E-06	42	7.52E-10	9.15E-06
20	7.51E-10	9.15E-06	43	7.33E-10	9.15E-06
21	7.50E-10	9.15E-06	44	7.58E-10	9.15E-06
22	7.51E-10	9.15E-06	45	7.43E-10	9.15E-06
23	7.48E-10	9.15E-06	46	7.41E-10	9.15E-06
24	7.35E-10	9.15E-06	47	7.39E-10	9.15E-06
25	7.54E-10	9.15E-06	48	7.38E-10	9.15E-06
26	7.40E-10	9.15E-06	49	7.66E-10	9.15E-06

Table 6.4: Comparison of the absolute error of critical Rayleigh numbers and wavenumbers for Chebyshev collocation method-1.

No. of pol.	Ra	a_c^2	No. of pol.	Ra	a_c^2
4	6.01E-01	2.25E-03	27	3.29E-08	8.12E-06
5	1.05E-01	3.93E-04	28	3.60E-09	3.58E-05
6	1.24E-03	6.97E-06	29	7.40E-08	1.21E-05
7	1.34E-05	9.15E-06	30	2.64E-08	9.15E-06
8	1.86E-07	9.15E-06	31	8.88E-10	3.05E-05
9	9.08E-08	9.15E-06	32	1.98E-08	1.66E-05
10	5.38E-10	8.11E-07	33	4.88E-08	9.15E-06
11	5.37E-10	9.15E-06	34	3.64E-08	4.59E-05
12	9.52E-10	9.15E-06	35	5.54E-08	6.76E-06
13	1.34E-09	3.00E-06	36	2.69E-08	9.40E-07
14	2.21E-10	4.62E-06	37	1.43E-08	4.27E-06
15	2.07E-09	9.15E-06	38	3.26E-08	2.44E-06
16	1.77E-09	9.15E-06	39	8.74E-08	4.22E-05
17	5.56E-09	8.11E-07	40	8.69E-09	3.86E-05
18	2.03E-09	9.15E-06	41	8.36E-08	6.21E-05
19	4.12E-09	4.41E-06	42	7.79E-08	9.40E-05
20	8.86E-09	3.00E-06	43	3.98E-08	8.25E-05
21	2.83E-09	1.85E-05	44	1.47E-07	2.99E-05
22	5.20E-09	1.91E-05	45	1.78E-07	2.69E-05
23	3.47E-09	3.31E-05	46	6.07E-08	4.93E-05
24	7.38E-09	1.93E-05	47	1.89E-07	5.37E-05
25	2.93E-08	2.23E-06	48	3.95E-08	1.04E-04
26	2.86E-09	3.52E-05	49	3.05E-08	6.33E-05

Table 6.5: Comparison of the absolute error of critical Rayleigh numbers and wavenumbers for Chebyshev collocation method-2.

		FD		HFD	
h	Ra	a_c^2	Ra	a_c^2	
0.5	2.70E+00	1.01E-02	1.20E+00	8.99E-03	
0.4	1.73E+00	6.50E-03	7.69E-01	5.74E-03	
0.2	4.32E-01	1.61E-03	1.92E-01	1.39E-03	
0.1	1.08E-02	5.30E-04	4.81E-03	2.80E-04	
0.01	2.82E-03	2.99E-05	1.32E-04	1.75E-05	

Table 6.6: Comparison of the absolute error of critical Rayleigh numbers and wavenumbers for finite differences (FD) and high order finite differences (HFD) methods.

λ	FEM	Che-tau	Che-C-1	Che-C-2	FD	HFD
1.E-05	1707.6026	1707.6810	1707.7071	1707.6525	1706.3158	1707.2809
1.E-04	1706.6700	1707.0793	1707.2157	1706.6702	1705.3357	1706.3364
1.E-03	1696.9550	1700.9850	1702.3283	1696.9550	1695.6419	1696.6268
1.E-02	1609.4775	1644.3853	1656.0212	1609.4774	1608.3469	1609.1948
1.E-01	1186.0566	1313.4363	1355.8963	1186.0566	1185.5812	1185.9377
1	761.2043	822.7658	843.2863	761.2042	761.0558	761.1671
10	669.1816	677.6847	680.5191	669.1816	669.0695	669.1536
1.E+02	658.6940	659.5783	659.8730	658.6939	658.5854	658.6668
1.E+03	657.6298	657.7186	657.7482	657.6298	657.5216	657.6027
1.E+04	657.5232	657.5321	657.5351	657.5232	657.4151	657.4962
1.E+05	657.5125	657.5134	657.5137	657.5125	657.4044	657.4855

Table 6.7: The critical Rayleigh and wavenumbers for symmetric-slip case for a selection of λ values. These numbers are evaluated by using finite element, Chebyshev tau, Chebyshev collocation-1, Chebyshev collocation-2, finite difference and fourth order finite difference.

λ_U	FEM	Che-tau	Che-C-2	FD	HFD
1.E-05	1707.6557	1707.6943	1707.7071	1706.3704	1707.0130
1.E-04	1707.2157	1707.2158	1707.2159	1705.8802	1706.5479
1.E-03	1702.3478	1702.3478	1702.3478	1701.0229	1701.6854
1.E-02	1657.7442	1657.7442	1657.7442	1656.5143	1657.1292
1.E-01	1422.7335	1422.7335	1422.7335	1421.9144	1422.3239
1	1163.5803	1163.5803	1163.5803	1163.0497	1163.3150
10	1107.6329	1107.6329	1107.6329	1107.1443	1107.3886
1.E+02	1101.3557	1101.3558	1101.3558	1100.8714	1101.1136
1.E+03	1100.7203	1100.7203	1100.7203	1100.2364	1100.4783
1.E+04	1100.6567	1100.6567	1100.6567	1100.1728	1100.4147
1.E+05	1100.6503	1100.6503	1100.6503	1100.1664	1100.4084

Table 6.8: The critical Rayleigh and wavenumbers for fixed-slip case for a selection of λ_U values. These numbers are evaluated by using finite element, Chebyshev tau, Chebyshev collocation-2, finite difference and fourth order finite difference.

Chapter 7

Structural stability for convection models in a reacting porous medium with magnetic field effect

7.1 Introduction

Structural stability is the study of stability of the model itself. The classical definition of stability involves continuous dependence of the solution on changes in the initial data. However, it is increasingly being realised that continuous dependence on changes in the coefficients, in the model, in boundary data, or even in the partial differential equations themselves, is very important. This aspect of continuous dependence, or stability, is what we refer to as structural stability. Hirsch and Smale [88] were prominent in introducing the ideas of structural stability. In this chapter we focus on the structural stability in the context of the convection models of porous media. It is extremely important, because if a small change in the equations, or a coefficient in an equation, causes a major change in the solution it may well say something about how accurate the model is as a vehicle to describe flow in porous media.

Early articles dealing with structural stability questions in porous flows are those of Ames and Payne [2], Franchi and Straughan [54, 57], and Payne and Straughan [149–151] investigates in some detail the continuous dependence of the solution

on changes in the initial-time geometry. Payne and Straughan [152] establish continuous dependence on the coefficients of Forchheimer and of Brinkman, and also investigate how the solution to the Brinkman equations converges to that of the Darcy equations as the Brinkman coefficient tends to zero.

There has also been considerable recent interest in questions of structural stability in porous media. Straughan [196] explains a system of equations to describe the double diffusive convective flow in a porous medium using the Brinkman model. In [200] Straughan and Hutter established continuous dependence of the solution on the Soret coefficient. Lin and Payne [108] further extended the work of [200]. They investigate the structural stability of the Brinkman equations modeling on the gravity vector coefficients and Brinkman coefficient. Then in [109] they established the structural stability of the Brinkman equations on the Soret coefficient when the boundary conditions are nonhomogeneous Dirichlet type. Continuous dependence of the solution of the Darcy equations on the Soret coefficient is established by Lin and Payne in [110]. Harfash in [78], proves that the solution depends continuously on changes in the magnetic and the gravity vector coefficients for Darcy model. For details of the Darcy model see e.g. Rionero [172]. Straughan in chapter 2 in his book [197] introduces a very important review of the studies on structural stability.

In Chapter 3, we consider the convection of a reacting solute in a viscous incompressible fluid occupying a horizontal plane layer subject to a vertical magnetic field, while in Chapter 4, we study the double-diffusive convection in a reacting fluid in the presence of a magnetic field. This study continues the investigation of continuous dependence properties of models which introduced in Chapter 3 and 4 when these models include porous media. We concentrate on a Brinkman porous medium, cf. Rionero and Vergori [178].

Convection in a porous medium is a highly active subject of research due to the immense variety of applications such as bio-remediation, geothermal reservoir systems, contaminant movement in soil, solid matrix heat exchangers, solar power converters and oil extraction. These and many other examples are described in Nield and Bejan [138], and specific references may be found on pages 238, 239 of Straughan [196]. An example of the novel use of porous medium, drawn from these

references, is in heat transfer mechanisms through the use of porous foams and heat pipes, see e.g. Amili and Yortsos [6]. Cimatti [39] studied the flow of an incompressible fluid in a porous medium represented by an open and bounded subset of \mathbb{R}^3 with a regular boundary consisting of two disjoint surfaces. A linear and nonlinear stability analyses of the motionless state of thermosolutal second-order fluid in porous Bénard layer is investigated by Xu and Yang [225] via Lyapunov direct method on the basis of Brinkman's modification of the Darcy's model. Capone et al [23] studied a linear and nonlinear stability analyses of vertical throughflow in a fluid layer, where the density is quadratic in temperature.

The first model which is studied in this study is the problem of convection with a dissolved reacting porous medium layer and a vertically imposed magnetic field

$$v_i = -p_{,i} + \nu \Delta v_i + g_i c + \mathbf{j} \times \mathbf{B}, \quad (7.1.1)$$

$$v_{i,i} = 0, \quad (7.1.2)$$

$$c_{,t} + v_i c_{,i} = D \Delta c - K_1 c, \quad (7.1.3)$$

$$v_i = 0, \quad \frac{\partial c}{\partial n} = 0, \quad \text{on} \quad \partial\Omega, \quad (7.1.4)$$

$$c(\mathbf{x}, 0) = f_1(\mathbf{x}), \quad \text{in} \quad \Omega, \quad (7.1.5)$$

where \mathbf{v} is the velocity vector, c is the concentration field, p is pressure field, D is the diffusion coefficient, g_i is the gravity vector, \mathbf{B} is the magnetic induction field, \mathbf{j} is the current and K_1 is the chemical reaction rate. This system hold on a bounded spatial domain Ω in \mathbb{R}^3 with boundary $\partial\Omega$ sufficiently smooth to allow applications of the divergence theorem. Standard indication notation is employed with Δ denoting the Laplacian. The function f_1 is assumed to be smooth function. In general, the magnetic induction field \mathbf{B} has a separate evolution equation for its determination, cf. Rionero [165–168, 170, 171]. However, in certain situations one can avoid direct use of this equation and employ a quasi-static magnetohydrodynamics MHD approximation. This leads to a particular form for the term $\mathbf{j} \times \mathbf{B}$, and this is explained in detail at the end of this section.

The second model which is studied in this study is the problem of double diffusive convection with a dissolved reacting porous medium layer and a vertically imposed magnetic field

$$v_i = -p_{,i} + v\Delta v_i + h_i T + g_i c + \mathbf{j} \times \mathbf{B}, \quad (7.1.6)$$

$$v_{i,i} = 0, \quad (7.1.7)$$

$$T_{,t} + v_i T_{,i} = K\Delta T, \quad (7.1.8)$$

$$c_{,t} + v_i c_{,i} = D\Delta c - K_1 c, \quad (7.1.9)$$

$$v_i = 0, \quad \frac{\partial c}{\partial n} = 0, \quad \frac{\partial T}{\partial n} = 0, \quad \text{on} \quad \partial\Omega, \quad (7.1.10)$$

$$c(\mathbf{x}, 0) = f_1(\mathbf{x}), \quad T(\mathbf{x}, 0) = f_2(\mathbf{x}), \quad \text{in} \quad \Omega, \quad (7.1.11)$$

where \mathbf{v} is the velocity vector, c is the concentration field, T is the temperature field, p is pressure field, D is the diffusion coefficient, \mathbf{B} is the magnetic induction field, \mathbf{j} is the current, K_1 is the chemical reaction rate and K is the thermal diffusivity. This system hold on a bounded spatial domain Ω in \mathbb{R}^3 with boundary $\partial\Omega$ sufficiently smooth to allow applications of the divergence theorem. Again, we employ the quasi-static magnetohydrodynamics approximation for the term $\mathbf{j} \times \mathbf{B}$, as discussed below. The functions f_1 and f_2 are assumed to be smooth functions. In (7.1.6) we have employed a Boussinesq approximation in the sense that the density is linear in T and c so that the gravity term may be written as

$$-k_i g(\alpha T - \alpha_c c)$$

where α and α_c are the thermal and salt expansion coefficients respectively, and g is gravity, cf. Straughan [196] page 102. Then $g_i = gk_i\alpha_c$ and $h_i = -gk_i\alpha$ are gravity coefficients, where $k_i = (0, 0, 1)$.

Research exploring double-diffusive convection in a fluid-saturated porous layer has been an active area for many years, making this work considerably relevant to the wider literature. These phenomena of combined heat and mass transfer appear in numerous physical problems such as contaminant transport in spreading of pollutants. Comprehensive reviews of the literature concerning double-diffusive natural convection in a fluid-saturated porous medium can be found in the review article

by Trevisan and Bejan [217], in the book of Nield and Bejan [138], and in chapter 14 of the book by Straughan [196]. Recent novel contributions include Mahidjiba et al. [119] for a vertical porous medium enclosure, Mahidjiba et al. [118] for mixed boundary conditions, and Guo and Kaloni [71] with the introduction of the Brinkman effect. In particular there are very interesting recent studies of stability in double diffusive convection by Rionero [173] and by Capone et al. [29]. Furthermore, the more technical problem of stability in a triply diffusive convection situation is analysed in detail by Rionero [174–176] and by Capone and de luca [28]. The latter class of problem is one where we may fruitfully apply the techniques of this chapter to study continuous dependence on the various parameters which arise.

Now, according to the quasi-static MHD approximation of Galdi and Straughan [61], we have

$$\mathbf{j} \times \mathbf{B} = \sigma(\mathbf{v} \times \mathbf{B}_0) \times \mathbf{B}_0,$$

where σ is the electrical conductivity and $\mathbf{B}_0 = (0, 0, B_0)$ is a magnetic field with only the vertical component. This obviates the need to employ the full MHD equations which also involve an equation for the evaluation of the magnetic field, \mathbf{H} , cf. Rionero [165–168, 170, 171] and Rionero and Mulone [177]. Then, equation (7.1.1) reduces to

$$v_i = -p_{,i} + v\Delta v_i + g_i c + \sigma[(\mathbf{v} \times \mathbf{B}_0) \times \mathbf{B}_0]_i, \quad (7.1.12)$$

and equation (7.1.6) reduces to

$$v_i = -p_{,i} + v\Delta v_i + h_i T + g_i c + \sigma[(\mathbf{v} \times \mathbf{B}_0) \times \mathbf{B}_0]_i. \quad (7.1.13)$$

Throughout the chapter, $\|\cdot\|$ and (\cdot, \cdot) denote the norm and inner product on $L^2(\Omega)$ and $\|\cdot\|_\infty$ denotes the norm on $L^\infty(\Omega)$. In addition, without loss of generality, the gravity vectors are assumed constant and the models are scaled so that

$$|h|, |g| \leq 1. \quad (7.1.14)$$

The goal of this chapter is to establish continuous dependence on changes in the chemical reaction K_1 coefficient, and on changes in the coefficient of the magnetic

term σ . The plan of the chapter is as follows. In Section 7.2 we study the continuous dependence for the model of convective motion in a porous medium layer with a dissolved reacting porous medium layer. In Section 7.3 we investigate the continuous dependence for the model of double diffusive convection with a dissolved reacting porous medium layer.

The results in this chapter were published in the article Harfash [76].

7.2 Continuous dependence for the first model

In this section we consider a solution to equations (7.1.12) and (7.1.2)-(7.1.5). In the beginning we shall prove bounds for our solution.

Lemma 7.2.1 If $c(\mathbf{x}, 0) \in L^\infty(\Omega)$, then

$$\|c(\mathbf{x}, t)\|_\infty \leq c_\infty, \quad (7.2.15)$$

where $c_\infty = \|c(\mathbf{x}, 0)\|_\infty$.

Proof: Multiply (7.1.3) by c^{p-1} for $p > 1$ (where we assume the concentration is scaled to be non-negative, otherwise p is chosen as an even integer). Thus,

$$\frac{d}{dt} \int_\Omega c^p dx = -p(p-1) \int_\Omega c^{p-2} |\nabla c|^2 dx - K_1 p \int_\Omega c^p dx. \quad (7.2.16)$$

We may integrate this and drop non-positive terms on the right to deduce

$$\left\{ \int_\Omega c^p dx \right\}^{1/p} \leq \left\{ \int_\Omega c_0^p dx \right\}^{1/p}. \quad (7.2.17)$$

Let now $p \rightarrow \infty$ in (7.2.17) to find the desired result. \square

Lemma 7.2.2

$$\|\mathbf{v}\| \leq \|c\|.$$

Proof: Multiply (7.1.12) by v_i , we have

$$\|\mathbf{v}\|^2 = -v \|\nabla \mathbf{v}\|^2 + g(w, c) - \sigma B_0^2 (\|\mathbf{v}\|^2 - \|w\|^2),$$

where w and g are the third component of velocity and gravity vectors, respectively. Next, by using the Cauchy-Schwarz inequality, the Poincarés inequality and then dropping non-positive terms on the right, we deduce the required result. \square

7.2.1 Continuous dependence on σ

Now, to investigate continuous dependence on σ , we let (v_{i1}, c_1, p_1) and (v_{i2}, c_2, p_2) be solutions to (7.1.12) and (7.1.2)-(7.1.5) for the same boundary-initial-value problems for different electrical conductivity coefficients σ_1 and σ_2 . Define the difference variables and constant as

$$u_i = v_{i1} - v_{i2}, \quad \phi = c_1 - c_2, \quad \pi = p_1 - p_2, \quad \sigma = \sigma_1 - \sigma_2, \quad (7.2.18)$$

and then from (7.1.12) and (7.1.2)-(7.1.5), (u_i, ϕ, π) is found to satisfy the partial differential equations

$$u_i = -\pi_{,i} + v\Delta u_i + g_i\phi + \sigma b_0^2[(v_1 \times k) \times k]_i + \sigma_2 b_0^2[(u \times k) \times k]_i, \quad (7.2.19)$$

$$u_{i,i} = 0, \quad (7.2.20)$$

$$\phi_{,t} + v_{1i}\phi_{,i} + u_i c_{2,i} = D\Delta\phi - K_1\phi, \quad (7.2.21)$$

where $\mathbf{k} = (0, 0, 1)$. The boundary and initial conditions are as follows

$$u_i = 0, \quad \frac{\partial\phi}{\partial n} = 0, \quad \text{on} \quad \partial\Omega, \quad (7.2.22)$$

$$\phi(\mathbf{x}, 0) = 0, \quad \text{in} \quad \Omega. \quad (7.2.23)$$

The proof of continuous dependence commences by multiplying (7.2.19) by u_i and integrating over Ω to find also with the aid of (7.2.15), Lemma 7.2.2 and the Cauchy-Schwarz inequality,

$$\|\mathbf{u}\|^2 \leq \|\phi\| \|\mathbf{u}\| + 2\sigma b_0^2 c_{1\infty} \|\mathbf{u}\|, \quad (7.2.24)$$

where $c_{1\infty} = \|c_1(\mathbf{x}, 0)\|_{\infty}$. We next use arithmetic-geometric mean inequality on the first and the second term on the right of (7.2.24) to find

$$\|\mathbf{u}\|^2 \leq 2\|\phi\|^2 + 8\sigma^2 b_0^4 c_{1\infty}^2. \quad (7.2.25)$$

Next, multiply (7.2.21) by ϕ and integrate over Ω to obtain

$$\frac{1}{2} \frac{d}{dt} \|\phi\|^2 = (u_i c_{2,i}, \phi_{,i}) - D \|\nabla\phi\|^2 - K_1 \|\phi\|^2. \quad (7.2.26)$$

Using the Cauchy-Schwarz inequality, arithmetic-geometric mean inequality and (7.2.15) we have

$$\frac{d}{dt} \|\phi\|^2 \leq \frac{c_{2\infty}^2}{2D} \|\mathbf{u}\|^2, \quad (7.2.27)$$

where $c_{2\infty} = \|c_2(\mathbf{x}, 0)\|_\infty$. Substituting (7.2.25) in (7.2.27)

$$\frac{d}{dt} \|\phi\|^2 \leq \frac{c_{2\infty}^2}{D} [\|\phi\|^2 + 4\sigma^2 b_0^4 c_{1\infty}^2]. \quad (7.2.28)$$

After integration (7.2.28), we arrive at the continuous dependence inequality

$$\|\phi\|^2 \leq 4\sigma^2 b_0^4 c_{1\infty}^2 [\exp(c_{2\infty}^2 t/D) - 1]. \quad (7.2.29)$$

If we use inequality (7.2.25), we find

$$\|\mathbf{u}\|^2 \leq 8\sigma^2 b_0^4 c_{1\infty}^2 \exp(c_{2\infty}^2 t/D).$$

7.2.2 Continuous dependence on K_1

We commence with a study of continuous dependence on the coefficient K_1 . Therefore, let (v_{i1}, c_1, p_1) and (v_{i2}, c_2, p_2) be solutions to equations (7.1.12) and (7.1.2)-(7.1.5) for the same boundary conditions (7.1.4) and the same initial data function $c(\mathbf{x}, 0)$ in (7.1.5), but for different chemical reaction coefficient K_{11} and K_{12} . Define the difference variables u_i, ϕ and π and constant K_1 by

$$u_i = v_{i1} - v_{i2}, \quad \phi = c_1 - c_2, \quad \pi = p_1 - p_2, \quad K_1 = K_{11} - K_{12}, \quad (7.2.30)$$

and then we find that (u_i, ϕ, π) satisfy the boundary-initial value problem

$$u_i = -\pi_{,i} + v\Delta u_i + g_i \phi + \sigma b_0^2 [(u \times k) \times k]_i, \quad (7.2.31)$$

$$u_{i,i} = 0, \quad (7.2.32)$$

$$\phi_{,t} + v_{1i} \phi_{,i} + u_i c_{2,i} = D\Delta c - K_{11}\phi - K_1 c_2. \quad (7.2.33)$$

in $\Omega \times (0, \infty)$, and

$$u_i = 0, \quad \frac{\partial \phi}{\partial n} = 0, \quad \text{on} \quad \partial\Omega, \quad (7.2.34)$$

$$\phi(\mathbf{x}, 0) = 0, \quad \text{in} \quad \Omega. \quad (7.2.35)$$

To establish continuous dependence on K_1 , we then multiply (7.2.31) by u_i and integrate over Ω to find, with the aid of the Cauchy-Schwarz inequality and after dropping a non-positive term on the right, that we may establish

$$\|\mathbf{u}\| \leq \|\phi\|. \quad (7.2.36)$$

Next, multiply (7.2.33) by ϕ and integrate over Ω to obtain

$$\frac{1}{2} \frac{d}{dt} \|\phi\|^2 = (u_i c_2, \phi_{,i}) - D \|\nabla \phi\|^2 - K_{11} \|\phi\|^2 - K_1(\phi, c_2). \quad (7.2.37)$$

We then use (7.2.15), the Cauchy-Schwarz and arithmetic-geometric mean inequalities, and then drop a non-positive term on the right to see that

$$\frac{d}{dt} \|\phi\|^2 \leq \frac{c_{2\infty}^2}{2D} \|u\|^2 + 2K_1 c_{2\infty} \|\phi\|^2. \quad (7.2.38)$$

Substituting (7.2.36) in (7.2.38) and then using the arithmetic-geometric mean inequality to obtain

$$\frac{d}{dt} \|\phi\|^2 \leq \frac{c_{2\infty}^2}{D} \|\phi\|^2 + 2DK_1^2. \quad (7.2.39)$$

Upon integration of (7.2.39), we arrive at the continuous dependence inequality

$$\|\phi\|^2 \leq 2 \frac{D^2 K_1^2}{c_{2\infty}^2} [\exp(c_{2\infty}^2 t / D) - 1], \quad (7.2.40)$$

Due to (7.2.36), clearly $\|\mathbf{u}\|^2$ satisfies the same bound (7.2.40) as $\|\phi\|^2$.

7.3 Continuous dependence for the second model

In this section we consider a solution to equations (7.1.13) and (7.1.7)-(7.1.11). Firstly, we need to get some bounds for our solution.

Lemma 7.3.1 If $T(\mathbf{x}, 0) \in L^\infty(\Omega)$, then

$$\|T(\mathbf{x}, t)\|_\infty \leq T_\infty, \quad (7.3.41)$$

where $T_\infty = \|T(\mathbf{x}, 0)\|_\infty$.

Proof: The proof of this lemma can be achieved by using the same argument which is used in the proof of lemma 7.2.1. \square

Lemma 7.3.2

$$\|\mathbf{v}\| \leq \|c\| + \|T\|.$$

Proof: The proof of this lemma is very similar to the proof of Lemma 7.2.2, and follows directly after multiplying (7.1.13) by v_i and use the Cauchy-Schwarz inequality. \square

7.3.1 Continuous dependence on σ

To study continuous dependence on the coefficient σ in equations (7.1.13) and (7.1.7)-(7.1.11), we let (v_{i1}, T_1, c_1, p_1) and (v_{i2}, T_2, c_2, p_2) be solutions to these equations for the same boundary and initial data, but for different electrical conductivity of the fluid σ_1 and σ_2 . Define the difference variables and constant as

$$u_i = v_{i1} - v_{i2}, \quad \theta = T_1 - T_2, \quad \phi = c_1 - c_2, \quad \pi = p_1 - p_2, \quad \sigma = \sigma_1 - \sigma_2, \quad (7.3.42)$$

and then from (7.1.13) and (7.1.7)-(7.1.11), (u_i, θ, ϕ, π) is found to satisfy the partial differential equations

$$u_i = -\pi_{,i} + v\Delta u_i + h_i\theta + g_i\phi + \sigma b_0^2[(v_1 \times k) \times k]_i + \sigma_2 b_0^2[(u \times k) \times k]_i, \quad (7.3.43)$$

$$u_{i,i} = 0, \quad (7.3.44)$$

$$\theta_{,t} + v_{1i}\theta_{,i} + u_i T_{2,i} = K\Delta\theta. \quad (7.3.45)$$

$$\phi_{,t} + v_{1i}\phi_{,i} + u_i c_{2,i} = D\Delta\phi - K_1\phi, \quad (7.3.46)$$

and the boundary and initial conditions

$$u_i = 0, \quad \frac{\partial\theta}{\partial n} = 0, \quad \frac{\partial\phi}{\partial n} = 0, \quad \text{on} \quad \partial\Omega, \quad (7.3.47)$$

$$\theta(\mathbf{x}, 0) = 0, \quad \phi(\mathbf{x}, 0) = 0, \quad \text{in} \quad \Omega. \quad (7.3.48)$$

From multiplication of (7.3.43) by u_i , integration over Ω and use (7.2.15), (7.3.41), Lemma 7.3.2 and the Cauchy-Schwarz inequality, one finds

$$\|\mathbf{u}\|^2 \leq \|\theta\|\|\mathbf{u}\| + \|\phi\|\|u\| + 2\sigma b_0^2\|\mathbf{v}_1\|\|\mathbf{u}\|$$

Therefore, we arrive at

$$\|\mathbf{u}\|^2 \leq 4\|\theta\|^2 + 4\|\phi\|^2 + 16\sigma^2 b_0^4(\|c_1\| + \|T_1\|)^2$$

$$\begin{aligned}
&\leq 4\|\theta\|^2 + 4\|\phi\|^2 + 32\sigma^2 b_0^4 (\|c_1\|^2 + \|T_1\|^2) \\
&\leq 4\|\theta\|^2 + 4\|\phi\|^2 + 32|\Omega|\sigma^2 b_0^4 (c_{1\infty}^2 + T_{1\infty}^2), \tag{7.3.49}
\end{aligned}$$

where $T_{1\infty} = \|T_1(\mathbf{x}, 0)\|_\infty$. Next, multiply (7.3.45) by θ and (7.3.46) by ϕ and integrate over Ω , using (7.2.15), (7.3.41) and arithmetic-geometric mean inequality to obtain

$$\frac{d}{dt}\|\theta\|^2 \leq \frac{T_{2\infty}^2}{2K}\|\mathbf{u}\|^2, \tag{7.3.50}$$

$$\frac{d}{dt}\|\phi\|^2 \leq \frac{c_{2\infty}^2}{2D}\|\mathbf{u}\|^2, \tag{7.3.51}$$

where $T_{2\infty} = \|T_2(\mathbf{x}, 0)\|_\infty$.

Let $b_1 = (T_{2\infty}^2/K) + (c_{2\infty}^2/D)$ and $b_2 = 16|\Omega|\sigma^2 b_0^4 (c_{1\infty}^2 + T_{1\infty}^2)$. We add (7.3.50) and (7.3.51) and then substitute (7.3.49) to find

$$\frac{d}{dt}(\|\theta\|^2 + \|\phi\|^2) \leq b_1[2(\|\theta\|^2 + \|\phi\|^2) + b_2]. \tag{7.3.52}$$

This expression is easily integrated to yield

$$\|\theta\|^2 \leq \frac{b_2}{2}[\exp(2b_1 t/D) - 1]. \tag{7.3.53}$$

$$\|\phi\|^2 \leq \frac{b_2}{2}[\exp(2b_1 t/D) - 1]. \tag{7.3.54}$$

From (7.3.49), (7.3.53) and (7.3.54), one may establish the continuous dependence of u_i on σ .

7.3.2 Continuous dependence on K_1

To study continuous dependence of the solution to (7.1.13) and (7.1.7)-(7.1.11) upon changes in K_1 we let (v_{i1}, T_1, c_1, p_1) and (v_{i2}, T_2, c_2, p_2) be solutions to equations (7.1.13) and (7.1.7)-(7.1.11) for the boundary conditions (7.1.10) and the same initial data function $c(\mathbf{x}, 0)$ and $T(\mathbf{x}, 0)$ in (7.1.11), but for chemical reaction coefficient K_{11} and K_{12} . Define the difference variables u_i, ϕ and π and constant K_1 by

$$u_i = v_{i1} - v_{i2}, \quad \theta = T_1 - T_2, \quad \phi = c_1 - c_2, \quad \pi = p_1 - p_2, \quad K_1 = K_{11} - K_{12}. \tag{7.3.55}$$

The difference of the two solutions (u_i, θ, ϕ, π) then satisfies

$$u_i = -\pi_{,i} + v\Delta u_i + g_i\phi + \sigma b_0^2[(u \times k) \times k]_i, \tag{7.3.56}$$

$$u_{i,i} = 0, \quad (7.3.57)$$

$$\theta_{,t} + v_{1i} \theta_{,i} + u_i T_{2,i} = K \Delta \theta. \quad (7.3.58)$$

$$c_{,t} + v_{1i} \phi_{,i} + u_i c_{2,i} = D \Delta c - K_{11} \phi - K_1 c_2, \quad (7.3.59)$$

in $\Omega \times (0, \infty)$, with the boundary and initial conditions

$$u_i = 0, \quad \frac{\partial \theta}{\partial n} = 0, \quad \frac{\partial \phi}{\partial n} = 0, \quad \text{on} \quad \partial \Omega, \quad (7.3.60)$$

$$\theta(\mathbf{x}, 0) = 0, \quad \phi(\mathbf{x}, 0) = 0, \quad \text{in} \quad \Omega. \quad (7.3.61)$$

Multiplying (7.3.53) by u_i and integrating over Ω to find after discarding the non-positive term on the right also with the aid of the Cauchy-Schwarz and arithmetic-geometric inequalities,

$$\|\mathbf{u}\|^2 \leq 2(\|\theta\|^2 + \|\phi\|^2). \quad (7.3.62)$$

Next, multiply (7.3.58) by θ and (7.3.59) by ϕ and integrate over Ω , respectively, and then use (7.2.15), (7.3.41) and arithmetic-geometric mean inequality to obtain

$$\frac{d}{dt} \|\theta\|^2 \leq \frac{T_{2\infty}^2}{2K} \|\mathbf{u}\|^2. \quad (7.3.63)$$

$$\frac{d}{dt} \|\phi\|^2 \leq \frac{c_{2\infty}^2}{2D} \|\mathbf{u}\|^2 + \frac{c_{2\infty}^2}{2D} \|\phi\|^2 + 2DK_1^2. \quad (7.3.64)$$

Let b_1 has the same value in last section and $b_3 = (T_{2\infty}^2/K) + (3c_{2\infty}^2/2D)$. Summing (7.3.63) and (7.3.64) and then using (7.3.62), we get

$$\frac{d}{dt} (\|\theta\|^2 + \|\phi\|^2) \leq b_3 (\|\theta\|^2 + \|\phi\|^2) + 2DK_1^2. \quad (7.3.65)$$

Upon integration of (7.3.65), we arrive at the continuous dependence on K_1 inequality

$$\|\theta\|^2 \leq \frac{2DK_1^2}{b_3} [\exp(b_3 t) - 1]. \quad (7.3.66)$$

$$\|\phi\|^2 \leq \frac{2DK_1^2}{b_3} [\exp(b_3 t) - 1]. \quad (7.3.67)$$

A similar continuous dependence estimate for u_i may then be established with the help of (7.3.62).

Chapter 8

Structural stability for two convection models in a reacting fluid with magnetic field effect

8.1 Introduction

There has been much recent interest in obtaining stability estimates for solutions to physical problems in partial differential equations where changes in coefficients are allowed, or even the equations themselves change. This type of stability, which is often called structural stability to distinguish it from continuous dependence on the initial data, is studied for example in Ames and Payne [1–4], Franchi and Straughan [54–57], Lin and Payne [106–110], Payne and Song [144–146], and Payne and Straughan [147–151], Payne et al. [143], Straughan and Hutter [200], Harfash [76, 78], and also occupies attention in the books of Bellomo and Preziosi [19], Ames and Straughan [5] and Straughan [197]. Such stability estimates are fundamental to analysing whether a small change in a coefficient or other data leads to a drastic change in the solution. A concrete example of structural stability, and in particular continuous dependence on modelling, is provided in the paper by Payne and Straughan [147], where it is shown how a solution to the Stokes equation for slow viscous flow approximates that to the Navier-Stokes equations. Thus, questions of continuous dependence on the model itself are fundamental and in many ways are

as important as a study of stability itself.

This chapter continues the investigation of continuous dependence properties of models which are introduced in Chapter 3 and 4. The first model which is studied in this study is the problem of convection with a dissolved reacting fluid layer and a vertically imposed magnetic field

$$v_{i,t} + v_j v_{i,j} = -p_{,i} + v \Delta v_i + g_i c + \mathbf{j} \times \mathbf{B}, \quad (8.1.1)$$

$$v_{i,i} = 0, \quad (8.1.2)$$

$$c_{,t} + v_i c_{,i} = D \Delta c - K_1 c, \quad (8.1.3)$$

$$v_i = 0, \quad \frac{\partial c}{\partial n} = 0, \quad \text{on} \quad \partial \Omega, \quad (8.1.4)$$

$$v_i(\mathbf{x}, 0) = \psi_i(\mathbf{x}), \quad c(\mathbf{x}, 0) = f_1(\mathbf{x}), \quad \text{in} \quad \Omega, \quad (8.1.5)$$

where \mathbf{v} is the velocity vector, c is the concentration field, p is pressure field, D is the diffusion coefficient, g_i is the gravity vector, \mathbf{B} is the magnetic induction field, \mathbf{j} is the current and K_1 is the chemical reaction rate. This system hold on a bounded spatial domain Ω in \mathbb{R}^3 with boundary $\partial \Omega$ sufficiently smooth to allow applications of the divergence theorem. Standard indication notation is employed with Δ denoting the Laplacian. The functions ψ_i and f_1 are assumed to be smooth functions.

The second model which is studied in this study is the problem of double diffusive convection with a dissolved reacting fluid layer and a vertically imposed magnetic field,

$$v_{i,t} + v_j v_{i,j} = -p_{,i} + v \Delta v_i + h_i T + g_i c + \mathbf{j} \times \mathbf{B}, \quad (8.1.6)$$

$$v_{i,i} = 0, \quad (8.1.7)$$

$$T_{,t} + v_i T_{,i} = K \Delta T, \quad (8.1.8)$$

$$c_{,t} + v_i c_{,i} = D \Delta c - K_1 c, \quad (8.1.9)$$

$$v_i = 0, \quad \frac{\partial c}{\partial n} = 0, \quad \frac{\partial T}{\partial n} = 0, \quad \text{on} \quad \partial \Omega, \quad (8.1.10)$$

$$v_i(\mathbf{x}, 0) = \psi_i(\mathbf{x}), \quad c(\mathbf{x}, 0) = f_1(\mathbf{x}), \quad T(\mathbf{x}, 0) = f_2(\mathbf{x}), \quad \text{in} \quad \Omega, \quad (8.1.11)$$

where \mathbf{v} is the velocity vector, c is the concentration field, T is the temperature field, p is pressure field, D is the diffusion coefficient, \mathbf{B} is the magnetic induction field, \mathbf{j} is the current, K_1 is the chemical reaction rate and K is the thermal diffusivity. This system hold on a bounded spatial domain Ω in \mathbb{R}^3 with boundary $\partial\Omega$ sufficiently smooth to allow applications of the divergence theorem. The functions ψ_i , f_1 and f_2 are assumed to be smooth functions.

Now, according to the quasi-static MHD approximation of Galdi and Straughan [61], we have

$$\mathbf{j} \times \mathbf{B} = \sigma(\mathbf{v} \times \mathbf{B}_0) \times \mathbf{B}_0,$$

where σ is the electrical conductivity and $\mathbf{B}_0 = (0, 0, B_0)$ is a magnetic field with only the vertical component.

In Both models, we establish that the solution depends continuously on change in the chemical reaction and magnetic coefficients. The plan of this chapter is as follows. In Section 8.2 we study the continuous dependence for the model of convective motion with a dissolved reacting fluid layer. In Section 8.3 we investigate the continuous dependence for the model of double diffusive convection with a dissolved reacting fluid layer.

The results in this chapter were published in the article Harfash [77].

8.2 Continuous dependence for the first model

Lemma 8.2.1 If $c(\mathbf{x}, 0)$ and $T(\mathbf{x}, 0) \in L^\infty(\Omega)$, then

$$\|c(\mathbf{x}, t)\|_\infty \leq c_\infty, \quad (8.2.12)$$

$$\|T(\mathbf{x}, t)\|_\infty \leq T_\infty, \quad (8.2.13)$$

where $c_\infty = \|c(\mathbf{x}, 0)\|_\infty$, $T_\infty = \|T(\mathbf{x}, 0)\|_\infty$.

Proof: Multiply (8.1.3) by c^{p-1} for $p > 1$ (where we assume the concentration is scaled to be non-negative, otherwise p is chosen as an even integer). Thus,

$$\frac{d}{dt} \int_\Omega c^p dx = -p(p-1) \int_\Omega c^{p-2} |\nabla c|^2 dx - K_1 p \int_\Omega c^p dx. \quad (8.2.14)$$

We may integrate this and drop non-positive terms on the right to deduce

$$\left\{ \int_{\Omega} c^p dx \right\}^{1/p} \leq \left\{ \int_{\Omega} c_0^p dx \right\}^{1/p}. \quad (8.2.15)$$

Let now $p \rightarrow \infty$ in (8.2.15) to find the desired result. Similar argument can be used to prove (8.2.13). \square

Lemma 8.2.2 If $c(\mathbf{x}, 0) \in L^2(\Omega)$, then

$$\|c(\mathbf{x}, t)\|^2 \leq c_l, \quad (8.2.16)$$

where $c_l = \|c(\mathbf{x}, 0)\|^2$.

Proof: Multiply (8.1.3) by c and integrating over Ω . we have

$$\frac{d}{dt} \|c\|^2 = -2D \|\nabla c\|^2 - 2K_1 \|c\|^2.$$

We may integrate this and drop non-positive terms on the right to deduce

$$\|c(\mathbf{x}, t)\|^2 \leq \|c(\mathbf{x}, 0)\|^2.$$

\square

Lemma 8.2.3 If $v_i(\mathbf{x}, 0) \in L^2(\Omega)$, then

$$\|\mathbf{v}(\mathbf{x}, t)\|^2 \leq v_l, \quad (8.2.17)$$

where $v_l = (c_l + \|\mathbf{v}(\mathbf{x}, 0)\|^2)e^T$.

Proof: Multiply (8.1.1) by v_i and integrating over Ω . By using the Cauchy-Schwarz inequality, arithmetic-geometric mean inequality and and drop a non-positive term on the right, we have

$$\frac{1}{2} \frac{d}{dt} \|\mathbf{v}\|^2 \leq \int_{\Omega} g_i v_i c dx \leq \|\mathbf{v}\| \|c\| \leq \frac{1}{2} \|\mathbf{v}\|^2 + \frac{c_l}{2}.$$

We may integrate this, we get

$$\begin{aligned} \|\mathbf{v}\|^2 &\leq c_l(e^t - 1) + e^t \|\mathbf{v}(\mathbf{x}, 0)\|^2 \\ &\leq (c_l + \|\mathbf{v}(\mathbf{x}, 0)\|^2)e^t \leq (c_l + \|\mathbf{v}(\mathbf{x}, 0)\|^2)e^T. \end{aligned}$$

\square

Lemma 8.2.4 If $v_i(\mathbf{x}, 0) \in L^2(\Omega)$ and $c(\mathbf{x}, 0) \in L^2(\Omega)$, then

$$\int_{\Omega} v_{i,j} v_{i,j} dx \leq \frac{1}{v} [v_i^{1/2} (\int_{\Omega} v_{i,t} v_{i,t} dx)^{1/2} + (v_i c_i)^{1/2}]. \quad (8.2.18)$$

Proof: Multiply (8.1.1) by v_i and integrating over Ω and drop a non-positive term on the right, we have

$$\int_{\Omega} v_{i,t} v_i dx \leq -v \int_{\Omega} v_{i,j} v_{i,j} dx + \int_{\Omega} g_i v_i c dx.$$

Hence, employing (8.2.16) and (8.2.17) in the above inequality, we find, with use of the Cauchy-Schwarz inequality,

$$\begin{aligned} \int_{\Omega} v_{i,j} v_{i,j} dx &\leq \frac{1}{v} [- \int_{\Omega} v_{i,t} v_i dx + \int_{\Omega} g_i v_i c dx] \\ &\leq \frac{1}{v} [(\int_{\Omega} v_{i,t} v_{i,t} dx)^{1/2} (\int_{\Omega} v_i v_i dx)^{1/2} + (\int_{\Omega} v_i v_i dx)^{1/2} (\int_{\Omega} c^2 dx)^{1/2}] \\ &\leq \frac{1}{v} [v_i^{1/2} (\int_{\Omega} v_{i,t} v_{i,t} dx)^{1/2} + (v_i c_i)^{1/2}]. \end{aligned}$$

□

We now derive an a priori bound for $v_{i,t}$. Here we have two different values for the bound of $v_{i,t}$. This is because we split the proof into two parts depending on the availability of the Sobolev inequalities. For the two dimensions case, we have the following inequality [196]:

$$\int_{\Omega} v^4 dx \leq (\int_{\Omega} v^2 dx) (\int_{\Omega} v_{,i} v_{,i} dx), \quad (8.2.19)$$

while in three dimensions, we cannot use the above inequality, thus we will use the following inequality [196]:

$$\int_{\Omega} v^4 dx \leq \beta (\int_{\Omega} v^2 dx)^{1/2} (\int_{\Omega} v_{,i} v_{,i} dx)^{3/2}, \quad (8.2.20)$$

Lemma 8.2.5 For two dimensions, if $v_{i,t}(\mathbf{x}, 0) \in L^2(\Omega)$ and $c_{,t}(\mathbf{x}, 0) \in L^2(\Omega)$, then

$$\int_{\Omega} v_{i,t} v_{i,t} dx \leq v_{tl}(t), \quad (8.2.21)$$

where

$$v_{tl}(t) = \left(\frac{R_2 \sqrt{\Phi(0)}}{R_1 \sqrt{\Phi(0)} (e^{-R_2 t} - 1) + R_2 e^{-R_2 t}} \right)^2,$$

$$\Phi = \Phi_v + \Phi_c, \quad \Phi_v = \int_{\Omega} v_{i,t} v_{i,t} dx \quad \Phi_c = \int_{\Omega} c_{,t} c_{,t} dx, \quad R_1 = \frac{v_l^{1/2}}{2v^2}, \quad R_2 = \frac{v_l^{1/2} c_l^{1/2}}{2v^2} + \frac{c_{\infty}^2}{2D} + 1$$

Proof:

$$\begin{aligned} \Phi_{c,t} &= 2 \int_{\Omega} c_{,t} c_{,tt} dx = 2 \int_{\Omega} c_{,t} [-v_i c_{,i} + D\Delta c - K_1 c]_{,t} dx \\ &= 2D \int_{\Omega} c_{,t} \Delta c_{,t} dx - 2K_1 \int_{\Omega} c_{,t} c_{,t} dx - 2 \int_{\Omega} c_{,t} v_{i,t} c_{,i} dx - 2 \int_{\Omega} c_{,t} v_{i,t} c_{,it} dx \\ &\leq -2D \int_{\Omega} c_{,it} c_{,it} dx + 2 \int_{\Omega} c_{,it} v_{i,t} c_{,i} dx = -2D \int_{\Omega} c_{,it} c_{,it} dx + 2c_{\infty} \int_{\Omega} c_{,it} v_{i,t} dx \\ &\leq -2D \int_{\Omega} c_{,it} c_{,it} dx + 2c_{\infty} \left(\int_{\Omega} c_{,it} c_{,it} dx \right)^{1/2} \left(\int_{\Omega} v_{i,t} v_{i,t} dx \right)^{1/2} \\ &\leq -2D \int_{\Omega} c_{,it} c_{,it} dx + 2D \int_{\Omega} c_{,it} c_{,it} dx + \frac{c_{\infty}^2}{2D} \int_{\Omega} v_{i,t} v_{i,t} dx. \end{aligned}$$

Thus we have,

$$\frac{d}{dt} \Phi_c \leq \frac{c_{\infty}^2}{2D} \Phi_v. \quad (8.2.22)$$

Next, we will perform the same work for $\Phi_{v,t}$,

$$\begin{aligned} \Phi_{v,t} &= 2 \int_{\Omega} v_{i,t} v_{i,tt} dx = 2 \int_{\Omega} v_{i,t} [-v_j v_{i,j} - p_{,i} + v\Delta v_i + g_i c + \sigma b_0^2 (k_i w - v_i)]_{,t} dx \\ &= -2v \int_{\Omega} v_{i,jt} v_{i,jt} dx - 2 \int_{\Omega} v_{i,t} v_{j,t} v_{i,j} dx + 2 \int_{\Omega} g_i v_{i,t} c_t dx + 2\sigma b_0^2 \int_{\Omega} (k_i w_{,t} v_{i,t} - v_{i,t} v_{i,t}) dx \\ &\leq -2v \int_{\Omega} v_{i,jt} v_{i,jt} dx - 2 \int_{\Omega} v_{i,t} v_{j,t} v_{i,j} dx + 2 \int_{\Omega} g_i v_{i,t} c_t dx \\ &\leq -2v \int_{\Omega} v_{i,jt} v_{i,jt} dx + 2 \left(\int_{\Omega} v_{i,j} v_{i,j} dx \right)^{1/2} \left(\int_{\Omega} (v_{i,t} v_{i,t})^2 dx \right)^{1/2} + \Phi_v + \Phi_c. \end{aligned}$$

where $\mathbf{k} = (0, 0, 1)$.

Now, the arithmetic-geometric mean inequality is used on the right-hand side together with the Sobolev inequality (8.2.19) and (8.2.18) to find

$$\begin{aligned} \Phi_{v,t} &\leq -2v \int_{\Omega} v_{i,jt} v_{i,jt} dx + 2 \left(\int_{\Omega} v_{i,j} v_{i,j} dx \right)^{1/2} \left(\int_{\Omega} v_{i,t} v_{i,t} dx \right)^{1/2} \left(\int_{\Omega} v_{i,jt} v_{i,jt} dx \right)^{1/2} + \Phi_v + \Phi_c \\ &\leq \frac{1}{2v} \Phi_v \int_{\Omega} v_{i,j} v_{i,j} dx + \Phi_v + \Phi_c \leq \frac{1}{2v^2} \Phi_v [v_l^{1/2} \Phi_v^{1/2} + (v_l c_l)^{1/2}] + \Phi_v + \Phi_c. \quad (8.2.23) \end{aligned}$$

Now, summing (8.2.22) and (8.2.23), we have

$$\frac{d}{dt} (\Phi_v + \Phi_c) \leq R_1 \Phi_v^{3/2} + R_2 \Phi_v + \Phi_c$$

$$\begin{aligned} &\leq R_1 \Phi_v (\Phi_v + \Phi_c)^{1/2} + R_2 (\Phi_v + \Phi_c) \leq R_1 \Phi_v (\Phi_v + \Phi_c)^{1/2} + R_1 \Phi_c (\Phi_v + \Phi_c)^{1/2} + R_2 (\Phi_v + \Phi_c) \\ &\quad \frac{d}{dt} (\Phi_v + \Phi_c) \leq R_1 (\Phi_v + \Phi_c)^{3/2} + R_2 (\Phi_v + \Phi_c). \end{aligned} \quad (8.2.24)$$

Integrating (8.2.24), we find the desired result (8.2.21) for the two dimensions case.

□

Lemma 8.2.6 For three dimensions, if $v_{i,t}(\mathbf{x}, 0) \in L^2(\Omega)$ and $c_{,t}(\mathbf{x}, 0) \in L^2(\Omega)$, then

$$\int_{\Omega} v_{i,t} v_{i,t} dx \leq v_{il}(t), \quad (8.2.25)$$

where

$$\begin{aligned} v_{il}(t) &= \frac{R_4 \Phi(0)}{R_3 \Phi(0)(e^{-R_4 t} - 1) + R_4 e^{-R_4 t}} \\ \Phi &= \Phi_v + \Phi_c, \quad R_3 = \frac{27v_l \beta^4}{64v^5}, \quad R_4 = \frac{27v_l c_l \beta^4}{64v^5} + \frac{c_{\infty}^2}{2D} + 1. \end{aligned}$$

It is clear that for three dimensions the bound (8.2.25) valid just for $t < \frac{1}{R_4} \ln(1 + \frac{R_4}{R_3 \Phi(0)})$, thus we have conditional continuous dependence in this case.

Proof: Using similar technique which is used for two dimensions case we have

$$\frac{d}{dt} \Phi_c \leq \frac{c_{\infty}^2}{2D} \Phi_v, \quad (8.2.26)$$

and

$$\Phi_{v,t} \leq -2v \int_{\Omega} v_{i,jt} v_{i,jt} dx + 2 \left(\int_{\Omega} v_{i,j} v_{i,j} dx \right)^{1/2} \left(\int_{\Omega} (v_{i,t} v_{i,t})^2 dx \right)^{1/2} + \Phi_v + \Phi_c.$$

Next, using the Sobolev inequalities (8.2.20), Young's inequality and (8.2.18) we derive

$$\begin{aligned} \Phi_{v,t} &\leq -2v \int_{\Omega} v_{i,jt} v_{i,jt} dx + 2\beta \left(\int_{\Omega} v_{i,j} v_{i,j} dx \right)^{1/2} \left(\int_{\Omega} v_{i,t} v_{i,t} dx \right)^{1/4} \left(\int_{\Omega} v_{i,jt} v_{i,jt} dx \right)^{3/4} + \Phi_v + \Phi_c \\ &\leq \frac{27\beta^4}{128v^3} \Phi_v \left(\int_{\Omega} v_{i,j} v_{i,j} dx \right)^2 + \Phi_v + \Phi_c \\ &\leq \frac{27\beta^4}{128v^5} \Phi_v [v_l^{1/2} \Phi_v^{1/2} + (v_l c_l)^{1/2}]^2 + \Phi_v + \Phi_c \\ &\leq \frac{27\beta^4}{64v^5} \Phi_v [v_l \Phi_v + v_l c_l] + \Phi_v + \Phi_c. \end{aligned} \quad (8.2.27)$$

Now, summing (8.2.26) and (8.2.27), we have

$$\begin{aligned} \frac{d}{dt}(\Phi_v + \Phi_c) &\leq R_3\Phi_v^2 + R_4\Phi_v + \Phi_c \\ &\leq R_3(\Phi_v^2 + 2\Phi_v\Phi_c + \Phi_c^2) + R_4(\Phi_v + \Phi_c). \end{aligned}$$

Thus, we deduce

$$\frac{d}{dt}(\Phi_v + \Phi_c) \leq R_3(\Phi_v + \Phi_c)^2 + R_4(\Phi_v + \Phi_c). \quad (8.2.28)$$

Upon integration of (8.2.28), we find the desired result (8.2.25) for the three dimensions case.

□

8.2.1 Continuous dependence on σ

This section is devoted to establishing continuous dependence of the solution on σ . Let (v_{i1}, c_1, p_1) and (v_{i2}, c_2, p_2) be two solutions of (8.1.1)-(8.1.3) with the same data (8.1.4), (8.1.5), but with different electrical conductivity of the fluid σ_1 and σ_2 . Now set

$$u_i = v_{i1} - v_{i2}, \quad \phi = c_1 - c_2, \quad \pi = p_1 - p_2, \quad \sigma = \sigma_1 - \sigma_2. \quad (8.2.29)$$

The difference of the two solutions (u_i, ϕ, π) then satisfies

$$u_{i,t} + v_{1j}u_{i,j} + u_j v_{2i,j} = -\pi_{,i} + v\Delta u_i + g_i\phi + \sigma b_0^2[(v_1 \times k) \times k]_i + \sigma_2 b_0^2[(u \times k) \times k]_i, \quad (8.2.30)$$

$$u_{i,i} = 0, \quad (8.2.31)$$

$$\phi_{,t} + v_{1i}\phi_{,i} + u_i c_{2,i} = D\Delta\phi - K_1\phi, \quad (8.2.32)$$

with the boundary and initial conditions

$$u_i = 0, \quad \frac{\partial\phi}{\partial n} = 0, \quad \text{on} \quad \partial\Omega, \quad (8.2.33)$$

$$\theta(\mathbf{x}, 0) = 0, \quad u_i(\mathbf{x}, 0) = 0, \quad \text{in} \quad \Omega. \quad (8.2.34)$$

The proof of continuous dependence commences by multiplying (8.2.30) by u_i and integrating over Ω to find,

$$\frac{d}{dt}\|\mathbf{u}\|^2 = 2 \int_{\Omega} u_i u_{i,t} dx$$

$$\begin{aligned}
&= 2 \int_{\Omega} u_i [-v_{1j} u_{i,j} - u_j v_{2i,j} - \pi_{,i} + v \Delta u_i + g_i \phi + \sigma b_0^2 (k_i w_1 - v_{1i}) + \sigma_2 b_0^2 (k_i w - u_i)] dx \\
&\leq -2v \int_{\Omega} u_{i,j} u_{i,j} dx - 2 \int_{\Omega} u_i u_j v_{2i,j} dx + 2 \int_{\Omega} g_i u_i \phi dx + 2\sigma b_0^2 \int_{\Omega} (k_i w_1 u_i - v_{1i} u_i) dx \\
&\leq -2v \int_{\Omega} u_{i,j} u_{i,j} dx + 2 \left(\int_{\Omega} v_{2i,j} v_{2i,j} dx \right)^{1/2} \left(\int_{\Omega} (u_i u_i)^2 dx \right)^{1/2} + 2 \left(\int_{\Omega} u_i u_i dx \right)^{1/2} \left(\int_{\Omega} \phi \phi dx \right)^{1/2} \\
&\quad + 4\sigma b_0^2 v_{l1}^{1/2} \left(\int_{\Omega} u_i u_i dx \right)^{1/2},
\end{aligned}$$

where $v_{l1} = (c_{l1} + \|\mathbf{v}_1(\mathbf{x}, 0)\|^2) e^T$, $c_{l1} = \|c_1(\mathbf{x}, 0)\|^2$ and w, w_1 is the third component of the velocities u_i, v_{i1} , respectively. By using the Sobolev inequality (8.2.20), arithmetic-geometric mean inequality and (8.2.18) we obtain

$$\begin{aligned}
\frac{d}{dt} \|\mathbf{u}\|^2 &\leq -2v \int_{\Omega} u_{i,j} u_{i,j} dx + 2\beta \left(\int_{\Omega} v_{2i,j} v_{2i,j} dx \right)^{1/2} \left(\int_{\Omega} u_i u_i dx \right)^{1/4} \left(\int_{\Omega} u_{i,j} u_{i,j} dx \right)^{3/4} \\
&\quad + \int_{\Omega} u_i u_i dx + \int_{\Omega} \phi \phi dx + \sigma^2 b_0^4 v_{l1} + \int_{\Omega} u_i u_i dx \\
&\leq \frac{27\beta^4}{128v^3} \|u\|^2 \left(\int_{\Omega} v_{2i,j} v_{2i,j} dx \right)^2 + 2\|u\|^2 + \|\phi\|^2 + \sigma^2 b_0^4 v_{l1} \\
&\leq \frac{27\beta^4}{128v^5} \|u\|^2 [v_{l2}^{1/2} v_{lt2}(t)^{1/2} + (v_{l2} c_{l2})^{1/2}]^2 + 2\|u\|^2 + \|\phi\|^2 + \sigma^2 b_0^4 v_{l1} \\
&\leq \frac{27\beta^4}{64v^5} \|u\|^2 [v_{l2} v_{lt2}(t) + v_{l2} c_{l2}] + 2\|u\|^2 + \|\phi\|^2 + \sigma^2 b_0^4 v_{l1}, \tag{8.2.35}
\end{aligned}$$

where $v_{l2} = (c_{l2} + \|\mathbf{v}_2(\mathbf{x}, 0)\|^2) e^T$, $c_{l2} = \|c_2(\mathbf{x}, 0)\|^2$, the value $v_{lt1}(t)$ is equal to the value of $v_{lt}(t)$ which is defined in Lemma 8.2.5 and 8.2.6 at the solution (v_{i2}, c_2, p_2) . Next, multiply (8.2.32) by ϕ and integrate over Ω and using the Cauchy-Schwarz inequality, arithmetic-geometric mean inequality and (8.2.12) we have

$$\frac{d}{dt} \|\phi\|^2 \leq \frac{c_{2\infty}^2}{2D} \|u\|^2. \tag{8.2.36}$$

Let $R_5(t) = \frac{27\beta^4}{64v^5} [v_{l2} v_{lt2}(t) + v_{l2} c_{l2}] + \frac{c_{2\infty}^2}{2D} + 2$, and $R_6(t) = \int R_5(t) dt$. Summing (8.2.35) and (8.2.36), we get

$$\frac{d}{dt} (\|\mathbf{u}\|^2 + \|\phi\|^2) \leq R_5(t) (\|\mathbf{u}\|^2 + \|\phi\|^2) + \sigma^2 b_0^4 v_{l1}. \tag{8.2.37}$$

Integrating (8.2.37) we obtain the continuous dependence inequality on σ

$$\|\mathbf{u}\|^2 + \|\phi\|^2 \leq \sigma^2 b_0^4 v_{l1} \int_0^t e^{R_6(t)-R_6(s)} ds. \tag{8.2.38}$$

8.2.2 Continuous dependence on K_1

In this section we demonstrate briefly how to establish a continuous dependence result for the chemical reaction rate K_1 in (8.1.1)-(8.1.3). Let (v_{i1}, c_1, p_1) and (v_{i2}, c_2, p_2) be two solutions of problem (8.1.1)-(8.1.3) for different chemical reaction coefficients K_{11} and K_{12} , respectively. Then, as previously, (u_i, ϕ, π) will solve the problem

$$u_{i,t} + v_{1j}u_{i,j} + u_jv_{2i,j} = -\pi_{,i} + v\Delta u_i + g_i\phi + \sigma b_0^2[(u \times k) \times k]_i, \quad (8.2.39)$$

$$u_{i,i} = 0, \quad (8.2.40)$$

$$\phi_{,t} + v_{1i}\phi_{,i} + u_i c_{2,i} = D\Delta c - K_{11}\phi - K_1 c_2, \quad (8.2.41)$$

subject to conditions

$$u_i = 0, \quad \frac{\partial \phi}{\partial n} = 0, \quad \text{on} \quad \partial\Omega, \quad (8.2.42)$$

$$\theta(\mathbf{x}, 0) = 0, \quad u_i(\mathbf{x}, 0) = 0, \quad \text{in} \quad \Omega. \quad (8.2.43)$$

Multiplying by u_i and integrating by parts over Ω , we find

$$\begin{aligned} \frac{d}{dt}\|u\|^2 &= 2 \int_{\Omega} u_i u_{i,t} dx \\ &= 2 \int_{\Omega} u_i [-v_{1j}u_{i,j} - u_jv_{2i,j} - \pi_{,i} + v\Delta u_i + g_i\phi + \sigma b_0^2(k_i w - u_i)] dx \\ &= -2v \int_{\Omega} u_{i,j}u_{i,j} dx - 2 \int_{\Omega} u_i u_j v_{2i,j} dx + 2 \int_{\Omega} g_i u_i \phi dx + 2\sigma b_0^2 \int_{\Omega} (k_i w \cdot u_i - u_i u_i) dx \\ &\leq -2v \int_{\Omega} u_{i,j}u_{i,j} dx + 2 \left(\int_{\Omega} v_{2i,j}v_{2i,j} dx \right)^{1/2} \left(\int_{\Omega} (u_i u_i)^2 dx \right)^{1/2} + 2 \left(\int_{\Omega} u_i u_i dx \right)^{1/2} \left(\int_{\Omega} \phi^2 dx \right)^{1/2}. \end{aligned}$$

By using the Sobolev inequality (8.2.20), Young's inequality and (8.2.18) we get

$$\begin{aligned} \frac{d}{dt}\|\mathbf{u}\|^2 &\leq -2v \int_{\Omega} u_{i,j}u_{i,j} dx + 2\beta \left(\int_{\Omega} v_{2i,j}v_{2i,j} dx \right)^{1/2} \left(\int_{\Omega} u_i u_i dx \right)^{1/4} \left(\int_{\Omega} u_{i,j}u_{i,j} dx \right)^{3/4} \\ &\quad + \int_{\Omega} u_i u_i dx + \int_{\Omega} \phi^2 dx \\ &\leq \frac{27\beta^4}{128v^3} \|\mathbf{u}\|^2 \left(\int_{\Omega} v_{2i,j}v_{2i,j} dx \right)^2 + \|\mathbf{u}\|^2 + \|\phi\|^2 \\ &\leq \frac{27\beta^4}{128v^5} \|\mathbf{u}\|^2 [v_{l2}^{1/2} v_{lt2}(t)^{1/2} + (v_{l2} c_{l2})^{1/2}]^2 + \|\mathbf{u}\|^2 + \|\phi\|^2 \end{aligned}$$

$$\leq \frac{27\beta^4}{64v^5} \|\mathbf{u}\|^2 [v_{l2}v_{lt2}(t) + v_{l2}c_{l2}] + \|\mathbf{u}\|^2 + \|\phi\|^2. \quad (8.2.44)$$

Next, multiply (8.2.41) by ϕ and integrate over Ω to obtain

$$\frac{1}{2} \frac{d}{dt} \|\phi\|^2 = (u_i c_2, \phi_i) - D \|\nabla \phi\|^2 - K_{11} \|\phi\|^2 - K_1(\phi, c_2). \quad (8.2.45)$$

Next, the Cauchy-Schwarz and arithmetic-geometric mean inequalities are employed and then drop a non-positive term on the right to see that

$$\frac{d}{dt} \|\phi\|^2 \leq \frac{c_{2\infty}^2}{2D} \|\mathbf{u}\|^2 + \frac{c_{2\infty}^2}{2D} \|\phi\|^2 + 2DK_1^2. \quad (8.2.46)$$

Let $R_7(t) = (27\beta^4/64v^5)[v_{l2}v_{lt2}(t) + v_{l2}c_{l2}] + (c_{2\infty}^2/2D) + 1$, and $R_8(t) = \int R_7(t) dt$.

Summing (8.2.44) and (8.2.46), we get

$$\frac{d}{dt} (\|\mathbf{u}\|^2 + \|\phi\|^2) \leq R_7(t) (\|\mathbf{u}\|^2 + \|\phi\|^2) + 2DK_1^2. \quad (8.2.47)$$

An integration yields

$$\|\mathbf{u}\|^2 + \|\phi\|^2 \leq 2DK_1^2 \int_0^t e^{R_8(t)-R_8(s)} dt, \quad (8.2.48)$$

which is the desired continuous dependence result, thus the continuous dependence for u_i and ϕ follows from (8.2.48).

8.3 Continuous dependence for the second model

Lemma 8.3.1 If $T(\mathbf{x}, 0) \in L^2(\Omega)$, then

$$\|T(\mathbf{x}, t)\|^2 \leq T_l, \quad (8.3.49)$$

where $T_l = \|T(\mathbf{x}, 0)\|^2$.

Proof: The proof of this lemma follows directly using the same argument in lemma 8.2.2. \square

Lemma 8.3.2 If $v_i(\mathbf{x}, 0) \in L^2(\Omega)$, then

$$\|\mathbf{v}(\mathbf{x}, t)\|^2 \leq v_l, \quad (8.3.50)$$

where $v_l = (2c_l + 2T_l + \|\mathbf{v}(\mathbf{x}, 0)\|^2)e^T$.

Proof: The first step involves multiplying (8.1.6) by v_i and integrating over Ω . By using the Cauchy-Schwarz inequality, arithmetic-geometric mean inequality and and drop a non-positive term on the right, we have

$$\begin{aligned} \frac{1}{2} \frac{d}{dt} \|\mathbf{v}\|^2 &= \int_{\Omega} g_i v_i c \, dx + \int_{\Omega} h_i v_i T \, dx \leq \|\mathbf{v}\| \|c\| + \|\mathbf{v}\| \|T\| \\ &\leq \frac{1}{2} \|\mathbf{v}\|^2 + c_l + T_l. \end{aligned}$$

We may integrate this, we get

$$\begin{aligned} \|\mathbf{v}\|^2 &\leq (2c_l + 2T_l)(e^t - 1) + e^t \|\mathbf{v}(\mathbf{x}, 0)\|^2 \\ &\leq (2c_l + 2T_l + \|\mathbf{v}(\mathbf{x}, 0)\|^2) e^t \leq (2c_l + 2T_l + \|\mathbf{v}(\mathbf{x}, 0)\|^2) e^T. \end{aligned}$$

□

Lemma 8.3.3 If $v_i(\mathbf{x}, 0) \in L^2(\Omega)$ and $c(\mathbf{x}, 0) \in L^2(\Omega)$, then

$$\int_{\Omega} v_{i,j} v_{i,j} \, dx \leq \frac{1}{v} [v_l^{1/2} (\int_{\Omega} v_{i,t} v_{i,t} \, dx)^{1/2} + (v_l c_l)^{1/2} + (v_l T_l)^{1/2}]. \quad (8.3.51)$$

Proof: Multiply (8.1.6) by v_i and integrating over Ω and drop a non-positive term on the right, we have

$$\int_{\Omega} v_{i,t} v_i \, dx \leq -v \int_{\Omega} v_{i,j} v_{i,j} \, dx + \int_{\Omega} g_i v_i c \, dx + \int_{\Omega} h_i v_i T \, dx.$$

Hence, use (8.2.16), (8.3.49), (8.3.50) in this inequality together with the Cauchy-Schwarz inequality to arrive at

$$\begin{aligned} \int_{\Omega} v_{i,j} v_{i,j} \, dx &\leq \frac{1}{v} \left[- \int_{\Omega} v_{i,t} v_i \, dx + \int_{\Omega} g_i v_i c \, dx + \int_{\Omega} h_i v_i T \, dx \right] \\ &\leq \frac{1}{v} \left[\left(\int_{\Omega} v_{i,t} v_{i,t} \, dx \right)^{1/2} \left(\int_{\Omega} v_i v_i \, dx \right)^{1/2} + \left(\int_{\Omega} v_i v_i \, dx \right)^{1/2} \left(\int_{\Omega} c^2 \, dx \right)^{1/2} \right. \\ &\quad \left. + \left(\int_{\Omega} v_i v_i \, dx \right)^{1/2} \left(\int_{\Omega} T^2 \, dx \right)^{1/2} \right] \\ &\leq \frac{1}{v} [v_l^{1/2} (\int_{\Omega} v_{i,t} v_{i,t} \, dx)^{1/2} + (v_l c_l)^{1/2} + (v_l T_l)^{1/2}]. \end{aligned}$$

□

Lemma 8.3.4 For two dimensions, if $v_{i,t}(\mathbf{x}, 0) \in L^2(\Omega)$ and $c_{i,t}(\mathbf{x}, 0) \in L^2(\Omega)$, then

$$\int_{\Omega} v_{i,t} v_{i,t} dx \leq v_{il}(t), \quad (8.3.52)$$

where

$$v_{il}(t) = \left(\frac{I_2 \sqrt{\Phi(0)}}{I_1 \sqrt{\Phi(0)} (e^{-I_2 t} - 1) + I_2 e^{-I_2 t}} \right)^2$$

$$\Phi = \Phi_v + \Phi_c + \Phi_T, \quad \Phi_v = \int_{\Omega} v_{i,t} v_{i,t} dx, \quad \Phi_T = \int_{\Omega} T_{i,t} T_{i,t} dx, \quad \Phi_c = \int_{\Omega} c_{i,t} c_{i,t} dx,$$

$$I_1 = \frac{v_l^{1/2}}{2v^2}, \quad I_2 = \frac{(v_l c_l)^{1/2} + (v_l T_l)^{1/2}}{2v^2} + \frac{T_{\infty}^2}{2K} + \frac{c_{\infty}^2}{2D} + 2.$$

Proof: Firstly, observe that

$$\begin{aligned} \Phi_{c,t} &= 2 \int_{\Omega} c_{i,t} c_{i,tt} dx = 2 \int_{\Omega} c_{i,t} [-v_i c_{i,i} + D \Delta c - K_1 c]_{,t} dx \\ &= 2D \int_{\Omega} c_{i,t} \Delta c_{i,t} dx - 2K_1 \int_{\Omega} c_{i,t} c_{i,t} dx - 2 \int_{\Omega} c_{i,t} v_{i,t} c_{i,i} dx - 2 \int_{\Omega} c_{i,t} v_{i,i} c_{i,t} dx \\ &\leq -2D \int_{\Omega} c_{i,tt} c_{i,t} dx + 2 \int_{\Omega} c_{i,tt} v_{i,t} c_{i,t} dx = -2D \int_{\Omega} c_{i,tt} c_{i,t} dx + 2c_{\infty} \int_{\Omega} c_{i,tt} v_{i,t} dx \\ &\leq -2D \int_{\Omega} c_{i,tt} c_{i,t} dx + 2c_{\infty} \left(\int_{\Omega} c_{i,tt} c_{i,t} dx \right)^{1/2} \left(\int_{\Omega} v_{i,t} v_{i,t} dx \right)^{1/2} \\ &\leq -2D \int_{\Omega} c_{i,tt} c_{i,t} dx + 2D \int_{\Omega} c_{i,tt} c_{i,t} dx + \frac{c_{\infty}^2}{2D} \int_{\Omega} v_{i,t} v_{i,t} dx, \end{aligned}$$

thus we have,

$$\frac{d}{dt} \Phi_c \leq \frac{c_{\infty}^2}{2D} \Phi_v. \quad (8.3.53)$$

Similar argument can be apply for Φ_T , to obtain

$$\frac{d}{dt} \Phi_T \leq \frac{T_{\infty}^2}{2K} \Phi_v \quad (8.3.54)$$

Next, we will preform similar work for $\Phi_{v,t}$,

$$\begin{aligned} \Phi_{v,t} &= 2 \int_{\Omega} v_{i,t} v_{i,tt} dx = 2 \int_{\Omega} v_{i,t} [-v_j v_{i,j} - p_{,i} + v \Delta v_i + g_i c + h_i T + \sigma b_0^2 (k_i w - v_i)]_{,t} dx \\ &= -2v \int_{\Omega} v_{i,jt} v_{i,jt} dx - 2 \int_{\Omega} v_{i,t} v_{j,t} v_{i,j} dx + 2 \int_{\Omega} g_i v_{i,t} c_t dx \\ &\quad + 2 \int_{\Omega} h_i v_{i,t} T_t dx + 2\sigma b_0^2 \int_{\Omega} (k_i w_t v_{i,t} - v_{i,t} v_{i,t}) dx \end{aligned}$$

$$\begin{aligned}
&\leq -2v \int_{\Omega} v_{i,jt} v_{i,jt} dx - 2 \int_{\Omega} v_{i,t} v_{j,t} v_{i,j} dx + 2 \int_{\Omega} g_i v_{i,t} c_t dx + 2 \int_{\Omega} h_i v_{i,t} T_t dx \\
&\leq -2v \int_{\Omega} v_{i,jt} v_{i,jt} dx + 2 \left(\int_{\Omega} v_{i,j} v_{i,j} dx \right)^{1/2} \left(\int_{\Omega} (v_{i,t} v_{i,t})^2 dx \right)^{1/2} + 2\Phi_v + \Phi_c + \Phi_T.
\end{aligned}$$

Now, we use the Sobolev inequality (8.2.19), arithmetic-geometric mean inequality and (8.3.51), we have

$$\begin{aligned}
\Phi_{v,t} &\leq -2v \int_{\Omega} v_{i,jt} v_{i,jt} dx + 2 \left(\int_{\Omega} v_{i,j} v_{i,j} dx \right)^{1/2} \left(\int_{\Omega} v_{i,t} v_{i,t} dx \right)^{1/2} \left(\int_{\Omega} v_{i,jt} v_{i,jt} dx \right)^{1/2} \\
&\quad + 2\Phi_v + \Phi_c + \Phi_T \\
&\leq \frac{1}{2v} \Phi_v \int_{\Omega} v_{i,j} v_{i,j} dx + 2\Phi_v + \Phi_c + \Phi_T \\
&\leq \frac{1}{2v^2} \Phi_v [v_l^{1/2} \Phi_v^{1/2} + (v_l c_l)^{1/2} + (v_l T_l)^{1/2}] + 2\Phi_v + \Phi_c + \Phi_T. \tag{8.3.55}
\end{aligned}$$

Now, summing (8.3.53), (8.3.54) and (8.3.55), we have

$$\begin{aligned}
\frac{d}{dt}(\Phi_v + \Phi_c + \Phi_T) &\leq I_1 \Phi_v^{3/2} + I_2 \Phi_v + \Phi_c + \Phi_T \\
&\leq I_1 \Phi_v (\Phi_v + \Phi_c + \Phi_T)^{1/2} + I_2 (\Phi_v + \Phi_c + \Phi_T) \\
&\leq I_1 \Phi_v (\Phi_v + \Phi_c + \Phi_T)^{1/2} + I_1 \Phi_c (\Phi_v + \Phi_c + \Phi_T)^{1/2} \\
&\quad + I_1 \Phi_T (\Phi_v + \Phi_c + \Phi_T)^{1/2} + I_2 (\Phi_v + \Phi_c + \Phi_T) \\
\frac{d}{dt}(\Phi_v + \Phi_c + \Phi_T) &\leq I_1 (\Phi_v + \Phi_c + \Phi_T)^{3/2} + I_2 (\Phi_v + \Phi_c + \Phi_T). \tag{8.3.56}
\end{aligned}$$

Upon integration of (8.3.56), we find the desired result (8.3.52) for the two dimensions case.

□

Lemma 8.3.5 For three dimensions, if $v_{i,t}(\mathbf{x}, 0) \in L^2(\Omega)$ and $c_{,t}(\mathbf{x}, 0) \in L^2(\Omega)$, then

$$\int_{\Omega} v_{i,t} v_{i,t} dx \leq v_u(t), \tag{8.3.57}$$

where

$$v_u(t) = \frac{I_4 \Phi(0)}{I_3 \Phi(0)(e^{-I_4 t} - 1) + I_4 e^{-I_4 t}}$$

$$\Phi = \Phi_v + \Phi_c + \Phi_T, \quad \Phi_v = \int_{\Omega} v_{i,t} v_{i,t} dx, \quad \Phi_T = \int_{\Omega} T_{,t} T_{,t} dx, \quad \Phi_c = \int_{\Omega} c_{,t} c_{,t} dx,$$

$$I_3 = \frac{27v_l\beta^4}{64v^5}, \quad I_4 = \frac{27\beta^4(v_l c_l + v_l T_l)}{32v^5} + \frac{T_\infty^2}{2K} + \frac{c_\infty^2}{2D} + 2.$$

It is clear that for three dimensions the bound (8.3.57) valid just for $t < \frac{1}{I_4} \ln(1 + \frac{I_4}{I_3\Phi(0)})$, thus we have conditional continuous dependence in this case.

Proof: Similar argument can be apply for three dimensions case, to obtain

$$\frac{d}{dt}\Phi_c \leq \frac{c_\infty^2}{2D}\Phi_v, \quad (8.3.58)$$

$$\frac{d}{dt}\Phi_T \leq \frac{T_\infty^2}{2K}\Phi_v, \quad (8.3.59)$$

and

$$\Phi_{v,t} \leq -2v \int_{\Omega} v_{i,jt} v_{i,jt} dx + 2 \left(\int_{\Omega} v_{i,j} v_{i,j} dx \right)^{1/2} \left(\int_{\Omega} (v_{i,t} v_{i,t})^2 dx \right)^{1/2} + 2\Phi_v + \Phi_c + \Phi_T.$$

Next, using the Sobolev inequality (8.2.20), Young's inequality and (8.3.51) we get

$$\begin{aligned} \Phi_{v,t} &\leq -2v \int_{\Omega} v_{i,jt} v_{i,jt} dx + 2\beta \left(\int_{\Omega} v_{i,j} dx \right)^{1/2} \left(\int_{\Omega} v_{i,t} v_{i,t} dx \right)^{1/4} \left(\int_{\Omega} v_{i,jt} v_{i,jt} dx \right)^{3/4} \\ &\quad + 2\Phi_v + \Phi_c + \Phi_T \\ &\leq \frac{27\beta^4}{128v^3} \Phi_v \left(\int_{\Omega} v_{i,j} v_{i,j} dx \right)^2 + 2\Phi_v + \Phi_c + \Phi_T \\ &\leq \frac{27\beta^4}{128v^5} \Phi_v [v_l^{1/2} \Phi_v^{1/2} + (v_l c_l)^{1/2} + (v_l T_l)^{1/2}]^2 + 2\Phi_v + \Phi_c + \Phi_T \\ &\leq \frac{27\beta^4}{64v^5} \Phi_v [v_l \Phi_v + 2(v_l c_l + v_l T_l)] + 2\Phi_v + \Phi_c + \Phi_T. \end{aligned} \quad (8.3.60)$$

Now, summing (8.3.58), (8.3.59) and (8.3.60), we obtain

$$\frac{d}{dt}(\Phi_v + \Phi_c + \Phi_T) \leq I_3 \Phi_v^2 + I_4 \Phi_v + \Phi_c + \Phi_T$$

$$\frac{d}{dt}(\Phi_v + \Phi_c + \Phi_T) \leq I_3 (\Phi_v + \Phi_c + \Phi_T)^2 + I_4 (\Phi_v + \Phi_c + \Phi_T). \quad (8.3.61)$$

Upon integration of (8.3.61), we find the desired result (8.3.57) for the three dimensions case.

□

8.3.1 Continuous dependence on σ

In this section, we establish continuous dependence on the electrical conductivity coefficient σ . To do this, let (v_{i1}, T_1, c_1, p_1) and (v_{i2}, T_2, c_2, p_2) be solutions of (8.1.6)-(8.1.9) with the same boundary and initial conditions, but with different electrical conductivity coefficients σ_1 and σ_2 . Now, we define

$$u_i = v_{i1} - v_{i2}, \quad \theta = T_1 - T_2, \quad \phi = c_1 - c_2, \quad \pi = p_1 - p_2, \quad \sigma = \sigma_1 - \sigma_2, \quad (8.3.62)$$

Then, (u_i, θ, ϕ, π) is a solution of the problem

$$u_{i,t} + v_{1j}u_{i,j} + u_jv_{2i,j} = -\pi_{,i} + v\Delta u_i + h_i\theta + g_i\phi + \sigma b_0^2[(v_1 \times k) \times k]_i + \sigma_2 b_0^2[(u \times k) \times k]_i, \quad (8.3.63)$$

$$u_{i,i} = 0, \quad (8.3.64)$$

$$\theta_{,t} + v_{1i}\theta_{,i} + u_i T_{2,i} = K\Delta\theta, \quad (8.3.65)$$

$$\phi_{,t} + v_{1i}\phi_{,i} + u_i c_{2,i} = D\Delta\phi - K_1\phi, \quad (8.3.66)$$

subject to the boundary and initial conditions

$$u_i = 0, \quad \frac{\partial\theta}{\partial n} = 0, \quad \frac{\partial\phi}{\partial n} = 0, \quad \text{on} \quad \partial\Omega, \quad (8.3.67)$$

$$\theta(\mathbf{x}, 0) = 0, \quad \phi(\mathbf{x}, 0) = 0, \quad u_i(\mathbf{x}, 0) = 0, \quad \text{in} \quad \Omega. \quad (8.3.68)$$

The proof of continuous dependence commences by multiplying (8.3.63) by u_i and integrating over Ω to find,

$$\begin{aligned} & \frac{d}{dt} \|\mathbf{u}\|^2 = 2 \int_{\Omega} u_i u_{i,t} dx \\ & = 2 \int_{\Omega} u_i [-v_{1j}u_{i,j} - u_jv_{2i,j} - \pi_{,i} + v\Delta u_i + g_i\phi + h_i\theta + \sigma b_0^2(k_i w_1 - v_{1i}) + \sigma_2 b_0^2(k_i w - u_i)] dx \\ & \leq -2v \int_{\Omega} u_{i,j}u_{i,j} dx - 2 \int_{\Omega} u_i u_j v_{2i,j} dx + 2 \int_{\Omega} g_i u_i \phi dx + 2 \int_{\Omega} h_i u_i \theta dx \\ & \quad + 2\sigma b_0^2 \int_{\Omega} (k_i w_1 u_i - v_{1i} u_i) dx \\ & \leq -2v \int_{\Omega} u_{i,j}u_{i,j} dx + 2 \left(\int_{\Omega} v_{2i,j}v_{2i,j} dx \right)^{1/2} \left(\int_{\Omega} (u_i u_i)^2 dx \right)^{1/2} \\ & + 2 \left(\int_{\Omega} u_i u_i dx \right)^{1/2} \left(\int_{\Omega} \phi^2 dx \right)^{1/2} + 2 \left(\int_{\Omega} u_i u_i dx \right)^{1/2} \left(\int_{\Omega} \theta^2 dx \right)^{1/2} + 4\sigma b_0^2 v_{11}^{1/2} \left(\int_{\Omega} u_i u_i dx \right)^{1/2}, \end{aligned}$$

where $v_{l1} = (2c_{l1} + 2T_{l1} + \|\mathbf{v}(\mathbf{x}, 0)\|^2)e^T$, $c_{l1} = \|c_1(\mathbf{x}, 0)\|^2$, $T_{l1} = \|T_1(\mathbf{x}, 0)\|^2$. By using the Sobolev inequality (8.2.20), arithmetic-geometric mean inequality and (8.3.51), we obtain

$$\begin{aligned} \frac{d}{dt}\|u\|^2 &\leq -2v \int_{\Omega} u_{i,j}u_{i,j} dx + 2\beta \left(\int_{\Omega} v_{2i,j}v_{2i,j} dx \right)^{1/2} \left(\int_{\Omega} u_i u_i dx \right)^{1/4} \left(\int_{\Omega} u_{i,j}u_{i,j} dx \right)^{3/4} \\ &\quad + 3 \int_{\Omega} u_i u_i dx + \int_{\Omega} \phi^2 dx + \int_{\Omega} \theta^2 dx + \sigma^2 b_0^4 v_{l1} \\ &\leq \frac{27\beta^4}{128v^3} \|\mathbf{u}\|^2 \left(\int_{\Omega} v_{2i,j}v_{2i,j} dx \right)^2 + 3\|\mathbf{u}\|^2 + \|\phi\|^2 + \|\theta\|^2 + \sigma^2 b_0^4 v_{l1} \\ &\leq \frac{27\beta^4}{128v^5} \|\mathbf{u}\|^2 [v_{l2}^{1/2} v_{lt2}(t)^{1/2} + (v_{l2}c_{l2})^{1/2} + (v_{l2}T_{l2})^{1/2}]^2 + 3\|\mathbf{u}\|^2 + \|\phi\|^2 + \|\theta\|^2 + \sigma^2 b_0^4 v_{l1} \\ &\leq \frac{27\beta^4}{64v^5} \|\mathbf{u}\|^2 [v_{l2}v_{lt2}(t) + v_{l2}c_{l2} + v_{l2}T_{l2}] + 3\|\mathbf{u}\|^2 + \|\phi\|^2 + \|\theta\|^2 + \sigma^2 b_0^4 v_{l1}, \end{aligned} \quad (8.3.69)$$

where $v_{l2} = (2c_{l2} + 2T_{l2} + \|\mathbf{v}_2(\mathbf{x}, 0)\|^2)e^T$, $c_{l2} = \|c_2(\mathbf{x}, 0)\|^2$, $T_{l2} = \|T_2(\mathbf{x}, 0)\|^2$, the value $v_{lt1}(t)$ is equal to the value of $v_{lt}(t)$ which is defined in Lemma 8.3.4 and 8.3.5 at the solution (v_{i2}, T_2, c_2, p_2) .

Next, multiply (8.3.65) and (8.3.66) by θ and ϕ , respectively, and integrate over Ω and using the Cauchy-Schwarz inequality, arithmetic-geometric mean inequality we have

$$\frac{d}{dt}\|\phi\|^2 \leq \frac{c_{2\infty}^2}{2D} \|\mathbf{u}\|^2. \quad (8.3.70)$$

$$\frac{d}{dt}\|\theta\|^2 \leq \frac{T_{2\infty}^2}{2K} \|\mathbf{u}\|^2. \quad (8.3.71)$$

Let $I_5(t) = (27\beta^4/64v^5)[v_{l2}v_{lt2}(t) + v_{l2}c_{l2} + v_{l2}T_{l2}] + (c_{2\infty}^2/2D) + (T_{2\infty}^2/2K) + 3$, and $I_6(t) = \int I_5(t)dt$. Summing (8.3.69), (8.3.70) and (8.3.71), we get

$$\frac{d}{dt}(\|\mathbf{u}\|^2 + \|\phi\|^2 + \|\theta\|^2) \leq I_5(t)(\|\mathbf{u}\|^2 + \|\phi\|^2 + \|\theta\|^2) + \sigma^2 b_0^4 v_{l1}. \quad (8.3.72)$$

Upon integration of (8.3.72), we arrive at the continuous dependence on σ inequality

$$\|\mathbf{u}\|^2 + \|\phi\|^2 + \|\theta\|^2 \leq \sigma^2 b_0^4 v_{l1} \int_0^t e^{I_6(t)-I_6(s)} ds. \quad (8.3.73)$$

Thus, (8.3.73) establishes the continuous dependence on the coefficient σ .

8.3.2 Continuous dependence on K_1

In this section we show that the solution of the problem (8.1.6)-(8.1.9) depends continuously on the coefficient K_1 . Let us consider two solutions (v_{i1}, T_1, c_1, p_1) and (v_{i2}, T_2, c_2, p_2) of (8.1.6)-(8.1.9) and have the same initial and boundary data corresponding to two different nonzero values K_{11} and K_{12} . Set

$$u_i = v_{i1} - v_{i2}, \quad \theta = T_1 - T_2, \quad \phi = c_1 - c_2, \quad \pi = p_1 - p_2, \quad K_1 = K_{11} - K_{12}, \quad (8.3.74)$$

so that (u_i, θ, ϕ, π) is a solution of the problem

$$u_i = -\pi_{,i} + v\Delta u_i + g_i\phi + \sigma b_0^2[(u \times k) \times k]_i, \quad (8.3.75)$$

$$u_{i,i} = 0, \quad (8.3.76)$$

$$\theta_t + v_{1i}\theta_{,i} + u_i T_{2,i} = K\Delta\theta, \quad (8.3.77)$$

$$\phi_t + v_{1i}\phi_{,i} + u_i c_{2,i} = D\Delta c - K_{11}\phi - K_1 c_2, \quad (8.3.78)$$

in $\Omega \times (0, \infty)$, and

$$u_i = 0, \quad \frac{\partial\theta}{\partial n} = 0, \quad \frac{\partial\phi}{\partial n} = 0, \quad \text{on} \quad \partial\Omega, \quad (8.3.79)$$

$$\theta(\mathbf{x}, 0) = 0, \quad \phi(\mathbf{x}, 0) = 0, \quad u_i(\mathbf{x}, 0) = 0, \quad \text{in} \quad \Omega. \quad (8.3.80)$$

The proof of continuous dependence commences by multiplying (8.3.75) by u_i and integrating over Ω to find ,

$$\begin{aligned} \frac{d}{dt}\|u\|^2 &= 2 \int_{\Omega} u_i u_{i,t} dx \\ &= 2 \int_{\Omega} u_i [-v_{1j} u_{i,j} - u_j v_{2i,j} - \pi_{,i} + v\Delta u_i + g_i\phi + h_i\theta + \sigma b_0^2(k_i w - u_i)] dx \\ &= -2v \int_{\Omega} u_{i,j} u_{i,j} dx - 2 \int_{\Omega} u_i u_j v_{2i,j} dx + 2 \int_{\Omega} g_i u_i \phi dx + 2 \int_{\Omega} h_i u_i \theta dx + 2\sigma b_0^2 \int_{\Omega} (k_i w \cdot u_i - u_i u_i) dx \\ &\leq -2v \int_{\Omega} u_{i,j} u_{i,j} dx + 2 \left(\int_{\Omega} v_{2i,j} v_{2i,j} dx \right)^{1/2} \left(\int_{\Omega} (u_i u_i)^2 dx \right)^{1/2} + 2 \left(\int_{\Omega} u_i u_i dx \right)^{1/2} \left(\int_{\Omega} \phi^2 dx \right)^{1/2} \\ &\quad + 2 \left(\int_{\Omega} u_i u_i dx \right)^{1/2} \left(\int_{\Omega} \theta^2 dx \right)^{1/2}. \end{aligned}$$

By using the Sobolev inequality (8.2.20), Young's inequality and (8.3.51) we have

$$\frac{d}{dt}\|u\|^2 \leq -2v \int_{\Omega} u_{i,j} u_{i,j} dx + 2\beta \left(\int_{\Omega} v_{2i,j} v_{2i,j} dx \right)^{1/2} \left(\int_{\Omega} u_i u_i dx \right)^{1/4} \left(\int_{\Omega} u_{i,j} u_{i,j} dx \right)^{3/4}$$

$$\begin{aligned}
& +2 \int_{\Omega} u_i u_i dx + \int_{\Omega} \phi^2 dx + \int_{\Omega} \theta^2 dx \\
& \leq \frac{27\beta^4}{128v^3} \|\mathbf{u}\|^2 \left(\int_{\Omega} v_{2i,j} v_{2i,j} dx \right)^2 + 2\|\mathbf{u}\|^2 + \|\phi\|^2 + \|\theta\|^2 \\
& \leq \frac{27\beta^4}{128v^5} \|\mathbf{u}\|^2 [v_{l2}^{1/2} v_{l2}(t)^{1/2} + (v_{l2} c_{l2})^{1/2} + (v_{l2} T_{l2})^{1/2}]^2 + 2\|\mathbf{u}\|^2 + \|\phi\|^2 + \|\theta\|^2 \\
& \leq \frac{27\beta^4}{64v^5} \|\mathbf{u}\|^2 [v_{l2} v_{l2}(t) + 2(v_{l2} c_{l2} + v_{l2} T_{l2})] + 2\|\mathbf{u}\|^2 + \|\phi\|^2 + \|\theta\|^2. \quad (8.3.81)
\end{aligned}$$

Next, multiply (8.3.77) by θ and (8.3.78) by ϕ and integrate over Ω , respectively, and arithmetic-geometric mean inequality to obtain

$$\frac{d}{dt} \|\theta\|^2 \leq \frac{T_{2\infty}^2}{2K} \|\mathbf{u}\|^2. \quad (8.3.82)$$

Similarly, by multiplying (8.3.78) by ϕ and integrate over Ω and using the Cauchy-Schwarz inequality, arithmetic-geometric mean inequality and drop a non-positive terms on the right, we have

$$\frac{d}{dt} \|\phi\|^2 \leq \frac{c_{2\infty}^2}{2D} \|\mathbf{u}\|^2 + \frac{c_{2\infty}^2}{2D} \|\phi\|^2 + 2DK_1^2. \quad (8.3.83)$$

Let $I_7(t) = (27\beta^4/64v^5)[v_{l2} v_{l2}(t) + 2(v_{l2} c_{l2} + v_{l2} T_{l2})] + (c_{2\infty}^2/2D) + (T_{2\infty}^2/2K) + 2$, and $I_8(t) = \int I_7(t) dt$. Summing (8.3.81), (8.3.82), and (8.3.83), we get

$$\frac{d}{dt} (\|\mathbf{u}\|^2 + \|\phi\|^2 + \|\theta\|^2) \leq I_7(t) (\|\mathbf{u}\|^2 + \|\phi\|^2) + 2DK_1^2. \quad (8.3.84)$$

An integration of (8.3.84) leads to

$$\|\mathbf{u}\|^2 + \|\phi\|^2 + \|\theta\|^2 \leq 2DK_1^2 \int_0^t e^{I_8(t)-I_8(s)} ds. \quad (8.3.85)$$

We thus conclude that the nonzero solutions of double diffusive convection problem depend continuously on the effective chemical reaction coefficient.

Chapter 9

Continuous dependence on the coefficients for double diffusive convection in Darcy flow with Magnetic field effect

9.1 Introduction

Straughan [196] explains a system of equations to describe the double diffusive convective flow in a porous medium using the Brinkman model. In [200] Straughan and Hutter established continuous dependence of the solution on the Soret coefficient. Lin and Payne [108] further extended the work of [200]. They investigate the structural stability of the Brinkman equations modeling on the gravity vector coefficients and Brinkman coefficient. Then in [109] they established the structural stability of the Brinkman equations on the Soret coefficient which describes the flow of a fluid containing a solute. In [200] the boundary conditions are nonhomogeneous Dirichlet type while in [109] they employ homogeneous Neumann ones. Thus the Sobolev inequalities which are used in [200] are not available for functions satisfying homogeneous Neumann boundary conditions. However, if the viscosity contribution to the flow is negligible and this term is neglected, then the Brinkman equations reduce to the Darcy equations. Continuous dependence of the solution of the Darcy

equations on the Soret coefficient is established by Lin and Payne in [110].

This chapter is devoted to studying the influence of the magnetic and the gravity vector coefficients on the Darcy equations. The governing equations for Darcy flow with magnetic field effect in a region Ω for time $t > 0$ may be written as

$$\begin{aligned} v_i &= -p_{,i} + g_i T + h_i C + \sigma[(\mathbf{v} \times \mathbf{B}_0) \times \mathbf{B}_0]_i, \\ T_{,t} + v_i T_{,i} &= \Delta T, \\ C_{,t} + v_i C_{,i} &= \Delta C + \gamma \Delta T, \\ v_{i,i} &= 0, \end{aligned} \tag{9.1.1}$$

where v_i, T, C and p represent velocity, temperature, salt concentration and pressure fields, respectively, g_i and h_i are the gravity vector terms arising in the density equation of state. Standard indicial notation is used throughout, Δ is the Laplacian operator, γ is the Soret coefficient and $\mathbf{B}_0 = (0, 0, B_0)$ is a magnetic field with only the vertical component. In deriving (9.1.1) we take a particular magnetic field, as in e.g. Galdi and Straughan [61]

We assume that Ω is a bounded, simply connected domain with boundary $\partial\Omega$ of bounded curvature. (For convex domains, we in fact require less smoothness of the boundary.) Associated with (9.1.1) we impose the boundary conditions

$$v_i n_i = 0; \quad T = f_1; \quad C = f_2, \quad \text{on} \quad \partial\Omega \times t > 0, \tag{9.1.2}$$

for prescribed functions f_1 and f_2 . We also impose initial conditions

$$T(x, 0) = T_0(x); \quad C(x, 0) = C_0(x); \quad \text{in} \quad \Omega, \tag{9.1.3}$$

for prescribed functions T_0 and C_0 .

The plan of the chapter is as follows. In the next section we derive a priori bounds which are very useful in the next sections. In Section 9.3 we study continuous dependence of a solution to the Darcy equations on the magnetic coefficient σ . In section 9.4 we derive continuous dependence on the gravity vector coefficients g_i and h_i for (9.1.1)-(9.1.3).

The results in this chapter were published in the article Harfash [78].

9.2 A priori bounds

In this section, we derive bounds for various norms of v_i , T and C in terms of data. These bounds will be used in the next sections in the continuous dependence proof. Before we commence the analysis it is opportune to present some useful bounds which are easy to prove.

$$[(\mathbf{v} \times \mathbf{B}_0) \times \mathbf{B}_0]_i = B_0^2(k_i w - v_i), \quad (9.2.4)$$

$$\int_{\Omega} v_i(k_i w - v_i) dx \leq 0, \quad (9.2.5)$$

$$2 \int_{\Omega} v_{i,j}(v_{i,j} - v_{j,i}) dx = \int_{\Omega} (v_{i,j} - v_{j,i})(v_{i,j} - v_{j,i}) dx, \quad (9.2.6)$$

where $\underline{k} = (0, 0, 1)$ and $w = v_3$. Now suppose that η is the third component of the vector $\nabla \times (\nabla \times (\underline{g}T))$, where $\underline{g} = (g_1, g_2, g_3)$, then we have

$$\eta = -\nabla \left(g_3 \frac{\partial T}{\partial x}, g_3 \frac{\partial T}{\partial y}, -g_1 \frac{\partial T}{\partial x} - g_2 \frac{\partial T}{\partial y} \right). \quad (9.2.7)$$

Then from (9.2.7) we construct the following form

$$\int_{\Omega} \eta w dx = - \int_{\Omega} w \nabla \left(g_3 \frac{\partial T}{\partial x}, g_3 \frac{\partial T}{\partial y}, -g_1 \frac{\partial T}{\partial x} - g_2 \frac{\partial T}{\partial y} \right) dx. \quad (9.2.8)$$

Now, by using the Cauchy-Schwarz inequality and the arithmetic-geometric mean inequality, we have

$$\begin{aligned} \int_{\Omega} \eta w dx &= \int_{\Omega} \nabla w \cdot \left(g_3 \frac{\partial T}{\partial x}, g_3 \frac{\partial T}{\partial y}, -g_1 \frac{\partial T}{\partial x} - g_2 \frac{\partial T}{\partial y} \right) dx \\ &\leq \frac{1}{2\alpha_1} \int_{\Omega} w_{,i} w_{,i} dx + \frac{\alpha_1}{2} \int_{\Omega} \left| g_3 \frac{\partial T}{\partial x}, g_3 \frac{\partial T}{\partial y}, -g_1 \frac{\partial T}{\partial x} - g_2 \frac{\partial T}{\partial y} \right|^2 dx \\ &\leq \frac{1}{2\alpha_1} \int_{\Omega} w_{,i} w_{,i} dx + \frac{\alpha_1}{2} \int_{\Omega} \left[\left(g_3 \frac{\partial T}{\partial x} \right)^2 + \left(g_3 \frac{\partial T}{\partial y} \right)^2 + \left(g_1 \frac{\partial T}{\partial x} + g_2 \frac{\partial T}{\partial y} \right)^2 \right] dx \\ &\leq \frac{1}{2\alpha_1} \int_{\Omega} w_{,i} w_{,i} dx + \frac{g^2 \alpha_1}{2} \int_{\Omega} \left[\left(\frac{\partial T}{\partial x} \right)^2 + \left(\frac{\partial T}{\partial y} \right)^2 + \left(\frac{\partial T}{\partial x} + \frac{\partial T}{\partial y} \right)^2 \right] dx \\ &\leq \frac{1}{2\alpha_1} \int_{\Omega} w_{,i} w_{,i} dx + \frac{3g^2 \alpha_1}{2} \int_{\Omega} \left[\left(\frac{\partial T}{\partial x} \right)^2 + \left(\frac{\partial T}{\partial y} \right)^2 \right] dx \\ &\leq \frac{1}{2\alpha_1} \int_{\Omega} w_{,i} w_{,i} dx + \frac{3g^2 \alpha_1}{2} \int_{\Omega} T_{,i} T_{,i} dx, \end{aligned} \quad (9.2.9)$$

where $g^2 = \max g_i g_i$. Later, we apply (9.2.9) for different functions and we use different values for α_1 . Now, we look at norms of $\|\mathbf{v}\|^2$.

9.2.1 A bound for \mathbf{v}

To find a bound for $\int_{\Omega} v_i v_i dx$, we multiply (9.1.1)₁ by v_i and use (9.2.5), the Cauchy-Schwarz inequality and the arithmetic-geometric mean inequality, then we have

$$\begin{aligned} \int_{\Omega} v_i v_i dx &\leq g \|\mathbf{v}\| \|T\| + h \|\mathbf{v}\| \|C\| \\ &\leq g^2 \|T\|^2 + h^2 \|C\|^2 + \frac{1}{2} \|\mathbf{v}\|^2. \end{aligned}$$

Thus, we have

$$\|\mathbf{v}\|^2 \leq 2g^2 \|T\|^2 + 2h^2 \|C\|^2, \quad (9.2.10)$$

where $h^2 = \max h_i h_i$.

9.2.2 A bound for T

Now, the next step is to find bounds for $\|T\|^2$, $\|C\|^2$, $\|\nabla T\|^2$ and $\|\nabla C\|^2$. To this end we introduce the harmonic function, ψ , which adopts the same boundary values as T , so define

$$\begin{aligned} \Delta \psi &= 0, \quad \text{in } \Omega \times t > 0, \\ \psi(x, t) &= f_1, \quad \text{on } \partial\Omega. \end{aligned} \quad (9.2.11)$$

We then form the identity

$$\int_0^t \int_{\Omega} (T - \psi)(T_{,t} + v_i T_{,i} - \Delta T) dx d\eta = 0. \quad (9.2.12)$$

Next, we perform several integrations in (9.2.12) and use the boundary values and properties of ψ to see that,

$$\begin{aligned} \frac{1}{2} \|T\|^2 - \frac{1}{2} \|T_0\|^2 + \int_{\Omega} T_0 \psi_0 dx - \int_{\Omega} T \psi dx + \int_0^t \int_{\Omega} T \psi_{,\eta} dx d\eta - \int_0^t \int_{\Omega} T_{,i} v_i \psi dx d\eta \\ + \int_0^t \int_{\Omega} T_{,i} T_{,i} dx d\eta - \int_0^t \int_{\partial\Omega} f_1 \frac{\partial \psi}{\partial n} dA d\eta = 0. \end{aligned} \quad (9.2.13)$$

Let f_{1m} be the maximum value of f_1 on $\partial\Omega \times [0, \tau)$ (f_{1m} is taken to be positive) and then since ψ is harmonic we know by the maximum principle that $\psi \leq f_{1m}$. Upon employing the Cauchy-Schwarz inequality, arithmetic-geometric mean inequality

and (9.2.10), we can drive a bound for the cubic term of (9.2.13)

$$\begin{aligned} \int_0^t \int_{\Omega} T_{,i} v_i \psi \, dx d\eta &\leq f_{1m} \left(\int_0^t \int_{\Omega} v_i v_i \, dx d\eta \right)^{1/2} \left(\int_0^t \int_{\Omega} T_{,i} T_{,i} \, dx d\eta \right)^{1/2} \\ &\leq \frac{f_{1m}^2}{2} \int_0^t \int_{\Omega} v_i v_i \, dx d\eta + \frac{1}{2} \int_0^t \int_{\Omega} T_{,i} T_{,i} \, dx d\eta \\ &\leq f_{1m}^2 (g^2 \int_0^t \int_{\Omega} T^2 \, dx d\eta + h^2 \int_0^t \int_{\Omega} C^2 \, dx d\eta) + \frac{1}{2} \int_0^t \int_{\Omega} T_{,i} T_{,i} \, dx d\eta. \end{aligned} \quad (9.2.14)$$

By use of the Cauchy-Schwartz inequality one finds

$$\int_0^t \int_{\partial\Omega} f_1 \frac{\partial\psi}{\partial n} \, dAd\eta = \left(\int_0^t \int_{\partial\Omega} f_1^2 \, dAd\eta \right)^{1/2} \left(\int_0^t \int_{\partial\Omega} \left(\frac{\partial\psi}{\partial n} \right)^2 \, dAd\eta \right)^{1/2},$$

and from the arithmetic-geometric mean inequality it follows that

$$\begin{aligned} \int_{\Omega} T_0 \psi_0 \, dx &\leq \frac{1}{2} \int_{\Omega} \psi_0^2 \, dx + \frac{1}{2} \int_{\Omega} T_0^2 \, dx, \\ \int_{\Omega} T \psi \, dx &\leq \int_{\Omega} \psi^2 \, dx + \frac{1}{4} \int_{\Omega} T^2 \, dx, \\ \int_0^t \int_{\Omega} T \psi_{, \eta} \, dx d\eta &\leq \frac{1}{2} \int_0^t \int_{\Omega} \psi_{, \eta}^2 \, dx d\eta + \frac{1}{2} \int_0^t \int_{\Omega} T^2 \, dx d\eta. \end{aligned}$$

We next employ these estimates together with (9.2.14) in (9.2.13) to arrive at

$$\begin{aligned} \frac{1}{4} \|T\|^2 + \frac{1}{2} \int_0^t \|\nabla T\|^2 \, dx &\leq \|T_0\|^2 + \|\psi\|^2 + \frac{1}{2} \|\psi_0\|^2 + \frac{1}{2} \int_0^t \|\psi_{, \eta}\|^2 \, dx \\ + \left(\int_0^t \int_{\partial\Omega} f_1^2 \, dAd\eta \right)^{1/2} \left(\int_0^t \int_{\partial\Omega} \left(\frac{\partial\psi}{\partial n} \right)^2 \, dAd\eta \right)^{1/2} &+ \left(\frac{1}{2} + f_{1m}^2 g^2 \right) \int_0^t \|T\|^2 \, dx + f_{1m}^2 h^2 \int_0^t \|C\|^2 \, dx. \end{aligned} \quad (9.2.15)$$

Now, using well-known inequalities (see for example [153]) we have

$$\|\psi\|^2 + \frac{1}{2} \|\psi_0\|^2 \leq \frac{3}{2} c_3 \int_{\partial\Omega} f_1^2 \, dA + \frac{3}{2} c_4 \int_{\partial\Omega} |\text{grad}_s f_1|^2 \, dA, \quad (9.2.16)$$

$$\int_0^t \|\psi_{, \eta}\|^2 \, dx \leq c_5 \int_0^t \int_{\partial\Omega} f_{1, \tau}^2 \, dAd\tau + c_6 \int_0^t \int_{\partial\Omega} |\text{grad}_s f_{1, \tau}|^2 \, dAd\tau, \quad (9.2.17)$$

$$\int_0^t \int_{\partial\Omega} \left(\frac{\partial\psi}{\partial n} \right)^2 \, dAd\eta \leq c_2 \int_0^t \int_{\partial\Omega} |\text{grad}_s f_1|^2 \, dAd\tau, \quad (9.2.18)$$

where grad_s denotes the surface gradient on $\partial\Omega$.

Setting

$$D_1(t) = 4\|T_0\|^2 + 6c_3 \int_{\partial\Omega} f_1^2 \, dA + 6c_4 \int_{\partial\Omega} |\text{grad}_s f_1|^2 \, dA + 2c_5 \int_0^t \int_{\partial\Omega} f_{1, \tau}^2 \, dAd\tau$$

$$+2c_6 \int_0^t \int_{\partial\Omega} |\text{grad}_s f_{1,\tau}|^2 dAd\tau + 4c_2^{1/2} \left(\int_0^t \int_{\partial\Omega} f_1^2 dAd\eta \right)^{1/2} \left(\int_0^t \int_{\partial\Omega} |\text{grad}_s f_1|^2 dAd\eta \right)^{1/2},$$

and substituting (9.2.16)-(9.2.18) in (9.2.15) we arrive at the following result

$$\|T\|^2 + 2 \int_0^t \|\nabla T\|^2 dx \leq D_1(t) + (2 + 4f_{1m}^2 g^2) \int_0^t \|T\|^2 dx + 4f_{1m}^2 h^2 \int_0^t \|C\|^2 dx. \quad (9.2.19)$$

9.2.3 A bound for C

Now, we introduce another harmonic function, φ , which has the same boundary values as C , so define

$$\begin{aligned} \Delta\varphi &= 0, \quad \text{in } \Omega \times t > 0, \\ \varphi(x, t) &= f_2, \quad \text{on } \partial\Omega. \end{aligned} \quad (9.2.20)$$

Let f_{2m} be the maximum value of f_2 on $\partial\Omega \times [0, \tau]$, and by using the similar argument to prove (9.2.19) we can establish

$$\begin{aligned} \|C\|^2 + 2 \int_0^t \|\nabla C\|^2 dx &\leq D_2(t) + (2 + 8f_{2m}^2 g^2) \int_0^t \|C\|^2 dx + 8f_{2m}^2 h^2 \int_0^t \|C\|^2 dx \\ &\quad + 4\gamma^2 \int_0^t \|\nabla T\|^2 dx, \end{aligned} \quad (9.2.21)$$

where

$$\begin{aligned} D_2(t) &= 4\|C_0\|^2 + 6c_3 \int_{\partial\Omega} f_2^2 dA + 6c_4 \int_{\partial\Omega} |\text{grad}_s f_2|^2 dA + 2c_5 \int_0^t \int_{\partial\Omega} f_{2,\tau}^2 dAd\tau \\ &+ 2c_6 \int_0^t \int_{\partial\Omega} |\text{grad}_s f_{2,\tau}|^2 dAd\tau + 4c_2^{1/2} \left(\int_0^t \int_{\partial\Omega} f_2^2 dAd\eta \right)^{1/2} \left(\int_0^t \int_{\partial\Omega} |\text{grad}_s f_2|^2 dAd\eta \right)^{1/2} \\ &\quad + 4c_2^{1/2} \sigma_1 \left(\int_0^t \int_{\partial\Omega} f_1^2 dAd\eta \right)^{1/2} \left(\int_0^t \int_{\partial\Omega} |\text{grad}_s f_2|^2 dAd\eta \right)^{1/2}. \end{aligned}$$

We now let Γ be a constant such that $\Gamma > 2\gamma_1^2$ and then form Γ (9.2.19)+(9.2.21).

In this way we obtain

$$\begin{aligned} \Gamma\|T\|^2 + (2\Gamma - 4\gamma^2) \int_0^t \|\nabla T\|^2 dx + \|C\|^2 + 2 \int_0^t \|\nabla C\|^2 dx &\leq \Gamma D_1(t) + D_2(t) \\ + [\Gamma(2 + 4f_{1m}^2 g^2) + 8f_{2m}^2 h^2] \int_0^t \|T\|^2 dx + (4\Gamma f_{1m}^2 h^2 + 2 + 8f_{2m}^2 g^2) \int_0^t \|C\|^2 dx. \end{aligned} \quad (9.2.22)$$

Define now K as

$$K = \max\{2 + 4f_{1m}^2 g^2 + \Gamma^{-1} 8f_{2m}^2 h^2, 4\Gamma f_{1m}^2 h^2 + 2 + 8f_{2m}^2 g^2\},$$

then from (9.2.22) one derives

$$\Gamma \|T\|^2 + \|C\|^2 \leq \Gamma D_1(t) + D_2(t) + K[\Gamma \int_0^t \|T\|^2 dx + \int_0^t \|C\|^2 dx]. \quad (9.2.23)$$

Setting $D_3(t) = e^{K\tau} \int_0^t [\Gamma D_1(\eta) + D_2(\eta)] d\eta$ and after integrating (9.2.23), we have

$$\Gamma \int_0^t \|T\|^2 dx + \int_0^t \|C\|^2 dx \leq D_3(t). \quad (9.2.24)$$

By using Gronwall's inequality on (9.2.23) we can derive another priori bound,

$$\Gamma \|T\|^2 + \|C\|^2 \leq D_4(t), \quad (9.2.25)$$

where

$$D_4(t) = \Gamma D_1(t) + D_2(t) + K D_3(t).$$

9.2.4 Bounds for $\nabla T, \nabla C$

Finally, to establish the bound for $\|\nabla T\|^2$ and $\|\nabla C\|^2$, we substitute the bound (9.2.24) in (9.2.22) to obtain the following results

$$\int_0^t \|\nabla T\|^2 dx \leq \frac{D_4(t)}{2}. \quad (9.2.26)$$

$$\int_0^t \|\nabla C\|^2 dx \leq \frac{D_4(t)}{(2\Gamma - 4\gamma^2)}. \quad (9.2.27)$$

9.2.5 A bounds for ∇w

To find a bound for $\|\nabla w\|$ where $w = v_3$, take the double curl of (9.1.1)₁, using the third component, (and the fact that \underline{v} is solenoidal) to find

$$\begin{aligned} -\Delta w &= -\nabla(g_3 \frac{\partial T}{\partial x}, g_3 \frac{\partial T}{\partial y}, -g_1 \frac{\partial T}{\partial x} - g_2 \frac{\partial T}{\partial y}) \\ &\quad -\nabla(h_3 \frac{\partial C}{\partial x}, h_3 \frac{\partial C}{\partial y}, -h_1 \frac{\partial C}{\partial x} - h_2 \frac{\partial C}{\partial y}) + \sigma B_0^2 D^2 w, \end{aligned} \quad (9.2.28)$$

where $D = d/dz$. Multiplying (9.2.28) by w and integrating over Ω , and then using the similar argument which is used to prove (9.2.9) with $\alpha_1 = 2$ we have

$$\int_{\Omega} w_{,i} w_{,i} dx \leq \frac{1}{2} \int_{\Omega} w_{,i} w_{,i} dx + 3g^2 \int_{\Omega} T_{,i} T_{,i} dx + 3h^2 \int_{\Omega} C_{,i} C_{,i} dx - \sigma B_0^2 \int_{\Omega} w_{,3} w_{,3} dx. \quad (9.2.29)$$

Dropping a negative term involving σ , finally, we obtain

$$\|\nabla w\|^2 \leq 6g^2 \|\nabla T\|^2 + 6h^2 \|\nabla C\|^2. \quad (9.2.30)$$

9.2.6 A bounds for $\nabla \mathbf{v}$

We shall also require a bound for the Dirichlet integral of \mathbf{v} . We start with the fact

$$\|\nabla \mathbf{v}\|^2 = \int_{\Omega} v_{i,j}(v_{i,j} - v_{j,i})dx + \int_{\Omega} v_{i,j}v_{j,i}dx. \quad (9.2.31)$$

Now, we find a bound for the last term in the right hand side of (9.2.31) as follows

$$\int_{\Omega} v_{i,j}v_{j,i}dx = \oint_{\partial\Omega} v_{i,j}v_j n_i dS = \oint_{\partial\Omega} (v_i n_i)_j v_j dS - \oint_{\partial\Omega} v_i v_j n_{i,j} dS. \quad (9.2.32)$$

Note that $\oint_{\partial\Omega} (v_i n_i)_j v_j dS$ contain the product of a tangential vector and a normal vector, thus its value equal to zero . Moreover, if Ω is convex it follows that since v_i is a tangential vector on $\partial\Omega$, hence $\oint_{\partial\Omega} v_i v_j n_{i,j} dS \geq 0$. Thus we conclude that

$$\int_{\Omega} v_{i,j}v_{j,i}dx \leq 0, \quad (9.2.33)$$

while for nonconvex Ω with boundary of bounded curvature

$$\int_{\Omega} v_{i,j}v_{j,i}dx \leq \kappa_0 \oint_{\partial\Omega} |\mathbf{v}|^2 dS, \quad (9.2.34)$$

where κ_0 depends on the Gaussian curvature of $\partial\Omega$ (see Weatherburn [221], p. 86).

Next, if we use a trace inequality

$$\oint_{\partial\Omega} |\mathbf{v}|^2 dS \leq \kappa_1 \int_{\Omega} |\mathbf{v}|^2 dx + \kappa_2 \int_{\Omega} |\nabla \mathbf{v}|^2 dx, \quad (9.2.35)$$

where the constant κ_2 may be small. It follows then that whether Ω is convex or nonconvex we have after inserting (9.2.35) into (9.2.34) and the result into (9.2.31), having chosen k_2 sufficiently small, we have

$$\|\nabla \mathbf{v}\|^2 \leq M \left[\int_{\Omega} v_{i,j}(v_{i,j} - v_{j,i})dx + \|\mathbf{v}\|^2 \right], \quad (9.2.36)$$

where M is a computable constant. From this point on we shall use the symbol M to denote a computable constant, and in the different inequalities where it occurs it will in general have different values. To find a bound for the first term of (9.2.36), we use (9.2.4), (9.2.30), the arithmetic-geometric mean inequality and the Cauchy-Schwarz inequality, to arrive at

$$\int_{\Omega} v_{i,j}(v_{i,j} - v_{j,i})dx = \int_{\Omega} v_{i,j}[-p_{,ij} + g_i T_{,j} + h_i C_{,j} + \sigma B_0^2(k_i w_{,j} - v_{i,j})]dx$$

$$\begin{aligned}
& - \int_{\Omega} v_{i,j}[-p_{,ij} + g_j T_{,i} + h_j C_{,i} + \sigma B_0^2(k_j w_{,i} - v_{j,i})] dx \\
& = \int_{\Omega} v_{i,j}[g_i T_{,j} + h_i C_{,j}] - \int_{\Omega} v_{i,j}[g_j T_{,i} + h_j C_{,i}] dx - \sigma B_0^2 \int_{\Omega} v_{i,j}[v_{i,j} - v_{j,i}] dx \\
& \quad + \sigma B_0^2 \int_{\Omega} v_{i,j}[k_i w_{,j} - k_j w_{,i}] dx \\
& = \int_{\Omega} [g_i T_{,j}(v_{i,j} - v_{j,i}) + h_i C_{,j}(v_{i,j} - v_{j,i})] dx - \sigma B_0^2 \int_{\Omega} v_{i,j}[v_{i,j} - v_{j,i}] dx - \sigma B_0^2 \int_{\Omega} k_j w_{,i}[v_{i,j} - v_{j,i}] dx \\
& \leq 2g^2 \|\nabla C\|^2 + 2h^2 \|\nabla T\|^2 + \frac{1}{4} \int_{\Omega} (v_{i,j} - v_{j,i})^2 dx + \frac{\sigma B_0^2}{2} \int_{\Omega} w_{,i} w_{,i} dx \\
& \leq 2g^2 \|\nabla C\|^2 + 2h^2 \|\nabla T\|^2 + \frac{1}{2} \int_{\Omega} v_{i,j}(v_{i,j} - v_{j,i}) dx + 3\sigma B_0^2 [g^2 \|\nabla T\|^2 + h^2 \|\nabla C\|^2].
\end{aligned} \tag{9.2.37}$$

Therefore, we arrive to the following bound

$$\begin{aligned}
\int_{\Omega} v_{i,j}(v_{i,j} - v_{j,i}) dx & \leq 4g^2 \|\nabla C\|^2 + 4h^2 \|\nabla T\|^2 + 6\sigma B_0^2 [g^2 \|\nabla T\|^2 + h^2 \|\nabla C\|^2] \\
& \leq M[\|\nabla C\|^2 + \|\nabla T\|^2].
\end{aligned} \tag{9.2.38}$$

Thus, it follows directly from (9.2.10), (9.2.36) and (9.2.38) the inequality

$$\|\nabla \mathbf{v}\|^2 \leq M[\|C\|^2 + \|T\|^2 + \|\nabla C\|^2 + \|\nabla T\|^2]. \tag{9.2.39}$$

9.3 Continuous dependence on the coefficient σ

In this section, we establish continuous dependence on the magnetic field coefficient.

To do this, let (v_i, T, C, P) and (v_i^*, T^*, C^*, P^*) be solutions of (9.1.1)-(9.1.3) with the same boundary and initial conditions, but with different magnetic coefficients σ_1 and σ_2 . Now, we define

$$u_i = v_i - v_i^*, \theta = T - T^*, \phi = C - C^*, \pi = p - p^*, \sigma = \sigma_1 - \sigma_2.$$

Then, (u_i, θ, ϕ, π) is a solution of the problem

$$\begin{aligned}
u_i & = -\pi_{,i} + g_i \theta + h_i \phi + \sigma[(\mathbf{v}^* \times \mathbf{B}_0) \times \mathbf{B}_0]_i + \sigma_1[(\mathbf{u} \times \mathbf{B}_0) \times \mathbf{B}_0]_i, \\
\theta_{,t} + v_i \theta_{,i} + u_i T_{,i}^* & = \Delta \theta, \\
\phi_{,t} + v_i \phi_{,i} + u_i C_{,i}^* & = \Delta \phi + \gamma \Delta \theta, \\
u_{i,i} & = 0,
\end{aligned} \tag{9.3.40}$$

in $\Omega \times t > 0$, together with the boundary and initial conditions,

$$u_i \cdot n_i = 0; \quad \theta = 0; \quad \phi = 0, \quad \text{on} \quad \partial\Omega \times t > 0, \quad (9.3.41)$$

$$\theta(x, 0) = 0; \quad \phi(x, 0) = 0; \quad \text{in} \quad \Omega. \quad (9.3.42)$$

Theorem 9.3.1 The solution (v_i, T, C, P) to the boundary-initial value problem (9.1.1)-(9.1.3) depends continuously on change in the magnetic coefficient σ , as shown explicitly in inequality (9.3.71) which derives a relation of the form

$$\alpha \|T - T^*\| + \|C - C^*\| \leq L_1 \sigma^2$$

where α is a computable constant and L_1 is likewise an a priori constant. Here (T, C) and (T^*, C^*) are two solutions to (9.1.1)-(9.1.3) for different σ values σ_1 and σ_2 . Further the velocity field \mathbf{v} depends continuously on σ in the manner

$$\|\mathbf{v} - \mathbf{v}^*\| \leq L_2 \sigma^2$$

where L_2 is also an a priori constant. Precise details of these statements are continued in inequalities (9.3.46) and (9.3.71).

Proof: Multiplying (9.3.40)₁ by u_i , and integrating over Ω , with aid of the Cauchy-Schwarz inequality and (9.2.28), we obtain

$$\|\mathbf{u}\|^2 \leq g\|\theta\|\|\mathbf{u}\| + h\|\phi\|\|\mathbf{u}\| + \sigma B_0^2 \int_{\Omega} u_i(k_i w^* - v_i^*) dx + \sigma_1 B_0^2 \int_{\Omega} u_i(k_i w - u_i) dx, \quad (9.3.43)$$

where $w = u_3, w^* = u_3^*$. From (9.2.5) we see that

$$\int_{\Omega} u_i(k_i w - u_i) dx \leq 0. \quad (9.3.44)$$

In addition, applying the Cauchy-Schwarz inequality we obtain

$$\begin{aligned} \sigma B_0^2 \int_{\Omega} u_i(k_i w^* - v_i^*) dx &\leq \sigma B_0^2 [\|\mathbf{u}\| \|w^*\| + \|\mathbf{u}\| \|\mathbf{v}^*\|] \\ &\leq 2\sigma B_0^2 \|\mathbf{u}\| \|\mathbf{v}^*\|. \end{aligned} \quad (9.3.45)$$

Now, substituting (9.3.45) into (9.3.43) and then using the arithmetic-geometric mean inequality and (9.2.10), we have

$$\|\mathbf{u}\|^2 \leq 4g^2 \|\theta\|^2 + 4h^2 \|\phi\|^2 + 8\sigma^2 B_0^4 \|\mathbf{v}^*\|^2 + 2\sigma_1 B_0^2 \int_{\Omega} u_i(k_i w - u_i) dx$$

$$\begin{aligned} &\leq 4g^2\|\theta\|^2 + 4h^2\|\phi\|^2 + 8\sigma^2 B_0^4[2g^2\|T\|^2 + 2h^2\|C\|^2] \\ &\leq M[\|\theta\|^2 + \|\phi\|^2 + \sigma^2(\|T\|^2 + \|C\|^2)], \end{aligned} \quad (9.3.46)$$

where we have dropped a negative term involving σ_1 . To find a bound for $\|\nabla w\|$ where $w = u_3$, take the double curl of (9.3.40)₁, use the third component and use (9.3.40)₄, to drive

$$\begin{aligned} -\Delta w &= -\nabla(g_3 \frac{\partial \theta}{\partial x}, g_3 \frac{\partial \theta}{\partial y}, -g_1 \frac{\partial \theta}{\partial x} - g_2 \frac{\partial \theta}{\partial y}) \\ &\quad -\nabla(h_3 \frac{\partial \phi}{\partial x}, h_3 \frac{\partial \phi}{\partial y}, -h_1 \frac{\partial \phi}{\partial x} - h_2 \frac{\partial \phi}{\partial y}) + \sigma B_0^2 D^2 w^* + \sigma_1 B_0^2 D^2 w. \end{aligned} \quad (9.3.47)$$

Multiplying (9.3.47) by w_i and use the similar argument which is used to prove (9.2.9) with $\alpha_1 = 2$ we have

$$\begin{aligned} \int_{\Omega} w_{,i} w_{,i} dx &\leq \frac{1}{2} \int_{\Omega} w_{,i} w_{,i} dx + g^2 \int_{\Omega} \theta_{,i} \theta_{,i} dx + h^2 \int_{\Omega} \phi_{,i} \phi_{,i} dx \\ &\quad -\sigma_1 B_0^2 \int_{\Omega} w_{,3} w_{,3} dx - \sigma B_0^2 \int_{\Omega} w_{,3}^* w_{,3} dx. \end{aligned} \quad (9.3.48)$$

Now, applying the Cauchy-Schwarz inequality and the arithmetic-geometric mean inequality to the last term, we have

$$\begin{aligned} \frac{1}{2} \int_{\Omega} w_{,i} w_{,i} dx &\leq g^2 \int_{\Omega} \theta_{,i} \theta_{,i} dx + h^2 \int_{\Omega} \phi_{,i} \phi_{,i} dx + \frac{\sigma^2 B_0^2}{4\sigma_1} \int_{\Omega} w_{,3}^* w_{,3}^* dx \\ &\leq g^2 \int_{\Omega} \theta_{,i} \theta_{,i} dx + h^2 \int_{\Omega} \phi_{,i} \phi_{,i} dx + \frac{\sigma^2 B_0^2}{4\sigma_1} \int_{\Omega} w_{,i}^* w_{,i}^* dx. \end{aligned} \quad (9.3.49)$$

Now, using the bound (9.2.30), we obtain

$$\begin{aligned} \|\nabla w\|^2 &\leq 2g^2\|\nabla\theta\|^2 + 2h^2\|\nabla\phi\|^2 + \frac{3\sigma^2 B_0^2}{\sigma_1}[g^2\|\nabla T\|^2 + h^2\|\nabla C\|^2] \\ &\leq M[\|\nabla\theta\|^2 + \|\nabla\phi\|^2 + \sigma^2(\|\nabla T\|^2 + \|\nabla C\|^2)]. \end{aligned} \quad (9.3.50)$$

Next, using the similar argument which is used in the proof of (9.2.36), we find

$$\|\nabla \mathbf{u}\|^2 \leq M[\int_{\Omega} u_{i,j}(u_{i,j} - u_{j,i})dx + \|\mathbf{u}\|^2]. \quad (9.3.51)$$

Now, our aim is to find a bound to the first term of (9.3.51), and to this end from (9.3.40), we form

$$\int_{\Omega} u_{i,j}(u_{i,j} - u_{j,i})dx = \int_{\Omega} u_{i,j}[-\pi_{,ij} + g_i \theta_{,j} + h_i \phi_{,j} + \sigma B_0^2(k_i w_{,j}^* - v_{i,j}^*) + \sigma_1 B_0^2(k_i w_{,j} - u_{i,j})]dx$$

$$\begin{aligned}
& - \int_{\Omega} u_{i,j} [-\pi_{i,j} + g_j \theta_{i,j} + h_j \phi_{i,j} + \sigma B_0^2 (k_j w_{i,j}^* - v_{j,i}^*) + \sigma_1 B_0^2 (k_j w_{i,j} - u_{j,i})] dx \\
& = \int_{\Omega} u_{i,j} [g_i \theta_{i,j} - g_j \theta_{j,i}] + \int_{\Omega} u_{i,j} [h_i \phi_{i,j} - h_j \phi_{j,i}] \\
& + \sigma_1 B_0^2 \int_{\Omega} u_{i,j} [(k_i w_{i,j} - u_{i,j}) - (k_j w_{i,j} - u_{j,i})] dx \\
& + \sigma B_0^2 \int_{\Omega} u_{i,j} [(k_i w_{i,j}^* - v_{i,j}^*) - (k_j w_{i,j}^* - v_{j,i}^*)] dx. \tag{9.3.52}
\end{aligned}$$

Now, we shall deal with each term of (9.3.52). Firstly, Using (9.2.6), the Cauchy-Schwarz inequality and the arithmetic-geometric mean inequality we have

$$\begin{aligned}
& \int_{\Omega} u_{i,j} [g_i \theta_{i,j} - g_j \theta_{j,i}] = \int_{\Omega} g_j \theta_{j,i} (u_{i,j} - u_{j,i}) dx \\
& \leq 4g^2 \int_{\Omega} \theta_{j,i} \theta_{i,j} dx + \frac{1}{16} \int_{\Omega} (u_{i,j} - u_{j,i})(u_{i,j} - u_{j,i}) dx = 4g^2 \|\nabla \theta\| + \frac{1}{8} \int_{\Omega} u_{i,j} (u_{i,j} - u_{j,i}) dx. \tag{9.3.53}
\end{aligned}$$

Similarly,

$$\int_{\Omega} u_{i,j} [h_i \phi_{i,j} - h_j \phi_{j,i}] \leq 4h^2 \|\nabla \phi\| + \frac{1}{8} \int_{\Omega} u_{i,j} (u_{i,j} - u_{j,i}) dx. \tag{9.3.54}$$

Again, using the Cauchy-Schwarz inequality, the arithmetic-geometric mean inequality and (9.3.50)

$$\begin{aligned}
& \sigma_1 B_0^2 \int_{\Omega} u_{i,j} [(k_i w_{i,j} - u_{i,j}) - (k_j w_{i,j} - u_{j,i})] dx \\
& = -\sigma_1 B_0^2 \int_{\Omega} u_{i,j} (u_{i,j} - u_{j,i}) dx + \sigma_1 B_0^2 \int_{\Omega} u_{i,j} (k_i w_{i,j} - k_j w_{i,j}) dx \\
& = -\sigma_1 B_0^2 \int_{\Omega} u_{i,j} (u_{i,j} - u_{j,i}) dx + \sigma_1 B_0^2 \int_{\Omega} k_j w_{i,j} (u_{i,j} - u_{j,i}) dx \\
& \leq \frac{\sigma_1 B_0^2}{2} \int_{\Omega} w_{i,j} w_{i,j} dx \\
& \leq M [\|\nabla \theta\|^2 + \|\nabla \phi\|^2 + \sigma^2 (\|\nabla T\|^2 + \|\nabla C\|^2)]. \tag{9.3.55}
\end{aligned}$$

Applying the Cauchy-Schwarz inequality, the arithmetic-geometric mean inequality, (9.2.30) and (9.2.38), we have

$$\begin{aligned}
& \sigma B_0^2 \int_{\Omega} u_{i,j} [(k_i w_{i,j}^* - v_{i,j}^*) - (k_j w_{i,j}^* - v_{j,i}^*)] dx \\
& = -\sigma B_0^2 \int_{\Omega} u_{i,j} (v_{i,j}^* - v_{j,i}^*) dx + \sigma B_0^2 \int_{\Omega} u_{i,j} (k_i w_{i,j}^* - k_j w_{i,j}^*) dx
\end{aligned}$$

$$\begin{aligned}
&= -\frac{\sigma B_0^2}{2} \int_{\Omega} (u_{i,j} - u_{j,i})(v_{i,j}^* - v_{j,i}^*) dx - \sigma B_0^2 \int_{\Omega} k_j w_{,i}^* (u_{i,j} - u_{j,i}) dx \\
&\leq \frac{3}{16} \int_{\Omega} u_{i,j} (u_{i,j} - u_{j,i}) dx + 2\sigma^2 B_0^4 \int_{\Omega} v_{i,j}^* (v_{i,j}^* - v_{j,i}^*) dx + 4\sigma^2 B_0^4 \int_{\Omega} w_{,i}^* w_{,i}^* dx \\
&\leq \frac{3}{16} \int_{\Omega} u_{i,j} (u_{i,j} - u_{j,i}) dx + \sigma^2 M [\|C\|^2 + \|T\|^2 + \|\nabla C\|^2 + \|\nabla T\|^2]. \quad (9.3.56)
\end{aligned}$$

Substituting (9.3.53), (9.3.54), (9.3.55) and (9.3.56) into (9.3.52), we arrive at

$$\int_{\Omega} u_{i,j} (u_{i,j} - u_{j,i}) dx \leq M [\|\nabla \phi\|^2 + \|\nabla \theta\|^2 + \sigma^2 (\|C\|^2 + \|T\|^2 + \|\nabla C\|^2 + \|\nabla T\|^2)]. \quad (9.3.57)$$

Now, substituting (9.3.57) into (9.3.51) and then using (9.3.46), we have

$$\|\nabla \mathbf{u}\|^2 \leq M [\|\nabla \phi\|^2 + \|\nabla \theta\|^2 + \sigma^2 (\|C\|^2 + \|T\|^2 + \|\nabla C\|^2 + \|\nabla T\|^2)]. \quad (9.3.58)$$

here we have used the relation

$$\|\chi\|^2 \leq \lambda_1 \|\nabla \chi\|^2, \quad (9.3.59)$$

where λ_1 is the first eigenvalue of

$$\Delta \chi + \lambda_1 \chi = 0, \quad \text{in } \Omega,$$

$$\chi = 0, \quad \text{on } \partial\Omega.$$

Lower bounds for λ_1 are well known (see, e.g. Bandle [13]).

Next, we will find a bound for $\|\theta\|^2$ and $\|\phi\|^2$.

$$\begin{aligned}
&\frac{d}{dt} (\alpha \|\theta\|^2 + \|\phi\|^2) = 2 \int_{\Omega} (\alpha \theta \theta_t + \phi \phi_t) dx \\
&= 2 \int_{\Omega} \alpha \theta (\Delta \theta - v_i \theta_{,i} - u_i T_{,i}^*) dx + 2 \int_{\Omega} \phi (\Delta \phi - v_i \phi_{,i} - u_i C_{,i}^* + \gamma \Delta \theta) dx \\
&= -2\alpha \|\nabla \theta\|^2 - 2\|\nabla \phi\|^2 + 2\alpha \int_{\Omega} \theta_{,i} u_i T^* dx + 2 \int_{\Omega} \phi_{,i} u_i C^* dx - 2\gamma \int_{\Omega} \theta_{,i} \phi_{,i} dx \\
&\leq -\left(2\alpha - \frac{\gamma^2}{\alpha_1} - \frac{\alpha}{\alpha_3}\right) \|\nabla \theta\|^2 - \left(2 - \alpha_1 - \frac{1}{\alpha_4}\right) \|\nabla \phi\|^2 + \alpha \alpha_3 \|\mathbf{u}\|_4^2 \|T\|_4^2 + \alpha_4 \|\mathbf{u}\|_4^2 \|C\|_4^2. \quad (9.3.60)
\end{aligned}$$

Now, we choose the constant as follows

$$\alpha = \gamma^2, \quad \alpha_1 = 1, \quad \alpha_2 = \frac{1}{4}, \quad \alpha_3 = 2, \quad \alpha_4 = 4. \quad (9.3.61)$$

Thus, we have

$$\frac{d}{dt}(\alpha\|\theta\|^2 + \|\phi\|^2) \leq -\frac{1}{2}(\|\nabla\theta\|^2 + \|\nabla\phi\|^2) + \|\mathbf{u}\|_4^2(2\gamma^2\|T\|_4^2 + 4\|C\|_4^2). \quad (9.3.62)$$

Now, we use the bounds of $\|\mathbf{u}\|_4^2$, $\|T\|_4^2$ and $\|C\|_4^2$ which were derived in [110] in the forms

$$\|\mathbf{u}\|_4^2 \leq M[(1 + \frac{\delta}{4})\|\mathbf{u}\|^2 + \frac{3}{4}\delta^{-1/3}\|\nabla\mathbf{u}\|^2], \quad (9.3.63)$$

$$\|T\|_4^2 \leq D_5(t), \quad (9.3.64)$$

$$\|C\|_4^2 \leq D_6(t). \quad (9.3.65)$$

Substituting these bound into (9.3.62) and removing the non positive terms, we obtain

$$\begin{aligned} \frac{d}{dt}(\alpha\|\theta\|^2 + \|\phi\|^2) &\leq M[(1 + \frac{\delta}{4})(\|\theta\|^2 + \|\phi\|^2 + \sigma^2(\|T\|^2 + \|C\|^2)) \\ &+ \frac{3}{4}\delta^{-1/3}(\|\nabla\phi\|^2 + \|\nabla\theta\|^2 + \sigma^2(\|C\|^2 + \|T\|^2 + \|\nabla C\|^2 + \|\nabla T\|^2))] \\ &\quad \times [2\gamma^2 D_5(t) + 4D_6(t)]. \end{aligned} \quad (9.3.66)$$

Since the constant δ is at our disposal then provided $D_5(t)$ and $D_6(t)$ are bounded we may choose δ so large that the first term on the right dominates the other term involving $\|\nabla\phi\|^2 + \|\nabla\theta\|^2 + \sigma^2(\|C\|^2 + \|T\|^2 + \|\nabla C\|^2 + \|\nabla T\|^2)$. We are then left with

$$\begin{aligned} \frac{d}{dt}(\alpha\|\theta\|^2 + \|\phi\|^2) &\leq M[\alpha\|\theta\|^2 + \|\phi\|^2 + \sigma^2(\|T\|^2 + \|C\|^2)] \\ &\quad \times [2\gamma^2 D_5(t) + 4D_6(t)]. \end{aligned} \quad (9.3.67)$$

Setting

$$D_7(t) = 2\gamma^2 D_5(t) + 4D_6(t), \quad (9.3.68)$$

and

$$D_8(t) = D_7(t) \times [\|T\|^2 + \|C\|^2], \quad (9.3.69)$$

then, we have from (9.3.67)

$$\frac{d}{dt}[(\alpha\|\theta\|^2 + \|\phi\|^2)e^{-M \int_0^t D_7(\varrho)d\varrho}] \leq M\sigma^2 D_8(t)e^{-M \int_0^t D_7(\varrho)d\varrho}. \quad (9.3.70)$$

Upon integration, we further obtain

$$\alpha\|\theta\|^2 + \|\phi\|^2 \leq M\sigma^2 \int_0^t D_8(\varrho)e^{-M \int_0^t D_7(\eta)d\eta}d\varrho, \quad (9.3.71)$$

which is the desired continuous dependence result. The continuous dependence for u_i follows directly from (9.3.46). \square

9.4 Continuous dependence on the coefficients g_i and h_i

We have develop an analysis that establishes continuous dependence of the solution on changes in the gravity vectors g_i and h_i in equations (9.1.1)₁. To do this, let (v_i, T, C, P) and (v_i^*, T^*, C^*, P^*) be solutions of (9.1.1)-(9.1.3) with the same boundary and initial conditions, but with different (g_i, h_i) and (g_i^*, h_i^*) . Now, we define $u_i = v_i - v_i^*$, $\theta = T - T^*$, $\phi = C - C^*$, $\pi = p - p^*$, $\mu_i = g_i - g_i^*$, $\zeta_i = h_i - h_i^*$. Then, (u_i, θ, ϕ, π) is a solution of the problem

$$\begin{aligned} u_i &= -\pi_{,i} + \mu_i T^* + g_i \theta + \zeta_i C^* + h_i \phi + \sigma[(\mathbf{u} \times \mathbf{B}_0) \times \mathbf{B}_0]_i, \\ \theta_{,t} + v_i \theta_{,i} + u_i T_{,i}^* &= \Delta \theta, \\ \phi_{,t} + v_i \phi_{,i} + u_i C_{,i}^* &= \Delta \phi + \gamma \Delta \theta, \\ u_{i,i} &= 0, \end{aligned} \tag{9.4.72}$$

in $\Omega \times t > 0$, together with the boundary and initial conditions,

$$u_i n_i = 0; \quad \theta = 0; \quad \phi = 0, \quad \text{on} \quad \partial\Omega \times t > 0, \tag{9.4.73}$$

$$\theta(x, 0) = 0; \quad \phi(x, 0) = 0; \quad \text{in} \quad \Omega. \tag{9.4.74}$$

Theorem 9.4.1 The solution (v_i, T, C, P) to the boundary-initial value problem (9.1.1)-(9.1.3) depends continuously on change in the gravity vectors g_i and h_i , as shown explicitly in inequality (9.4.81) which derives a relation of the form

$$\alpha \|T - T^*\| + \|C - C^*\| \leq L_3 \mu^2 + L_4 \zeta^2$$

where α is a computable constant and L_3, L_4 are likewise a priori constants. Further the velocity field \mathbf{v} depends continuously on g_i and h_i in the manner

$$\|\mathbf{v} - \mathbf{v}^*\| \leq L_5 \mu^2 + L_6 \zeta^2$$

where L_5, L_6 are a priori constants. The terms μ and ζ are the differences in the gravity coefficients g_i and h_i , respectively. Precise details of these statements are continued in inequalities (9.4.75) and (9.4.81).

Proof: Using the similar argument of the last section, we have

$$\|\mathbf{u}\|^2 \leq M[\|\phi\|^2 + \|\theta\|^2 + \mu^2\|T\|^2 + \zeta^2\|C\|^2], \quad (9.4.75)$$

and

$$\|\nabla\mathbf{u}\|^2 \leq M[\|\nabla\phi\|^2 + \|\nabla\theta\|^2 + \mu^2(\|\nabla T\|^2 + \|T\|^2) + \zeta^2(\|\nabla C\|^2 + \|C\|^2)]. \quad (9.4.76)$$

where $\zeta = \max \zeta_i \zeta_i$ and $\mu = \max \mu_i \mu_i$.

Now, (9.3.62) still valid and again we shall use the bounds of $\|\mathbf{u}\|_4^2$, $\|T\|_4^2$ and $\|C\|_4^2$ which were derived in [110]. Substituting (9.4.75) and (9.4.76) into (9.3.62) and use (9.3.63)-(9.3.65) and (9.3.68), we arrive after removing the non positive terms in (9.3.62) to the following bound estimate

$$\begin{aligned} \frac{d}{dt}(\alpha\|\theta\|^2 + \|\phi\|^2) &\leq M\left(1 + \frac{\delta}{4}\right)(\|\phi\|^2 + \|\theta\|^2 + \mu^2\|T\|^2 + \zeta^2\|C\|^2) \\ &+ \frac{3}{4}\delta^{-1/3}(\|\nabla\phi\|^2 + \|\nabla\theta\|^2 + \mu^2(\|\nabla T\|^2 + \|T\|^2) + \zeta^2(\|\nabla C\|^2 + \|C\|^2)) \times D_7(t). \end{aligned} \quad (9.4.77)$$

Similarly, if we choose δ so large such that the first term on the right dominates the other term involving $\|\nabla\phi\|^2 + \|\nabla\theta\|^2 + \mu^2(\|\nabla T\|^2 + \|T\|^2) + \zeta^2(\|\nabla C\|^2 + \|C\|^2)$ and Since $D_7(t)$ are bounded, Thus, we have

$$\frac{d}{dt}(\alpha\|\theta\|^2 + \|\phi\|^2) \leq M[\alpha\|\theta\|^2 + \|\phi\|^2 + \mu^2\|T\|^2 + \zeta^2\|C\|^2] \times D_7(t). \quad (9.4.78)$$

Setting

$$\begin{aligned} D_9(t) &= D_7(t) \times \|T\|^2, \\ D_{10}(t) &= D_7(t) \times \|C\|^2, \end{aligned} \quad (9.4.79)$$

then, we have from (9.4.78)

$$\frac{d}{dt}[(\alpha\|\theta\|^2 + \|\phi\|^2)e^{-M \int_0^t D_7(\varrho)d\varrho}] \leq M[\mu^2 D_9(t) + \zeta^2 D_{10}(t)]e^{-M \int_0^t D_7(\varrho)d\varrho}. \quad (9.4.80)$$

Upon integration, we further obtain

$$\alpha\|\theta\|^2 + \|\phi\|^2 \leq M\sigma^2 \int_0^t [\mu^2 D_9(\varrho) + \zeta^2 D_{10}(\varrho)]e^{-M \int_0^t D_7(\eta)d\eta} d\varrho, \quad (9.4.81)$$

which is the desired continuous dependence result. The continuous dependence for u_i follows directly from (9.4.75). \square

Chapter 10

Three dimensional simulation for the problem of a layer of non-Boussinesq fluid heated internally with prescribed heat flux on the lower boundary and constant temperature upper surface

10.1 Introduction

The Rayleigh-Bénard problem is the major section for the problem of the onset of convection in a horizontal fluid layer uniformly heated from below. Rayleigh [163] provided an analysis on the assumption that the convection was induced by buoyancy effects. Rayleigh introduced an approximation to the basic equations of motion that he ascribed to Boussinesq [22]. However, Joseph [92] found that the approximation had been earlier applied by Oberbeck [139]. The parameter whose value determines

the onset of convection is called the Rayleigh number. Joseph [92] noticed that this parameter appeared in a study by Lorenz [113], who also used the approximation employed by Oberbeck.

The Oberbeck-Boussinesq approximation is the basis of most of the contemporary studies on natural or mixed convection flows. In the Oberbeck-Boussinesq approximation, all fluid properties such as viscosity and density can be taken as constants except that a buoyancy term proportional to a density difference is retained in the momentum equation. Thus, the fluid is taken as quasi-incompressible, the divergence of the velocity is approximated by zero in the continuity equation, and the term involving the product of the pressure and the divergence of the velocity is neglected in the thermal energy equation; see, for example, Section 8 of Chandrasekhar [32]. Several Oberbeck-Boussinesq approximations have been applied on the full Navier-Stokes equations. It is generally used in the framework of the natural convection problems such as the Rayleigh-Bénard configuration, and provides a simplified set of equations which is much more tractable for both numerical and analytical purposes, since all the acoustic scales have been eliminated. Rayleigh [163] employed the simplified thermal energy equation and he ascribed it to Boussinesq [22]. In [161], Rajagopal et al. intend to provide a rigorous derivation of the Oberbeck-Boussinesq approximation in the framework of a full thermodynamical theory of the Navier-Stokes equations. Hills and Roberts [85] provided important idea to adapt a new method of treating the constraint of mechanical incompressibility. Recently, the Oberbeck-Boussinesq approximation have been developed intensively by Rajagopal [160], Rajagopal et al. [162], Barletta [14] and Barletta and Nield [15, 16].

Straughan [194] obtained quantitative non-linear stability estimates which guarantee nonlinear stability for the problem of penetrative convection in a plane layer with a nonuniform heat source, and a constant temperature upper surface, while the lower surface is subject to a prescribed heat flux. In addition to the non-linear results which establish a critical Rayleigh number below which convection cannot occur, Straughan [194] calculated the linear value above which convection occurs. In this chapter we study the problem of penetrative convection in a plane layer with

a nonuniform heat source, and a constant temperature upper surface, while the lower surface is subject to a prescribed heat flux. Especially, the accuracy of linear instability and nonlinear stability thresholds are tested using a three dimensions simulation. Regions of possible very large subcritical instabilities, i.e. where agreement between the linear instability thresholds and nonlinear stability thresholds is poor, are studied by solving for the full three-dimensional system. The results indicate that linear theory is very accurate in predicting the onset of convective motion, and thus, regions of stability.

In the next Section we present the governing equations of motion and derive the associated perturbation equations and then in section 10.3, we introduce the linear and nonlinear analysis of our system. In section 10.4, we transform our system to velocity-vorticity formulation. Section 10.5 is devoted to a study of numerical solution of the problem in three dimensions. The results of our numerical investigation are then compiled and discussed in the final Section of the paper.

The results in this chapter were published in the article Harfash [79].

10.2 Governing equations

Consider then a layer of heat-conducting viscous fluid with a quadratic equation of state, occupying the horizontal layer $z \in (0, d)$ with the lower boundary $z = 0$ heated by radiation and with the temperature scale selected so that the temperature at $z = d$ remains a constant, T_u . By assuming the validity of the Oberbeck-Boussinesq approximation, the following local balance equations hold:

$$v_{i,t} + v_j v_{i,j} = -\frac{1}{\rho_m} p_{,i} + \nu \Delta v_i - g k_i [1 - \alpha(T - T_m)^2], \quad (10.2.1)$$

$$v_{i,i} = 0, \quad (10.2.2)$$

$$T_{,t} + v_i T_{,i} = \kappa \Delta T + Q, \quad (10.2.3)$$

where v, p, T, ν, g, α , and κ are respectively velocity, pressure, temperature, viscosity, gravity, a thermal expansion coefficient, and thermal diffusivity, $k = (0, 0, 1)$, and standard indicial notation is employed. These equations are defined on the spatial

region $\mathbb{R}^2 \times [0, d]$. Here, we have to mention that the effects of pressure work are not taken into account in the energy balance. The boundary conditions are

$$\mathbf{v} = 0, \quad \text{at } z = 0, d, \quad T = T_u, \quad \text{at } z = d, \quad \frac{\partial T}{\partial z} = \gamma, \quad \text{at } z = 0. \tag{10.2.4}$$

We here consider the heat supply function as $Q = Q_0(e^{z/d} - 1)$, where Q_0 and γ are constants. The steady solution $(\bar{\mathbf{v}}, \bar{T})$ corresponding to boundary conditions (10.2.4) is

$$\bar{\mathbf{v}} = 0, \quad \bar{T} = T_u - \gamma(d - z) + \frac{Q_0 d^2}{\kappa} \left(e - \frac{3}{2} - e^{\frac{z}{d}} + \frac{z}{d} + \frac{z^2}{2d^2} \right),$$

the hydrostatic pressure being determined from the momentum equation.

To investigate the stability of these solutions, we introduce perturbations (u, θ, π) by

$$v_i = \bar{v}_i + u_i, \quad T = \bar{T} + \theta, \quad p = \bar{p} + \pi.$$

Then, the perturbation equations are nondimensionalized according to the scales (stars denote dimensionless quantities)

$$t = t^* \frac{d^2}{\nu}, \quad U = \frac{\nu}{d}, \quad x = x^* d, \quad \theta = \theta^* T^\sharp, \quad \delta = \frac{\kappa(T_m - T_u)}{Q_0 d^2},$$

$$Pr = \frac{\nu}{\kappa}, \quad T^\sharp = U \sqrt{\frac{\nu}{\alpha g d \kappa}}, \quad R^2 = \frac{Q_0^2 d^7 g \alpha}{\kappa^3 \nu}, \quad \hat{\gamma} = \frac{\kappa \gamma}{Q_0 d}.$$

Here Pr is the Prandtl number and R^2 is a Rayleigh number. The dimensionless perturbation equations are (after omitting all stars)

$$u_{i,t} + u_j u_{i,j} = -\pi_{,i} + \Delta u_i + 2Rf_1(z)\theta k_i + Prk_i\theta^2, \tag{10.2.5}$$

$$u_{i,i} = 0, \tag{10.2.6}$$

$$Pr(\theta_{,t} + u_i \theta_{,i}) = -Rf_2(z)w + \Delta \theta, \tag{10.2.7}$$

where $w = u_3$, $f_1(z) = \hat{\gamma}(z - 1) - \delta + e - \frac{3}{2} - e^z + z + \frac{1}{2}z^2$, and $f_2(z) = 1 + z + \hat{\gamma} - e^z$. Equations (10.2.5)-(10.2.7) hold on $\mathbb{R}^2 \times [0, 1]$ and the boundary conditions adopted are

$$u = v = w = 0, \tag{10.2.8}$$

$$\theta = 0, \quad \text{at } z = 1, \tag{10.2.9}$$

$$\frac{\partial \theta}{\partial z} = 0, \quad \text{at } z = 0, \tag{10.2.10}$$

$$\mathbf{u}, \theta, \pi \text{ have a periodic structure in } x, y. \tag{10.2.11}$$

10.3 Linear and nonlinear energy stability theories

Linear instability results for stationary convection are obtained via the application of standard procedures to the linearized version of Eqs. (10.2.5)-(10.2.7). Straughan [194] found the critical Rayleigh number of linear theory by determining the lowest eigenvalue of the system

$$(D^2 - a^2)^2 W = 2f_1(z)Ra^2\Theta, \quad (10.3.12)$$

$$(D^2 - a^2)\Theta = Rf_2(z)W, \quad (10.3.13)$$

on $z \in (0, 1)$. Here $D = d/dz$, $w = We^{i(mx+ny)}$, $\theta = \Theta e^{i(mx+ny)}$ and $a^2 = m^2 + n^2$ is a horizontal wavenumber. These equations are subject to the boundary conditions

$$W = DW = \Theta = 0, \quad \text{at } z = 0, 1. \quad (10.3.14)$$

We solve the eigenvalue system (10.3.12) and (10.3.14) for σ numerically using the Chebyshev collocation method-1.

Straughan [194] presented a nonlinear energy stability analysis for arbitrary initial perturbations. They employed a weight in the temperature part of the energy in order to eliminate the nonlinearities that are introduced through the equation of state and thereby obtained stability results that were not amplitude dependent. Their eigenvalue problem of nonlinear theory is

$$2(D^2 - a^2)^2 W = -R_E M(z)a^2\Theta, \quad (10.3.15)$$

$$2\hat{\lambda}(D^2 - a^2)\Theta - 4D\Theta = R_E M(z)W, \quad (10.3.16)$$

where $M(z) = -f_1(z) + \frac{\hat{\lambda}}{2}f_2(z)$, $\hat{\lambda} = \lambda - 2z$ and λ is a parameter to be chosen. Then the lowest eigenvalue $R_E(a^2; \lambda)$ can be found from

$$Ra_E = \max_{\lambda > 2} \min_{a^2} R_E^2(a^2; \lambda).$$

For more detail about derivation of these system, see Straughan [194]. To achieve this, we have used again the Chebyshev collocation method-1. In our use of the Chebyshev collocation method, we used between 20 and 30 polynomials. Usually 25

was found to be sufficient but convergence was checked by varying the number of polynomials and by examining the convergence of the associated eigenvector (which yields the approximate associated eigenfunction).

10.4 Velocity-vorticity formulation

The mathematical formulations that are commonly used to simulate three-dimensional incompressible viscous flows include the primitive variables [96] (velocity-pressure), vorticity-vector potential [9, 123] and vorticity-velocity [42] formulations. As indicated in an overview of these formulations by Gresho [69], each formulation has its own advantages as well as shortcomings with respect to the others. Both the vorticity-vector potential formulations and the vorticity-velocity approach have a distinct advantage over the velocity-pressure formulation in that the pressure need not be calculated explicitly.

In this paper, we present an efficient, stable, and accurate finite difference schemes in the vorticity-vector potential formulation for computing the dynamics of viscous incompressible fluids. The emphasis is on three dimensions and nonstaggered grids. We introduce a second-order accurate method based on the vorticity-vector potential formulation on the nonstaggered grid whose performance on uniform grids is comparable with the finite scheme. We will pay special attention to how accurately the divergence-free conditions for vorticity, velocity, and vector potential are satisfied. We will derive the three-dimensional analog of the local vorticity boundary conditions.

By using the curl operator to Equation (10.2.5), one gets the following dimensionless form of the vorticity transport equation:

$$\omega_{,t} + (\mathbf{v} \cdot \nabla)\omega = (\omega \cdot \nabla)\mathbf{v} + \Delta\omega + 2R\nabla \times F(z)\theta\mathbf{k} + Pr\nabla \times \mathbf{k}\theta^2, \quad (10.4.17)$$

where the vorticity vector $\omega = (\xi_1, \xi_2, \xi_3)$ is defined as

$$\omega = \nabla \times \mathbf{v}. \quad (10.4.18)$$

To calculate velocity from vorticity, it is convenient to introduce a vector potential $\psi = (\psi_1, \psi_2, \psi_3)$, which may be looked upon as the three-dimensional counterpart

of a two-dimensional stream function. The vector potential are defined by

$$\mathbf{v} = \nabla \times \psi. \quad (10.4.19)$$

It easy to show the existence of such a vector potential for a solenoidal vector field ($\nabla \cdot \mathbf{v} = 0$). Such a vector potential can be required to be solenoidal, i.e.,

$$\nabla \cdot \psi = 0. \quad (10.4.20)$$

Substituting Eq. (10.4.19) in Eq. (10.4.18) and using Eq. (10.4.20) yields

$$\nabla^2 \psi = -\omega. \quad (10.4.21)$$

The set of equations (10.2.7), (10.4.17), (10.4.19) and (10.4.21) with appropriate boundary conditions were found to be a convenient form for numerical computations.

The boundary conditions for the vector potential are given below

$$\frac{\partial \psi_1}{\partial x} = \psi_2 = \psi_3 = 0, \quad \text{at } x = 0, 1, \quad (10.4.22)$$

$$\psi_1 = \frac{\partial \psi_2}{\partial y} = \psi_3 = 0, \quad \text{at } y = 0, 1, \quad (10.4.23)$$

$$\psi_1 = \psi_2 = \frac{\partial \psi_3}{\partial z} = 0, \quad \text{at } z = 0, 1, \quad (10.4.24)$$

The boundary conditions on vorticity follow directly and may expressed as

$$\xi_1 = 0, \quad \xi_2 = -\frac{\partial w}{\partial x}, \quad \xi_3 = \frac{\partial v}{\partial x}, \quad \text{at } x = 0, 1, \quad (10.4.25)$$

$$\xi_1 = \frac{\partial w}{\partial y}, \quad \xi_2 = 0, \quad \xi_3 = -\frac{\partial u}{\partial y}, \quad \text{at } y = 0, 1, \quad (10.4.26)$$

$$\xi_1 = -\frac{\partial v}{\partial z}, \quad \xi_2 = \frac{\partial u}{\partial z}, \quad \xi_3 = 0, \quad \text{at } z = 0, 1. \quad (10.4.27)$$

10.5 Numerical schemes

The first step in the numerical computational is to give an initial values for the vorticity vectors $\xi_{1ijk}^n, \xi_{2ijk}^n, \xi_{3ijk}^n, i, j, k = 0, 1, \dots, m$. Next, the Poisson equations (10.4.21) are discretized in space using an implicit scheme as follows

$$(\delta_x^2 + \delta_y^2 + \delta_z^2)\psi_{1ijk}^{n+1} = -\xi_{1ijk}^n, \quad (10.5.28)$$

$$(\delta_x^2 + \delta_y^2 + \delta_z^2)\psi_{2ijk}^{n+1} = -\xi_{2ijk}^n, \quad (10.5.29)$$

$$(\delta_x^2 + \delta_y^2 + \delta_z^2)\psi_{3ijk}^{n+1} = -\xi_{3ijk}^n. \quad (10.5.30)$$

where $\delta_x^2, \delta_y^2, \delta_z^2$ are the second-order central difference operators, which are define as

$$\delta_x^2\phi = \frac{\phi_{i+1jk} - 2\phi_{ijk} + \phi_{i-1jk}}{(\Delta x)^2},$$

$$\delta_y^2\phi = \frac{\phi_{ijk+1} - 2\phi_{ijk} + \phi_{ij-1k}}{(\Delta y)^2},$$

$$\delta_z^2\phi = \frac{\phi_{ijk+1} - 2\phi_{ijk} + \phi_{ijk-1}}{(\Delta z)^2}.$$

We used the Gauss-Seidel iteration method to evaluate $\psi_{1ijk}^{n+1}, \psi_{2ijk}^{n+1}, \psi_{3ijk}^{n+1}, i, j, k = 1, \dots, m-1$ from Eqs. (10.5.28), (10.5.29), (10.5.30), respectively. The next step is to discretize Eqs.(10.4.22)-(10.4.24) to evaluate the $\psi_{10jk}^{n+1}, \psi_{1mj}^{n+1}, \psi_{2i0k}^{n+1}, \psi_{2imk}^{n+1}, \psi_{3ij0}^{n+1}, \psi_{3ijm}^{n+1}, i, j, k = 0, \dots, m$ i.e. we used Eqs.(10.4.22)-(10.4.24) to evaluate the potential vectors at the boundary. Now, the velocity vector can be calculated explicitly by using a second order finite difference scheme to Eq.(10.4.19) as follows:

$$u_{ijk}^{n+1} = \delta_y\psi_{3ijk}^{n+1} - \delta_z\psi_{2ijk}^{n+1}, \quad (10.5.31)$$

$$v_{ijk}^{n+1} = \delta_z\psi_{1ijk}^{n+1} - \delta_x\psi_{3ijk}^{n+1}, \quad (10.5.32)$$

$$w_{ijk}^{n+1} = \delta_x\psi_{2ijk}^{n+1} - \delta_y\psi_{1ijk}^{n+1}, \quad (10.5.33)$$

$$i, j, k = 1, \dots, m-1,$$

where $\delta_x, \delta_y, \delta_z$ are the first-order central difference operators, which are define as

$$\delta_x\phi = \frac{\phi_{i+1jk} - \phi_{i-1jk}}{2\Delta x},$$

$$\delta_y\phi = \frac{\phi_{ij+1k} - \phi_{ij-1k}}{2\Delta y},$$

$$\delta_z\phi = \frac{\phi_{ijk+1} - \phi_{ijk-1}}{2\Delta z}.$$

The vorticity transport equations (10.4.17) are discretized in time using the explicit scheme. The discretized form of the vorticity transport equations (10.4.17) for the three vorticity components and energy equation (10.2.7) can be written as

$$\frac{\xi_{1ijk}^{n+1} - \xi_{1ijk}^n}{\Delta t} + u_{ijk}^n \delta_x \xi_{1ijk}^n + v_{ijk}^n \delta_y \xi_{1ijk}^n + w_{ijk}^n \delta_z \xi_{1ijk}^n$$

$$= \xi_{1ijk}^n \delta_x u_{ijk}^n + \xi_{2ijk}^n \delta_y u_{ijk}^n + \xi_{3ijk}^n \delta_z u_{ijk}^n + (\delta_x^2 + \delta_y^2 + \delta_z^2) \xi_{1ijk}^n + 2Rf_{1k} \delta_y \theta_{ijk}^n + 2Pr \theta_{ijk}^n \delta_y \theta_{ijk}^n, \quad (10.5.34)$$

$$\begin{aligned} & \frac{\xi_{2ijk}^{n+1} - \xi_{2ijk}^n}{\Delta t} + u_{ijk}^n \delta_x \xi_{2ijk}^n + v_{ijk}^n \delta_y \xi_{2ijk}^n + w_{ijk}^n \delta_z \xi_{2ijk}^n \\ &= \xi_{1ijk}^n \delta_x v_{ijk}^n + \xi_{2ijk}^n \delta_y v_{ijk}^n + \xi_{3ijk}^n \delta_z v_{ijk}^n + (\delta_x^2 + \delta_y^2 + \delta_z^2) \xi_{2ijk}^n - 2Rf_{1k} \delta_x \theta_{ijk}^n - 2Pr \theta_{ijk}^n \delta_x \theta_{ijk}^n, \end{aligned} \quad (10.5.35)$$

$$\begin{aligned} & \frac{\xi_{3ijk}^{n+1} - \xi_{3ijk}^n}{\Delta t} + u_{ijk}^n \delta_x \xi_{3ijk}^n + v_{ijk}^n \delta_y \xi_{3ijk}^n + w_{ijk}^n \delta_z \xi_{3ijk}^n \\ &= \xi_{1ijk}^n \delta_x w_{ijk}^n + \xi_{2ijk}^n \delta_y w_{ijk}^n + \xi_{3ijk}^n \delta_z w_{ijk}^n + (\delta_x^2 + \delta_y^2 + \delta_z^2) \xi_{2ijk}^n, \end{aligned} \quad (10.5.36)$$

$$Pr \left(\frac{\theta_{ijk}^{n+1} - \theta_{ijk}^n}{\Delta t} + u_{ijk}^n \delta_x \theta_{ijk}^n + v_{ijk}^n \delta_y \theta_{ijk}^n + w_{ijk}^n \delta_z \theta_{ijk}^n \right) = -Rf_{2k} w_{ijk}^n + (\delta_x^2 + \delta_y^2 + \delta_z^2) \theta_{ijk}^n, \quad (10.5.37)$$

$$i, j, k = 1, \dots, m-1,$$

The temperature on the boundary can be compute explicitly using Eqs. (10.2.10) - (10.2.11). However, a second order implicit technique has been used to evaluated the vorticity vector at the boundary form Eqs.(10.4.25)-(10.4.27).

10.6 Results and conclusions

In this section, Ra_L , is the critical Rayleigh number for linear instability and Ra_E similarly denotes the global nonlinear stability threshold. The corresponding critical wavenumbers of the linear instability will be denoted by a_L^2 . In Table 10.1, we present the results of numerical results of linear instability and nonlinear stability analyses. The dimensions of the box, which are calculated according to the critical wavenumber, are shown in Table 10.1. In this table Lx and Ly are box dimensions in the x and y directions, respectively, while, the box dimension in z direction is always equal 1. we select a solution so that these two values are similar to avoid any possible stabilisation effect from of walls.

As we mention in section 2, we assume that the perturbation fields (u, θ, π) are periodic in the x and y direction and denote by $\Omega = [0, 2\pi/a_x] \times [0, 2\pi/a_y] \times [0, 1]$ the periodicity cell, where a_x and a_y are the wavenumbers in the x and y directions, respectively. a_x and a_y are evaluated according to the critical wavenumbers a_L^2 where

$a_L^2 = a_x^2 + a_y^2$, then we computed $Lx = 2\pi/a_x$ and $Ly = 2\pi/a_y$. The values of Lx and Ly in Table 10.1 may be rearranged to yield the number of possible solutions for each value of the critical wavenumber. However, we select a solution so that these two values are similar to avoid any possible stabilisation effect from of walls.

For numerical solutions of the three dimensional problem, we used $\Delta t = 5 \times 10^{-5}$ and $\Delta x = \Delta y = \Delta z = 0.02$. The convergence criteria has been selected to make sure that the solutions arrive at an steady state. The convergence criteria is

$$\varphi = \max_{i,j,k} \{ |\xi_{1ijk}^{n+1} - \xi_{1ijk}^n|, |\xi_{2ijk}^{n+1} - \xi_{2ijk}^n|, |\xi_{3ijk}^{n+1} - \xi_{3ijk}^n|, |\theta_{ijk}^{n+1} - \theta_{ijk}^n| \},$$

and we select $\varphi = 10^{-6}$. The program will continue computing the results of the temperature, velocity, vorticity and potential vector for new time levels until the results satisfy the convergence criteria, otherwise, we stop the program after 80000 time levels, i.e at the time $\tau = 4$.

To solve eqs. (10.5.28)- (10.5.30) using Gauss-Seidel iteration method, in the first time level we give an initial values to potential vector and we denote $\psi_{1ijk}^{1,k}$, $\psi_{2ijk}^{1,k}$, $\psi_{3ijk}^{1,k}$. Then using these initial values we compute new values which we denote by $\psi_{1ijk}^{1,k+1}$, $\psi_{2ijk}^{1,k+1}$, $\psi_{3ijk}^{1,k+1}$ and then we use these values to evaluated new values and the program will continue in this process until satisfying the convergence criteria which is

$$\eta = \max_{i,j,k} \{ |\psi_{1ijk}^{1,k+1} - \psi_{1ijk}^{1,k}|, |\psi_{2ijk}^{1,k+1} - \psi_{2ijk}^{1,k}|, |\psi_{3ijk}^{1,k+1} - \psi_{3ijk}^{1,k}| \} < 10^{-5}.$$

In the next time levels, the values of ψ_{1ijk} , ψ_{2ijk} , ψ_{3ijk} in the time level n will be the initial values to the next time level.

In order to display the numerical results clearly, the temperature, velocity and vorticity contours are plotting in Figures 10.1 and 10.2 at $z = 0.5$, $\tau = 4$, $\delta = -1$, $\hat{\gamma} = 0.3$ and $R^2 = 155000$, with mesh size of $71 \times 71 \times 51$. In these Figures, the temperature and velocity contours are presented at the time level $\tau = 4$ as as it is impossible to arrive at any steady state. Figure 10.1 shows the contours of u , v , w , and θ at $z = 0.5$ in (a), (b), (c) and (d) respectively. The contours of ξ_1 , ξ_2 and ξ_3 at $z = 0.5$ are presented in Figure 10.2 in (a), (b) and (c), respectively.

In Table 10.2- 10.8, we show the summery of the numerical results where we introduce the maximum and minimum values of temperature, velocity, vorticity and

$\hat{\gamma}$	Ra_L	a_L^2	Ra_E	a_E^2	Lx	Ly
0.28	114766.015	35.003	59632.100	16.818	1.5	1.5
0.29	133165.864	37.399	64280.001	16.625	1.5	1.4
0.3	154816.654	39.981	68802.297	16.446	1.4	1.4
0.31	180365.749	42.764	73174.607	16.282	1.6	1.2
0.32	210613.017	45.767	77376.734	16.132	1.7	1.1
0.34	289395.588	52.556	85204.774	15.868	1.4	1.1
0.36	402309.378	60.608	92178.900	15.642	1.2	1.1

Table 10.1: Critical Rayleigh and wavenumbers Ra_L , Ra_E , a_L^2 , a_E^2 at $\delta = -1$.

potential vectors. In Table 10.2, we select $\delta = -1$, $\hat{\gamma} = 0.28$, then according to the stability analysis we have $Ra_L = 114766.015$, $Ra_E = 59632.1$. It clear there is big difference between the critical Rayleigh numbers of linear and nonlinear theories. From Table 10.2, for $R^2 = 107000$, we can see that the values of temperature, velocity, vorticity and potential vectors satisfy the convergence criteria at $\tau = 1.94845$ while for $R^2 = 111000$, the program need $\tau = 2.5697$ to arrive at the steady stat solutions. However, for $R^2 = 116000$, we can see that the solutions can not arrive at any steady state and the program stopes at $\tau = 4$. For $R^2 = 116000$, we let the program work to long time to see the behaviors of the solution for a long time and to see if it is possible that the solutions could arrive at any steady state. We see that the values of velocities increased at $\tau = 8$, then the values decreased at $\tau = 12$ and the velocities continue in this oscillation. Here, according to the numerical results, the linear instability threshold is the actual threshold, i.e. the solutions arrive to the basic steady state before the linear instability threshold. However, the results of Tables 10.3-10.8 explain that the stability behavior is absolutely similar to the stability behavior of Table 10.2, as we found that the linear instability threshold is the actual threshold.

	$R^2 = 107000$		$R^2 = 111000$		$R^2 = 116000$	
	$\tau = 1.94845$		$\tau = 2.5697$		$\tau = 4$	
	Max	Min	Max	Min	Max	Min
u	1.99E-04	-1.99E-04	2.78E-04	-2.78E-04	0.01647	-0.01646
v	2.00E-04	-1.99E-04	2.78E-04	-2.78E-04	0.01648	-0.01646
w	4.10E-04	-1.00E-04	5.73E-04	-1.40E-04	0.03394	-0.00823
ξ_1	4.48E-03	-4.47E-03	6.29E-03	-6.27E-03	0.37587	-0.37562
ξ_2	4.47E-03	-4.48E-03	6.27E-03	-6.28E-03	0.37563	-0.37586
ξ_3	1.91E-04	-1.92E-04	2.53E-04	-2.53E-04	0.01340	-0.01340
ψ_1	3.56E-05	-3.57E-05	4.95E-05	-4.95E-05	0.00291	-0.00291
ψ_2	3.57E-05	-3.56E-05	4.95E-05	-4.95E-05	0.00291	-0.00291
ψ_3	3.15E-07	-3.15E-07	4.07E-07	-4.08E-07	0.00002	-0.00002
θ	1.77E-04	-3.70E-05	2.47E-04	-5.10E-05	0.01467	-0.00302

Table 10.2: Summary of numerical results for $\delta = -1$, $\hat{\gamma} = 0.28$, $Ra_L = 114766.015$, $Ra_E = 59632.1$, $Lx = 1.5$ and $Ly = 1.5$.

	$R^2 = 125000$		$R^2 = 131000$		$R^2 = 136000$	
	$\tau = 1.8639$		$\tau = 3.5053$		$\tau = 4$	
	Max	Min	Max	Min	Max	Min
u	1.83E-04	-1.82E-04	3.94E-04	-3.93E-04	0.06589	-0.06585
v	1.71E-04	-1.71E-04	3.67E-04	-3.66E-04	0.06115	-0.06113
w	3.64E-04	-8.89E-05	7.83E-04	-1.91E-04	0.13067	-0.03204
ξ_1	3.98E-03	-3.98E-03	8.63E-03	-8.62E-03	1.45141	-1.45118
ξ_2	4.22E-03	-4.23E-03	9.18E-03	-9.20E-03	1.55105	-1.55163
ξ_3	2.61E-04	-2.62E-04	5.23E-04	-5.24E-04	0.08371	-0.08374
ψ_1	2.96E-05	-2.97E-05	6.32E-05	-6.33E-05	0.01050	-0.01051
ψ_2	3.18E-05	-3.17E-05	6.81E-05	-6.79E-05	0.01133	-0.01133
ψ_3	4.24E-07	-4.27E-07	8.24E-07	-8.28E-07	0.00013	-0.00013
θ	1.57E-04	-3.27E-05	3.39E-04	-6.92E-05	0.05672	-0.01166

Table 10.3: Summary of numerical results for $\delta = -1$, $\hat{\gamma} = 0.29$, $Ra_L = 133165.864$, $Ra_E = 64280.001$, $Lx = 1.5$ and $Ly = 1.4$.

	$R^2 = 145000$		$R^2 = 150000$		$R^2 = 155000$	
	$\tau = 1.85045$		$\tau = 2.64285$		$\tau = 4$	
	Max	Min	Max	Min	Max	Min
u	1.75E-04	-1.75E-04	2.68E-04	-2.68E-04	0.00205	-0.00205
v	1.75E-04	-1.75E-04	2.68E-04	-2.68E-04	0.00205	-0.00205
w	3.59E-04	-8.62E-05	5.52E-04	-1.32E-04	0.00423	-0.00101
ξ_1	4.19E-03	-4.19E-03	6.48E-03	-6.47E-03	0.04992	-0.04990
ξ_2	4.19E-03	-4.19E-03	6.47E-03	-6.48E-03	0.04990	-0.04992
ξ_3	1.78E-04	-1.78E-04	2.56E-04	-2.56E-04	0.00183	-0.00183
ψ_1	2.95E-05	-2.96E-05	4.51E-05	-4.52E-05	0.00034	-0.00034
ψ_2	2.96E-05	-2.95E-05	4.52E-05	-4.51E-05	0.00034	-0.00034
ψ_3	2.58E-07	-2.58E-07	3.66E-07	-3.66E-07	2.57E-06	-2.57E-06
θ	1.56E-04	-3.26E-05	2.40E-04	-4.95E-05	0.00184	-0.00038

Table 10.4: Summary of numerical results for $\delta = -1$, $\hat{\gamma} = 0.3$, $Ra_L = 154816.654$, $Ra_E = 68802.297$, $Lx = 1.4$ and $Ly = 1.4$.

	$R^2 = 169000$		$R^2 = 179000$		$R^2 = 183000$	
	$\tau = 1.79825$		$\tau = 3.76835$		$\tau = 4$	
	Max	Min	Max	Min	Max	Min
u	1.69E-04	-1.70E-04	4.00E-04	-4.24E-04	0.06425	-0.07184
v	1.18E-04	-1.18E-04	2.83E-04	-2.83E-04	0.04586	-0.04586
w	2.96E-04	-9.81E-05	7.14E-04	-2.77E-04	0.11717	-0.04979
ξ_1	3.04E-03	-3.04E-03	7.36E-03	-7.36E-03	1.20230	-1.20229
ξ_2	4.20E-03	-4.18E-03	1.07E-02	-1.01E-02	1.80962	-1.62091
ξ_3	4.74E-04	-4.71E-04	1.16E-03	-1.15E-03	0.18827	-0.18816
ψ_1	1.93E-05	-1.93E-05	4.60E-05	-4.60E-05	0.00741	-0.00741
ψ_2	2.77E-05	-2.79E-05	6.50E-05	-6.90E-05	0.01043	-0.01169
ψ_3	7.09E-07	-7.05E-07	1.68E-06	-1.67E-06	0.00028	-0.00028
θ	1.28E-04	-3.94E-05	3.08E-04	-1.11E-04	0.05069	-0.02055

Table 10.5: Summary of numerical results for $\delta = -1$, $\hat{\gamma} = 0.31$, $Ra_L = 180365.749$, $Ra_E = 73174.607$, $Lx = 1.6$ and $Ly = 1.2$.

	$R^2 = 197000$		$R^2 = 206000$		$R^2 = 216000$	
	$\tau = 1.55835$		$\tau = 3.0146$		$\tau = 4$	
	Max	Min	Max	Min	Max	Min
u	1.56E-04	-1.70E-04	3.64E-04	-5.09E-04	3.96811	-5.99826
v	8.74E-05	-8.74E-05	2.30E-04	-2.30E-04	3.72197	-3.72072
w	2.56E-04	-1.44E-04	6.74E-04	-5.30E-04	4.57103	-10.88875
ξ_1	2.42E-03	-2.42E-03	6.42E-03	-6.42E-03	93.56001	-93.53506
ξ_2	4.40E-03	-4.07E-03	1.32E-02	-9.68E-03	149.12978	-107.62974
ξ_3	6.22E-04	-6.19E-04	1.77E-03	-1.77E-03	17.70996	-17.73222
ψ_1	1.39E-05	-1.39E-05	3.66E-05	-3.66E-05	0.64347	-0.64367
ψ_2	2.46E-05	-2.69E-05	5.67E-05	-8.05E-05	0.64702	-0.99582
ψ_3	8.37E-07	-8.33E-07	2.39E-06	-2.38E-06	0.02736	-0.02739
θ	1.09E-04	-5.94E-05	2.89E-04	-2.22E-04	1.93564	-3.88420

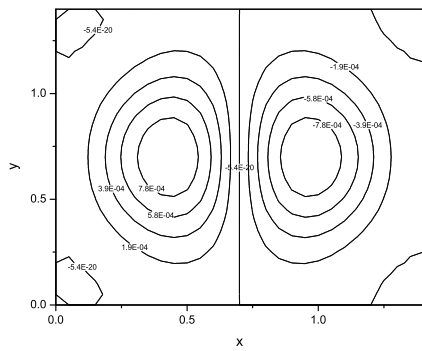
Table 10.6: Summary of numerical results for $\delta = -1$, $\hat{\gamma} = 0.32$, $Ra_L = 210613.017$, $Ra_E = 77376.734$, $Lx = 1.7$ and $Ly = 1.1$.

	$R^2 = 272000$		$R^2 = 282000$		$R^2 = 291000$	
	$\tau = 1.67595$		$\tau = 2.7606$		$\tau = 4$	
	Max	Min	Max	Min	Max	Min
u	1.33E-04	-1.33E-04	2.40E-04	-2.40E-04	0.03775	-0.03912
v	9.98E-05	-9.96E-05	1.79E-04	-1.79E-04	0.02802	-0.02801
w	2.51E-04	-7.33E-05	4.54E-04	-1.34E-04	0.07173	-0.02343
ξ_1	2.93E-03	-2.93E-03	5.30E-03	-5.29E-03	0.83860	-0.83848
ξ_2	3.75E-03	-3.76E-03	6.86E-03	-6.83E-03	1.12349	-1.07741
ξ_3	3.90E-04	-3.91E-04	6.89E-04	-6.89E-04	0.10748	-0.10737
ψ_1	1.54E-05	-1.54E-05	2.75E-05	-2.75E-05	0.00431	-0.00431
ψ_2	2.04E-05	-2.04E-05	3.67E-05	-3.67E-05	0.00577	-0.00598
ψ_3	4.71E-07	-4.72E-07	8.15E-07	-8.13E-07	0.00013	-0.00013
θ	1.06E-04	-2.77E-05	1.92E-04	-5.14E-05	0.03026	-0.00886

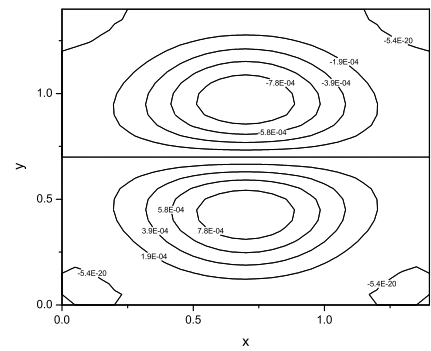
Table 10.7: Summary of numerical results for $\delta = -1$, $\hat{\gamma} = 0.34$, $Ra_L = 289395.588$, $Ra_E = 85204.774$, $Lx = 1.4$ and $Ly = 1.1$.

	$R^2 = 379000$		$R^2 = 395000$		$R^2 = 404000$	
	$\tau = 1.69925$		$\tau = 3.8083$		$\tau = 4$	
	Max	Min	Max	Min	Max	Min
u	1.19E-04	-1.18E-04	3.14E-04	-3.13E-04	0.12174	-0.12169
v	1.08E-04	-1.08E-04	2.85E-04	-2.85E-04	0.11014	-0.11013
w	2.52E-04	-6.04E-05	6.67E-04	-1.60E-04	0.25815	-0.06217
ξ_1	3.44E-03	-3.44E-03	9.18E-03	-9.18E-03	3.58302	-3.58280
ξ_2	3.72E-03	-3.73E-03	9.96E-03	-9.98E-03	3.90202	-3.90308
ξ_3	2.29E-04	-2.31E-04	5.76E-04	-5.79E-04	0.21958	-0.21970
ψ_1	1.62E-05	-1.63E-05	4.27E-05	-4.28E-05	0.01651	-0.01651
ψ_2	1.79E-05	-1.78E-05	4.71E-05	-4.69E-05	0.01822	-0.01821
ψ_3	2.36E-07	-2.39E-07	5.78E-07	-5.82E-07	0.00022	-0.00022
θ	1.04E-04	-2.23E-05	2.75E-04	-5.82E-05	0.10657	-0.02240

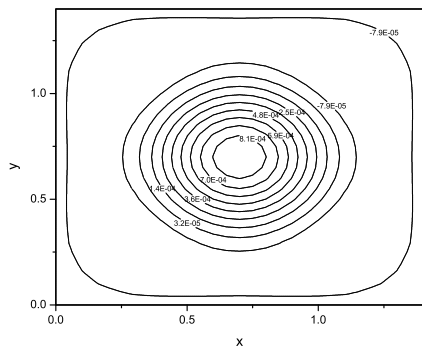
Table 10.8: Summary of numerical results for $\delta = -1$, $\hat{\gamma} = 0.36$, $Ra_L = 402309.378$, $Ra_E = 92178.900$, $Lx = 1.2$ and $Ly = 1.1$.



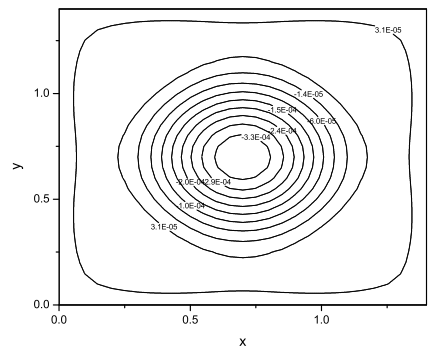
(a)



(b)

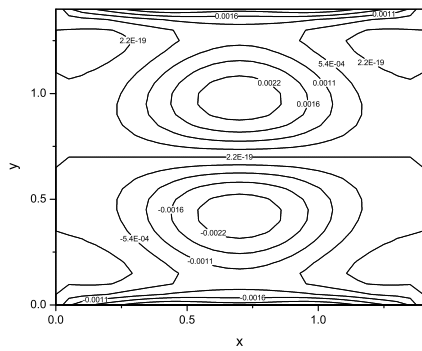


(c)

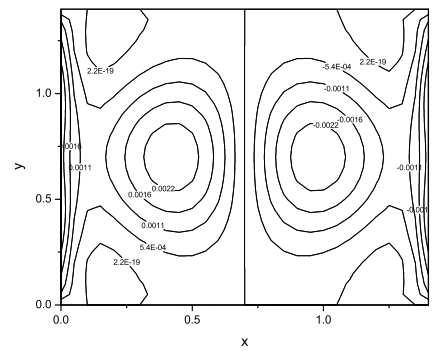


(d)

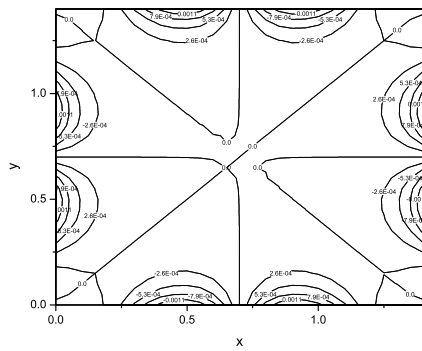
Figure 10.1: The contours map at $z = 0.5$. $\tau = 4$, $\delta = -1$, $\hat{\gamma} = 0.3$, $R^2 = 155000$, $Lx = 1.4$, $Ly = 1.4$, $\Delta t = 5 \times 10^{-5}$, $\Delta x = \Delta y = \Delta z = 0.02$. (a) u , (b) v , (c) w , (d) θ .



(a)

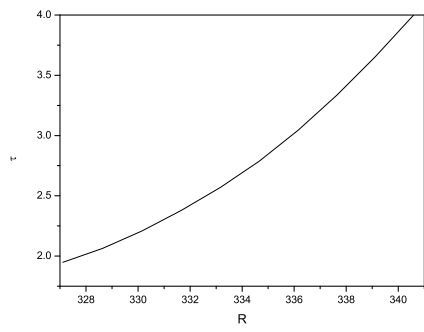


(b)

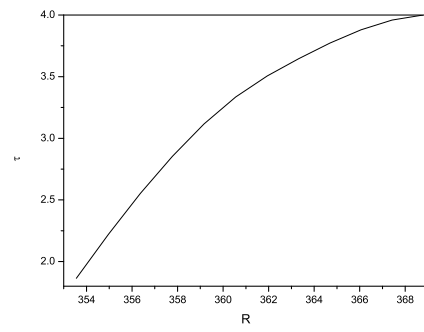


(c)

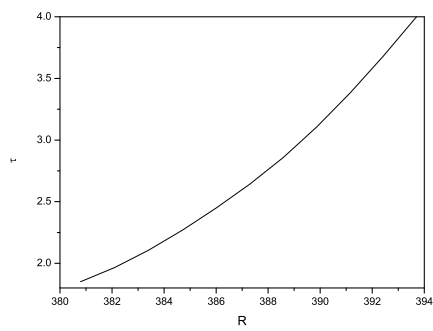
Figure 10.2: The contours map at $z = 0.5$, $\tau = 4$, $\delta = -1$, $\hat{\gamma} = 0.3$, $R^2 = 155000$, $Lx = 1.4$, $Ly = 1.4$, $\Delta t = 5 \times 10^{-5}$, $\Delta x = \Delta y = \Delta z = 0.02$. (a) ξ_1 , (b) ξ_2 , (c) ξ_3 .



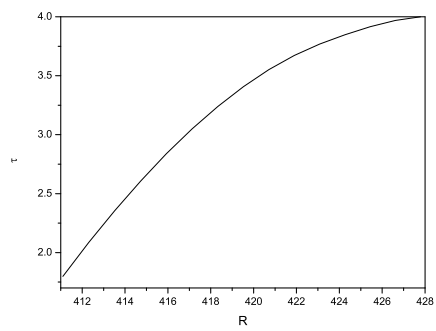
(a)



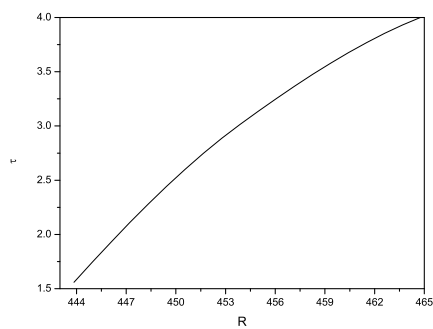
(b)



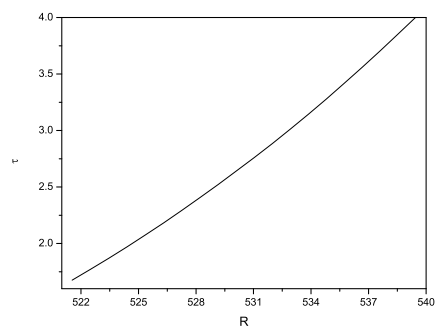
(c)



(d)



(e)



(f)

Figure 10.3: The required time to arrive at steady state versus R at $\delta = -1$ *a.* $\hat{\gamma} = 0.28$,
b. $\hat{\gamma} = 0.29$, *c.* $\hat{\gamma} = 0.3$, *d.* $\hat{\gamma} = 0.31$ *e.* $\hat{\gamma} = 0.32$, *f.* $\hat{\gamma} = 0.34$.

Chapter 11

Conclusions

The main aims of this thesis have been to investigate convection in fluid and porous media, and to develop efficient numerical methods to improve on the more commonly used techniques for these types of problems. Linear instability and nonlinear stability analyses have been employed to assess critical thresholds for the onset and type of convection involved, where a variety of numerical methods have been utilised including those developed in the thesis.

In Chapter 2, the problem of convection in a variable gravity field with magnetic field effect is studied by using methods of linear instability theory and nonlinear energy theory. Three numerical methods have been applied to get the numerical results of our problem, namely Chebyshev tau, finite difference (FD) and High order finite difference (HFD). One of the key reasons to apply different numerical methods is to see the advantages and disadvantages of each method when it is used to find the solution of linear and nonlinear problems. The advantage of Chebyshev tau method is that it can achieve the required accuracy using a small number of polynomials. However, the (FD) method need a large number of divisions to reach the required accuracy, whilst the (HFD) method can reach to the desired accuracy by using fewer divisions. However, in the problems of variable coefficients, the Chebyshev tau method is complicated to implement as this method depends on writing all functions in the system of equations in the form of Chebyshev polynomials, which could be very difficult in some cases.

Chapter 3 analyses the problem of convective movement of a reacting solute in

a viscous incompressible fluid occupying a plane layer and subjected to a vertical magnetic field. The results show the stabilizing effect of increasing the magnetic field and the chemical reaction on the critical Rayleigh number. We have chosen to employ a finite difference method to solve the eigenvalue system rather than Chebyshev tau or compound matrices, such as in Dongarra et al. [43], Straughan and Walker [201–203]. This is largely due to the finite difference method leading to matrices of the eigenvalue system that are non-singular and so we may employ LU decomposition, unlike the D^2 and D methods of Dongarra et al. [43] which necessarily have singular matrices and so necessitate use of the QZ algorithm. In addition, we found no occurrence of spurious eigenvalues which frequently arises with the Chebyshev tau method, cf., Dongarra et al. [43].

In Chapter 4, we study the problem of double-diffusive convection in a reacting fluid and magnetic field effect based internal heat source. We found that when the layer is heated above and salted below, the system is always stable. For the case where the layer is salted above and heated below, the spectrum σ is always real. However, when the layer is salted and heated from below, the spectrum σ has a complex value and the linear analysis stability is difficult because it includes an oscillatory convection. We found that the values of wave numbers for oscillatory convection are very close to the values of wave numbers for stationary convection, thus the computations of the critical Rayleigh numbers was especially difficult in the period around the intersection points. The results demonstrate the stabilizing effect of the magnetic field and the chemical reaction on the double-diffusive convection problem.

Further work could assess the practicality of developing numerical techniques for evaluating the eigenvalues. Now, we are developing the Newton-Raphson technique instead of the Secant method to evaluate the eigenvalues.

The problem of Poiseuille flow in a channel which is filled with a porous medium saturated with a linear viscous fluid has been studied in Chapter 5. We analyse when instability will commence and determine the critical Reynolds number as a function of the slip coefficient. For this problem, a referee has raised the interesting question as to how accurate we expect the linear instability results to be compared

to a nonlinear theory. This is one of the major problems in Poiseuille flow theory even in a clean fluid with no-slip boundary conditions, see e.g. Straughan [195], Chapter 8. Linear instability results guarantee that the solution will be unstable for a Rayleigh number which exceeds the linear threshold. It does not guarantee stability if the Rayleigh number is below this. One can sometimes calculate nonlinear energy stability thresholds which will guarantee nonlinear stability if the Rayleigh number is below this threshold although they say nothing about instability. We can calculate nonlinear energy stability thresholds for the problem considered here, just as was done in a porous medium with no-slip boundary conditions by Hill & Straughan [87], and as was done for a clear fluid with slip boundary conditions by Webber & Straughan [222]; the latter results are also carefully reported in Chapter 3 of Webber [223]. However, for the present problem the nonlinear energy stability thresholds which do guarantee the solution is stable, are well below those of linear theory. This is one area where nonlinear energy stability theory is not so useful. Such scenarios are not unknown in other areas of fluid mechanics, cf. Straughan [198], where exactly the same discrepancy is found between the linear instability boundaries and the global nonlinear stability thresholds. This does mean that there is a potential area between the two boundaries in which sub-critical instabilities may arise. In future, we intend, to compute a full three-dimensional simulation to calculate if and when sub-critical instabilities may arise. For many convection problems, ongoing computations do suggest there is a region of sub-critical instability below the linear instability threshold, but well above the nonlinear energy stability boundary.

In Chapter 6, we solve the stability problem of standard thermal convection in a thin fluid layer with free-free, slip-slip, and fixed-slip boundary conditions. We use different numerical methods to check their flexibility and accuracy where we use the following numerical methods: the second order finite difference method, the high order finite difference scheme, p order finite element method, the Chebyshev collocation method-1 and method-2 and Chebyshev tau technique. In conclusion, we believe that the finite difference and finite element methods are very flexible methods and we can apply them to solve any problem easily. However, the accuracy

of these methods is fewer than the accuracy of the Chebyshev methods. However, Chebyshev tau and Chebyshev collocation-1 are very accurate methods but not flexible. Thus, we strongly recommend the use of Chebyshev collocation method-2 as we found that this method was very accurate and flexible.

The purpose of following three chapters was to derive a priori continuous dependence estimates for some fundamental models. Chapter 7 deals with two fundamental models for convection in a reacting porous medium with magnetic field effect. We demonstrate that the solution depends continuously on changes in the chemical reaction and the electrical conductivity coefficients. We use Chapter 8 to deal with two fundamental models for convection in a reacting fluid and porous medium with magnetic field effect. We demonstrate that the solution depends continuously on changes in the chemical reaction and the electrical conductivity coefficients. The continuous dependence is unconditional in two-dimensions but conditional in three-dimensions. Finally, in Chapter 9, the Darcy model is used to describe the double diffusive flow of a fluid containing a solute. An a priori result is established whereby we show the solution depends continuously on changes in the magnetic and the gravity vector coefficients.

The problem of a layer of non-Boussinesq fluid heated internally (non-uniformly), with prescribed heat flux on the lower boundary and constant temperature on the upper surface has been studied in Chapter 10. The validity of both the linear instability and global nonlinear energy stability thresholds are tested using three dimensional simulation. Our results show that the linear threshold accurately predicts the onset of instability in the basic steady state. However, the required time to arrive at the steady state increases significantly as the Rayleigh number tends to the linear threshold. Numerically, we find that the convection has three different patterns. The first picture, where R^2 is less than Ra_L , is that the temperature, velocity, vorticity and potential perturbations vanish, sending the solution back to the steady state, before the linear thresholds are reached. The second picture, where R^2 is close to Ra_L , is that solutions can tend to a steady state which is different to the basic steady state. In the third picture, where $R^2 > Ra_L$, the solution does not arrive at any steady state and oscillate.

Although this thesis has concentrated on convection problems, the new methods presented can be adapted to many other classes of stability problem in Continuum Mechanics. For example, stability in fluid and porous media with a different governing law such as that of viscoelastic flows, and stability problems in elasticity or thermoelasticity.

Bibliography

- [1] K. A. Ames and L. E. Payne (1994), Continuous dependence results for solutions of the Navier- Stokes equations backward in time, *Nonlinear Anal., Theor., Meth., Appl.*, **23**, 103-113.
- [2] K. A. Ames and L. E. Payne (1994), On stabilizing against modeling errors in a penetrative convection problem for a porous medium, *Math. Models Meth. Appl. Sci.* **4**, 733-740.
- [3] K. A. Ames and L. E. Payne (1997), Continuous dependence results for a problem in penetrative convection, *Q. Appl. Math.* **55**, 769-790.
- [4] K. A. Ames and L. E. Payne (1998), Asymptotic behavior for two regularizations of the Cauchy problem for the backward heat equation, *Math. Models Meth. Appl. Sci.* **8**, 187-202.
- [5] K. A. Ames and B. Straughan (1997), Non-standard and improperly posed problems, New York: Academic, *Math. in Sci. and Engng. Series*, vol. 194.
- [6] P. Amili and Y. C. Yortsos (2004), Stability of heat pipes in vapor-dominated system, *Int. J. Heat Mass Trans.* **47**, 1223-1246.
- [7] M. Ashouri, B. Ebrahimi, M.B. Shafii, M.H. Saidi and M.S. Saidi (2010), Correlation for Nusselt number in pure magnetic convection ferrofluid flow in a square cavity by a numerical investigation, *J. Magnetism and Magnetic Materials* **322**, 3607-3613.

- [8] R. Avila, E. Ramos, and S. N. Atluri (2009), The Chebyshev tau spectral method for the solution of the linear stability equations for Rayleigh - Bénard convection with melting, *Comput. Modell. in Engng. and Sci.* **51**, 73–92.
- [9] K. Aziz and J. D. Hellums (1967), Numerical solution of the three-dimensional equations of motion of laminar natural convection, *Phys. Fluids* **10**, 314–324.
- [10] J. Badur, M. Karcz, and M. Lemanski (2011), On the mass and momentum transport in the Navier - Stokes slip layer, *Microfluid Nanofluid* **11**, 439–449.
- [11] P. G. Baines and A. E. Gill (1969), On thermohaline convection with linear gradients, *J. Fluid Mech.* **37**, 289–306.
- [12] D. Bandyopadhyay, P. D. S. Reddy, A. Sharma, S. W. Joo, and S. Qian (2012), Electro-magnetic field induced flow and interfacial instabilities in confined stratified liquid layers, *Theor. Comput. Fluid Dyn.* **26**, 23–28.
- [13] C. Bandle (1980), *Isoperimetric Inequalities and Their Applications*, Pitman Press, London.
- [14] A. Barletta (2009), Local energy balance, specific heats and the Oberbeck-Boussinesq approximation, *Int. J. Heat Mass Trans.* **52**, 5266–5270.
- [15] A. Barletta and D. A. Nield (2009), Effect of pressure work and viscous dissipation in the analysis of the Rayleigh-Bénard problem, *Int. J. Heat Mass Trans.* **52**, 3279–3289.
- [16] A. Barletta and D. A. Nield (2010), Extended Oberbeck-Boussinesq approximation study of convective instabilities in a porous layer with horizontal flow and bottom heating, *Int. J. Heat Mass Trans.* **53**, 577–585.
- [17] A. P. Bassom, M. G. Blyth, and D. T. Papageorgiou (2012), Using surfactants to stabilize two-phase pipe flows of core-annular type, *J. Fluid Mech.* **704**, 333–359.

- [18] M. Basurto and S. Lombardo (2003), Global nonlinear stability in the Bénard problem for a mixture near the bifurcation point, *Continuum Mech. Thermodyn.* **15**, 265-274.
- [19] N. Bellomo and L. Preziosi (1995), Modelling mathematical methods and scientific computation, Boca Raton, FL: CRC Press.
- [20] P. Bera and A. Khalili (2006), Influence of Prandtl number on stability of mixed convective flow in a vertical channel filled with a porous medium, *Phys. Fluids* **18**, 124103.
- [21] P. Bera, J. Kumar and A. Khalili (2011), Hot springs mediate spatial exchange of heat and mass in the enclosed sediment domain: A stability perspective, *Advances in Water Resources* **34**, 817-828.
- [22] J. Boussinesq (1903), Théorie Analytique de la Chaleur, *Gauthier-Villars, Paris* **2**, 172.
- [23] F. Capone, M. Gentile and A. A. Hill (2008), Penetrative convection in a fluid layer with throughflow, *Ricerche mat.* **57**, 251-260.
- [24] F. Capone, M. Gentile and A. A. Hill (2009), Anisotropy and symmetry in porous media convection, *Acta Mech.* **208**, 205-214.
- [25] F. Capone, M. Gentile and A. A. Hill (2010), Penetrative convection via internal heating in anisotropic porous media, *Mech. Res. Communications* **37**, 441-444.
- [26] F. Capone, M. Gentile and A. A. Hill (2011), Penetrative convection in anisotropic porous media with variable permeability, *Acta Mech.* **216**, 49-58.
- [27] F. Capone, M. Gentile and A. A. Hill (2011), Double - diffusive penetrative convection simulated via internal heating in an anisotropic porous layer with throughflow, *Int. J. Heat Mass Trans.* **54**, 1622-1626.

- [28] F. Capone and R. D. Luca (2012), Ultimately boundedness and stability of triply diffusive mixtures in rotating porous layers under the action of Brinkman law, *Int. J. non-linear Mech.* **57**, 799-805.
- [29] F. Capone, R. D. Luca and I. Torricollo (2013), Longtime behavior of vertical throughflows for binary mixtures in porous layers, *Int. J. non-linear Mech.*, **57**, 1-7.
- [30] M. A. Celia, J. S. Kindred and I. Herrera (1989), Contaminant transport and biodegradation. I. A numerical model for reactive transport in porous media, *Water Resources Res.* **25**, 1141-1148.
- [31] C. Cercignani (1988), The Boltzmann equation and its applications, Springer, Berlin.
- [32] S. Chandrasekhar (1981), Hydrodynamic and hydromagnetic stability, *Dover*, New York.
- [33] B. Chen, A. Cunningham, R. Ewing, R. Peralta and E. Visser (1994), Two-dimensional modelling of microscale transport and biotransformation in porous media, *Numer. Meth. PDEs* **10**, 65-83.
- [34] R. Chertovskih, S.M.A. Gama, O. Podvigina and V. Zheligovsky (2010), Dependence of magnetic field generation by thermal convection on the rotation rate: A case study, *Physica D: Nonlinear Phenomena*, **239**, 1188-1209.
- [35] X. Chen, S. Wang and J. Tao (2011), Stability analysis of thermosolutal convection in a horizontal porous layer using a thermal non-equilibrium model, *Int. J. Heat Fluid Flow* **32**, 78-87.
- [36] P. Cheng (1978), Heat transfer in geothermal systems, *Advances in Heat Trans.*, **14** (1978) 1-105.
- [37] W. K. Chu (2000), Stability of incompressible helium II: a two fluid system, *J. Phys.: Condensed Matter* **12**, 8065-8069.

- [38] A. K. Chu (2004), Instability of Navier slip flow of liquids, *Comptes Rendue, Mécanique* **332**, 895–900.
- [39] G. Cimatti (2010), A class of explicit solutions for the Soret-Dufour boundary value problem in arbitrary domains, *Ricerche mat.* **59**, 199-205.
- [40] M. C. Curran and M. B. Allen (1990), Parallel computing for solute transport models via alternating direction collocation, *Advances in Water Resources* **13**, 70-75.
- [41] J. Delgado, H. N. Nunez-Yepey and A. L. Salas-Brito (2004), On the Lagrangian form of the variational equations of Lagrangian dynamical systems, *Chaos Solitions Fractals* **20**, 925-935.
- [42] S. C. R. Dennis, D. B. Ingham and R. W. Cook (1979), Finite difference methods for calculating steady incompressible flows in three dimensions, *J. Comp. Phys.* **33**, 325-339.
- [43] J. J. Dongarra, B. Straughan, and D. W. Walker (1996), Chebyshev tau - QZ algorithm methods for calculating spectra of hydrodynamic stability problems, *Appl. Numer. Math.* **22**, 399–435.
- [44] I. Dragomirescu and A. Georgescu (2006), Linear stability bounds in a convection problem for variable gravity field, *buletinul academiei de stiinte a republicii moldova. matematica* **3(52)**, 51-56.
- [45] F. I. Dragomirescu and C. I. Gheorghiu (2010), Analytical and numerical solutions to an electrohydrodynamic stability problem, *Appl. Math. Comp.* **59**, 3718–3727.
- [46] P. G. Drazin and W. H. Reid (1981), Hydrodynamic Stability, *Cambridge University Press, Cambridge*.
- [47] Z. Duan and Y. S. Muzychka (2007), Slip flow in non-circular microchannels, *Microfluid Nanofluid* **3**, 473–484.

- [48] Z. Duan (2012), Second-order gaseous slip flow models in long circular and noncircular microchannels and nanochannels, *Microfluid Nanofluid*, **12**, 805–820.
- [49] I. A. Eltayeb, E. A. Hamza, J. A. Jervase, E.V. Krishnan and D. E. Loper (2004), Compositional convection in the presence of a magnetic field. I. A single interface, *Proc. Roy. Soc. Lond. A* **460**, 3505-3528.
- [50] I. A. Eltayeb, E.A. Hamza, J. A. Jervase, E.V. Krishnan and D.E. Loper (2005), Compositional convection in the presence of a magnetic field. I. Cartesian plume, *Proc. Roy. Soc. Lond. A* **461**, 2605-2633.
- [51] R. E. Ewing and S. Weekes (1998), Numerical methods for contaminant transport in porous media, *Marcel Decker, Inc.: New York* **Vol. 202**, 75-95.
- [52] M. Fabrizio and A. Morro (2003), Electromagnetism of continuous media, *Oxford University Press*, Oxford.
- [53] L. Fox (1962), Chebyshev methods for ordinary differential equations, *Computer J.* **4**, 318-331.
- [54] F. Franchi and B. Straughan (1993), Continuous dependence on the body force for solutions to the Navier-Stokes equations and on the heat supply in a model for double-diffusive porous convection, *J. Math. Anal. Appl.* **172**, 117-129.
- [55] F. Franchi and B. Straughan (1994), Continuous dependence on the relaxation time and modelling, and unbounded growth, *J. Math. Anal. Appl.* **185**, 726-746.
- [56] F. Franchi and B. Straughan (1994), Spatial decay estimates and continuous dependence on modelling for an equation from dynamo theory, *Proc. R. Soc. Lond. A* **445**, 437-451.
- [57] F. Franchi and B. Straughan (1996), Structural stability for the Brinkman equations of porous media, *Math. Meth. Appl. Sci.* **19**, 1335-1347.

- [58] F. Franchi and B. Straughan (2001), A comparison of the Graffi and Kazhikhov-Smagulov models for top heavy pollution instability, *Advances in Water Resources* **24**, 585-594.
- [59] S.N. Gaikwad, M.S. Malashetty and K. R. Prasad (2007), An analytical study of linear and non-linear double diffusive convection with Soret and Dufour effects in couple stress fluid, *Int. J. of Non-Linear Mech.* **42**, 903-913.
- [60] G.P. Galdi (1985), Nonlinear stability of the magnetic Bénard problem via a generalized energy method, *Arch. Rat. Mech. Anal.* **87**, 167-186.
- [61] G. P. Galdi and B. Straughan (1985), Exchange of stabilities, symmetry and nonlinear stability, *Arch. Rat. Mech. Anal.* **89**, 211-228.
- [62] A. Georgescu and I. Dragomirescu (2009), Linear stability results in a magneto-thermoconvection problem, *An. Șt. Univ. Ovidius Constanța* **17**, 119-129.
- [63] B. Ghasemi, S.M. Aminossadati and A. Raisi (2011), Magnetic field effect on natural convection in a nanofluid-filled square enclosure, *Int. J. Therm. Sci.* **50**, 1748-1756.
- [64] C. I. Gheorghiu, F. Dragomirescu (2009), Spectral methods in linear stability. Applications to thermal convection with variable gravity field, *Appl. Numer. Math.* **59**, 1290-1302.
- [65] C. I. Gheorghiu and I. S. Pop (1997), A modified Chebyshev-tau method for a hydrodynamic stability problem, *Proc. ICAOR '97, Transylvania Press, Cluj-Napoca* **2**, 119-126.
- [66] C. I. Gheorghiu and J. Rommes (2012), Application of the Jacobi - Davidson method to accurate analysis of singular linear hydrodynamic stability problems, *Int. J. Numer. Meth. Fluids*, doi: 10.1002/flid.3669.
- [67] A. Gilman and J. Bear (1996), The influence of free convection on soil salinization in arid regions, *Transp. Porous Media* **23**, 275-301.

- [68] L. Greenberg L and M. Marletta (2004), The Ekman flow and related problems: spectral theory and numerical analysis, *Math. Proc. Camb. Phil. Soc.* **136**, 719-764.
- [69] P. M. Gresho (1991), Incompressible fluid dynamics: some fundamental formulation issues, *Ann. Rev. Fluid Mech.* **23**, 413-453.
- [70] R. W. Grichth (1981), Layered double-diffusive convection in porous media, *J. Fluid Mech.* **102**, 221-248.
- [71] J. Guo and Kaloni (2005), Double-diffusive convection in porous medium, nonlinear stability, *Stud. Appl. Math.* **94**, 341-358.
- [72] A. J. Harfash (2014), Convection in a variable gravity field with magnetic field effect, manuscript.
- [73] A. J. Harfash and B. Straughan (2012), Magnetic effect on instability and nonlinear stability in a reacting fluid, *Meccanica.* **47**, 1849-1857.
- [74] A. J. Harfash (2013), Magnetic effect on instability and nonlinear stability of double diffusive convection in a reacting fluid, *Continuum Mech. Thermodyn.* **25**, 89-106.
- [75] A. J. Harfash(2014), Numerical methods for solving some hydrodynamic stability problems. manuscript.
- [76] A. J. Harfash (2014), Structural stability for convection models in a reacting porous medium with magnetic field effect, *Ricerche mat.* **63**, 1-13.
- [77] A. J. Harfash (2014), Structural stability for two convection models in a reacting fluid with magnetic field effect, *Ann. Henri Poincaré*, doi 10.1007/s00023-013-0307-z.
- [78] A. J. Harfash (2013), Continuous dependence on the coefficients for double diffusive convection in Darcy flow with Magnetic field effect, *Anal. Math. Phys.* **3**, 163-181.

- [79] A. J. Harfash (2014), Three dimensions simulation for the problem of a layer of non-Boussinesq fluid heated internally with prescribed heat flux on the lower boundary and constant temperature upper surface, *Int. J. Engng. Sci.* **74**, 91-102.
- [80] T. Hayat and M. Nawaz (2011), Unsteady stagnation point flow of viscous fluid caused by an impulsively rotating disk, *J. Taiwan Inst. Chem. Engng.* **42**, 41-49.
- [81] K. Hibino, H. Ishikawa and K. Ishioka (2012), Effect of a capping inversion on the stability of an Ekman boundary layer, *J. Meteorological Soc. Japan*, **90** 311–319.
- [82] A. A. Hill (2008), Global stability for penetrative double-diffusive convection in a porous medium, *Acta Mech.* **200**, 1-10.
- [83] A. A. Hill and M. Carr (2010), Sharp global nonlinear stability for a fluid overlying a highly porous material, *Proc. Roy. Soc. Lond. A* **7**, 127-140.
- [84] A. A. Hill and M. S. Malashetty (2012), An operative method to obtain sharp nonlinear stability for systems with spatially dependent coefficients, *Proc. Roy. Soc. Lond. A* **468**, 2695-2705.
- [85] R. N. Hills and P. H. Roberts (1991), On the motion of a fluid that is incompressible in a generalized sense and its relationship to the Boussinesq Approximation, *SAACM* **1**, 205-212.
- [86] A.A. Hill and B. Straughan (2003), A Legendre spectral element method for eigenvalues in hydromagnetic stability, *J. Comp. Appl. Math.* **193**, 363-381.
- [87] A. A. Hill and B. Straughan (2010), Stability of Poiseuille flow in a porous medium, In R. Rannacher and A. Sequeira, editors, *Advances in Mathematical Fluid Mechanics*, pages 287–293. Springer, Heidelberg.
- [88] M. W. Hirsch and S. Smale (1974), Differential equation, dynamical systems, and linear algebra, *Academic Press*, New York.

- [89] D. D. Joseph (1965), On the stability of the Boussinesq equations, *Arch. Rat. Mech. Anal.*, **20** (1965) 59-71.
- [90] D. D. Joseph (1966), Nonlinear stability of the Boussinesq equations by the method of energy, *Arch. Rat. Mech. Anal.* **22**, 163-184.
- [91] D. D. Joseph (1970), Global stability of the conduction-diffusion solution, *Arch. Rat. Mech. Anal.* **36**, 285-292.
- [92] D.D. Joseph (1976), Stability of Fluid Motions II, *Springer, Berlin*.
- [93] R. Kaiser and G. Mulone (2005), A note on nonlinear stability of plane parallel shear flows, *J. Math. Anal. Appl.* **302**, 543-556.
- [94] P. N. Kaloni and A. Mahajan (2011), Stability of magnetic fluid motions in a saturated porous medium, *ZAMP* **62**, 529-538.
- [95] A. Khoshnood and M. A. Jalali (2012), Long-lived and unstable modes of Brownian suspensions in microchannels, *J. Fluid Mech.* **701**, 407-418.
- [96] I. H. C. Ku, R. S. Hirsh and T. D. Taylor (1987), A pseudospectral method for solution of the three-dimensional incompressible, *J. Comp. Phy.* **70**, 439-462.
- [97] A. Kumar, P. Bera and A. Khalili (2010), Influence of inertia and drag terms on the stability of mixed convection in a vertical porous-medium channel, *Int. J. Heat Mass Trans.* **53**, 23-24.
- [98] A. Kumar, P. Bera and J. Kumar (2011), Non-Darcy mixed convection in a vertical pipe filled with porous medium, *Int. J. Therm. Sci.* **50**, 725-735.
- [99] M. Landeau and J. Aubert (2011), Equatorially asymmetric convection inducing a hemispherical magnetic field in rotating spheres and implications for the past martian dynamo, *Phy. of the Earth and Planetary Interiors* **185**, 61-73.
- [100] L. Landau, E. Lifshitz and L. Pitaevskii (1984), Electrodynamics of continuous media, *Pergamon, London*.

- [101] E. Lauga, M. P. Brenner and H. A. Stone (2007), Microfluidics: the no-slip boundary condition. In C. Tropea, A. Yarin, and J. F. Foss, editors, *Handbook of Experimental Fluid Dynamics*, pages 1219–1240. Springer, 2007.
- [102] E. Lauga and C. Cossu (2005), A note on the stability of slip channel flows, *Phys. Fluids* **17**, 088106.
- [103] J. Leblanca, A. Akbarzadeha, J. Andrews a and H. Lub, P. Goldingb (2011), Heat extraction methods from salinity-gradient solar ponds and introduction of a novel system of heat extraction for improved efficiency, *Solar Energy* **85**, 3103-3142.
- [104] Y. S. Lee and C. H. Chun (1999), Effects of a cusp magnetic field on the oscillatory convection coupled with crucible rotation in Czochralski crystal growth, *J. of Crystal Growth* **197**, 307-316.
- [105] L. P. Lefebvre, J. Banhart and D. C. Dunand (2008), Porous metals and metallic foams: current status and recent developments, *Adv. Engng. Materials* **10**, 775–787.
- [106] C. Lin and L. E. Payne (1993), On the spatial decay of ill-posed parabolic problems, *Math. Meth. Appl. Sci.* **3**, 563-575.
- [107] C. Lin and L. E. Payne (1994), The influence of domain and diffusivity perturbations on the decay of end effects in heat conduction, *SIAM J. Math. Anal.* **25**, 1242-1258.
- [108] C. Lin and L. E. Payne (2007), Structural stability for a Brinkman fluid, *Math, Math. Meth. Appl. Sci.* **30**, 567-578.
- [109] C. Lin and L. E. Payne (2007), Structural stability for the Brinkman equations of flow in double diffusive convection, *J. Math. Anal. Appl.* **325**, 1479-1490.
- [110] C. Lin and L. E. Payne (2008), Continuous dependence on the Soret coefficient for double diffusive convection in Darcy flow, *J. Math. Anal. Appl.* **342**, 311-325.

- [111] S. Lombardo, G. Mulone and S. Rionero (2001), Global nonlinear exponential stability of the conduction-diffusion solution for Schmidt numbers greater than Prandtl numbers, *J. Math. Anal. Appl.* **262**, 191-207.
- [112] S. Lombardo, G. Mulone and B. Straughan (2001), Non-linear stability in the Benard problem for a double-diffusive mixture in a porous medium, *Math. Meth. Appl. Sci.* **24**, 1229-1246.
- [113] L. Lorenz (1881), über das Leitungsvermögen der Metalle für Wärme und Elektrizität, *Ann. Phys. Chem.* **13**, 581.
- [114] A. Ludvigsen, E. Palm and R. Mckibbin (1992), Convective momentum and mass transport in porous sloping layers, *J. Geophys. Res. B* **97**, 12315-12325.
- [115] C. Ma (2009), Lattice BGK simulations of double diffusive natural convection in a rectangular enclosure in the presences of magnetic field and heat source, *Nonlinear Anal.: Real World Appl.* **10**, 2666-2678.
- [116] S. Maehlmann and D. T. Papageorgiou (2011), Interfacial instability in electrified plane Couette flow, *J. Fluid Mech.* **666**, 155-188.
- [117] A. Mahdy, A.J. Chamkha and Y. Baba (2010), Double-diffusive convection with variable viscosity from a vertical truncated cone in porous media in the presence of magnetic field and radiation effects, *Comp. Math. with Appl.* **59**, 3867-3878.
- [118] A. Mahidjiba, A. Mamou and P. Vasseur (2000), onset of double-diffusive convection in in rectangular porous cavity subject to mixed boundary conditions, *Int. J. Heat Mass Trans.* **43**, 1505-1522.
- [119] A. Mahidjiba, P. Vasseur, and E. Bilgen (1995), Multiple solution for double-diffusive convection in porous enclosures, *Int. J. Heat Mass Trans.* **38**, 623-630.
- [120] M. S. Malashetty and B. S. Biradar (2011), The onset of double diffusive reaction - convection in an anisotropic porous layer, *Phys. Fluids*, **23**, 064102.

- [121] M. S. Malashetty, I. Pop and R. Heera (2009), Linear and nonlinear double diffusive convection in a rotating sparsely packed porous layer using a thermal non-equilibrium model, *Continuum Mech. Thermodyn.*, **21** (2009) 317-339.
- [122] S. V. Malik and A. P. Hooper (2007), Three-dimensional disturbances in channel flows, *Phys. Fluids* **19**, 052102–052102.
- [123] G. D. Mallinson and G. de Vahl Davis (1977), Three-dimensional natural convection in a box: a numerical study, *J. Fluid Mech.* **83**, 1-31.
- [124] M. Mamou (2002), Stability analysis of double-diffusive convection in porous enclosures, In: Ingham, D.B., Pop, I. (eds.) *Transport Phenomena in Porous Media II*. Elsevier, Oxford, 113-154.
- [125] L. Massa and P. Jha (2012), Linear analysis of the Richtmyer - Meshov instability in shock flame interactions, *Phys. Fluids* **24**, 056101.
- [126] J. C. Maxwell (1879), On stresses in rarefied gases arising from inequalities of temperature, *Phil. Trans. Roy. Soc. Lond.* **170**, 231–256.
- [127] A. Mojtabi and M. C. Charrier-Mojtabi (2005), Double-diffusive convection in porous media. In: Vafai, K. (ed.) *Handbook of Porous media*, 2nd edn. Taylor and Francis, New York , 269-320.
- [128] G. L. Morini, M. Lorenzini and M. Spiga (2005), A criterion for experimental validation of slip - flow models for incompressible rarefied gases through microchannels, *Microfluid Nanofluid* **1**, 190–196.
- [129] G. Mulone (1994), On the nonlinear stability of a fluid layer of a mixture heated and salted from below. *Continuum Mech. Thermodyn.* **6**, 161-184.
- [130] C. E. Nanjundappa, M. Ravisha, J. Lee and I. S. Shivakumara (2011), Penetrative ferroconvection in a porous layer, *Acta Mech.* **216**, 243-257.
- [131] C. L. M. H. Navier (1823), Mémoire sur les lois du mouvement des fluides, *Mémoires de l'Academie Royale des Sciences d l'Institut de France* **6**, 389-440.

- [132] B. S. Ng and W. H. Reid (1979), An initial-value method for eigenvalue problems using compound matrices, *J. Comp. Phys.* **30**, 125-136.
- [133] B. S. Ng and W. H. Reid (1980), On the numerical solution of the Orr-Sommerfeld problem: asymptotic initial conditions for shooting methods, *J. Comp. Phys.* **38**, 275-293.
- [134] B. S. Ng and W. H. Reid (1985), The compound matrix method for ordinary differential systems, *J. Comp. Phys.* **58**, 209-228.
- [135] Z. Nie, L. Bu, M. Zheng and W. Huang (2011), Experimental study of natural brine solar ponds in Tibet, *Solar Energy* **85**, 1537-1542.
- [136] D. A. Nield (1968), Onset of thermohaline convection in a porous medium, *Water Resources Res.*, **4**, 553-560.
- [137] D. A. Nield (2003), The stability of flow in a channel or duct occupied by a porous medium, *Int. J. Heat Mass Trans.* **46**, 4351-4354.
- [138] D. A. Nield and A. Bejan (2013), *Convection in Porous Media. 4th edn.* Springer-Verlag.
- [139] A. Oberbeck (1879), Über die Wärmeleitung der Flüssigkeiten bei der Berücksichtigung der Strömungen infolge von Temperaturdifferenzen, *Ann. Phys. Chem.* **7**, 271.
- [140] S. Orszag (1971), Accurate solutions of OrrSommerfeld stability equation, *J. Fluid Mech.* **50**, 689-703.
- [141] M. Padula (1986), Non-linear energy stability for the compressible Benard problem, *Boll. U.M.I. B (6)* **5**, 581-602.
- [142] N. C. Papanicolaou, C. Christov and P.M. Jordan (2011), The influence of thermal relaxation on the oscillatory properties of two-gradient convection in a vertical slot, *European J. Mech. B - Fluids* **30**, 68-75.

- [143] L. E. Payne, J. C. Song and B. Straughan (1999), Continuous dependence and convergence results for Brinkman and Forchheimer models with variable viscosity, *Proc. R. Soc. Lond.* **A 455**, 2173-2190.
- [144] L. E. Payne and J. C. Song (1997), Spatial decay estimates for the Brinkman and Darcy flows in a semi-infinite cylinder, *Continuum Mech. Thermodyn.* **9** 175-190.
- [145] L. E. Payne and J. C. Song (2000), Spatial decay for a model of double diffusive convection in Darcy and Brinkman flows, *ZAMP* **51**, 867-880.
- [146] L. E. Payne and J. C. Song (2007), Spatial decay bounds in double diffusive convection in Darcy flow, *J. Math. Anal. Appl.* **330**, 864-875.
- [147] L. E. Payne and B. Straughan (1989), A Comparison of viscous flows backward in time with small data, *Int. J. Nonlinear Mech.* **24**, 209-214.
- [148] L. E. Payne and B. Straughan (1990), Error estimates for the temperature of a piece of cold ice, given data on only part of the boundary, *Nonlinear Anal., Theor., Meth., Appl.*, **14**, 443-452.
- [149] L. E. Payne and B. Straughan (1996), Stability in the initial-time geometry problem for the Brinkman and Darcy equations of flow in porous media, *J. Math. Pures Appl.* **75**, 225-271.
- [150] L. E. Payne and B. Straughan (1998), Analysis of the boundary condition at the interface between a viscous and a porous medium and related modelling questions, *J. Math. Pures Appl.* **77**, 317-354.
- [151] L. E. Payne and B. Straughan (1998), Structural stability for the Darcy equations of flow in porous media, *Proc. R. Soc. Lond.* **A 454**, 1691-1698.
- [152] L. E. Payne and B. Straughan (1999), Convergence and continuous dependence for Brinkman-Forchheimer equations, *Stud. Appl. Math.* **A 102**, 419-439.
- [153] L.E. Payne and H.F. Weinberger (1958), New bounds for solutions of second order elliptic partial differential equations, *Pacific J. Math.* **8**, 551-573.

- [154] D. Poulikakos (1986), Double diffusive convection in a horizontally sparsely packed porous layer, *Int. Communications Heat Mass Transf.* **13**, 587-598.
- [155] G. K. Pradhan and P. C. Samal (1987), Thermal stability of a fluid layer under variable body forces, *J. Math. Anal. Appl.* **122**, 487-495.
- [156] N. V. Priezjev (2013), Molecular dynamics simulations of oscillatory Couette flows with slip boundary conditions, *Microfluid Nanofluid* **14**, 225–233.
- [157] M. M. Rahman and M. Al-Lawatia (2010), Effects of higher order chemical reaction on micropolar fluid flow on a power law permeable stretched sheet with variable concentration in a porous medium, *Can. J. Chem. Eng.* **88**, 23-32.
- [158] M. M. Rahman, M. A. Al-Lawatia, I. A. Eltayeb and N. Al-Salti (2012), Hydromagnetic slip flow of water based nanofluids past a wedge with convective surface in the presence of heat generation or absorption, *Int. J. Therm. Sci.* **57**, 172–182.
- [159] M. M. Rahman, R. Saidur and N. A. Rahim (2011), Conjugated effect of joule heating and magneto-hydrodynamic on double-diffusive mixed convection in a horizontal channel with an open cavity, *Int. J. Heat Mass Trans.* **54**, 3201-3213.
- [160] K. R. Rajagopal (2006), On implicit constitutive theories. *J. Fluid Mech.* **550**, 243-249.
- [161] K. R. Rajagopal, M. Ruzicka and A. R. Srinivasa (1996), On the Oberbeck-Boussinesq approximation, *Math. Models and Meth. in Appl. Sci.* **6**, 1157-1167.
- [162] K. R. Rajagopala, G. Saccomandi and L. Vergori (2009), On the Oberbeck-Boussinesq approximation for fluids with pressure dependent viscosities, *Non-linear Anal.: Real World Appl.* **10**, 1139-1150.
- [163] Lord Rayleigh (1916), On convective currents in a horizontal layer of fluid, when the higher temperature is on the under side, *Philosophical Magazine* **32**, 529-546.

- [164] P. D. S. Reddy, D. Bandyopadhyay, S. W. Joo, A. Sharma and S. Qian (2011), Parametric study on instabilities in a two-layer electromagnetohydrodynamic channel flow confined between two parallel electrodes, *Phys. Rev. E* **83**, 036313.
- [165] S. Rionero (1967), Sulla stabilità asintotica in media in magnetoidrodinamic, *Annali di Matematica Pura ed Applicata* **76**, 75-92.
- [166] S. Rionero (1967), Sulla stabilità asintotica in media in magnetoidrodinamica non isoterma, *Ricerche mat.* **16**, 250-263.
- [167] S. Rionero (1968), Metodi variazionali stabilità asintotica in media in magnetoidrodinamica, *Annali di Matematica Pura ed Applicata* **78**, 339-364.
- [168] S. Rionero (1968), Sulla stabilità magnetoidrodinamica in media con vari tipi di condizioni al contorno, *Ricerche mat.* **17**, 64-78.
- [169] S. Rionero (1968), Metodi variazionali per la stabilità asintotica in media in magnetoidrodinamica, *Annali di Matematica Pura ed Applicata* **78**, 339-364.
- [170] S. Rionero (1970), Sulla stabilità nonlinear asintotica in media in magnetoidrodinamica, *Ricerche mat.*, 19, (1970) 269-285.
- [171] S. Rionero (1971), Sulla stabilità magnetoidrodinamica nonlinear asintotica in media in presenza di effetto hall, *Ricerche mat.* **20**, 285-296.
- [172] S. Rionero (2011), Onset of convection in porous materials with vertically stratified porosity, *Acta Mech* **222**, 261-272.
- [173] S. Rionero (2012), Global non-linear stability in double diffusive convection via hidden symmetries, *Int. J. non-linear mechanics* **47**, 61-66.
- [174] S. Rionero (2012), Global nonlinear stability for a triply diffusive convection in a porous layer, *Continuum Mech. Thermodyn.* **24**, 629-641.
- [175] S. Rionero (2012), Absence of subcritical instabilities and global nonlinear stability for porous ternary diffusive-convective fluid mixtures, *Physics of fluids* **24**, 104101.

- [176] S. Rionero (2013), Triple diffusive convection in porous media, *Acta Mech* **224**, 447-458.
- [177] S. Rionero and G. Mulone (1988), Nonlinear stability analysis of the magnetic Bénard problem through the Lyapunov direct method, *Arch. Rat. Mech. Anal.* **103**, 347-368.
- [178] S. Rionero and L. Vergori (2010), Long-time behaviour of fluid motions in porous media according to the Brinkman model, *Acta Mech* **210**, 221-240.
- [179] P. H. Roberts (1967), An introduction to magnetohydrodynamics, *Longman*, London.
- [180] H. Rubin (1973), Effect of nonlinear stabilizing salinity profiles on thermal convection in a porous medium layer, *Water Resources Research* **9**, 211-248.
- [181] N. Rudraiah and M. S. Malashetty (1986), The influence of coupled molecular diffusion on the double diffusive convection in a porous medium, *ASME J. Heat Transf.* **108**, 872-876.
- [182] N. Rudraiah, P. K. Srimani and R. Friedrich (1982), Finite amplitude convection in a two component fluid saturated porous layer, *Heat Mass Transf.* **25**, 715-722.
- [183] S. Saravanan and D. Brindha (2011), Linear and non-linear stability limits for centrifugal convection in an anisotropic layer, *Int. J Nonlinear Mech.* **46**, 65-72.
- [184] S. Saravanan, and T. Sivakumar, Onset of thermovibrational filtration convection: departure from thermal equilibrium. *Phys. Rev. E*, **84** (2011) 026307.
- [185] I. S. Shivakumara, J. Lee, , K. Vajravelu and A. L. Mamatha (2011), Effects of thermal nonequilibrium and non-uniform temperature gradients on the onset of convection in a heterogeneous porous medium, *Int. Communications Heat Mass Trans.* **38**, 906-910.

- [186] I. S. Shivakumara, J. Lee and K. B. Chavaraddi (2011), Onset of surface tension driven convection in a fluid layer overlying a layer of an anisotropic porous medium, *Int. J. Heat Mass Trans.* **54**, 994-1001.
- [187] I. S. Shivakumara, J. Lee, M. Ravisha and R. G. Raddy (2011), Effects of MFD viscosity and LTNE on the onset of ferromagnetic convection in a porous medium, *Int. J. Heat Mass Trans.* **54**, 2630-2641.
- [188] I. S. Shivakumara, C. O. Ng and M. S. Nagashree (2011), The onset of electrothermoconvection in a rotating Brinkman porous layer, *Int. J. Engng. Sci.* **49**, 6464-663.
- [189] M. Shojaeian and M. Shojaeian (2012), Analytical solution of mixed electromagnetic / pressure driven gaseous flows in microchannels, *Microfluid Nanofluid* **12**, 553-564.
- [190] A. Spille, A. Rauh and H. Bühring (2000), Critical curves of plane Poiseuille flow with slip boundary conditions, *Nonlinear Phenomena In Complex Systems* **3**, 171-173.
- [191] E. A. Spiegel (1964), Convective instability in a compressible atmosphere, I, *Astrrophys. J.* **139**, 1068-1090.
- [192] J. Stebel (2012), On shape stability of incompressible fluids subject to Navier's slip condition, *J. Math. Fluid Mech.* **14**, 575-589.
- [193] B. Straughan (1989), Convection in a variable gravity field, *J. Math. Anal. Appl.* **140**, 467-475.
- [194] B. Straughan (1991), Continuous dependence on the heat source and nonlinear stability in penetrative convection, *Int. J. Non-Linear Mech.* **2**, 221-231.
- [195] B. Straughan (1998), Explosive instabilities in mechanics, Springer, Heidelberg, 1998.
- [196] B. Straughan (2004), The energy method, stability, and nonlinear convection, 2nd edn., Springer, *Series in Applied Mathematical Sciences* vol. 91.

- [197] B. Straughan (2008), Stability and wave motion in porous media, Springer, *Series in Applied Mathematical Sciences*, vol. 165.
- [198] B. Straughan (2012), Triply resonant penetrative convection, *Proc. Roy. Soc. Lond. A* **468**, 3804–3823.
- [199] B. Straughan and A. J. Harfash (2013), Instability in Poiseuille flow in a porous medium with slip boundary conditions, *Microfluid Nanofluid* **15**, 109-115.
- [200] B. Straughan and K. Hutter (1999), A priori bounds and structural stability for double diffusive convection incorporating the Soret effect, *Proc. R. Soc. Lond. A* **455**, 767-777.
- [201] B. Straughan and D. W. Walker (1996), Two very accurate and efficient methods for computing eigenvalues and eigenfunctions in porous convection problems, *J. Comp. Phys.* **127**, 128-141.
- [202] B. Straughan and D. W. Walker (1996), Anisotropic porous penetrative convection, *Proc. Roy. Soc. Lond. A* **452**, 97-115.
- [203] B. Straughan and D.W. Walker (1997), Multi component diffusion and penetrative convection, *Fluid Dyn. Res.* **19**, 77-89.
- [204] B. J. Suchomel, B. M. Chen and M. B. Allen (1998), Network model of flow, transport and biofilm effects in porous media, *Transp. Porous Media* **30**, 1-23.
- [205] Sunil, Anupama and R. C. Sharma (2005), The effect of magnetic field dependent viscosity on thermosolutal convection in ferromagnetic fluid, *Appl. Math. and Comp.* **163**, 1197-1214.
- [206] Sunil, P. Chand and P. K. Bharti (2007), Double-diffusive convection in a micropolar ferromagnetic fluid, *Appl. Math. and Comp.* **189**, 1648-1661.
- [207] Sunil, P. Chand, P. K. Bharti and A. Mahajan (2008), Thermal convection in micropolar ferrofluid in the presence of rotation, *J. Magnetism and Magnetic Materials* **320**, 316-324.

- [208] Sunil, R. Devi and A. Mahajan (2011), Global stability for thermal convection in a couple-stress fluid, *Int. Communications in Heat and Mass Trans.* **38**, 938942.
- [209] Sunil and A. A. Mahajan (2008), Nonlinear stability analysis for magnetized ferrofluid heated from below, *Proc. Roy. Soc. Lond. A* **464**, 83-98.
- [210] Sunil and A. Mahajan (2009), A nonlinear stability analysis of a double-diffusive magnetized ferrofluid with magnetic field-dependent viscosity, *J. of Magnetism and Magnetic Materials* **321**, 2810-2820.
- [211] Sunil, A. Sharma, P. K. Bharti and R. G. Shandil (2007), Linear stability of double-diffusive convection in a micropolar ferromagnetic fluid saturating a porous medium, *Int. J. of Mech. Sci.* **49**, 1047-1059.
- [212] Sunil, P. Sharma and A. Mahajan (2010), Onset of Darcy-Brinkman double-diffusive convection in a magnetized ferrofluid layer using a thermal non-equilibrium model: a nonlinear stability analysis, *J. Geophys. Engng.* **7**, 417-430.
- [213] Sunil, P. Sharma and A. Mahajan (2011), A nonlinear stability analysis of a rotating double-diffusive magnetized ferrofluid, *Appl. Math. and Comp.* **218**, 2785-2799.
- [214] Sunil, P. Sharma and A. Mahajan (2011), Onset of Darcy-Brinkman ferroconvection in a rotating porous layer using a thermal non-equilibrium model: A nonlinear stability analysis. *Transp. Porous Media* **88**, 421-439.
- [215] M. A. Teamah (2008), Numerical simulation of double diffusive natural convection in rectangular enclosure in the presences of magnetic field and heat source, *Int. J. of Therm. Sci.* **47**, 237-248.
- [216] M. A. Teamah, A. F. Elsafty and E. Z. Massoud (2012), Numerical simulation of double-diffusive natural convective flow in an inclined rectangular enclosure in the presence of magnetic field and heat source, *Int. J. of Therm. Sci.* **52**, 161-175.

- [217] O. V. Trevisan and A. Bejan (1990), Combined Heat and mass transfer by natural convection in a porous medium, *Adv. Heat Trans.* **28**, 1587-1611.
- [218] J. C. Umavathi and M. S. Malashetty (2005), Magnetohydrodynamic mixed convection in a vertical channel, *Int. J. of Non-Linear Mech.* **40**, 91-101.
- [219] H. Varshney and M. F. Baig (2008), Rotating Rayleigh-Bénard convection under the influence of transverse magnetic field, *Int. J. Heat Mass Trans.* **51**, 4095-4108.
- [220] G. Veronis (1963), Penetrative convection, *Astrophys. J.* **137**, 641-663.
- [221] C.E. Weatherburn (1980), Differential Geometry of Three Dimensions, Cambridge Univ. Press.
- [222] M. Webber (2006), The destabilizing effect of boundary slip on Bénard convection, *Math. Meth. Appl. Sci.* **29**, 819-838.
- [223] M. Webber (2007), Instability of fluid flows, including boundary slip, PhD thesis, Durham University.
- [224] M. Webber and B. Straughan (2006), Stability of pressure driven flow in a microchannel, *Rend. Circolo Matem. Palermo* **29**, 343-357.
- [225] L. Xu and S. Yang (2007), Stability analysis of thermosolutal second-order fluid in porous Bénard layer, *Ricerche mat.* **56**, 149-160.
- [226] D. Yang, R. Zeng, and D. Zhang (2011), Numerical simulation of convective stability of the short-term storage of CO₂ in saline aquifers, *Int. J. Greenhouse Gas Control* **5**, 986-994.
- [227] X. Yong and L. T. Zhang (2013), Slip in nanoscale shear flow: mechanisms of interfacial friction, *Microfluid Nanofluid* **14**, 299-308.
- [228] M. Zakaria (2003), Free convection effects on the oscillatory flow of a viscoelastic fluid with thermal relaxation in the presence of a transverse magnetic field, *Appl. Math. Comp.* **139**, 265-286.

-
- [229] A. Zebib (1996), Thermal convection in a magnetic fluid, *J. Fluid Mech.* **321**, 121-136.
- [230] H. Zhang, Z. Zhang and H. Ye (2012), Molecular dynamics - based prediction of boundary slip of fluids in nanochannels, *Microfluid Nanofluid* **12**, 107–115.
- [231] W. M. Zhang, G. Meng and X. Wei (2012), A review on slip models for gas microflows, *Microfluid Nanofluid* **14**, 845–882.